Cranfield University

School of Industrial and Manufacturing Science

PhD Thesis

P. Shore

Machining of Optical Surfaces in Brittle Materials using an Ultra-Precision Machine Tool

Supervisor : Dr D. J. Stephenson

March 1995

Abstract

Investigations of machining optical surfaces into brittle materials using an ultra precision machine tool are presented. The newly developed ultra precision NION machine is evaluated to gain a good appreciation of its operating performance. The machining accuracy capability of this machine is established by careful measurement of its; motion accuracy, thermal and dimensional stability and loop stiffness. Corroboration of these measurements are provided by assessment of surfaces which were produced in soft "easily machined" metal materials. It was found that surfaces smooth to ~ 1 nm Ra could be produced on the NION machine and with a form error of less than 100 nm P-V. The main source of figure error, approximately 80 nm, was found to be caused by the synchronous axial error motion of the workhead spindle. Other elements of the machine, including thermal effects, incurred less than 25 nm of additional figure error.

Assessment of the diamond turning process for the producing optical surfaces made in a number of important optical materials, which are ostensibly brittle, were undertaken. Turning tests were carried out to establish the relative difficulty for machining optical surfaces in these materials and to define the most important parameters which affect the attained surface quality. Assessment of the produced surfaces was based on their roughness quality, surface morphology and residual stress condition. It was found that diamond tool edge quality degraded with total cut distance. Tool cut distance was found to be a major influence on achievable material removal rate before micro-fractures became present at the surface. Surface quality and residual stress condition were also greatly influenced by the overall tool cut distance.

Diamond grinding trials were also carried out using the NION machine tool. These grinding trials were carried out using a mode of grinding which permits complex shape optical surfaces to be produced. Various grinding technologies were employed to establish the optimum methods. Selected grinding trials were carried out to establish the dominate parameters affecting the optical quality. Assessment of the machined surfaces was in regard of their surface roughness, residual stress and severity of sub-surface micro cracking. It was found that grinding wheel specification was a major influence on surface quality and sub-surface damage. The level of residual stress associated with “ductile” mode grinding was not found to prohibit its application toward the direct manufacture of optical elements.

Selection of grinding parameters which ensured the grain depth of cut, GDOC, parameter did not exceed the materials critical depth, d_c, allowed glass surfaces to be ground to 1-2 nm Ra. These ground glass surfaces appeared free of any surface fractures. Sub-surface assessments did however reveal small levels of micro-fractures hidden below the surface.

Discussion of both machining processes is provided. Available material removal rates for each process is given when cutting a number of important optical materials. Conclusions regarding the production of both Infrared and visible wavelength optics using the NION machine tool are provided. Recommendations for future work to improve both; the understanding of the processes and the effectiveness of applying the processes are suggested.

LIST OF CONTENTS

Page No.

CHAPTER 3 : Experimental Procedures and Equipment

Page No.

List of Tables

Page No.

List of Figures

Page No.

CHAPTER 1

Introduction

The increasing requirement for precise and complex shaped optics, made in a wide range of ostensibly brittle materials, has resulted in a need for more controllable and repeatable manufacturing methods.

Traditional machining methods for producing optical elements have been highly dependant on the use of the loose abrasive processes, lapping and polishing. Indeed these processes have proved extremely successful in the manufacture of high quality planar and spherical surfaces. However, the implementation of such machining processes for the manufacture of more complex shape objectives, e.g. aspheric, diffractive, binary or "hybrid's", have been far less successful when assessed from both a quality and cost effectiveness standpoint.

Optical designers have generally been encouraged to design systems having simple planar and spherical surfaces. Spherical and chromatic aberrations which may result from using elements of this shape were then "designed out" by careful selection of; the element's material (variance of refractive index), the size / shape and the total number of optical elements used. This "spherical design" approach therefore leads to systems having increased size, weight and overall total cost.

Advanced optical systems are now often specified with a critical maximum weight and / or size limit. This has forced the optical designers to advocate the use of more complex shape objectives. This in turn has placed much more pressure on the optical manufacturers to supply precise elements having an aspheric and even diffractive shape. This is presently the case for some of the more advanced systems operating in the infra-red regions, 2-5 μm and 8-10μm wave-lengths. It is widely thought that other systems manufacturers will ultimately demand similar complex elements for systems operating in the visible region, 0.4-0.7 μm wave-lengths.

The manufacture of optical surfaces which depart significantly from a planar or spherical shape, using a free abrasive force controlled process (e.g. Polishing), has proved difficult, slow and expensive. More success has been found in machining aspherical surfaces using machining processes which are controlled by accurately positioning the tool with respect to the workpiece. These so-called "position controlled" processes include, diamond turning and fixed abrasive grinding.

For many years cost effective use of diamond turning as a manufacturing process was limited to soft plastic and non-ferrous metals. Typical optical components being X ray mirror elements, contact lenses and other optical mirror systems.

The increased need for more precise and complex optical objectives has placed arduous requirements on both the machine tools and the associated tooling. These demands are compounded by harder and more brittle objective materials. These brittle materials offer important performance criteria. All of this is coupled by lower cost and lead-time expectations of the system manufacturers.

The advantages offered by position controlled processes such as turning and fixed abrasive grinding is in regard of their suitability for computer control, automation and repeatability of product quality.

The limitations attached to these processes are defined by;
i) the machine tool's motion accuracy
ii) the consistency and quality of the cutting tool
and iii) non-linearities of the material removal mechanisms

Recent developments have taken place in all of the above areas. Higher precision machine tools have been developed. Tool preparation methods have been optimised. Basic research into "ductile" machining of ostensible brittle materials has revealed that these hard materials can be machined, albeit at low tool penetration levels, with a ductile type removal mechanism where surface and near surface damage is minimised.

Other investigations into fixed abrasive diamond grinding of brittle materials, such as advanced ceramics has shown that a ductile type removal mechanism is achievable. Other grinding investigations carried out on glass materials have shown that super smooth "optical type" surfaces can be achieved by fixed abrasive grinding. Surface textures approaching that obtained by traditional polishing methods have been reliably produced. The implementation of advanced grinding techniques on machine tools having the same precision quality as diamond turning machines has been adopted. It is claimed that significant advantages in manufacturing advanced optical elements is thus made possible.

Some investigation of the condition of the near surface regions has been carried out on surfaces which have been precisely machined by the diamond turning and fixed abrasive grinding processes. This limited work has shown that damaged regions can range from 100 nm up to a number of microns. The condition of the near surface region is a major influence on the performance of an optical element. This particularly influences absorption and coherence qualities, together with the stability of the form profile through residual stress levels.

In this study a newly developed ultra precision machining research facility, the "NION" machine, has been carefully characterised for its precision of motion control, long term stability and overall machine "loop" stiffness. Machining trials were then carefully carried out to support the measurements of machine accuracy. A clear indication of the attainable accuracy from this machine was gained. Sources of the NION machine's error are identified and discussed.

Subsequent investigations into the effectiveness of using "ductile" machining methods to produce optical quality surfaces, in a range of advanced optical materials, using the NION machine, were carried out. Machining trials employed both single point diamond turning and multi-point fixed abrasive diamond grinding.

The machining tests were set out to establish the important machining and tooling requirements which attain the highest quality surface and sub-surface conditions. Investigation of the resulting surface and sub-surface conditions permitted an overall assessment of the effectiveness of producing such surfaces in that manner. Evaluation of surfaces were carried out using a range of non-destructive and destructive testing methods.

A review of the attainable quality, machining time and overall cost effectiveness is provided for both diamond turning and diamond grinding of complex shape optical surfaces.

CHAPTER 2

Literature Review

2.1 Optical Elements

Historically optical systems have generally comprised spherical shape objectives [1]. Although this shape of optic is often not an ideal one, for either a transmission or a reflective system, it benefits from being a shape which is easily generated to high levels of form accuracy.

Typically form accuracy of an optical component is measured in optical fringes. High quality optics are required to have accuracy's in the range of $\lambda/4$ up to $\lambda/50$, where λ ranges from 535-633 nm dependant on the lens manufacturer [2]. The most widely used value for λ is the wave length of a Helium Neon laser which is 633 nm. Form accuracy of high quality optics is stated either in transmission or as a surface wave front error. The former is the error of both of the surfaces of the element and is therefore the more demanding, the latter being the error on each individual surface. Commonly form accuracy specification for high quality spherical optics is $\lambda/20$, λ being 633 nm, and measured as a surface wave front error [3]. This means that each surface should not depart from the ideal by more than 31 nm peak to peak.

In recent years the range of objective shapes being used in high technology optical systems has become more diverse. Precision optical systems comprising purely spherical and planar elements are becoming less common. The reasons behind the move toward more complex shape optics are concerned with producing smaller, lighter and generally less complicated systems in regard to the number of elements. Quality aspects can also be attained with these more complex elements.

The use of aspherical shape objectives to reduce spherical aberration permits a reduction of the number of elements required in a given system and is becoming a more common practice [4], see Figure 1.

Diffractive surfaces, see Figure 2, are also becoming more commonly used [5]. Fresnel surfaces permit elements to remain thin and lightweight, yet have a high relative power aspect. Lower transmission performance is often associated with these Fresnel optics, but developments in their manufacture are improving this aspect [6].

For some of the most advanced systems it is the added benefits of utilising both refractive and diffractive surfaces together in one element which offers large scale

advantages, see Figure 3. These "hybrid" elements can be designed to ensure that they have no spherical or chromatic aberration [7].

The manner by which chromatic error is avoided is through a refractive surface giving chromatic aberration in the opposite direction to that of a diffractive surface, see Figure 4 [8]. The combination of a diffractive "binary" surface superimposed on a spherical or aspheric form provides the possibility of an "aberration free" objective, which is often referred to as an Achromatic singlet. These "hybrid" optics have already made some impact on systems operating in the IR wavelengths, 3-5 μm and 8-10μm, and prototype systems having "hybrid" IR elements have been manufactured.

It is predicted that the demand for aspheric and "hybrid" style optics is set to increase rapidly, especially as optical designers become aware of their availability [5]. As with all manufactured products, as the production numbers increase a significant reduction in cost will be anticipated by the end user. Significant improvement in the methods of manufacturing "hybrid" and other complex optics will therefore be necessary.

2.2 Fabrication Methods for Precise Optical Elements

2.2.1 Spherical Optics

Spherical type optics have traditionally been machined using a number of fixed and free abrasive grinding processes. A typical procedure for producing a spherical optic is given in this section [9,10].

2.2.1.1 Rough Machining of Bulk Material.

Initially slitting and milling of the rough overall dimensions is carried out using coarse grade metal bond diamond grinding wheels. This work is usually carried out on traditional glass working machines having force control. Metal cutting machine tools are sometimes used often having been fitted with higher speed rated spindles.

Roughly sized ground plates can be "marked" and "cut" into square pieces using a scribing guide and automated hammer. Assessment of the integrity of the glass pieces is possible at this stage. The cleaved edges are clear and permit inspection for defect bubbles and striae. The "sized" square glass pieces are subsequently fixed abrasively ground to give roughly flat and parallel surfaces. The pieces can then be "rounded", either individually or as a stack of components which have been waxed together. This "rounding" process is carried out using fixed abrasive grinding methods and using conventional metal cutting cylindrical grinding machines. The "rounding" process

whilst using fixed abrasive tools is often referred to as a "milling" operation. The cylindrical pieces are then ready to have the spherical surfaces machined.

2.2.1.2 Fixing Blanks to Block Holders

The cylindrical pieces, referred to as "blanks" must be fitted onto a block holder. The radius of the block holder is calculated using simple geometry and is dependant on the radius of curvature of the lens to be made.

The blanks are covered on one surface with a pellet of "pitch" (wax adhesive). A suitably chosen "laying in" shell is covered with a thin layer of pitch, see Figure 5. The blanks are fitted to the laying in shell, with their pitch covered surface, upward. The thin layer of pitch on the laying in shell should ensure the blanks do not slip during the blocking operation.

The block holder is heated, typically up to $70^{o}C$ and then lowered into the laying in shell. Previous to this three equi-spaced ball bearings are positioned in the laying in shell to obtain an even gap between the shell and the block holder. The heat of the block holder melts the pitch applied to the blanks, see Figure 6. The block holder is then cooled and subsequently removed with the blanks fixed onto it.

2.2.1.3 Grinding and Polishing of Blanks on Block Holders

The block holder is mounted into the grinding / polishing machine and is loose abrasively machined using different, tool shells, grade and type of abrasive. Diamond and cerium oxide abrasive are most commonly used. Three or four different grades of grinding / polishing are common practice for the most precise spherical elements.

For significant production numbers it is common for a block holder to be moved from one machine to another, each of the machines being identical but having a different grade / type of abrasive, different tool and / or suspension fluid (slurry mixture).

The most widely used machine is the "lever-arm" machine, see Figure 7. More modern machines have been developed but these in the main are based on similar lines to the lever arm approach. The process is ultimately force controlled by the weight applied to / by the tooling shell.

A high degree of accuracy from the machines motions is not necessary because the tool and the component run "unconstrained" with respect to each other. It is important for the machine operator to understand, how the "to" and "fro" movements

of the machine and the size of the tool shells influence the quality of lens. Suitable skilled craftsman can produce high accuracy spherical lenses using these methods, to better than $\lambda/10$.

2.2.2 Aspheric / Diffractive Optics

The initial stages of manufacturing these complex shape optics will often be very similar to that discussed in section 2.2.1.1. For many aspheric / diffractive optics they are made first into spherical elements which best fit the final shape needed, and subsequently worked to the final shape.

Successful finish machining methods for these type of optics are highly dependant on the required form accuracy, the optic material, its size and exact shape. This is clearly the case since aspheric and diffractive optics have made great impact in some areas of the optics industry and not at all in others. As stated in section 2.1 there are many advantages in using aspheric and diffractive optics, with the disadvantages being most often a consequence of difficulties in their manufacture.

Aspheric optics are more regularly used in systems operating at infra-red wavelengths. This is particularly so for the longer 8-10μm wavelength systems. The most common method for producing aspheric IR optics is by diamond turning. It is important to note that the surface roughness and form accuracy needed for these IR optics is less demanding than would be the case for a comparable visible wavelength element. IR materials include, Optical Germanium, Zinc Selenide, Zinc Sulphide and Silicon. These materials can with varying levels of difficulty be diamond turned. Aspheric optics in most of these materials are regularly manufactured by the diamond turning process.

Methods for producing precise aspheric optics for use at visible wavelengths have been less successful than for IR applications, especially with regard to cost effective manufacture. Diamond turning glass optics has not to-date proved a viable production method. This is a consequence of the difficulty in machining glass materials, see section 2.6.2. Precise visible wavelength aspherics can be obtained from a small number of companies who generally produce them using skill intensive free abrasive polishing methods. Both cost and delivery of such optics, compared to a similar size spherical surface, are dramatically increased. Therefore they are only used in the most demanding of applications. Full aperture and sub-aperture CNC polishing machines have been developed for aspheric optics [11,12]. However, these machines have generally been designed specifically for large and expensive optics, such as

telescope optics and synchrotron systems, etc.. A versatile aspheric polishing machine, aimed at rotationally symmetric optics having $\lambda/10$ capability, has not been marketed or discussed in the literature.

Direct grinding of precise glass aspheric surfaces using fixed abrasive grinding on ultra precision CNC machine tools has started to be investigated [13,14]. Machine tools have recently been designed specifically to accomplish this task and are under further development [15,16]. No evidence of this method being in general use without significant amounts of post polishing is to be found in the literature. Direct grinding of glasses where micro-fractures are not introduced reqiures an extremely high level of control of the grinding wheel grain penetration depth, GDOC, see sections 2.6.3 and 6.1.

Precise diffractive "hybrid" optics have to-date only been effectively used in a small number of IR systems [8], these elements have been exclusively produced by the diamond turning process.

General awareness of the benefits from using hybrid optics in both IR and visible systems has increased in recent years. Pressure by the optical designers has intensified the efforts of manufacturers to produce hybrid optics [7,8]. Along with the developments in diamond turning and diamond grinding processes investigation of "forming" such optics is being carried out [17].

2.2.3 Relative Cost of Advanced Optical Surfaces

To help establish the importance of improving the manufacturing methods for producing complex shape optical surfaces the relative manufacturing cost of various shapes has been obtained [18], these are given in Table 1. The costs are those for producing a typical 100 mm diameter IR surface having a figure accuracy of $\lambda/3$ or 0.2 μm p-p (λ = 633 nm) and made from optical germanium. It can be seen that the cost of the aspheric and hybrid surfaces are significantly greater than those for spherical and flat surfaces. This cost differential is due to the added difficulties and increased cost of the equipment which are needed to manufacture these type of optical surfaces.

2.3 Material Removal Mechanisms and Removal Rates

The material removal mechanisms of polishing, lapping and traditional grinding are discussed in this section. The mechanisms and associated removal rates of "ductile" mode turning and grinding are discussed in section 2.6.

2.3.1 Polishing

The removal mechanisms of the polishing process have been investigated in some depth. Several mechanisms have previously been proposed for the polishing of optical glass materials. These include:

i) the wear mechanism originally proposed by Rayleigh,
ii) the flow mechanism discussed by Beilby,
iii) the chemical mechanism discussed by Preston.

The fourth, and most widely accepted as being the correct mechanism, is some combination of the above three. This particular subject has been investigated in a great depth by the Hoya glass company and in particular by Izumitani [19].

The Rayleigh's wear theory suggested that molecular levels of glass is removed from the surface purely by a mechanical means. Beilby's flow mechanism theory is said to involve local heating of the glass surface caused by the friction generated as the polishing grains, under a high pressure, move over the glass surface. The material removal is obtained by plastic flow or viscous shear. The chemical theory initially proposed by Preston [20] suggested that a silica gel forms on the surface of the glass through a chemical reaction with the water based polishing slurry. This softer surface layer is then removed by the polishing compound. Further work [21] has identified the chemical reaction at the glass surface to be a very important factor of material removal during polishing glass.

Izumitani and others [19, 22] speculated that it was a combination of the above three mechanisms. Izumitani carried out in depth experiments to establish the contribution of each mechanism toward the overall material removal process, and has done so on a wide range of optical glasses. The intention of Izumitani's work was to establish any correlation between the polishing rate and other glass characteristics such as hardness, softening point and chemical durability. According to the wear theory the polishing rate should be highly dependant on the glass hardness level, the flow theory would be dependant on the softening point and finally the chemical theory would be dependant on the chemical durability of the glass. A carefully standardised polishing test was carried out on 18 different types of optical glass materials. The first finding from this test was that the hardness of the glasses investigated had little direct influence on the polishing rate, as shown in Figure 8. This graph clearly shows that the glass surface smoothness is not solely produced by a mechanical cutting process. This observation invalidates the wear mechanism proposed by Rayleigh. The second, equally important finding from Izumitani's polishing tests was that the softening point of the glass also

had no influence on the polishing rate, see Figure 9. In fact his findings were opposite to that expected in as much that the polishing rate was often higher for glasses having a high softening point. This observation clearly invalidates the flow mechanism proposed by Beilby.

To investigate the chemical mechanism Izumitani carried out other experiments and found that a linear relationship existed between the polishing rate (using an acidic slurry) and the percentage loss of weight of each glass material when submerged in a nitric acid solution, see Figure 10. The relationship is however different for the silicate and the lanthanum borate glasses and two lines are shown to express this difference. Another test of this type discussed by Izumitani showed that the polishing rate (using a water based slurry) showed a simple linear relationship with the percentage weight loss of glass samples submerged in water, see Figure 11. The rate of polishing is almost proportional to the water resistance. It can be said from these results that the chemical reaction between the glass and the polishing liquid plays an important role in the polishing process. It is clearly shown that there is a difference in the linear relationship between the polishing rate of silicate and lanthanum glasses when compared to their chemical durability in acid, see Figure 10. This suggests there must be another factor which controls the polishing rate.

The hardness of the glass surface layer was subsequently investigated. It was found that the hardness of the surface layer was significantly reduced when the glass surface was leached by soaking in a low concentrate hydrochloric acid solution. This shows that a soft surface layer was produced by a chemical reaction with the acid solution. It was also found that the less chemically durable glasses formed a softer surface layer more quickly after leaching in the acid solution. The softer surface layer, the hydrated layer, was investigated for hardness for a range of glasses and this was plotted against the glass polishing rate, as shown in Figure 12. From this another factor which influences the material removal during polishing is found; the formation rate of the hydrated layer and its hardness.

Polishing tests were carried out without using any abrasive grains in a water based polishing compound. During these tests no material removal occurred, indicating the importance of the abrasive grains.

Summarising, during the water polishing process a soft hydrated layer is formed on the surface by a chemical reaction and the smoothing process is due to the removal of this hydrated layer by the polishing grains. Thus, it can be concluded that the polishing

process is the forming of the hydrated layer by chemical reaction and then by mechanically removing this layer by use of abrasive grains. Polishing rate is determined by a combination of the chemical durability of the glass (rate of formation of the hydrated layer), the hardness of the hydrated layer and the mechanical action of the abrasive grains in removing this "hydrated" layer. The optimum hardness of the abrasive grains is such that they can themselves fracture during polishing but are harder than the "hydrated" layer formed on the glass material.

2.3.2 Lapping and Grinding

Before surfaces are polished they are generally lapped and / or ground. Lapping is a free abrasive machining process often using silicon carbide, boron carbide or aluminium oxide grains, whilst grinding is where diamond abrasives are bound in a metal or resin matrix tool. Traditionally lapping has been used for the so-called "smoothing" or "spherising" operation. However, an increasing trend is to carry out the smoothing operation using bound diamond abrasives. The shift to bound abrasives has in part been due to the development of new grinding tools and more advanced force controlled machines [23]. Bound diamond abrasive tools have proved to offer higher material removal rates than can generally be obtained from loose abrasive lapping methods.

The material removal mechanisms for both the lapping and grinding processes are thought to be extensively the same. The overriding removal mechanism is the initiation and propagation of micro cracks. These micro cracks are caused by grains penetrating the glass surface to an extent which causes micro cracks to appear from the edges of the indented region. Significant levels of micro fracture occur during lapping and grinding and material removal is obtained by brittle fracture.

The ease of lapping a material has traditionally been measured by the term "lapping hardness". The "lapping hardness" is an empirical or relative value which is determined from carefully carried out tests. "Lapping hardness" is the reciprocal of the ratio of the volume removal of a standard glass (often BK 7) and that of the glass of interest.

The "lapping hardness" is considerably influenced by the Knoop hardness of the glass. The higher the Knoop hardness the higher the lapping hardness. However this correlation is not always linear, lanthanum based glasses have relatively high Knoop hardness but a low "lapping hardness". This apparent anomaly has been clarified by showing that when the effects of water are removed from the lapping process, where

oil is used instead, the "lapping hardness" is more closely proportional to the Knoop hardness. The importance of water in the lapping process has been clearly demonstrated [19].

The ease of lapping a glass material has therefore been shown to be dependant on the resistance to fracture, expressed as a function of the size of the indentation caused by the lapping grains and the associated crack elongation extending from those indentations. It is therefore considered to be a property dependant upon the indentation hardness and the intrinsic strength of the glass. The intrinsic strength property is that which is influenced by the presence of water where extension of micro crack tips can occur.

2.3.3 Removal Rates and Surface Quality

The rate of material removal which can be obtained for lapping and polishing is greatly dependant on the shape of the optical surface, the element material and the permissible type and grade of abrasive. The typical lapping and polishing times and material removal rates for a 100 mm flat surface made in BK 7 optical glass are given in Table 2. The resulting surface finish quality for each of these processes is also given. The values given in Table 2 are those which can be obtained using modern optical manufacturing machines [24]. The parameter Ra, roughness average is used throughout the thesis to described surface roughness. However, this Ra value is that obtained from a Wyko 3D instrument and truly refers to the surface average of an assessed area. The Sa parameter itself is expected to become more widely used in the future.

The data obtained for the lapping process are when using 13 μm SiC abrasives, polishing rates are for 1 μm CrO abrasives. The removal rates for the polishing and lapping processes are significantly lower when used on harder materials such as silicon.

2.4 Important Materials for Advanced Optics

2.4.1 Infra-Red Applications

Important materials from which advanced IR optical objectives are made have been discussed previously [25]. Those which Riedl [8] considers to be most important are given in Table 3 together with some of their important mechanical properties.
The materials have been identified for their functioning properties as IR elements together with their mechanical / thermal properties, machinability and cost.

In general Silicon is the material which offers the best properties for use in the 3-5 μm region together with being the low cost option. Silicon is available in a high purity mono-crystalline and a polycrystalline form. Its low density makes it ideal for large aperture elements where overall system mass is critical. For the 8-10μm wavelength, Optical Germanium has an excellent operating performance and as with Silicon it is also available in high quality mono and polycrystalline forms.

Zinc Sulphide and Zinc Selenide have excellent operating performance in the 3-5 μm region Cleartran™ a form of Zinc Sulphide has the advantage that it is transparent in the visible region. This advantage is extremely useful when initially aligning systems. Zinc Selenide has one particular disadvantage in so much as it is toxic and must be handled and machined with some care ensuring extraction of swarf is provided.

The cost of Zinc Sulphide, Zinc Selenide and Optical Germanium in their highest quality format is very similar. Only Silicon has a significant cost advantage.

2.4.2 Visible Applications

There are many materials which are suitable as visible optical elements, including plastics, sol-gels and glasses. However, for the great majority of precision applications it is the glasses which are in prevalent usage. There are about 250 different optical glasses, each of which has its own particular optical, mechanical and chemical characteristics [26]. Glasses are selected for a given application depending on the required refractive indices, permissible weight, necessary abrasive wear resistance and cost. In many applications where fluctuation of the ambient temperature can not be controlled, e.g. aerospace and space applications, the coefficient of thermal expansion is also important.

The data in Tables 4 and 5 give some important details of three commonly used optical glasses and one special purpose Zerodur™[27] glass/ceramic material. The details of these particular glasses are given as they form a reasonable range of optical glasses that are important to many precision optical applications. These glasses posses very different mechanical and chemical compositions and have been used in experiments discussed in this thesis.

Whilst the mechanical properties listed in Table 4 are easily understood the chemical properties given in Table 5 need some explanation.

Acid resistance is classified to an SR specification. The SR measure is related to the time with which 0.1μm of glass is removed from a polished surface of a given glass when it is subjected to a strong nitric acid, pH 0.3 at 25°C. SR Class 1 is the most resistant and can be subject for over 1000 hours, classes 2, 3 and 4 are for 10-100 hours, 1-10 hours and 0.1-1 hour respectively.

The water resistance is stated by the CR classification. The CR classification is provided to give the optic manufacturer an indication of the resistance to changes caused to a polished surface when exposed to a water-vapour saturated atmosphere. An accelerated procedure is used for testing the climatic resistance of each glass. In this test un-coated polished surfaces of the glass are exposed to a water saturated environment which is cycled every hour from 45-55°C. Condensate forms on the surface during the heating phase and dries up during the cooling phase. After having been exposed for 30, 100 and 180 hours the samples are assessed for the amount of light scattering which each glass surface provides. Classification CR1 is given to glasses which have very limited, if any, deterioration after 180 hours of exposure. CR 4 is given to glasses which would noticeably deteriorate after 30 hours or less. Classes CR 2 and 3 are given to glasses which fall between classes 1 and 4.

2.5 Position Controlled Machines / Performance Assessment

2.5.1 Influences on Machining Accuracy Capability

Machining methods which have been most successfully applied to the manufacture of those optics which depart from simple spherical and planar shape are those which can be classified as "position controlled". With this type of machining process the actual position of the tool-to-workpiece is the controlled parameter, this being quite unlike the lapping and polishing processes which are predominantly force controlled.

Diamond turning and fixed abrasive diamond grinding are the most widely used positional controlled processes used in the manufacture of complex optical elements. The development of computer numerically controlled machines has permitted control of tool path in a manner which permits complex optics to be generated by a combination of linear and rotary motions.

The requirements of machine tools operating position controlled processes are significantly more arduous then for machines using force controlled processes. This is mainly through the relative difficulty of controlling position as opposed to force, but also that the force controlled processes are generally used for producing surfaces which are "self-generating", i.e. spherical.

The quality or accuracy of components made by positional controlled processes are influenced by many factors, see Figure 13 [28]. These influences include; changes of the environment, the machine tool's quality and the machining process stability. Therefore the achievable accuracy with which optical elements can be produced by diamond turning or fixed abrasive grinding is dependant on many interrelated factors. Assessment of a position controlled process therefore requires detailed test procedures to evaluate the true machining accuracy capability.

2.5.2 Aspheric Generators

Aspheric generators are ultra precision machine tools which have been developed for the manufacture of complex optical elements. These machines comprise computer numerically controlled rotary and linear axes of the most precise nature. A number of machine configurations has been used, the most popular of these are shown schematically in Figure 14.

The layout shown in Figure 14a is that of the Moore M18 AG. This machine was the first commercially successful aspheric generating diamond turning machine which is manufactured by the Moore Machine Tool company [15]. The M18 AG is a three axis CNC controlled machine having an air bearing work spindle which is rigidly fixed to the machine base structure. The diamond tool is mounted into a toolpost which is mounted onto a rotary B axis. This rotary B axis is in turn mounted on top of a stacked X-Y slideway system.

The M18 AG machine uses laser interferometers for positional measurement of the linear axes. These linear axes are mounted on very precise "opposed vee" type rolling element slideways and driven by specially prepared ball screw actuators.

In Figure 14b the layout used by the Rank Pnuemo for their MSG 325 is shown [29, 30]. This machine was developed subsequent to the Moore M18 and differs in a number of areas.

The most significant differences being ;

i) the air bearing workspindle is mounted on the in-feed Z slideway

ii) the linear motions are "floating" on hydrostatic oil bearings

In many other respects the MSG 325 and the M18 have similar sub-systems. The main reason behind Pnuemo implementing a moving workspindle was to permit the use of

smoother, but bulkier, hydrostatic oil bearings. This type of slideway bearing has many advantages over the rolling element bearings used by Moore, these include ease of manufacture, precision (repeatability), smoothness and increased stiffness. By changing the layout of the linear axes the Pnuemo machine benefited in other ways. Stacking axes as with Moore's M18, is not an ideal configuration for high precision since the straight-line motion errors tend to become additive and difficult to measure and compensate. The Abbe offset distances, see Section 2.5.5, become large and positioning of measurement encoders limited.

Figure 14c shows the configuration of the Cranfield Precision Nanocentre 250 aspheric generator [16]. This machine differs from both the M18 and MSG 325 in a number of ways. The configuration has the workspindle, an oil hydrostatic system, mounted into the X axis carriage, the tool in feed Z axis carries an integral rotary B axis. All the linear and rotary axes of the Nanocentre are "floating" on hydrostatic bearings. Unlike the MSG325 and the M18 the linear axes are driven by friction or traction drive systems, it is claimed that these drives are less prone to cyclic errors which can afflict ballscrew drives. A hydrostatic oil bearing workspindle was chosen to provide higher stiffness than can be obtained from an air spindle and also to provide a reduction of any thermal axial growth error. The choice of configuration for the linear and rotary axes permitted positioning of the laser interferometer transducers which ensured a minimal level of Abbe offset.

The addition of the rotary B axis used on both the Moore M18 and the Cranfield Precision Nanocentre is to permit diamond turning using a "Tool Normal" machining method. Tool normal turning ensures that a specific point on the radius of the diamond tool remains normal to the optical surface being cut. Therefore errors of form of the tool radius are not reflected in the component. The other benefit of the rotary B axis is found when turning with diamond tools having steep top rake angles. If Tool Normal operation is not used the top rake angle changes as the cutting position moves around the periphery of the tool.

All of the above machines can be provided with different systems which permit diamond turning and fixed abrasive grinding processes to be utilised.

2.5.3 Thermal Drift Errors

Thermal drift in machine tools has often been described as the largest contributing factor towards component form and size error [31]. Thermal drift is produced through a temperature change of machine elements which form part of the tool to

workpiece loop. Attempts to reduce thermal drift of machine tools has been carried out using three distinct approaches.

The first approach is concerned with improving the temperature control within and around the machine tool [32]. This method focuses on reducing the temperature variance and therefore reducing the dimensional effect. The second method is to reduce the effect which temperature variation has on dimensional stability. This insensitivity is achieved by utilising materials having a low coefficient of thermal expansion and by use of careful machine design practices [33, 34]. The third approach is that of compensation, here thermal distortions are measured, tool positions are then corrected in-line with any movement [35].

Thermal distortions of a machine tool are caused by both changes in ambient conditions [31], and by heat generated by the machine's sub-systems and machining process. Heat generation from machine operators has also been identified to cause machine distortion.

Analysis of the way thermal variations influence machine tool accuracy capability is complicated. This difficulty is found since machine tools are made from a variety of materials. Each material has its own level of thermal expansion, thermal mass and importantly, its own level of thermal conductivity. Thermal mass differences of machine sub-systems also make real time analysis of thermal distortion a complicated task. Little work on predictive compensation for thermal distortion has been carried out which could be the basis of improving the machine accuracy capability of complex ultra-precision CNC controlled machine tools. Improving machine tool accuracy capability has been most effectively achieved by use of high quality temperature systems.

2.5.4 Machine Tool Spindle Assessment

The machining performance of a machine tool is highly influenced by the qualities of its spindle systems [36]. For aspheric generating diamond turning machine tools it is the workhead spindle errors which are likely to be the largest contribution to overall component inaccuracy.

The methods of assessing the accuracy of machine tool spindles have been carefully investigated and a unification document has been drawn up [37]. The methods proposed for spindle assessment ensure spindles can be qualified for accuracy in a

standardised manner. The isolated use of poorly defined parameters such as "run out" levels have been identified as a serious error in the specification of spindle quality.

The three fundamental error motions of a spindle system have been proposed. These error motions are those which influence the accuracy of axis of rotation. These are;

i) Pure Radial error motion
ii) Pure Axial error motion
iii) Pure Tilt error motion

These pure error motions are shown in Figure 15. Pure radial error is where the axis of rotation remains parallel to the axis average line, and moves perpendicular to it. Pure axial error motion is where the axis of rotation remains co-axial with the axis average line, and moves axially with respect to it. Pure tilt (angular) error motion is where the axis of rotation moves angularly with respect to the axis average line, and in the plane of the axial and radial motions.

The importance of these error motions is in part dependant on the sensitive and non-sensitive directions of a particular machining process. For a turning type machine, such as an aspheric generator, the sensitive directions are fixed.

For each of the three pure error motions there are two distinct contributing modes of error, synchronous and asynchronous motions, synchronisation being relative to the rotation of the spindle shaft or housing.

Synchronous errors are those which occur in a repeatable way from one rotation of the spindle to the next. Asynchronous error is the lack of repeatability of position from one spindle rotation to the next. For an aspheric generating machine tool the synchronous errors translate themselves into component figure or form error, asynchronous errors translate into component surface roughness.

Thermal error within machine tool spindle systems has had much investigation [36, 38]. The amount of work in this area is fully justified since for most machine tools it is a very significant error which has influence on both, component accuracy and production rates. Power dissipation levels for spindles are generally the highest within a machine tool, a consequence being that significant thermal distortion can occur. The influence on production rate is a function of the axial thermal growth having a higher rate of growth after initial spindle start up. Since production cycles cannot generally

permit time to elapse, for the rate of thermal growth to reduce, much design effort has been focused on reducing this error [16]. Thermal growth is most sensitive in the axial direction for an aspheric generator machine.

Another spindle error which has been less well documented and occurs mainly with hydrostatic bearing spindles is that called hydrodynamic "yaw" or angle[39]. This error is a consequence of a shift of the axis of rotation with a change of spindle speed. For a turning machine it causes, tapered cylinders to be produced or, leads to an aberration on a spherical surface.

Methods of measuring spindle errors have been developed, as have specific measurement systems [40]. The most widely practised method of assessing spindle errors is through the use of non-contacting capacitance probes. This type of probe can have nanometric resolution [41] and be utilised with a low level of background noise. Synchronous and asynchronous error motions have been measured in this way, as have spindle thermal growth errors [42].

2.5.5 Linear Motion Accuracy

The contouring accuracy of a machine tool is influenced by the precision of its linear axes. Precision of linear axes are defined through their straight-line motion accuracy. The six degrees of freedom of a body are used to help define the precision of a linear slideway, see Figure 16. The six degrees of freedom are made up of, three rotational and three linear movements. The rotational movements are called pitch, roll and yaw,. The linear movements are, the positional error in the direction of the slideway, the two other movements are straightness errors orthogonal to the direction of motion. Full explanation of these errors are found in British Standards [43].

For an aspheric generator the importance of each of these degrees of freedom is dependant on the machine configuration. It is also important to differentiate the repeatable and non-repeatable contribution towards these errors. It is a common practice for the precision machine tool builder to error compensate the important error motions [44]. In-situ machine based precision straight edge have been employed such that workpiece errors can be measured whilst on the machine. Compensation of the "tool path" can then be entered into the CNC, the component is then re-cut to the desired shape. Error compensation methods can only be undertaken to the level of repeatability of the axis. Smooth hydrostatic oil bearing slideways generally have very good repeatability and can therefore be error corrected to very precise levels.

The method most widely used to assess straight-line motion quality of an axis is undertaken using an independent measuring system. Position error in the direction of the axis is often assessed using a laser interferometer. The pitch, roll and yaw errors can also be measured in this way, however the use of a high quality, calibrated and mapped straight edge used in conjunction with non-contacting measuring probes can be more useful. Error mapping and compensation of a linear axes can easily be undertaken on machines having the latest type of CNC controller. In order to ensure any errors in the master straight edge are minimised reversal methods can be employed. The reversal is obtained by turning the straight edge through 180 degrees; measured errors are then averaged to remove master introduced errors. Mapped errors from the master straight edge can also be used. Distortion of the master can easily be introduced if incorrect holding methods are used. Some diamond turning and grinding machines have been built with in-situ master straight edges [45, 46]. The straight edges are then used directly as the reference for the linear measuring transducers, active correction for errors of straight-line motion are gained.

2.5.6 Machine "loop" stiffness

The measure "loop" stiffness of a machine has been proposed [28, 47]. This parameter helps provide an understanding of how much the tool will deflect away from the component as a result of the machining force. Machine "loop" stiffness is an important measure of the quality of the machine. Both static and dynamic "loop" stiffness can be measured given the necessary equipment.

The so-called machine "loop" is that which encompasses all the stress bearing elements within the machine tool. No standardised method for measuring loop stiffness has been proposed, however the method described by Franse [47] is often cited as being a good procedure to provide comparable data. Very few machine tool manufacturers provide data on actual machine tool "loop" stiffness. A common practice among machine tool manufacturers is to provide stiffness data on particular elements or sub-systems. This information in isolation means little to the user (or potential customer) of the operational machine.

2.6 Precision Diamond Machining Processes

2.6.1 Introduction of Diamond Turning

Diamond turning as a machining process for soft metals such as copper and aluminium has been used for more than fifty years [48]. Diamond turning of optical mirror systems has been regularly used for the manufacture of X ray optical mirror systems

[44, 45, 48]. The development of producing precise mirror surfaces by diamond turning was led by these and other defence driven systems.

Commercially the contact lens industry commonly uses diamond turning as a machining process. The soft polymer materials used for contact lenses are easily turned. The form accuracy requirement of such elements are not particularly demanding for the latest contact lens turning machines [49].

Precise structured surfaces for the printing industry are often produced by diamond turning, or diamond fly cutting processes [50]. The materials used by this industry are in general limited to copper, aluminium and electro-less nickel plating. Single point diamond machining of copper has significant importance as a manufacturing process in the micro-electronics industry, particularly in a fly cutting mode.

The material removal mechanisms associated with the diamond turning of soft materials such as, copper and aluminium have been investigated [51, 52]. This plastic deformation removal method permits high quality surfaces to be produced with relatively large volumetric material removal rates. Until the mid 80's little consideration appears to have been given towards the direct diamond turning of optical surfaces in ostensibly brittle materials.

The attainable surface texture quality when diamond turning surfaces made from these soft materials is most significantly dependant on:

i) The level of the machine's overall error motions. Asynchronous error motions mainly dictating surface texture, synchronous motions affecting possible form accuracy [53].

ii) Diamond tool edge quality also has significant contribution to optical surface roughness. The tools wear rate and the regions of the tool which wear vary depending on the material being machined [54].

iii) The quality of these soft materials has a major influence on achievable surface quality. Residual stresses inherent in the material or, induced by the work holding method, greatly influence achievable form accuracy especially with low aspect optics.

The quality of surface roughness which can be achieved using the most modern of diamond turning machines is in the range of 1-2 nm Ra (10-20 nm Rt. peak to

valley)[55], see section 4.6. Form accuracy capability is at the 100 nm peak to valley level for optics up to 150 mm diameter [55], see section 4.7.

The quality of surface roughness which is achievable when diamond turning soft metal materials using conventional radius shape tools is geometrically limited, see Figure 17. The equation typically used [56] to express this geometric limit is given below:

$$R_t \approx \frac{f^2}{8 * T_r} \qquad \text{[Eqn 2.1]}$$

where

R_t is the surface roughness expressed as a peak to valley measurement

f is the feedrate per revolution of the work spindle

T_r is the tool radius

It should be understood that this equation does not take account of any of the machine errors. A more accurate equation is obtained by adding a term which describes the machines asynchronous error motion in the direction normal to the component's surface.

$$R_t \approx \frac{f^2}{8 * T_r} + f\{A_{syn}\} \qquad \text{[Eqn 2.2]}$$

where, A_{syn} is a measure of the asynchronous error motion in the direction normal to the machined surface, see section 3.2.2.

The early research into the diamond turning of brittle glass materials was concerned with a "crushing" process, [57]. This "crushing" process was dependant on brittle fracture occurring for the material removal mechanism. "Crush" turning as it became known, was indeed utilised for a short period in the machining of glass aspheric camera optics by the Rank Taylor Hobson company [58]. However, the resulting surface quality from this process required 20-80μm to be removed by a subsequent polishing technique in order to achieve the necessary optical quality.

In recent years diamond turning of ostensibly brittle materials by the process often called "ductile" mode machining has become a commercially useful machining process for the manufacture of optical elements operating in the infra-red wavelength regions [59]. The materials which have been found useful for IR applications have material properties, such as hardness, Young's modulus and fracture toughness, which permit these materials to be diamond turned, albeit at low tool penetration levels, whereby

the surface produced reflects that obtained when cutting softer metal materials and hence the so-called "ductile" mode machining [60, 61, 62, 63]. Direct "ductile" turning of optical surfaces in materials suitable for visible wavelength applications has been limited to fundamental research and basic investigations on flat surfaces [64, 65, 66]. Such experiments have however shown the possibility of removing glass in a mode which is unlike the traditional brittle fracture mechanism. The topic of "ductile" mode turning of brittle materials is discussed in detail in section 2.6.2

2.6.2 Ductile Mode Turning of Brittle Materials

Recent research into the diamond turning of brittle type electro-optic materials revealed significant non-linear characteristics in the mechanism's of material removal [60, 67]. It has been shown that a transition in the method of material removal exists when cutting brittle materials at low load and penetration levels. This change has been termed the "brittle-to-ductile" transition. The so-called "ductile" mode of material removal is important as high quality functional optical surfaces can be produced using this "removal mechanism", i.e. highly smooth surfaces having low levels of sub-surface micro cracking. The materials which have been most extensively tested for their apparent "ductile" mode machinability include, silicon, SiO_2, BK 7 glass, Zerodur and optical germanium.

A large body of data generated from indentation hardness investigations unequivocally demonstrates the fact that a limited amount of plastic deformation precedes the development of brittle fracture when considering localised-contact deformation under sharp point indentors [68, 69, 70].

The fracture systems associated with indentation deformation have been widely discussed. Figure 18 shows the progression of the plastic and fracture regions during an indentation test carried out using a sharp point indentor as proposed by Lawn [71]. Upon first contacting the surface, the indentor causes stress to occur in elastic / plastic stressed regions. At some critical load and penetration depth a median crack system develops which continues to grow with additional applied load / penetration. As the indentor is raised from the surface the median crack closes, internal stresses caused by mis-matching of the internal walls, developed by the median crack, cause internal cracks to grow. These internal or lateral cracks can propagate towards the surface which cause large levels of surface chipping to occur.

Lawn [70] has shown that formation of median cracks occurs at a critical load P^*, and that this critical load is given by

$$P^* \approx 1.6*10^4\left[\frac{K_c^4}{H^3}\right] \qquad \text{[Eqn 2.3]}$$

where,

K_c is the critical stress intensity factor or fracture toughness

H is the Micro-hardness.

The critical crack length C^*, associated with P^* is given by

$$C^* \approx 120\left[\frac{K_c}{H}\right]^2 \qquad \text{[Eqn 2.4]}$$

Hagan [72] has carried out similar indentation work to that of Lawn. Whilst Lawn observed the critical load to initiate a median crack Hagan dealt with the critical load to nucleate a micro-crack just beneath the elastic/plastic boundary. The critical load to nucleate this micro-crack is given by

$$P^* \approx 885\left[\frac{K_c^4}{H^3}\right] \qquad \text{[Eqn 2.5]}$$

The critical crack length is given by

$$C^* \approx 29.5\left[\frac{K_c}{H}\right]^2 \qquad \text{[Eqn 2.6]}$$

An important point which should be considered when applying both Lawn's and Hagan's equations is the method by which the fracture toughness has been calculated. Fracture toughness can be obtained using Lawn's method [70]. The radial crack length found after an indentation test is used in the following equation to define K_{1C}.

$$K_{1c} = 0.092 \bullet \frac{P}{c^{\frac{3}{2}}} \qquad \text{[Eqn 2.7]}$$

As discussed by Franse [73] there are a number of factors which strongly effect crack length, c. A critical factor found by Smith [74] being the time elapsed for measuring

the crack length after the indention has been carried out. Crack length was observed to grow for up to 24 hours. Franse carried out indentation experiments on a boro-silicate glass, FCA8866 and found the fracture toughness reduced from 1.3 MPa√m to 0.8 MPa√m after 24 hours. Franse states that the lower value is the more correct one. Since it correlates better with the value obtained from the double cantilever beam test.

The critical load P* for a median crack when calculated using Lawn's equation 2.3 for the boro-silicate glass FCA8866, is found to be 0.02 N, and the critical crack length C* is 1.6μm. Using Hagans equations 2.5 and 2.6 P* and C* are 0.001 N and 0.4 μ m respectively for nucleating a micro-crack beneath the elastic / plastic region.
Lawn and Marshall have proposed an "index of brittleness" for material's [70]. This index is developed from indentation test data and is primarily a function of the hardness and fracture toughness of materials. By normalising equations 2.3 and 2.4 and using suitable data, a so-called Universal deformation / fracture diagram, Figure 19, was produced. This diagram can prove useful in determining the relative brittleness of materials.

The basic hypothesis for ductile mode machining rests on the observation that plastic deformation can be achieved in brittle materials within a small controlled volume at the tool to workpiece interface before any fracture occurs. Scattergood [61] and Puttick [64] emphasise that there is a true size-scale effect for fracture initiation. The energy of plastic deformation scales with deformed volume, whereas the energy of fracture scales with crack surface area. Therefore plastic deformation becomes energetically favourable as the scale of deformation decreases, and there is a volume below which material will deform and not fracture. Theoretical models which predict the "critical depth of cut" which will lead to brittle fracture have been proposed, the two most widely discussed are those of Bifano and Puttick.

Bifano's model [75] is based on a fracture mechanics approach. The model is developed from Lawn's indentation work [70, 71] together with Bifano's own experimental data generated from diamond grinding trials carried out on glass samples.

Lawn's equation for the critical penetration for initiating a fracture is [70]

$$d_c = \Psi\left[\frac{E}{H}\right]\left[\frac{K_c}{H}\right]^2 \quad \text{[Eqn 2.8]}$$

where

d_c is the critical penetration depth for fracture initiation,

Ψ is a dimensionless constant depending on indentor geometry

E is the Young's Modulus

From his ductile mode glass grinding results, which are discussed in section 2.6.3, Bifano calculated a value for Ψ by fitting his test results to the calculated critical depth given from Lawns equation. Bifano defined the point of transition to brittle fracture by assessing the surfaces produced during his grinding trials. This was arbitrary defined as a surface having 10% of surface fracture and 90% of apparent ductile movement after grinding. This lead to the following equation for predicting the critical depth,

$$d_c = 0.15\left[\frac{E}{H}\right]\left[\frac{K_c}{H}\right]^2 \quad \text{[Eqn 2.9]}$$

The critical depth of cut, for a number of glasses was calculated by this method. These are shown in Table 6.

Puttick's model for predicting the critical depth of cut is based on an energy approach [64]. Verification of his equation is said to be provided by both compression and indentation experiments.

$$d_c = \left[\frac{\alpha E R_w}{\sigma_y^2}\right] \quad \text{[Eqn 2.10]}$$

where ,

d_c is the critical penetration depth for fracture initiation,

α is a dimensionless constant depending on indentor geometry

E is the Young's modulus

R_w is the specific work per unit area required to propagate a crack

σ_y is the yield stress for plastic flow

Puttick states that for fracture processes operated by residual stress on a typical glass material the following values apply, $\alpha \cong 6.25$, E = 70 GPa, R = 10 J/m^2 and $\sigma_y = 2 \times 10^9$ N/m^2

Puttick suggests that the critical depth, d_c should therefore be in the order of 1×10^{-6}m.

Of the two critical depth of cut models Bifano's is the most easily used. It does however heavily rely on the manner by which the materials fracture toughness is calculated. The measurement of fracture toughness by indentation methods is in an early state of development and requires further research. What is also important for Bifano's model is that the measure of hardness is obtained at the low penetration levels involved in ductile mode turning. The development of Nano-indentation equipment means that accurate hardness levels in these near surface regions is becoming available [76]. Residual surface stresses, caused for example by previous machining, can be of influence on the measured value of hardness [69]. Bifano however claims that his model should give a good indication of the critical depth.

In support of his theoretical work Puttick developed a special purpose diamond turning apparatus which was claimed to have a high loop stiffness, although this was not specified, and a tool in-feed capability of better than 0.1 μm. Using this apparatus Puttick et al [64] clearly demonstrated that grooves could be cut into fused quartz and soda lime glass where no evidence of brittle fracture could be seen. Indeed much is made of the curly ribbon like swarf which was found detached and in cases attached to the surface of the samples. The attached ribbons of swarf are said to have confirmed that at least part of the material removal takes place after the tool has passed over the surface. From these tests the critical depth of cut is claimed to be 0.25 and 1.5μm for the soda lime glass and fused quartz respectively.

Unfortunately the ability to directly diamond turn an optical quality surface in optical glass materials, those used for precise visible wavelength optics, has not been demonstrated. The ductile grooves which Puttick produced were done so in specially prepared polished surfaces. Izumitani [19] has previously shown that such surfaces can be up to 25% less hard than a typical "smoothed" or lapped surface of a particular glass material. This fact alone means that the critical depth Puttick measured was higher than could be achieved when working typical smoothed surfaces. Relatively expensive polished substrates could be used as the basis from

which to finish turn components but the cost effectiveness of doing so becomes highly questionable for surfaces departing greatly from a spherical shape.

Puttick's ductile turning work on glass materials was carried out where the grooves which were produced were separated by some distance and therefore do not reflect true machining of a surface. The machining of a surface does require each groove to overlap. Puttick used sharp tool shapes which gave relative, to other researchers, high values for the critical depth of cut. Such tools however only offer a limited feedrate capability. Other researchers have proposed that ductile diamond turning of amorphous optical glasses could be a viable proposition [58]. Gee et al, suggest a material removal rate based on 1μm per rev feedrate, 0.1 μm depth of cut and a maximum cutting speed of 10 m/sec, providing a volumetric removal rate of 0.05 mm3/sec, based on a 100 mm diameter flat surface. This figure itself compares very poorly with the removal rates for polishing given in section 2.3.3.

Tani [66] carried out ductile turning experiments on glass using a small diamond facing lathe having high quality spindle and linear motions. His conclusion was that whilst ductile turning of optical glasses was possible, the low material removal rates involved would not permit the process to be a viable production operation. His work suggested that the critical depth of cut to brittle fracture was in fact less than 100 nm for BK7 glass.

Research into ductile mode turning of materials used for infrared optical elements has been carried out in quite some depth. This work has revealed important information about ductile mode turning brittle materials. Most of this work has concentrated on optical germanium and silicon. Some early published work in this field was carried out by Gerchman and McLain [59], who took samples of high quality germanium, both single crystal and polycrystalline, and diamond turned them using a Rank Pnuemo MSG-325 aspheric generator. They produced surfaces which appeared to have been machined with a ductile mode and had surface roughness of approximately 5-6 nm Ra. These spherical surfaces of 50 mm diameter were made with constant feed rate, spindle speed and depth of cut. The material removal rate which was found to produce these smooth ductile like surfaces was expressed as feed per revolution of the workpiece and the applied depth of cut. These were stated as being up to 2.5μm/rev and 25μm respectively.

At first sight it would appear that the permissible depth of cut to provide ductile turning in silicon and germanium is between 1 and 2 orders of magnitudes greater

than that discussed by Puttick, Gee and Tani for glass materials. Whilst from a production stand-point this is quite true, it is the tool geometry together with these material's mechanical properties which contribute to the significant difference[61]. The effective depth of cut or effective chip thickness has been described by Blake and Scattergood. Figure 20 schematically illustrates the cutting geometry when conventional radius type tools are used. The chip cross section has a varying effective thickness t_{eff} as shown in Figure 21. It is important to note that, when tool radius (R) is much larger than the tool feed per revolution of the workpiece (f), the maximum uncut chip thickness (t_m) is most greatly influenced by feed per revolution. This is particularly important since feed rate is of prime importance in regard of machining times and material removal rate for rotationally symmetric optics.

Significant amounts of research into the diamond turning of germanium and silicon has been undertaken by Scattergood, [60, 61, 62]. The focus of his work has been to attain a clearer picture of how machining parameters, including tool geometry, effect the ductile to brittle transition when diamond turning these electro-optic materials.

Scattergood developed a novel means of gaining insight of the transition from ductile to brittle fracture, the "interrupted cut method". The "interrupted cut method" provided important details of where the ductile - brittle transition occurred across the uncut shoulder region, see Figure 22. The tests were carried out using a Rank Pnuemo aspheric generator, model ASG 2500. To this machine was fitted a special purpose low amplitude, high response "fast tool servo" tool holder similar to that discussed by Hara et al [77]. This particular fast tool servo was used to retract the tool rapidly from the surface of the workpiece. In doing so, it revealed the uncut shoulder region. This region was observed using an optical microscope to assess the point along the shoulder where transition from ductile to brittle fracture occurred, see Figure 22. Knowing the machining parameters and tool geometry involved in each test, the critical chip thickness (d_c) to the onset of brittle fracture could be calculated.

This approach to "the critical chip thickness" provides a system where the effect of the machining parameters on the material removal behaviour can be clearly investigated.

The first confirmation made by this type of test was that a so-called ductile mode machined surface was not necessarily produced solely by the ductile mode of material removal. In fact ductile mode turned surfaces in silicon and germanium were found to be produced by a combination of brittle fracture and ductile mode removal mechanisms. This is explained most clearly with the aid of figure 20 [60]. The critical

chip thickness (d_c) is defined as that which does not replicate fracture damage beyond the most proud point of the tool. It is suggested that true ductile mode machining only occurs near the apex of the tool.

Using his interrupted cut method Scattergood has developed equation 2.11 which is said to predict the maximum feedrate for a given tool such that the resulting surface is ductile like in morphology.

$$f_{\max} = d_c \sqrt{\frac{R}{2(d_c + y_c)}} \qquad \text{[Eqn 2.11]}$$

Another important finding from this work was that the nominal depth of cut (d), as shown in Figure 21, has little effect on the critical chip thickness (d_c). Also, the work confirmed Gerchmans[59] experience that a higher negative tool rake angle increased the ductility of silicon and germanium. This was confirmed by an increase of the critical chip thickness (d_c). If brittle fracture did however occur, the depth of propagation (y_c) would be higher for higher negative tools. As stated above, the feed of the tool has the most significant influence on the uncut chip geometry and as a consequence most greatly influences whether a surface appears to be have been produced in a ductile mode or not. Cutting speed was not found to be an important parameter.

Scattergood's work suggests that a larger tool radius is beneficial in terms of ductile mode turning silicon and germanium. The effect of using lager radius tools on the machined surface in terms of residual stress level has not been discussed. The effect of tool wear on removal mode is another important area which has little documentation.

Until recently the effect of crystal orientation had not been published. This topic is discussed in section 5.1.

2.6.3 Ductile Mode Grinding of Brittle Materials

Research into the grinding of glass, and other brittle materials, was until 1985 typified by the work carried out by Mairlot [78]. Mairlot's work demonstrated that when grinding glasses the removal mechanisms were dictated by fracture processes. Importantly, Mairlot found that grinding with diamond abrasives was significantly different from grinding with conventional abrasives. This difference was in respect of much lower grinding temperature occurring at the grinding zone when diamond wheels were used. Surfaces produced with this fracture based material removal

mechanism were poor in regard to their surface roughness, typically 0.4 μm Ra. Glass ground in this way was found to be opaque. Mairlot concluded that diamond grinding of glass was achieved purely through a mechanical removal process dominated by brittle fracture mechanisms.

However, Miyashita's work [79] made significant impact in respect of the grinding of glass materials. He built a cup wheel grinding machine which employed hydrostatic oil bearings and claimed it had extremely high overall loop stiffness. Using this stiff and precise machine Miyasita diamond ground flat glass surfaces to an unprecedented roughness quality, 2 nm Rmax. This level of surface roughness being as good as the best polishing methods can attain. These flat samples were assessed at a number of national laboratories for quantification [80]. Miyashita's work identified that it is possible to directly grind glass to the same surface roughness quality as can be achieved through conventional polishing. Also, investigation of the sub-surface regions of Miyashita glass samples revealed very little sub-surface defects [80]. Following on from Miyashita's work many researchers carried out more detailed investigations into the so called "ductile" or "shear" mode grinding of brittle materials [75, 81, 82].

The promise offered by this "ductile mode" grinding process is the ability to produce optical quality surface roughness without significant sub-surface damage and with cost effective removal rates. It is thought that when used in conjunction with high accuracy machine tools it could afford the ability of directly grinding high quality complex shape optics.

Bifano's research [75] into ductile mode grinding of glasses was carried out with the prime goal of investigating the mechanisms of what he termed "micro-grinding", establishing the machining parameters which afforded this "ductile mode" of material removal. For his research Bifano built a special purpose plunge mode grinding apparatus. This apparatus used cup shape grinding wheels mounted onto a high precision air bearing spindle, a single linear motion provided the in-feed motion to plunge the stationary component into the rotating grinding wheel. The loop stiffness of this simple machine was measured to be 50 N/ μm. Closed loop piezoelectric in-feed control permitted the specimen to be precisely advanced into the rotating grinding wheel. The grinding wheel was mounted onto a precise air bearing, in-situ wheel truing ensured wheel run out levels of 125 nm. A number of small specimens in a range of glasses were ground using different feedrates and grinding wheel types.

Bifano's findings showed that surfaces which appeared to have been produced by a ductile mode of machining were produced if the plunge in-feed rate was between 1.5 - 75 nm per revolution of the grinding wheel.. His work also indicated that grinding wheels having a resin bond gave higher levels of ductility than was found with metal bond wheels. The grain size which Bifano found suitable to give a surface which appeared predominantly ductile was 4μm sometimes defined as #4000 mesh size. From this work Bifano derived equation 2.9 discussed in section 2.6.2.

Whilst Bifano's test work showed that resin bond wheels gave higher levels of ductility than a corresponding metal bond wheel, operational difficulties have been associated with fine grain resin bonded wheels, with regard to their long term cutting stability [83]. Dressing is used to ensure grinding wheels have adequate grain exposure. A number of methods have been devised including, abrasive feed methods, loose abrasive methods and electrolytic methods.

An important development in dressing technology which has proved suitable for fine grain grinding wheels is that of electrolytic in-process dressing (ELID) [84]. This technique which was developed by Nakagawa and Ohmori and called ELID was an extension of earlier research carried out by Buttner [85]. Initially the ELID process was aimed towards the application of grinding silicon wafers for the microelectronics industry. Ohmori however, carried out grinding experiments in the area of "Mirror finish grinding of ceramics". High quality surface roughness 8-10 nm Ra was attained when grinding ceramics using fine grain cast-iron bonded diamond grind wheels and ELID.

The ELID technique ensures that an adequate grain exposure is maintained during grinding. I it can only however be applied when using grinding wheels having an electrically conductive bond. The necessary equipment for the ELID method is quite simple and is shown schematically, for a cup type grinding wheel, in Figure 23. An insulated copper electrode is positioned close to the surface of the grinding wheel, a second brush type electrode contacts the rotating grinding wheel. A water based electrolyte is passed through the gap between the grinding wheel and the copper electrode. Electrical potential is applied making the grinding wheel the positive pole and the copper electrode the negative pole. The ELID method has only proved effective when used with cast iron bond wheels [86]. When cast iron bond wheels are used the electrolytic cycle is "self-governing" due to the insulating properties of the ferrous oxide layer produced on the wheels surface. This provides a controllable

method of ensuring that the fine grains protrude the wheel bond. Details of the ELID dressing method is described in Appendix 1.

Ball et al [87] developed their own ELID system and suitable metal bonded grinding wheels. They carried out ELID grinding of optical glass materials using an ultra precision grinding machine having a loop stiffness of 135 N/μm. Their work showed that high quality surfaces of 1-2 nm Ra can be produced when using metal bond grinding wheels. Significantly their work showed that the normal grinding forces involved in ductile mode grinding greatly exceeded those found when brittle fracture grinding even if the material removal rate was lower. Although the normal grinding force was found to be high for ductile grinding, the level of sub-surface damage was limited to a small number of microns, see Appendix 1.

Namba's research into the ductile mode grinding of glass is also of importance [88]. His work has clearly demonstrated that the depth of cut which is applied to the grinding machine's axis is not limited to the calculated "critical depth" as described by Bifano. On his ultra-stiff grinding machine, Namba demonstrated that depths of cut as large as 10μm could successfully be taken in a ductile mode when grinding glass. Unfortunately the actual loop stiffness of his machine has not been published. His research however emphasises that it is the grain chip thickness which is limited to Bifano's "critical depth". This grain chip thickness parameter is dependant on the number of active grinding grains at the contact zone and the material removal rate. The ability to ensure each grain carries out its duty in the overall material removal, i.e. machine stiffness and precision, was stated to be a critical issue. Namba claims that the applied depth of cut on the machine can to a great extent be independent of removal mode when machining brittle materials.

The requirement of a "damage free" method for machining brittle materials other than glasses also exists, i.e. for advanced ceramics. Many advanced ceramic components need a controllable finishing technique whereby the strength properties of a ceramic component are not degraded by surface defects induced during previous machining This requirement has lead to significant research in the field of low damage grinding of advanced ceramics [89, 90].

Research into conventional grinding of advanced ceramics has previously shown that there is a marked difference in the grinding forces when compared to those of grinding metals [91]. Inasaki's work found that the ratio of the two primary grinding force components (F_n / F_t) was significantly different when compared to those found

when grinding steels. Ceramic grinding shows a marked increase in the level of normal force (Fn) when compared to a hardened steel. When grinding brittle materials the process can be regarded as a collection of indentations, where each of the abrasive grains are likened to the indentor used in a hardness test. It is therefore not surprising that Inasaki found the normal force to be relatively high for these hard ceramics. The magnitude of normal force was shown to reflect the hardness of the workpiece material. Each of the protruding abrasive grains acts like a sharp point indentor which generates an intense local stress field that causes irreversible deformation in the form of plastic flow or crack nucleation as discussed in section 2.6.2.

Whilst the majority of the grinding research carried out on advanced ceramics indicates that the dominant material removal mechanism is crack propagation from residual stress fields, ultra-precision grinding experiments have suggested plastic flow to be a significant removal mechanism. Shore's work [89] showed that high quality surface roughness could be attained by ultra-precision grinding whereby the surface appeared unlike that generally associated with brittle fracture. Importantly, an increase in mechanical strength could also be provided. Ker [90, 92] proved that ductile mode grinding could improve the strength of ceramics. He carried out detailed assessments of samples of silicon nitride, some of which had been ductile mode ground, and demonstrated that there was a potential to increase the strength of a ceramic component by this type of grinding. His work showed however that the overall machining "history" had a significant influence on resulting strength. The amount of ductile mode grinding necessary to improve strength was dependant on the severity of the prior machining and the depth of damage. Ker's work proved that a low damage mode of grinding was possible for brittle materials.

Ker also proposed that if the "real grain" normal grinding force was kept below P* as defined by Hagan then true damage free grinding of a brittle material could be achieved. This "real grain" force is that which each grain in the grinding wheel applies to the workpiece during grinding. The calculation of this is highly dependant on the grinding mode, which defines the grinding zone, and the number of active abrasives as a function of grinding wheel area.

Golini [93] has carried out important work with regard to ductile mode grinding brittle materials. Whilst Golini used a loose abrasive micro-grinding technique his findings are valuable for consideration of fixed abrasive ductile mode grinding. Loose abrasive "Micro-grinding" in Golini's context is the use of abrasive diamonds of 1-3μm size. This size of abrasive is not generally used in traditional loose abrasive

machining of glass optics. The reason for not using such small diamond abrasives is the lower material removal rate which is generally associated with the process. Most often opticians will lap / grind with abrasives down to a 9μm size, after which point polishing is carried out over a longer period using cerium oxide abrasives. The polishing operation removes any sub-surface damage induced during the earlier fabrication. Golini carried out grinding experiments using 1μm and 2-3μm abrasives together with a variety of slurry chemistries on Schott's Zerodur™ and Corning's ULE ™ glass ceramics. The object was to see if damage depths could be reduced with micro-grinding. Both the materials chosen are important materials because of their low thermal coefficient's of linear expansion.

His findings suggested that brittle fracture was dominant in both materials when used with 2-3μm size abrasives and brass tooling. This fracture dominance was the case for all slurry fluid's investigated including de-ionised water, which is known to increase micro fracture propagation. However, for abrasives of 1μm size, ductile mode grinding was found even when using de-ionised water as the slurry fluid. Golini investigated the residual surface stress and sub-surface condition of his samples. The method of assessment used is discussed in section 2.6.4. It was found that the micro-grinding process could remove the sub-surface micro cracks introduced during grinding / lapping. However, high levels of residual stress were introduced into the surface when the finer diamond abrasives were used with brass tooling. The majority of the stress was found to lie in the upper surface regions, typically to a depths of tens of nanometers. It is pointed out by Golini that polishing using cerium oxide leads to no measurable surface stress and that the residual stress levels found were a point of concern with the micro-grinding process. Distortion of ground samples was found for both the Zerodur and ULE glass ceramic materials.

2.6.4 Characterisation of Surface and Sub-surface Conditions

The measurement of surface roughness has been discussed in great detail [94]. For optical surfaces which have been produced using either the diamond turning or fixed abrasive grinding processes the methods and terminology used to describe engineering surfaces are more appropriate than those generally used in the traditional optics industry.

In recent years a number of surface roughness instruments of a non-contacting interferometer type have been developed [95]. Microscope based phase shift interferometers have been shown to be capable of measuring nanometric type

surfaces. These instruments typically have a vertical resolution below 1 nm and lateral resolutions of below 1 μm.

High quality contacting stylus instruments have also been developed which offer sub-nanometer resolution [96]. These stylus instruments benefit over the non-contacting systems through their traceability back to national standards held for instance at, NPL and NIST.

Scanning tip microscopes offer an increased resolution for investigation of surfaces, these instruments typically provide vertical resolution of below 0.1 nm and practical lateral resolution as small as 10 nm [97].

Surface morphology can be assessed using scanning and transmission electron microscopes. Higher magnification is offered from transmission electron microscopes, whilst better depth of field is provided from a scanning electron microscope.

Whilst the measurement of a surface's roughness is common practice for optical surfaces, measurement of residual stress is less widely carried out in the optics industry. The methods of measuring surface stress are not well established. High levels of surface stress can be problematic in both the manufacture and application of optical elements.

Golini's work [93] showed that the process of loose abrasive micro-grinding can induce significant levels of surface stress and lead to significant component distortion. The method Golini used to measure this surface stress was based on the Twyman effect. As early as 1905, F. Twyman found that if a thin piece of glass, lapped on both surfaces, has one of the surfaces polished the glass piece bows, see Figure 24 [98]. If the second surface is then polished the piece becomes flat again. The degree of the initial bow is a function of longitudinal surface stress. The stress level can be calculated from the following equation.

$$\sigma = dH \cdot \frac{T^2}{D^2}\left[\frac{E}{3(1-\nu)}\right] \qquad \text{[Eqn 2.12]}$$

where, σ is the longitudinal Twyman stress (N/m), D is the diameter of the glass sample (m), T is the thickness of the sample (m), dH is the peak to valley height change, E is the Young's Modulus and ν is Poisson's ratio.

Golini found that the stress his micro-grinding induced was concentrated over a very shallow depth. This was established by subsequently polishing the samples. After the micro-ground surface was lightly polished for 5 minutes, removing only 22 nm the stress had been removed and the sample became flat.

Other methods for measuring surface stress and stress profiles have been developed these have been reviewed by Bowen [99]. The use of indentation tests has been proposed whereby higher levels of surface residual stress would increase or decrease the measured hardness of a component. A model which calculates the effect of this surface stress has been put forward by Lawn [69]. Recently precise Nano-indentor machines [100] have emerged which make it possible to carry out indentation tests repeatably with very low levels of surface penetration.

A number of non-damaging methods for assessing surface stresses has been proposed and in certain cases proved useful, particularly for crystalline materials such as silicon and germanium. These techniques include; Raman spectroscopy, X-ray diffraction, Rutherford back scattering and Brillouin scattering and are discussed for their appropriate usage in some depth by Bowen [99].

Micro-Raman spectroscopy has been extensively researched by Paesler et al [101]. This method has recently been developed for measuring surface stress profiles in crystal materials and to some extent in opaque materials. Micro-Raman microscopes have recently been developed into commercial products [102].

Sparks et al [101,103] have used a micro-Raman microscope to investigate surface stress profiles of diamond turned germanium assessing the influence of machining parameters. His findings indicate that the machining parameters, feedrate and depth of cut have less effect on the depth and profile of surface stress as compared to the tool shape parameters, rake angle and clearance. The maximum compressive stress was found to be in the region of 0.05μm depth.

A number of destructive methods for investigating sub-surface conditions has previously been used. Puttick et al [104,105] has very effectively used transmission electron microscopy to investigate the sub-surface damage in ductile diamond turned and ground silicon specimens. Cross sectional views of the machined silicon surface were taken using TEM. Clear images of the sub-surface damage were produced, see Figures 25 and 26. This work clearly illustrates that the assessment of surface conditions can not be relied upon to indicate the material removal mechanisms

encountered when machining. The specimens investigated by Puttick were subjected to very fine levels of machining producing exceptionally smooth surfaces. SEM observations of these specimens revealed surfaces which appeared to be free from micro cracking. Surface finish of the specimens was measured using a Nanosurf instrument and found to be 11 nm Ra (60 nm Rmax) and 0.5 nm Ra (3 nm Rmax) for the ground and turned samples respectively. Yet when these specimens were assessed by XTEM they were found to have varying level's and types of damage. The ground specimens were shown to have actual micro-cracks hidden beneath the surface, these were typically 300 nm but in cases up to 500 nm. The turned samples were found to have a more consistent form of dislocation deformation up to 200 nm in depth. Evidence of micro cracking in the conventional sense was not detected on these turned specimens. Material removal rates were 0.06 mm^3 / minute and below 0.0015 mm^3 / minute for the grinding and turning trials respectively.

Assessment of sub-surface micro cracking in glass materials has often been investigated by a technique employing mild etching and light polishing [87,93]. The etching process removes a very thin layer from the surface of the substrate, typically below 50 nm. For amorphous materials the etching is even, smooth and repeatable. The newly revealed surface provided after etching can then be observed. After observation, light polishing can be used to remove more material from the surface. Repetition of the etch, observation and polishing can generate a good understanding of micro-crack densities and distributions, see Appendix 1.

An important non-destructive method for detecting micro-cracks in materials is acoustic microscopy, [106,107]. This technique has been shown to be able to detect micro-cracks which are invisible when viewed on the surface using optical microscopy. Scanning acoustic microscopes (SAM) have been developed which provide high quality images of crack shape. The operational resolution of SAM systems is dependant on a number of factors, including the operating frequency, the objective design and coupling media together with the mode of operation. The potential operating resolution of SAM systems has been stated as being 500 nm in the vertical direction and 10μm in the horizontal, or planar, directions.

Assessment of Rayleigh wave velocity has been proposed as a potential method to assess sub-surface defects in surfaces [106]. If ultrasonic acoustic waves are focused onto a surface using a sapphire objective and water as a coupling fluid, some of the acoustic energy will propagate as Rayleigh waves, in a direction parallel to the surface. The interesting feature of Rayleigh wave propagation is that it is tightly

bound to the surface to a depth of one Rayleigh wavelength. The Rayleigh wavelength is given by

$$\lambda_r = \frac{v_r}{f} \qquad \text{[Eqn 2.13]}$$

where, λ_r is the Rayleigh wavelength, v_r is the theoretical Rayleigh velocity determined by the samples material properties and f is the sampling frequency of the instrument. The theoretical Rayleigh surface wave velocity for some important optical glass materials is given in Table 7.

Therefore if sampling is carried out at 225 MHz in a material having a theoretical Rayleigh surface wavelength velocity of 3000 m/second the wavelength penetration depth will be 13μm, see Figure 27. Any features such as micro cracks within this distance from the surface will interact with the Rayleigh wave and generally cause a reduction in the measured surface wave velocity. Since near surface defects affect the surface wave velocity more than those at a depth approaching the 13μm wavelength the sensitivity of the measurement of surface wave velocity would prove useful for defects in the 0.2-3 μm range [106].

2.7 Summary Review

It is recognised that advanced optical systems could be made to higher quality specifications given reliable and cost effective methods for producing complex shape optical elements.

Advances in the manufacture of high precision machine tools potentially offers the ability to produce complex shape optics and do so cost effectively. An advanced aspheric generator machine, the NION machine, has been produced by Cranfield Precision Engineering Ltd under a jointly funded industrial and UK government programme. This programme was under the Link scheme and entitled, the Nanotechnology Initiative. The NION machine tool has been evaluated in this thesis in respect of its important performance features, such as motion control accuracy, loop stiffness, thermal stability, etc.

For optical systems operating at IR wavelengths the use of aspheric and "hybrid" shape optics has begun. In general manufacture has been provided by the diamond turning process. The cost effectiveness for producing these IR elements is greatly dependant on their processing time. The material removal rates available from the

diamond turning process, whereby high quality optical surfaces are produced, is therefore of both commercial and technical interest. Diamond turning of IR materials has been evaluated by machining trials discussed in this thesis. Whilst previous research in this area has shown some important phenomena and its influence on material removal mechanism's, the trials carried out here investigate the production effectiveness of diamond turning a number of IR materials. An assessment of diamond turning an amorphous glass was also carried out to reinforce previous researchers findings, this topic is discussed.

In recent years diamond grinding research into "ductile" mode machining of glass materials has been extremely active. Much work has been published on the ability of directly grinding "polished quality" optically smooth surfaces. The majority of this grinding work has been confined to small flat specimens produced by machine tools which have little, if any, contouring ability for producing more complex shapes. The mode of grinding used has also been that which ensures a high contact area between tool to workpiece, thus perhaps indicating higher levels of material removal in a "ductile" mode than could be found when contour grinding. The grinding trials discussed in this thesis have investigated the quality which can be attained by a contour grinding mode and the attainable material removal rate which can be found whilst producing optical type surfaces. New developments in grinding technology, e.g. ELID, have been incorporated into the grinding trials, evaluation of the important parameters and their influence is assessed and discussed.

Assessment of the surfaces produced by both the diamond turning and grinding experiments were closely evaluated in terms of their surface roughness, residual stress level and sub-surface damage. These sample assessments allowed the processes of diamond turning and grinding to be reviewed in regard of their suitability and cost effectiveness for producing optical elements. Where appropriate illustrations of the likely machining rates are given.

CHAPTER 3

Experimental Procedures and Equipment

3.1 Introduction

This chapter discusses the methods employed for both; assessment of the experimental machine tool, and the techniques and equipment used for investigating the machined samples surface and sub-surface conditions. Details of the objective for each experiment, choice of workpiece materials and process variables are also given.

The experimental machine tool which was used for the work described in this thesis was developed by Cranfield Precision Engineering Ltd under a LINK Nanotechnology project. At the onset of the research discussed here the "NION" machine tool had been assembled into a motion system but had not been assessed for its quality of motion or used in anyway to provide accurate profiling or machine optical surfaces.

The three main sections of this chapter are therefore concerned with ;

3.2 Assessment of the NION machine tool
3.3 Experimental methods, objectives and choice of important variables
3.4 Methods of assessing the surface and sub-surface regions of the machined samples

3.2 Assessment of the NION machine tool

The results of the assessments described in this section are discussed in Chapter 4.

3.2.1 Description of the NION machine tool

The "NION" Ultra Precision Machining Research Facility is a 4 axes, CNC aspheric generator, see Figure 28. The basis of the NION machine is a Cranfield Precision Engineering "Nanocentre", this is shown schematically in Figure 29.

The machine has a T base construction made from a synthetic granite material for high stiffness and damping. Two linear axes are mounted on the machine base, the carriages of which are carried on hydrostatic oil guide ways made from a high grade aluminium oxide ceramic material. The "X" cross-feed axis carries the "C" axis, a hydrostatic oil workhead spindle with a wide range velocity control, 0-1500 rpm. The "Z" in-feed axis has an integral "B" rotary axis which is also hydrostatic. Onto this rotary B axis a tool post can be mounted for diamond turning purposes. Removal of the B axis permits an air bearing grinding spindle to be fitted into the Z axis carriage to enable the machine to be used with the grinding process.

NION Metrology Frame

The X and Z linear axes are driven via friction (or traction) drive systems [16] and use laser interferometers as the position measurement transducers with resolution of 1.25 nm. This laser interferometer system is referenced to planar mirrors mounted into a metrology frame which is in turn fixed to the moving X carriage. The metrology frame concept provides good compliance with the Abbe principle in the X and Z directions. It also provides a metrology reference datum for the tool set station. High quality optical straight edges were chosen as the references for the X and Z linear motions, coupled using laser interferometers. The metrology frame is made of stabilised cast-iron and low thermal expansion super Invar. Zerodur "stick type" optical straight edges having very low coefficient of thermal expansion are fitted into the metrology frame.

The interferometer blocks are mounted off the Z axis carriage. A single laser path is used for the X axis position since this axis complies fully with Abbe Principles, i.e. no "offset" errors are present. The Z axis position is measured using two laser paths in order to measure and compensate for Abbe errors arising from yaw of the X and Z carriages. The adopted design is shown in Figure 30. A differential refractometer is built into the system to compensate for ambient changes which influence the refractive index of the laser "air" paths.

Temperature Control

The position control of the tool-to-workpiece in real time over a significant time scale would be greatly impaired if the heat generating systems are not stringently controlled. Thermal control was therefore provided by five individual temperature control systems, see Figure 31. These systems were specified to remove the heat from all major heat generating sources on the machine together with controlling the temperature of the machine structure and make it less susceptible to ambient changes. The five temperature control systems employed are for;

i) Workhead hydrostatic bearing oil
ii) Workhead motor coolant
iii) Oil shower system over the machine structure
iv) Linear and rotary hydrostatic bearing oil (X, Z, B axes)
v) Process coolant

All five temperature control systems were specified to operate to 0.01^{o}C accuracy of temperature control under normal operating conditions.

The intention of the oil shower system was to cover the machine structure in oil of a uniform temperature. Since the oil shower's ability to control the temperature of the machine structure would be degraded by significant levels of localised heat generated by specific machine sub-systems, these sub-systems are also individually temperature controlled.

In each of the control loops, the exit temperature for the fluid was set to be the controlled point. That is to say, the temperature probes would measure the fluid temperature directly as it exits the particular machine sub-system. This exit point would be controlled to better than 0.01^{o}C. The temperature sensors used for all five systems are specially developed high stability paired thermistor units. Each sensor comprising, a matched pair of thermistors which were carefully calibrated.

Fluids therefore enter the sub-systems at a lower temperature. The PID control systems adjust the entry temperature to an operating resolution of 0.001^{o} C and calculate the required entry temperature to suit the heat generated by the sub-system at that time.

To attain a control accuracy of 0.01^{o}C it was necessary to develop "dual loop" PID control systems for each of the 5 temperature systems. The first system was designed to control temperature to 0.1^{o}C, the second control loop would then heat the fluid to the required entry temperature, which would ensure the fluid would have an exit temperature of 20^{o}C +/- 0.01^{o}C.

Grinding Facility

Grinding systems had previously been built into aspheric generators of similar configuration to the NION machine [13]. However, these systems only provided the ability to grind brittle materials, such as glass, with a "brittle fracture" mode. With this mode of grinding, surface form or figure accuracy can be produced to a high quality with the attainable form accuracy dependant on the machine's motion accuracy. However, surface finish was particularly poor, > 200 nm Ra and sub-surface micro-cracking levels high.

The NION machine's grinding facility was aimed at providing a system and process which would achieve the optimum form accuracy, dictated by the machine's exceptional motion accuracy, as well as producing optical quality surface finish levels, approximately 1 nm Ra. Surface finish would be obtained by the ductile mode

grinding process (see Section 6). The associated levels of sub-surface micro-cracking could then be assessed against material removal rate when using this process.

To provide the highest stiffness for the grinding facility it was decided to remove the B axis from the Z axis carriage when grinding, and replace it with a high stiffness grinding spindle. A grinding speed of up to 60 metres/second was provided by use of an air bearing spindle design which has a maximum speed of 13,000 rpm. Vertical orientation of the spindle reduced the influence of any thermal axial growth on component form accuracy. The grinding spindle was designed to be fixed in position with no vertical adjustment, this was again to maximise stiffness. To ensure that the grinding wheel's operating diameter was centred for height, with respect to the centreline of the workhead spindle, a truing/forming station was provided. This truing station comprised, a vertically oriented linear Y axis carrying a precise air bearing spindle. To this spindle a truing wheel was mounted.

An electrolytic in-process dressing system and the necessary grinding wheels were developed and incorporated into the grinding facility. The dressing system was devised along similar lines to the research systems previously developed at Riken [85]. The grinding wheels and the necessary electrolytic power supply was develop through the glass grinding experiments discussed in Appendix 1.

3.2.2 Methods of Assessing Motion Accuracy

The machine's overall motion accuracy and stability was assessed. The important measurements which influence machining capability are discussed in this section. For many of the motion accuracy measurements a paired set of Pioneer PDG 500 capacitive sensors were used. These probes have a claimed accuracy of 25 nm and a operating resolution of 5 nm, where possible the probes were used in a differential mode to reduce the influence of external variations. The bandwidth capability of the Pioneer probes is 1 KHz.

Synchronous Axial Error Motion

The (systematic) synchronous axial error motion of the NION machine produces a predictable form profile error on the machined surfaces. The shape of this error has previously been analysed [53] and is shown in Figure 32. This type of error is a major limitation of diamond turning machines because it causes an astigmatic form error. Astigmatism is a significant error and adversely influences rotationally symmetric optics.

The synchronous axial error motion of the NION machine was measured using one of the Pioneer capacitive gauges, which was mounted off the rotary B axis and set against an optical flat mounted to the workhead spindle. The spindle system had previously been dynamically balanced using a Schenck Vibro-port dynamic analyser.

Movement of the Z axis to the machine base was also monitored during the test using a second capacitance sensor. This measurement would identify whether the spindle was the sole origin of any error or whether there was an input from a synchronous movement of the Z axis carriage.

Asynchronous Axial Error Motion

Asynchronous axial error is the uncertainty of tool position in the axial direction (Z direction) for each rotation of the workhead spindle. This form of "random" error manifests itself as surface roughness on machined surfaces. For diamond turning it is often the prime error which dictates the achievable surface finish quality.

The asynchronous axial error motion of the machine was measured using the "wax pencil" test [37]. A capacitance measuring probe was positioned against the face plate of the workhead spindle, at a radius of 50 mm, and mounted from the B axis rotary table. A radial line was drawn onto the face plate using a wax crayon type pencil. This line caused the output from the capacitance gauge to change as it passed underneath the gauge with each rotation of the work spindle. A second capacitance probe was set up as a "dummy" gauge and used in a differential mode to reduce any external effects.

The variance in the magnitude of the interrupt signal from the active probe is a measure of asynchronous axial error motion, from the workhead spindle to the B axis, i.e. the full machine loop.

Synchronous Radial / Tilt Error Motions

Synchronous radial error motion of NION machine gives rise to both a concentricity error and potentially a roundness form error when machining cylindrical features. Its influence on optical surfaces is dependant on the shape of the error motion itself. For example, a pure sinusoidal synchronous error would give only a non concentric geometric error which is less important to most optical elements. Other shapes of synchronous radial error do however influence the performance of an optical element.

Two capacitive gauges were used in a differential mode, in both, a horizontally opposed mode and an active/dummy mode. As with the previous synchronous test

these were mounted off the rotary B axis and mounted against a master cylinder mounted onto the work spindle. The horizontally opposed mode reduced most of the errors in the "master" and took out the pure sinusoidal error given from synchronous movement of the X axis to the workhead spindle.

Tilt error motion was calculated by carrying out two radial error motion tests at different distances from the work spindle face plate.

Asynchronous Radial Error Motion

The asynchronous radial error motion of the machine was also measured using the "wax pencil" test. The set up for this test was similar to that used for the axial direction.

A capacitance measuring probe was positioned against a master cylinder mounted to the face plate of the workhead spindle and mounted from the B axis rotary table. An axial line was drawn along the cylinder. This line caused the output from the capacitance gauge to change as it passed underneath the gauge with each rotation of the spindle. As previously described a second capacitance probe was set up as a "dummy" gauge and used in a differential mode to reduce any external effects.

The variance in the magnitude of the interrupt signal from the active probe is a measure of asynchronous radial error motion, from the workhead spindle to the B axis, i.e. the full machine loop. Asynchronous or "random" radial error manifests itself on components in the same manner as the axial asynchronous error, i.e. surface finish.

Precision of Straight-line motion of the linear X and Z axes

The metrology frame system was devised to improve the precision of the straight-line motion of the linear axes (X and Z). The system provided both the X and Z linear motions with a precise reference from which the laser interferometers operate. Within the metrology frame are mounted two very precise straight edge mirrors. The flatness of these two mirrors is shown in Figure 33. The overall "area" flatness quality is 60 nm and 108 nm peak to valley for the Z and X axis mirrors respectively. Cross sectional "line" straightness, which affects the lasers, is actually better than these values.

After the metrology frame system had been built into the NION machine it was set up and calibrated against a NAMAS accredited high quality straight edge. An example of the set up for assessing the Z axis straightness is shown in Figure 34. Capacitance gauges were used for measurement. Reversal methods were applied by rotating the

straight edge on a Moore Precision table, since this reversal method greatly reduces the errors inherent within the NAMAS straight edge. This NAMAS straight edge had been fully calibrated and its precision level was 30 nm peak to peak (as a line measurement).

After the error in the Z direction for the X axis, and in the X direction for the Z axis, had been measured, software error compensation was entered into the NION machine's CNC. The initial uncompensated errors arose from the inherent errors of the metrology frame mirrors, the offset of machine measurement / calibration and small thermal effects.

3.2.3 Machine "loop" Stiffness

The overall loop stiffness of the NION machine was measured in the more sensitive axial direction. This stiffness was measured using the set up shown schematically in Figure 35.

A strain gauge force transducer was fitted between the workhead spindle face plate and the tool holder, and in-line with a differential micrometer screw. Calibration of the force transducer had previously been carried out using precise masses. A capacitance probe was mounted on the tool post and up against the workhead spindle face plate. The capacitance gauge was calibrated against movements of the NION machine's Z axis, under laser interferometer closed loop servo control.

The differential micrometer screw was extended to apply a force between the tool post / work spindle and through the force transducer. Measurements of the applied force and displacement were taken.

3.2.4 Dynamic Characteristics of the NION Machine

The dynamic characteristics of the NION machine were evaluated. The important methods for assessing the dynamic performance of the machine included; data logging the laser signals of the metrology frame (linear X and Z axes), the use of velocity and acceleration sensors and assessment of the position error signals for the servo control. The metrology frame laser signals were assessed as both "history" in the time domain and "response" in the frequency domain.

3.2.5 Axial Thermal Growth

An important aspect for the NION machine's overall accuracy capability is its axial thermal drift. This drift causes a one for one profile error to occur on machined

components. A capacitance probe set up, as used for the synchronous axial error measurements, was used to measure the level of axial thermal drift.

An in-situ thermal axial growth measuring system was provided on the NION machine. This system was mounted directly onto the metrology frame and uses two inductive probes situated either side of a diamond turned disc which was mounted to the rear of the face plate of the workhead spindle, see Figure 36. The intention of this system was to feedback the output from the inductive probes into the machine's CNC control system to provide automatic compensation for any axial thermal growth of the workspindle.

3.2.6 Assessment of Temperature Control of the NION Machine Sub-systems

Data were taken directly from all five of the NION machine's temperature control systems. The dual type temperature probes which provided these data were previously calibrated against other thermistor type temperature sensors. The NION machine itself is housed in a temperature controlled laboratory having control to +/- 0.1 - 0.2^{o} C during any 24 hour period. The data obtained from the machine's own temperature control systems would be as stable and as accurate as that obtainable from any other proprietary device. Operating resolution of the temperature probes was 0.001° C, see section 4.3 for details.

3.2.7 Assessing Precision of Machine Motions by Component Accuracy

In order to demonstrate and confirm the motion accuracy of the NION machine a number of simple shape surfaces was machined.

To confirm the asynchronous motion quality a pure single crystal copper sample was diamond turned. This turning was carried out with machining parameters which permitted the resulting surface to be measured such that the level of asynchronous error motion could be clearly assessed.

Flat surfaces of 100 mm diameter were diamond turned into a high quality aluminium bar. Evaluation of the flatness of these surfaces would provided confirmation of the axial synchronous error motion.

The contouring quality of the NION machine was investigated by diamond turning concave spherical surfaces into the 100 mm diameter aluminium samples. The form accuracy quality of these surfaces would not only be influenced by the machines motions but also through the tool setting accuracy. Tool setting on the NION

machine is achieved using a specially developed optical tool setting station [108]. Appendix 2 discusses the optical tool setting system and the form accuracy which was achieved using the NION machine.

3.3 Experimental Details and Choice of Important Variables

Machining trials were defined such that both "ductile mode" turning and grinding, using the NION machine, could be assessed from a manufacturing effectiveness standpoint. Where little published data was available machining trials were carried out using two level, three factor experimental designs. This approach [109] both reduced the necessary number of test runs which were required to establish the fundamental interactions and quickly indicated the level of machining parameters for which brittle fracture was imposed into the various brittle test materials. Where previous work had been carried out, specific tests were used to assess the influence of individual parameters.

Test samples were carefully prepared such that each sample for a given test was consistent and therefore not of influence to the measured response. Preparation of test samples was closely monitored to ensure consistency. Preparation methods were however those which are realistic for serious production of high grade optics.

Flat test samples were used to ease subsequent assessments. Selecting flat surfaces would however in no way influence the results obtained and disc type samples were used for all experiments. Thin disc type samples were chosen for tests where residual stress was to be evaluated using the Twyman distortion method [98]. These thin disc samples were made to a 10-1 diameter to thickness ratio. This ratio was calculated to be appropriate for assessment of Twyman distortion and was representative of that expected for a precise optic. Where the attainable flatness quality from the process itself was to be assessed then test samples of, 2-1 diameter to thickness ratio were employed.

Selection of the exact size of the samples was determined by, the capacity of the metrology instruments to be subsequently used, the available time for the experiments since larger samples take longer to machine, and the capacity of the high quality machinery available for the preparation of the test samples.

Diamond turning trials were carried out on three material types, comprising optical germanium, silicon and zinc sulphide. Optical germanium was chosen since previous work has proved it suitable for diamond turning. Silicon was investigated since it

offers benefits over optical germanium for infra-red applications due to its lower cost and density. Zinc sulphide was assessed since optics of this material are often found in systems and used in conjunction with other optical germanium or silicon elements. A single diamond turning test was carried out on a polished BK7 glass sample. Details of the test samples used in the diamond turning trials are given in Table 8, other material properties are given in Tables 3 and 4.

Diamond grinding trials were carried out on three optical glasses and one glass-ceramic. The glasses included, BK7 which is a commonly used borosilicate glass and SF10 which is a relatively soft glass. Limited grinding trials were also carried out on a lanthanum based glass. The glass ceramic which was assessed was the low thermal expansion Zerodur™ material. The type and size of these grinding test samples are given in Table 9.

BK7 was selected since it is a commonly used glass for optical elements having a relatively high hardness. SF10 was chosen since it has a low hardness relative to BK7. Additional glass grinding trials were carried out on LaSFN30, this glass was investigated since it had a higher hardness than BK7 but with lower chemical durability.

Zerodur™ was investigated as previous research into loose abrasive micro-grinding this material was published which gave details of the induced surface stress. This work provided useful comparison data.

3.3.1 Diamond Turning Investigation (1)

Diamond Turning of Optical Germanium

Influence of Machining Parameters on Surface Morphology / Residual Stress Levels

Diamond turning has been shown to be useful for the production of IR optics which have aspheric and "hybrid" diffractive surfaces. The relative cost of these diamond turned surfaces is however considerably higher than that of polished spherics. Machining investigations were therefore carried out to assess the limitation of the material removal rate associated with the diamond turning process. In doing so, any advantage offered from the high loop stiffness of the NION machine could be evaluated.

Since previous research [59, 60] into diamond turning optical germanium had indicated that brittle fracture would occur at some critical point, investigation of this

transition was undertaken. The prime goal of these tests was the rate of material removal which could be attained from ductile mode turning germanium. Also of interest for these tests was the residual stress brought about by machining rate. Optical Germanium was selected for these test as it presently forms a significant proportion of IR optics.

In order to gain an understanding of any interactions between the machining variables and the influence on resulting surface morphology, a number of machining tests was carried out. These tests were selected from three factor, two level experimental designs. This approach was chosen because, the published work available, at the time of the trials, did not disclose levels for the machining or tooling parameters which would help identify the potential material removal rates for ductile mode turning. It was also hoped that the NION machine's higher performance may provide a higher material removal capability.

Diamond turning trials were carried out on disc type samples of optical germanium of 32 mm diameter and 3 mm thick. Thirty-two optical grade, N type, mono crystalline samples were acquired from the American company Eagle-Picher. Fourteen samples had <111> crystal orientation, a further fourteen had <100> orientation and four of <110> orientation. These "as sawn" test pieces were subsequently lapped on both sides using 13 μm grain size Silicon Carbide. One side was then polished to a high grade surface roughness and flat to better than 200 nm P-V. This polishing was done using 1 μm grain size Cerium Oxide. This lapping and polishing preparation work was carried out by the Pilkington Optronics company (UK) who ensured that consistency was maintained from sample to sample. Sample thickness was recorded after this preparation work for use in subsequent stress calculations.

The flatness of the polished face of each sample was measured using the Zygo/Wyko phase shift interferometer and saved for subsequent analysis. This measurement was carried out in such a way that the samples could be accurately repositioned under the interferometer and re-measured after being machined.

Samples having <111> and <100> orientation were treated as separate materials and most test runs were carried out on both orientations. This repetition of tests runs was done to identify the orientation which is best suited to the diamond turning process. Thirteen test runs were carried out on both <111> and <100> samples. Where coolant was used clear white spirit fluid was applied to the tool edge in the form of a spray mist. All diamond tools were supplied by Drukker Diamond Tooling (Holland).

Test runs were formed into three matrices of two level, three factor experimental designs. The three factors and the two levels selected for Matrix No.1 are shown schematically in Figure 37.

The diamond tools used in Matrix No. 1 had negative top rake angle of 25°, with a 10° front clearance. Work spindle speed was constant at 1200 rpm and depth of cut was set at 5μm. The three factors and the two levels selected for Matrix No. 2. are shown schematically below in Figure 38. The diamond tools used in Matrix No. 2 had negative top rake angle of 5° and 25°, with a 10° front clearance. The three factors and the two levels selected for Matrix No. 3. are shown schematically in Figure 39.

In all test runs samples were held on a special purpose vacuum chuck and mounted on their polished face. The chuck had previously been diamond turned on the NION machine to ensure its mounting face was flat. This mounting face was checked interferometrically before use to ensure it did not distort the test pieces during machining. A flatness of 90 nm peak to valley was obtained for the chuck mounting face.

The polished face of the machined samples was re-measured using the phase shift interferometer after being cut. This measurement was saved, then using a difference function in the Wyko software a value for Twyman distortion was obtained. This value being a function of the residual surface stresses induced or released during machining.

A full record of each test run was entered into a database which permitted other factors such as, tool cut distance and total material removed to be assessed against the surface roughness / morphology and the Twyman distortion/ residual stress levels.

Machined samples were assessed for their surface roughness using Wyko 3D instrument and visually assessed for the percentage surface fracture using an optical microscope.

3.3.2 Diamond Turning Investigation (2)

Diamond Turning of Optical Germanium and Silicon

Influence of Tool Cut Distance on Surface Morphology and Residual Stress

The results and findings of Investigation 1 indicated that the tool condition may be of a high significance and influence on the material removal mode, the resulting surface morphology and residual stress level. The results of investigation 1 suggested that for the purposes of cost effective manufacture the tool parameters and work done by the tool were a main consideration. Newly published work by Scattergood [111] however suggested that a formulae for defining maximum feed rate could be developed from the results of his plunge type experiments. If tool cut distance was important, as suggested from Investigation 1, this formulae for permissible feed rate would only be useful if the tool edge condition was known.

To investigate the importance of tool condition, diamond turning tests were carried out on both mono-crystalline Silicon and Optical Germanium. Samples of 32 mm diameter by 3 mm thickness were prepared in the same way as for investigation 1. Tooling and machining parameters were chosen which would provide, at least initially with a sharp tool, surfaces which appeared totally ductile in nature.

To evaluate any degradation of tool cutting performance, machining forces were measured using a Kistler force dynamometer. This dynamometer was designed into the toolpost of the NION machine, see Figure 40, and was calibrated using Correx force gauges.

Tool Life for Ductile Turning (1) : Silicon

Tool life, in respect of that which provides a fully ductile surface having no visible micro-fractures, was assessed by repeatedly cutting a single Silicon sample. The sample was cut with fixed machining parameters. After a number of cuts had been taken on the sample, the sample was removed from the machine and assessed for both surface morphology and Twyman distortion. Tool Forces were monitored during the machining cuts. The parameters chosen for this test are given below:

Tool Radius : 0.5 mm
Top Rake : -25°
Depth of Cut : 3 μm
Feed rate : 2 μm / rev
Work speed : 1000 rpm
Coolant : Spray mist white spirit

Tool Life for Ductile Turning (2) : Silicon

Tool life was assessed for with a smaller radius tool (0.15 mm) than used in Test (1). Machining and measurement procedure as described for test 1 was carried out. Other machining parameters were held constant.

Tool Life for Ductile Turning (3) : Optical Germanium

Tool life test (2) was repeated, using the same but newly reconditioned tool, on a single piece of optical germanium. Again the machining and measurement methods discussed for tool life test 1 was carried out.

3.3.3 Diamond Turning Investigation (3)

Diamond Turning of BK7, Silicon and Zinc Sulphide

Assessment of the "Ductile" Machinability

Diamond turning tests were carried out on amorphous BK7 glass, mono-crystalline silicon and poly-crystalline Zinc Sulphide. The objective of these tests was to establish the relative susceptibility of each material to propagate brittle fracture when diamond turned with relatively low tool penetration levels and material removal rates. This provided an indication of the level for difficulty and hence the cost effectiveness of ductile mode turning the various materials.

A flat nose diamond tool manufactured by Contour Fine Tooling having a 15° negative top rake and 10° front clearance, was used for turning the three material types stated.

The flat nose of the diamond tool was orientated at 2° to the cut plane of the surface of the sample, this is shown in Figure 41. This orientation was set using the optical tool set station of the NION machine. A standard test was carried out on each material; the parameters of this test are given overleaf :

Depth of Cut : 0.5 μm
Feed rate : 0.5 μm / rev
Work speed : 1200 rpm
Coolant : Spray mist white spirit

Each of the three machined samples were assessed for the presence of surface micro-fracture using optical and scanning electron microscopy.

3.3.4 Diamond Grinding Investigation (1)

Diamond Grinding of BK7, SF10 and LaSFN30 Glasses

Influence of Machining Parameters on Surface Morphology and Sub-Surface Damage

Direct grinding of glass materials has been an active area of research in recent years. The potential of direct grinding of complex aspheric and diffractive optics using CNC machine tools is said potentially to offer significant economic advantages over present day practice.

The purpose of the diamond grinding investigations discussed in this thesis was to assess the most advanced diamond grinding technologies when used on the newly developed NION machine. Assessing the available material removal rate in a ductile mode and the attainable quality which can be obtained when machining three important optical glasses. Investigation of the produced surfaces concentrated on surface roughness level and the extent of surface and sub-surface micro-fracture.

Previous research [75, 88] into the ductile mode grinding of glass has shown that surfaces which appear free from brittle fracture can be obtained by fixed abrasive grinding. This work has however been limited to either a simple plunge mode or surface mode of grinding generally using cup type wheels. Little work has been published on the ability to ductile grind surfaces where the mode of grinding is conducive to the production of complex aspheric optics.

The machining variables and their set levels were selected based on the previous work carried out in this area, this is discussed below:

Grinding wheels have a number of important parameters. Three which are considered to be of prime importance are; abrasive grain size, the bond type and the concentration.

It was considered that three levels of abrasive grain size should be investigated. The smallest grain size selected was 1-2 μm, this being the size which Golini's free abrasive work [93] gave a pure ductile mode removal when using water as the abrasive slurry. The largest grain size was 6-12μm, this being the size which Namba[88] had found possible to go up to when ductile mode surface grinding glass materials. The intermediate size of 3-6μm grain size being that used successfully by Ball et al [87] in their surface grinding trials.

The bond type which had most often been employed in the research of ductile mode grinding of glass is the resin type bond. A resin bond type was chosen from Shore's work [89] into low damage grinding of ceramics. The development of the ELID dressing method by Ohmori [84] led to Ball et al, [87] developing a new bond type specifically for ductile mode grinding of glass. This cast iron type bond was also used.

The concentration of a grinding wheel refers to the amount of abrasive grains in a given volume of bond. Concentration level of 100 equates to 4.4 carats of diamond in a given cubic centimetre of bond, this defines the number of abrasives contained in the grinding wheel. Glass grinding using resin wheels has most often been carried out using a 40 concentration. The development of the in-process ELID dressing method gave greater grain exposure for a given grinding wheel specification, therefore higher wheel concentration level might be possible. It was decided that wheels having 40 and 75 concentration should be assessed.

The grinding wheels acquired for all diamond grinding trials were provided by Diamant Boart (Belgium). The important parameters and levels chosen of the wheels are listed in Table 10.

The prime aim for this investigation was to assess the material removal rate afforded by the ductile mode grinding and the associated damage types and levels. Therefore, the key machining parameters were those which defined removal rate, these being; depth of cut (d) and feed rate (V_r). The mode of grinding used on the NION machine is somewhat more complex than on traditional grinding machines and it is shown schematically in Figure 42.

The workpiece rotational speed (V_w) was also seen as a critical parameter as it directly influences the grain chip thickness. Two modes of grinding operation were assessed. The first was referred to as constant surface speed (CSS). In this mode the rotational speed of the workspindle is a function of the radius which the grinding wheel is positioned with respect to the workspindle centre-line. This mode of grinding ensures that the feed rate of the workpiece across the face of the grinding wheel is constant. A maximum rotational speed is defined for the near centre regions. The second mode of grinding was that of constant rotational speed (CRPM) and in this mode the workpiece rotational speed is fixed throughout the machining pass.
Cylindrical glass samples of 50 mm diameter and 25 mm thick were specially prepared. The samples were carefully lapped and then fine polished on both sides to obtain a high quality surface roughness of better than 0.5 nm Ra. The two surfaces

were made flat and parallel to each other. After this polishing, one side of the samples was free abrasive lapped using carefully graded 13μm Silicon Carbide, each sample was lapped with the same pressure and for the same period of time. This preparation work ensured that each sample had a surface which was predominately produced by brittle fracture, but the extent of the brittle fracture was limited in depth. The depth of the damage was established by re-polishing one of the samples and found to be 15-20 microns in depth. The carefully produced lapped surfaces were ground using combinations of the machining parameters listed in Table 11 with a number of the grinding wheels listed in Table 10.

The procedure for the grinding trials was less well formalised than for the previous turning trials since very little was known about either the mode of grinding or the likely onset of brittle fracture for each glass type. These tests are discussed in detail in section 6.1.

3.3.5 Diamond Grinding Investigation (2)

Diamond Grinding of Zerodur™

Influence of "Ductile Mode" Grinding on Surface Morphology and Residual Stress Levels

Fixed abrasive grinding trials were carried out on specially prepared Zerodur™ samples. The two main objectives for this investigation were:

1. to establish that grinding parameters found to be suitable for glass materials were appropriate to this glass-ceramic material, and

2. to establish that fixed abrasive "ductile mode" grinding induces limited levels of residual surface stress which does not preclude the process from being used for producing high quality optic elements.

Zerodur™ was chosen for this investigation since comparable data have previously been generated by Golini [93] using free abrasive diamond grinding methods. Stress free samples were prepared by REOSC Optique (France). Samples were disc type of 32 mm diameter and 3 mm thick, these were lapped and fine pitch polished on both sides. Flatness quality of better than 150 nm peak to valley was achieved.

A number of samples was ground using fixed machining parameters which were selected as those which consistently provided high quality surface roughness on the BK7 glass material. These parameters are listed in Table 12.

Six samples were repeatedly ground using the above parameters removing between 29-31 μm from the surface. The surface roughness and Tywman distortion was measured on each sample.

A single Zerodur sample was ground using the above parameters where Tywman distortion was measured after removing certain amounts of material. This test provided details of the residual stress induced as a function of the amount of material cut from the original surface.

To ensure the Zerodur samples were actually supplied in a stress free state 6 samples were etched on one surface and the other surface was then measured for any Tywman distortion.

A number of these Zerodur samples were assessed for sub-surface damage using the polish and etch method discussed in section 3.3.4. Additionally, Nano-indentation measurements were taken on selected samples.

3.4 Methods of Surface and Sub-surface Characterisation

3.4.1 Surface Figure (or form) Accuracy

The figure accuracy of machined samples was measured using a helium neon laser based interferometer. A piezo-electric driven phase shift attachment was fitted to the laser to provide computational data analysis to be carried out. The measuring system was built up from components and software purchased from the Zygo and Wyko Corporations. The system is shown in Figure 43.

The vertical resolution of this system is claimed to be 0.3 nm. Lateral resolution is defined by the laser's aperture which is selectable at either 33 mm or 102 mm, providing a lateral resolution of 130 μm and 400 μm respectively. The measurement accuracy of the system is defined mainly by the master optic used. The master optics used were calibrated by Zygo to better than 30 nm p-p.

3.4.2 Surface Roughness Accuracy

Surface roughness of machined samples was measured using the following instruments:

Rank Taylor Hobson Form Talysurf Instrument

This instrument is of a contacting stylus type, the vertical resolution is 10 nm and is obtained using a laser interferometer measuring device. Lateral resolution is claimed to be 1μm but is dependant on the type of stylus used, a 5μm radius stylus was used throughout this work.

Wyko, Topo 3D phase shift (Linek) interferometer

This instrument is similar to the phase shift interferometer used for the figure accuracy measurements, however it is designed into a microscope system and as a result has a smaller aperture size. This non contacting white light interferometer is fitted with a 40 times magnification objective which provides a 250μm^2 assessment area. Vertical resolution is claimed to be 0.6 Angstrom, lateral resolution is 1μm. This instrument is commonly used as the method for assessing the best quality polished optics at < 0.5 nm Ra. The instrument is shown in Figure 43.

Digital instruments, Nanoscope III atomic force microscope

This type of instrument represents the most advanced method for investigating precise surfaces. This particular atomic force microscope has a vertical resolution $<$ 0.3 Angstrom. The lateral resolution is defined by the probe quality and is generally $<$ 0.2μm for small scan areas of 25μm^2. Measurements were carried out on ground glass surfaces by Pilkington's Group Research Surface Analysis Department.

3.4.3 Characterisation of Surface Morphology

Leitz Normarski Optical microscope

This Normarski type optical microscope, fitted with a number of magnification objectives, was used for general assessment of machined samples.

Jeol Transmission Electron Microscope

A transmission electron microscope was used to investigate the surface of ground glass samples using thin film replicas.

Philips Scanning Electron Microscope

A scanning electron microscope was used in the assessment of germanium and zinc sulphide samples. This instrument was also used to investigate wear regions of diamond tools. Grinding wheel surfaces were assessed using this instrument in a back scattered mode.

3.4.4 Assessment of Residual Surface Stress

Twyman distortion

The residual stress level of machined samples of germanium, Zerodur and BK7 were evaluated using the Twyman effect [98]. Twyman effect was measured using the Zygo/Wyko phase shift interferometer system. A selectable "difference" function, part of the Wyko software, permitted accurate measurement of the change of surface flatness, before and after tests to be measured. The longitudinal Twyman stress was calculated using equation 2.12.

Nano-indentation

A Digital instrument's Nano-Indentor II was used to assess if residual stress induced during the grinding of the Zerodur samples increase the measured hardness at low penetration levels. Previous indentation work [69] has shown that significant residual surface stresses can change the measured hardness of a material. The nano-indentation tests were undertaken to establish if ductile mode ground surfaces had significantly different hardness / surface stress than a polished surface. The tests were carried out with very low force and penetration depths. This work was carried out at the National Physical Laboratory.

Micro-Raman spectroscopy

Confirmation of a change in surface residual stress level of a diamond turned germanium sample was provided using a Micro-Raman microscope. This test was carried out by Renishaw Metrology Ltd. Micro-Raman spectroscopy is now often used to investigate the surface stress and stress profile of surfaces of materials of crystalline structure [103]. This test provided confirmation that the Twyman distortion method for assessing surface stress was valid.

3.4.5 Assessment of Sub-Surface Quality

Scanning Acoustic Microscopy (Rayleigh Wave Velocity)

A scanning acoustic microscope was used to measure the surface "Rayleigh" wave velocity of a number of ground glass and Zerodur samples. The SAM system was used with a sapphire lens and was coupled to the machined surface by a pure water droplet. Ultrasonic waves are emitted from the sapphire lens. Some of the acoustic energy which propagates as Rayleigh waves in a direction parallel to the machined surface was measured for velocity. As discussed in section 2.6.4 the interesting feature of Rayleigh wave propagation is that it is tightly bound to the surface to a depth of one Rayleigh wavelength. Any features which reside in the machined surface or the sub-surface region equating to the layer depth, defined by the Rayleigh wavelength, will interact with the measurement of surface wave velocity. Therefore,

the surface wave velocity of a machined surface will be influenced by the depth and density of defects which are found in the Rayleigh wavelength depth. The higher the concentration of surface /sub-surface defects, the greater the reduction in surface wave velocity.

The surface wave velocity of carefully polished surfaces of BK7, SF10 and Zerodur were measured to provide a datum from which other ground surfaces could be assessed.. Qualitative data of the level of sub-surface damage of the machined samples was gained through these measurements.

Measurements were undertaken by Mr Neil Stoodley and Dr Andrew Briggs of the Department of Materials, Oxford University. The SAM instrument was used at a frequency of 225 MHz and with a cylindrical shape objective lens. The defocus length was 500μm providing an assessment area of approximately 0.7 mm by 0.25 mm.

Measurements were taken in two scan modes on the disc shape samples:

i) Radially from the centre to the edge of the sample in steps of 0.17 mm, with the line focus perpendicular to the radial direction. This provided the radial variation from the samples edge to its centre.

ii) At a single point, but common on all samples, a scan was made by rotation of the line of focus, + / - 40^{o} in 5^{o} steps. This mode of measurement provided detail of the directionality or anisotropy of any sub-surface defects.

Polish and Etching methods

In order to permit a visual investigation of the regions below the immediate surface topography, ground glass samples were etched for 5 minutes using a 3% wt. solution of ammonium bifluoride ($NH_4.F.HF$). It was found that this time duration and solution strength removed in the region of 250 nm from the surface of glass samples.

To gain a full understanding of the depth and density of sub-surface defects selected samples were repeatedly etched, observed by an optical microscope, then finely polished using 0.3μm cerium oxide, re-etched, and again observed, etc. This highly time consuming method gave accurate detail of the density and distribution of the induced micro-cracking levels.

To provide information expediently on the sub-surface condition of machined samples the single etching operation was carried out on most glass samples. Half of the machined surface was protected from the etching process by insulating tape in order to allow other investigations to be carried out at a later date, e.g. surface wave velocity measurements.

Etching of a number of Zerodur samples was carried out to permit assessment of the residual stresses induced during the preparation polishing before machining took place. The stress level was measured using the Twyman method.

CHAPTER 4

"NION" Machine Performance

This chapter discusses the measured performance of the NION machine in respect of its precision capability and overall loop stiffness. The methods used for these assessments are as discussed in section 3.2.

4.1 Straight-line Motion Accuracy of Linear X and Z axes

The straight-line motion accuracy of the X and Z axes were assessed against a NAMAS accredited straight edge. The errors of motion were assessed at the workspindle centreline height ensuring that the error compensation was applied for the errors found at the tool height relative to the component centre-line. A Pioneer capacitance gauge was used for these measurements. Straight-line motion accuracy before and after CNC error compensation are given in Figures 44 and 45 for the X and Z axes respectively.

The quality of straightness obtained after one error correction procedure was:
X Axis, error in Z direction:- 55 nm peak to peak over full stroke (360 mm) of the axis.
Z Axis, error in X direction:- 110 nm peak to peak over full stroke (250 mm) of the axis.

4.2 Synchronous and Asynchronous Motion Accuracy

The NION machine's synchronous and asynchronous error motions, synchronous being relative to the workpiece spindle rotation, were assessed using capacitance gauges.

4.2.1 Synchronous Axial Error Motion

The axial synchronous error motion, i.e. in the direction of the Z axis, will generally be of most influence toward the form error of an optic cut using the NION machine. This error motion was therefore studied in some depth. The relative movement between an optical flat ($\lambda/20$ or 30 nm) mounted off the workspindle and a capacitance gauge fitted to the toolholder, mounted on the B axis, was measured at different spindle speeds. Also the relative motion of the Z axis carriage to the machine base was monitored at the different workspindle speeds. The results obtained are given in Table 13.

It was found that the Z axis carriage was moving synchronously with the workspindle and with respect to the machine base. This error was most noticeable at a workhead speed of 750 rpm. As can be seen in Table 13 the measured values for synchronous axial error varied significantly with workhead spindle speed, as did the relative movement of the Z axis carriage to the machine base. This test was carried out with the Z axis servo on, the test was subsequently repeated with the Z axis physically clamped into position, the measured axial error motion was then found to be consistent over the speed range, and found to be 60 nm p-p.

The speed dependency for this error was identified as a problem of machine dynamic stability through out of balance forces initiated by the workhead spindle. The workhead spindle had been dynamically balanced, using a Vibroport dynamic analyser to 0.04μm p-p. The dynamic instability is discussed in more detail in Section 4.5.

The lowest measured level of synchronous axial error however gives a good indication of the highest quality in terms of form accuracy which will be attainable from the NION machine. Synchronous axial error was smallest at a workhead speed of 600 rpm, 60 nm peak to peak.

4.2.2 Asynchronous Axial Error Motion

The asynchronous axial error of the NION machine was measured at different speed levels using the "wax" pencil test [37] , see Table 14. It was found that this error was not significantly influenced by the speed of the workhead spindle.

4.2.3 Synchronous Radial / Tilt Error Motions

The lowest measured value for synchronous radial error was obtained at 600 rpm and was 60 nm peak to peak which can be said to be the largest level of "pure" radial error motion of the NION workhead spindle. This measurement was carried out approximately 50 mm from the face of the workspindle. Tilt error motion was calculated by carrying out another radial error motion test at a different distance from the workspindle face plate. Tilt error was calculated to be 15 nm per 100 mm.

4.2.4 Asynchronous Radial Error Motion

Figure 46 shows the output from the probe at a workhead spindle speed of 600 rpm. This value of the machine asynchronous radial error was not influenced by changes in workhead spindle speed. Asynchronous radial error was 10 to 20 nm.

4.2.5 Overall Axial Thermal Growth

The thermal axial growth of the NION machine was measured with a capacitance probe mounted to the toolpost and set up to the centre of the faceplate of the NION workspindle. The change in position of the probe with respect to the faceplate is defined as the axial thermal growth. The output from the probe was logged over a 60 minute period. The workspindle was started from rest up to 750 rpm. The maximum thermal axial growth was measured to be 370 nm (+/- 50 nm) at 750 rpm when a 3.6 centistokes viscosity oil was used as the bearing fluid, see Figure 47. It can be seen that after 8-12 minutes a stability of 50-75 nm is obtained. Not surprisingly the settling period is very similar to that of the workhead spindle temperature control system which is shown in Figure 48.

In an attempt to remove the influence of thermal axial drift, a measuring system was provided which was mounted directly to the metrology frame. The measuring system uses two inductive probes situated either side of an in-situ diamond turned disc which was mounted to the rear of the face plate of the workhead spindle, see Figure 36.

It was found that the output from this measuring system was dependant on workspindle speed. This speed dependency was investigated and found to be a result of;

i) movement of the axis of rotation of the spindle with spindle speed, known as "hydrodynamic yaw", and to a lesser extent

ii) slight deformation of the reference disc with increased rotational speed

The output from the thermal growth measuring system at a maximum spindle speed of 1500 rpm is given in Figure 49. It can be seen that a large initial movement is measured after spindle start-up . This is caused by a combination of hydrodynamic yaw of the spindle and deformation of the reference disc.

If the initial movement is disregarded then the "pure" thermal axial drift is obtained, 350 nm at 1500 rpm. This is a lower value than that given in Figure 47 because a lower viscosity oil of 2.2 centistokes was used for the workhead spindle bearing fluid during this measurement. A stable output signal to 50 nm was obtained after an 8-12 minute stabilising period. The output from the system could be used for compensation of thermal growth but only when a constant work speed was used. This compensation was not adopted during the results discussed in the thesis.

4.3 Assessment of Temperature Control of the NION Machine Sub-systems

The following data were taken directly from the NION machine's temperature control systems. These systems use matched paired platinum thermistor sensors which had been carefully calibrated and found to be stable to +/- 0.003°C when compared against sensors of the same construction. The NION machine itself is housed in a temperature controlled laboratory. Laboratory temperature control is +/- 0.1- 0.2° C during any 24 hour period.

4.3.1 Workhead Spindle Bearing Oil System

Of the NION machine's five temperature control systems, the workhead spindle bearing system application is the most demanding. The high surface speed of this axis incurs a high heat input level developed as a consequence of fluid shearing the pressurised bearing oil. A limited level of flow rate for this system is a consequence of small gaps in the bearing; these were chosen to provide a high operational stiffness for the spindle.

Originally a very low viscosity oil (2.2 Centistokes) was chosen for this spindle and for the linear X, Z bearings. Unfortunately this oil was found to have been doped with white spirits which "out-gassed". This oil proved unsatisfactory from a health and safety stand-point.

Another oil was identified (3.6 Centistokes) which was a neat mineral oil. This had acceptable health and safety characteristics, but gave a reduced flow rate as a result of higher viscosity. The performance of the workhead spindle's temperature control system for this oil was found to have insufficient cooling capacity to control the oil bearing fluid at its maximum operating speed of 1500 rpm.

A third mineral oil was found which had a very low viscosity (< 2 Centistokes). The performance of the temperature control system was significantly improved even for the maximum operating speed. However, this third oil with its very low viscosity generated “noise” in the linear bearings and reduced the machine's stability.

A 60 / 40 mixture of the second and third oil was finally selected to give the optimum of temperature control and machine stability / performance. With this mixture temperature control of 0.01°C is met within 6 minutes of spindle start up for 750 rpm, 0.015°C is maintained at 1500 rpm after 12 minutes of operation, see Figure 48.

4.3.2 Workhead Spindle Motor Coolant System

The total heat generated by the workspindle drive motor was lower, <25%, than that generated in the Workhead spindle bearing system. A higher flow rate was possible in this system, therefore a high quality of temperature control was achieved. The temperature control from spindle start up is shown in Figure 50, +/- 0.01°C, is met within 5 minutes of spindle start up at 750 rpm and within 8 minutes at the maximum speed of 1500 rpm.

4.3.3 Linear Bearing Oil System

Again, compared to the workspindle bearing system, the flow rate of this particular system is high. Since the heat generated is low and importantly, very consistent it is ideal for temperature control. Temperature control capability is illustrated in Figure 51. This histogram of temperature variation helps illustrate the high quality of temperature stability achieved, i.e. 0.006°C at 1σ. The data are taken with both X and Z axes moving at a slewing speed of 5 mm/second.

4.3.4 Grinding Coolant System

The performance of this system is shown in Figure 52. The best position for measuring the temperature of the coolant was assessed. Temperature control capability was measured at the coolant nozzle and within the return tube from the machine to the coolant tank. Little degradation of the control quality is experienced when fine grinding on the machine. Temperature control of +/- 0.015°C is maintained for 90% of operating time when finish grinding operations are being carried out.

4.3.5 Oil Shower System and Positional Stability

The NION machine exhibits thermal stability of better than 0.01°C over significantly long machining periods when used in a diamond turning mode. The temperature controlled oil is applied through specially designed "baffles" which ensure oil flows uniformly over the machine structure, see Figures 53 and 54.

The performance of the oil shower when the NION machine is in a diamond turning mode is given in Figure 55. The temperature probe was sited in the oil flow leaving the machine near the exit point to the oil shower tray. This level of thermal stability provides positional stability as shown in Figure 56. These positional data were taken using a capacitance probe mounted off the toolpost measuring against the workspindle face plate, the workspindle being stationary.

4.4 Static Loop Stiffness

The axial loop stiffness of the NION machine was measured as described in section 2.5.6. The graph shown in Figure 57 shows the readings taken for force and deflection. The slope of this graph is the static loop stiffness, taken with the machine's linear axes enabled. The measured stiffness level was 60 N/ μm. This value of static loop stiffness in the axial direction is 25% better than other diamond turning machines for which data are available, e.g. the Lawrence Livermore PERL machine and other commercially made diamond turning machines installed at Lawrence Livermore National Laboratory [47].

4.5 Dynamic Characteristics of the NION Machine

As mentioned in Section 4.2.1 the level of the synchronous error motions, synchronous to the workhead spindle, were dependent on the workhead spindle rotational speed. This dependence was an important aspect of the machine's precision and was therefore investigated in some depth.

Since the workspindle is mounted to the X axis a synchronous input force to this motion is directly applied by any out of balance force generated within the spindle. Even though the spindle was dynamically balanced prior to testing and machining, it was considered possible that even with the low levels of "residual" out of balance a structural element within the measuring loops for the X and Z axes could be excited and resonant.

4.5.1 Assessment of Laser Signal Stability

The synchronous laser "noise" of the X and Z axis was assessed together with the spindle balance against spindle speed, Figure 58. This graph shows that there is 3 noticeable spindle speeds which cause balance level to degrade. It was found impossible to balance the spindle to a high quality at these three speeds. These were 300, 500 and 750 rpm.

The Z and X axis laser signals were both effected significantly at 750 rpm. Only the X axis was influenced at 500 rpm. It is important to note that the vibration isolation feet used at the time of testing were those having conventional restrictors in the control valves. An increase in speed over 1200 rpm had a noticeable effect on the synchronous laser noise of the X axis.

4.5.2 Dynamic Performance of Workspindle

It was found that the workhead spindle motor led to out of balance seen at both 300 and 500 rpm. This problem was found to be inherent in the NION Workhead Spindle motor design. These two speed levels were therefore avoided during all machining trials. The spindle motor has 18 electrical poles and these give rise to movements of the spindle shaft with respect to its housing. This is clearly shown through measurements of radial error motion, see Figure 59.

4.5.3 Dynamic Performance of Metrology Frame

The dynamic performance of the metrology frame was investigated to gain confidence that its dynamic stability was not influenced in the 0-20 Hz frequency range. Figure 60 was obtained by fitting accelerometers to the metrology frame and exciting the frame with an impact hammer. This response graph shows the metrology frame to have a first resonance frequency at approximately 100 Hz. It was concluded that the metrology frame was not influencing the 750 rpm apparent "resonance".

Assessment of the X and Z synchronous laser "noise" was subsequently carried out at different positions for X and Z carriages. Figure 61 shows the "noise" on the Z axis for 4 different positions. This graph shows that Z axis performance is not significantly degraded with position of the Z and X axis. Figure 62 shows the same details for the X axis. Again significant difference in "noise" is not seen, except at 1200 rpm and above. Above this speed level the negative positions of the X axis have higher levels of "noise". This corresponds to the position having the longest laser path length for the X axis. Figures 61 and 62 both show high "noise" at 750 rpm particularly for the Z axis.

4.5.4 Fitting of Laminar Flow Restrictors to Isolation Feet

Figure 63 shows the influence on the 750 rpm "resonance" resulting from in change of the type of control valves used in the vibration isolation feet. The initial Farrat systems were fitted with orifice type restrictors. The new Fabreeka feet that were subsequently fitted to the NION machine used laminar flow restrictors as advocated by DeBra [110]. A clear improvement of machine performance was gained by this modification, especially when operating with a workhead spindle speed of 750 rpm.

4.5.5 Positional Bandwidth of the Z Axis

Assessment of the positional bandwidth of the Z axis servo system indicated that it was the source of the resonance at 12.5 Hertz (750 rpm). The original restrictor type

isolation feet exasperated the amplitude of the vibration. The laminar flow restrictor type feet suppressed this problem to a more reasonable level.

4.6 Precision of the Machine Motions by Component Accuracy Assessments

The NION machine had been measured to have a 10-15 nm axial asynchronous error motion. Figure 64 is a surface finish measurement, using the Wyko Topo instrument, of a diamond turned single crystal copper surface which has been machined on NION at 600 rpm. The change in height of the base of each tool groove is approximately 15 nm, which correlates well with the measurements obtained from the wax pencil test discussed in section 2.5.4 and confirms the 15 nm asynchronous axial error.

In order to assess the quality of the NION machine to produce precise shape surfaces, aluminium samples of 100 mm diameter were diamond turned. Initially flat surfaces were made, these flat surfaces were turned at a workhead spindle speed of 600 rpm, the final cut having a cutting time of 20 minutes. These surfaces were measured using the Zygo / Wyko phase shift interferometer, discussed in section 3.4.1.

The highest quality of flatness achieved over the 100 mm surface was 90 nm peak to valley, see Figure 65. The form error observed is that which had previously been investigated [53] and was attributed to synchronous axial error motion. Axial synchronous error had been measured at 60 nm with a 600 rpm workhead spindle speed. The remaining 30 nm of form error would be incurred through any thermal drift and error of straight-line motion of the linear axes.

An interesting observation in measuring these flat surfaces was the quality of the fringes. When comparing these surfaces produced on the NION machine with surfaces diamond turned on other machines it is clear that the movements of the NION machine lead to lower levels of "waviness". This waviness is sometimes described as mid-term slope errors and can be found in some optic specifications.

The contouring quality of the NION machine was investigated by diamond turning concave spherical surfaces into the 100 mm diameter aluminium samples. The form accuracy quality of these surfaces would not only be influenced by the machine motions but also through the tool setting accuracy. Tool setting on the NION machine is achieved using a specially developed optical tool setting station [108]. Appendix 2 discusses in detail the optical tool setting system and the form accuracy which can be achieved using the NION machine. Figure 66 shows the surface form error of a concave aluminium mirror which was diamond turned on the NION

machine. The form error shown in Figure 66 again clearly shows that synchronous axial error is the major contribution to surface error. Of the 113 nm peak to valley error 60 nm must be attributed to the error within the workhead spindle, the remaining 53 nm of error will be incurred by a combination of; errors of precision of the linear motions, thermal drift and tool setting errors.

4.7 Conclusion of NION machine

The NION machine permits the machining of surface textures of 8-12 nm p-v, approximating to just under 1 nm Ra.. Other diamond turning machines having configurations similar to the NION machine have been credited with having a 3-5 nm Ra surface finish capability.

Form accuracy to better than $\lambda/6$ (100 nm p-v) can be obtained through the inherent precision and thermal stability of the machine and its sub-systems. The capability of other machines has been described as being no better than $\lambda/4$.

NION has a temperature control stability which greatly exceeds previous machine tools discussed in the literature. Thermal stability as good as 50 nm can be obtained over significant machining periods.

The errors of straightness of the NION machine's X and Z axes are at a 10-20 nm level for machining of optics up to 150 mm diameter with 25 mm sag.

The static loop stiffness for the NION machine is at a higher level than for any other machine of its size. Figure 67 shows the loop compliance of the NION machine in comparison with other machines discussed in the literature[47].

Smoothness of the NION machine's motions permits diamond turned components to have highly smooth interferometer fringe patterns, previously only achieved by polishing methods.

The main limitation of the machine's performance at this stage of its development is the axial error motion of the hydrostatic workhead spindle. This could be improved by re-grinding the main shaft and housing components to a higher precision level and by modification of the workhead motor drive. The influence of the out of balance force originating from the workhead spindle has previously been found to be the major influence on the attainable accuracy of diamond turning machines [30]. A

smoother workhead spindle motor would improve the potential accuracy of the NION machine.

More detailed investigation of the dynamic performance of the NION machine is required to gain a fuller understanding of its dynamic operating performance. The limited positional bandwidth of the Z axis is seen as an adverse characteristic of the machine.

CHAPTER 5

Diamond Turning Investigations

This chapter presents the results from the diamond turning trials introduced in sections 3.3.1, 3.3.2 and 3.3.3. The importance of all the findings are discussed in section 5.4.

5.1 Diamond Turning Investigation (1)

Diamond Turning of Optical Germanium

Influence of Machining Parameters on Surface Morphology and Residual Stress

The diamond turning experiments were carried out as described in section 3.3.1. Two level, three factor matrices were used as the format of the trials. The objective of the tests was to establish the maximum material removal rate for optical germanium whereby diamond turning provides surfaces which are useful for application as IR lenses, i.e. those having a ductile appearance.

The principal parameters which directly influence material removal rate are, depth of cut, and feedrate. Scattergood's [60,111] investigation of material removal mode indicated that feedrate per revolution of the component and tool radius would be the critical parameters. These two parameters were therefore investigated in the first matrix of these tests.

Experimental design matrix 1, shown in Figure 37, was carried out on germanium samples having <111> and <100> crystal orientations. The three parameters having two levels for matrix 1 were tool radius, feedrate per revolution of workspindle and use of coolant.

From traditional diamond turning of soft metals and equation 2.1, it would be expected that the lower feedrate and larger tool radius would give the best surface finish. Scattergood's work into transition from brittle to ductile removal also indicated larger tool radius and small feedrate to provide more ductile type surfaces and therefore provide a lower percentage of fractured surface regions.

After the samples were machined they were carefully investigated. Surface roughness was measured at a half radius position in the regions which appeared ductile, i.e. free of fracture. The Wyko Topo interferometer was used for the roughness measurement. Percentage of the surface area that was produced by fracture was estimated using the Lietz optical microscope. Twyman distortion was measured using the Zygo/Wyko interferometer to gain a measure of longitudinal surface stress. This method of stress measurement is discussed in section 3.3.4. The minor variations of the thickness of the samples gives rise to an error of less than +/-2% when calculating the longitudinal surface stress from the measured distortion. Sample thickness was nominally 2.95 mm

It was immediately apparent that crystal orientation had an influence on the material removal mode. The difference in material properties caused by the crystal orientation, anisotropy, showed through in the pattern produced by the brittle and ductile regions. Figure 68 is an optical micrograph of sample 4 of the <111> orientation samples. It can be seen that approximately 75% of the surface morphology is produced by brittle fracture. The percentage of surface fracture was estimated from visual inspection using an optical microscope. The "pie chart" shape of fractured regions eased estimation of this percentage value. The detail of the fracture regions are more clearly shown in Figures 69 and 70, which are SEM images. The pattern for each crystal orientation is shown in Figure 71. The reasoning for this pattern effect has recently been investigated by Scattergood [111]. The flatness of surfaces which show both ductile and brittle fracture regions is also noticeably influenced by the material removal modes, see Figure 72.

The assessment of residual surface stress using the Twyman effect clearly gave the spherical type distortion predicted. Figure 73 is a computerised image of the flatness of the mounting surface of sample 3 <111> before its front surface was diamond turned. Figure 74 is a measurement of the same surface after the front surface had been diamond turned. Clearly, the surface had been deformed through a change of the residual stress of the front surface. Figure 75 is the difference in the flatness of this surface before and after machining. This particular mounting surface became more concave indicating that the diamond turned surface had an increased compressive surface stress. The diamond turned surface becomes convex in an attempt to reduce the induced compressive stress. The magnitude of the Twyman distortion was found to be at a level that could easily be resolved by the phase shift interferometer.

The results of surface roughness, % surface fracture obtained from Matrix 1 for <111> and <100> samples are given in Tables 15 and 16 respectively. After some investigation of the results it became clear that another parameter influenced the measured responses. This was found to be the tool cut distance. The figure given for cut distance is the total tool cutting length at the end of each test run.

From these tests it can be seen that when the surface morphology is predominantly ductile in appearance, the peak to valley surface roughness is in-line with that predicted using equation 2.2.

This is clearly shown in the case of sample 6 <111> which measures 15.6 nm P-V. The predicted peak to valley roughness from equation 2.1 is 1 nm, however as set out by equation 2.2, the NION machine's asynchronous error motion of 12 nm must be added to the calculated 1 nm, giving an expected figure of 13 nm which compares favourably with the measured 15.6 nm. Similarly, for samples 1 and 5 <100> the expected and measured values correlate well. It is important to note that the tool cut distance in each of these cases, where low levels of brittle fracture are found, is itself low. In general the surface roughness values obtained in Matrix 1 were as expected.

The influence of tool cut distance on % surface fracture was not expected to be as significant as was suggested by samples 5 and 6 <100>. In this case a new tool was used at the higher feedrate on one sample and then used at the lower feedrate on the next sample. The % surface fracture dramatically increased on the second sample. This identified that the tool cutting effectiveness was reduced after only 2 Km cutting distance, such that even the three fold reduction of the feedrate was less significant than the change in the cutting effectiveness of the tool.

In all cases considered in Matrix 1 as the tool cut distance increases the Twyman distortion became more concave as indicated by a negative value in the tables. Samples which were cut with sharp unused tools tended to become more convex on their mounting surface implying the machined surface had become more tensile. However; as the tool wore the mounting surface became increasingly concave, indicating compressive stress at the machined surface. Surfaces having low levels of surface fracture had either low levels of compressive stress or were in tension.

The crystal orientation appears to have only a small effect on both % surface fracture and Twyman distortion. The <111> orientation appears to give a lower % of surface fracture and less compressive stress for a given tool type/condition.

The final suggestion from Matrix 1 is that coolant does reduce the % of surface fracture and reduces the induced compressive stress level when tool cut. This coolant effect can only be observed if tool cut distance is taken into account.

Experimental design matrix 2 is shown in Figure 38. The three parameters having two levels for matrix 2 were; tool radius, depth of cut and tool top rake angle.

The findings from this matrix supported that of matrix 1 in so much that tool cut distance is seen to have a significant effect on both % surface fracture and surface stress. Reduction in depth of cut is not seen to reduce % surface fracture. The results of surface roughness and % surface fracture obtained from Matrix 2 for both <111> and <100> samples are given in Tables 17 and 18 respectively. This is confirmed by samples 1 and 4 <100> where reduction in depth of cut was associated with an increase of % surface fracture and surface roughness. Note the much higher tool cut length for sample 4. A number of the surfaces for this matrix were of a very high quality roughness and in the case of sample 5 <111> sub-nanometre. This sample demonstrates an optical quality as found on the very best polished surfaces. A less negative tool top rake is not seen to cause higher % surface fracture when the tool is sharp, however the data does suggest that the -5° top rake tools degrade in their cutting ability more quickly and lead to higher % surface fracture. The surface stress associated with the lower rake angle tools was consistently tensile, see Table 18.

The results of surface roughness did not show that the larger tool radius provides better quality roughness as equation 2.1 would suggest. The % surface fracture was not noticeably influenced by tool radius in these tests.

Experimental design matrix 3 is shown in Figure 39. The three parameters having two levels for matrix 3 were depth of cut, tool top rake angle and workspindle speed. The results of surface roughness and % surface fracture obtained from Matrix 3 for both <111> and <100> samples are given in Tables 19 and 20 respectively.

The results obtained in matrix 3 suggest that cutting speed is not significant in the generation of surface roughness, % fracture or residual stress at the chosen levels. The additional tests using -5° top rake tools confirmed their tendency to induced tensile surface stress. Tool wear for these tools tended to reduce this level of tensile stress. Increasing the depth of cut to 10μm from 5μm did have an effect on the % surface fracture, even when tool wear is considered.

In order to confirm independently the principle of measuring surface stress by Twyman distortion specimen's were measured for surface stress using a Micro-Raman spectrometer. This method of assessing surface stress profiles in crystal materials has been widely researched by Sparks [103]. The measurements shown in Figure 76, taken using a Renishaw micro-Raman instrument, show comparable data from a carefully polished surface in a stress free state and that obtained from sample 5 <111>. It can be seen that the peak frequency on the spectrum obtained from the diamond turned sample 5 was shifted to the left. This shift has previously [103] been shown to indicate a higher level of tensile stress. This measurement provided confidence that the measurements of Tywman distortion gave an indication of the type of surface stress.

The suggestion from these data, that tool cut distance has a major influence on the % surface fracture and the induced surface stress, seriously questions the application of Scattergood's equation 2.11 for defining the maximum feedrate which will provide ductile type surfaces. Also, the change of the cutting effectiveness of the tool indicates the Indentor constant used in critical depth equations such as 2.9 and 2.10 is not actually a constant when considering diamond turning of germanium over realistic machining duration's at the levels tested.

Tool life, when measured as that which permits surfaces for IR applications to be machined, is limited to only 2-3 Km of cut length with the machining parameter levels tested. Application of coolant was seen to have a noticeable effect on surface stress and % surface fracture and it is likely that the tests where coolant was not used increased the overall tool wear. Another consideration which should be borne in mind is that numbers of cuts were taken on relatively small samples and tool life may be higher for continuous cutting of larger components.

The material removal rate, associated with a 2-3 Km tool life, which provided a high quality surface useful for IR applications, was 3.77 mm^3/minute. This figure is based on 100 mm diameter optics. In comparison to the polishing rate given in section 2.2.3 this is significantly higher. The total volume of material removal offered by a tool used in this way would be 40 mm^3.

The four <110> samples were machined at lower feed rates to assess the impact on the available tool life for producing ductile type surfaces. All four samples were machined using the same tool. This new sharp tool was of 2 mm radius and -25°

negative top rake. All four samples were machined with spray mist white spirit coolant. Rotational workspindle speed was increased up to 1200 rpm to maintain volumetric removal rate at the lower feed per revolution levels. The machining parameters and results are shown in Table 21.

Clearly, from these trials, tool life as measured in cut distance and ability to produce zero levels of surface fracture is higher than suggested in the previous tests, over 11 Km. Coolant was used for all tests carried out with this tool. Interestingly, the final test carried out on sample 4 <110> where a 10 μm depth of cut was used still gave a purely ductile surface. This corroborates Scattergood's claim that depth of cut is a secondary function on surface fracture [60]. In all four samples Twyman distortion indicated a slightly tensile stressed machined surface. For example the convex distortion of 100 nm in the case of sample 4 <110>, according to equation 2.12, equates to a longitudinal surface stress of 58 N/m.

The volumetric material removal rate for the test on sample 4 <110>, normalised for a 100 mm diameter component was 1.91 mm^3/min. If tool life is claimed to be 12 Km at the cutting parameters for sample 4 <110> then tool life provides 110 mm^3 of material removal.

5.2 Diamond Turning Investigation (2)

Diamond Turning of Silicon and Optical Germanium
Investigation of Tool Cut Distance and Machining Forces and their effect on Surface Morphology and Residual Stress

These tests were carried out in a similar manner to those of investigation 1. However; for these tests, lower feed rates, depth of cut and smaller tool radius were employed. Tools were supplied by Contour Fine Tooling Ltd in preference to Drukker since higher tool life was claimed. Contour orientated the diamond of the tool, such that the harder <111> plane is aligned to the cutting edge. Further details of this process were not disclosed. However; Drukker did confirm that the tools used in investigation 1, which they had supplied, were orientated to the softer <100> plane. This was said to be for ease of edge preparation.

Machining forces were measured during the tests using a dynamometer mounted under the toolpost shown in Figure 40. Each sample was assessed for Twyman distortion after varying amounts had been machined from the surface

Tool life for Ductile Turning (1) : Silicon

A single Silicon sample of 32 mm diameter and having <111> crystal orientation was diamond turned using the following parameters:

Tool Radius : 0.5 mm
Top Rake : -25°
Depth of cut : 3 μm
Feedrate : 2μm/rev (2 mm/minute)
Workspindle : 1000 rpm
Coolant : Spray mist white spirit

Purely ductile surfaces were produced on this Silicon sample until the tool had cut for an equivalent distance of 8 Km. For the machining parameters used this cut distance provides 48 mm^3 of material removal at 0.95 mm^3/min (normalised for a 100 mm optic). Cutting force, % surface fracture and Twyman distortion against the tool cut distance is given in Table 22.

It can be seen that both Twyman distortion and machining forces increase with tool cut distance. Silicon consistently shows a compressive surface stress condition when -25° top rake tools are employed. The magnitude of the compressive stress increases with tool cut distance. The reduction in the thickness of the sample, incurred during the overall test, will cause the Tywman distortion to artificially increase by approximately 5%. The maximum longitudinal surface stress for sample 1, given by equation 2.12.

$$\sigma = dH \cdot \frac{T^2}{D^2}\left[\frac{E}{3(1-\nu)}\right] \qquad \text{[Eqn 2.12]}$$

where, D = $32x10^{-3}$m, T= $2.95x10^{-3}$m, ν = 0.278, E = $159x10^9$ N/m with a change of flatness dH of -270 x 10^{-9} m, maximum longitudinal surface stress σ equates to 195 N/m.

A significant change of the level of machining forces are seen over the 8 Km of tool cutting length. Purely ductile surfaces were produced even after the tool forces had increased from 0.1 N up to 0.7N. Assessment of the diamond tool's edge condition by optical microscopy revealed little obvious wear regions. SEM observations did however show that the edge of the diamond tool had worn, see Figure 77. The wear

regions suggests a chemical wear mechanism as no visible markings or any suggestion of roughness can be seen in the worn region. Silicon is known to chemically modify diamond at high temperatures.

Tool life for Ductile Turning (2) : Silicon

As with tool life test (1) a single Silicon sample of 32 mm diameter and having <111> crystal orientation was diamond turned. All machining parameters except tool radius were kept as for tool life test (1).

Tool Radius : 0.15 mm
Top Rake : -25°
Depth of cut : 3 μm
Feedrate : 2 μm/rev (2 mm/min)
Workspindle : 1000 rpm
Coolant : Spray mist white spirit

In this test purely ductile surfaces were produced until the tool had cut for an equivalent distance of approximately 12 Km. As in tool life test (1) the machining parameters used provide a volumetric material removal rate of 0.95 mm^3/min. The total volume of material which can be removed equates to 72 mm^3. Cutting force, % surface fracture and Twyman distortion together with tool cut distance is given in Table 23.

The machining forces associated with the new tool both in the normal direction and the cutting direction are significantly smaller than was measured for the new 0.5 mm radius tool. However, the cutting force, F_c increased at a higher rate for this smaller tool. The increase in machining forces for both tools against tool cut distance is shown in Figure 78.

It is interesting to note that the normal force, F_n, which most closely represents the applied force P in an indentation test is at the same level for both tools used on the silicon when brittle fracture is first seen at the machined surface. This fact may well be a further indication that the tool cutting edge condition is of prime concern for turning ductile type surfaces in silicon. It is clear from the increasing machining forces that the tool edge is gradually degrading.

The smaller tool radius actually gave a longer tool life for producing useful optical surfaces. This result further questions the true usefulness of Scattergood's f_{max}

formula equation 2.11[112] when applied to turning of silicon. Significant increases in the level of Twyman distortion were found on the sample machined with the smaller radius tool. This is illustrated in Figure 79 which shows the longitudinal surface stress against tool cut distance for both the 0.5 mm and 0.15 mm radii tools. The maximum longitudinal surface stress induced with the 0.15 mm tool and after 12.1 Km cut distance is 960 N/m.

Tool life for Ductile Turning (3) : Optical Germanium

To obtain comparative data on optical germanium tool life test (1) was repeated on a single sample of germanium. The 32 mm diameter sample was of a <111> crystal orientation. This was diamond turned using the same parameters as for test (1) on the silicon. These being :

Tool Radius : 0.5 mm
Top Rake : -25°
Depth of cut : 3 μm
Feedrate : 2 μm/rev (2 mm/min), * 1 μm/rev (1 mm/min), ** 1.5 μm/rev (1.5 mm/min)
Workspindle : 1000 rpm
Coolant : Spray mist white spirit

Purely ductile surfaces were not produced on this germanium sample when using the same parameter levels which did so on the silicon sample 1. Five percent of the surface area was formed by brittle fracture. This value of surface fracture did not change over a 7 Km cut distance.

Assessment 6 was therefore carried out at a lower feedrate of 1 μm per rev, the surface produced for this assessment was free of any brittle fracture and measured ~ 2 nm Ra. Assessment 7 was carried out at 1.5 μm per rev and produced a surface having 3% fracture. Assessment 8 was carried out at 1 μm per rev feedrate and with a 10 μm depth of cut. This confirmed that reducing feedrate led to a surface free of brittle fracture even when depth of cut was significantly increased.

Machining forces and Twyman distortion remained almost constant throughout. Cutting force, % surface fracture and Twyman distortion against the tool cut distance is given in Table 24. Longitudinal surface stress induced was less than 50 N/m.

Tool wear regions were investigated using both optical and scanning electron microscopes none could be found. The fact that 5% surface fracture was produced even with an "as new" sharp tool suggests that germanium is more prone to brittle fracture than silicon. However, the machining forces for germanium are much more consistent. The potential tool life for producing purely ductile surfaces was not indicated from this test. It is fair to state that a feedrate of 1 μm per rev provides a tool life above 11.2 Km. The repeatable level for the machining forces indicate that tool edge degradation is at a much lower rate than experienced when cutting the silicon material. The consistent level of Twyman distortion and machining forces over the 11.2 Km tool cut distance imply that these are closely related.

The results obtained in this test show turning of germanium to be a stable process. The material removal rate involved for assessment 8 equates to 1.56 mm^3/min. Tool life of 11.2 Km would provide a total volume of material removal of 112 mm^3. It should be stressed at this point however that the overall tool life which provides purely ductile surfaces under these test conditions was not established due to a time limitation on the tests. Also whilst the maximum feedrate was established the associated maximum depth of cut was not established.

5.3 Diamond Turning Investigation (3)

Diamond Turning of BK7, Silicon and Zinc Sulphide

Assessment of "ductile" Machinability

The objective of this investigation was to gain some information on the relative ease of achieving "ductile" type surfaces in three materials which are considered important for optical elements. Silicon and zinc sulphide for IR applications and BK7 optical glass for visible applications.

Single samples of each material was machined using carefully formulated conditions such that repeatability was maintained for the three different materials. Sample size was as previously, 32 mm diameter. The diamond tool was reconditioned by Contour Fine Tooling before each test. Prior to the tests each sample had been finely polished. The machining parameters used are given below:

Tool Type : Flat nose tool
Top Rake : -15°
Depth of cut : 0.5 μm
Feedrate : 0.5 μm/rev (0.5 mm/min)

Workspindle : 1000 rpm
Coolant : Spray mist white spirit
The flat nose tool was carefully aligned to the surface of the samples. The alignment of the tool was set as shown in Figure 41 and achieved using the NION machines optical tool setting station. The aim of setting the tool in this manner was to provide a very simple chip geometry shown in Figure 80.

The samples were mounted onto the vacuum chuck and tested for swash. For all three samples swash was reduced to below 1 μm p-p. Four separate 0.5 μm depth cuts were taken on each sample. After which it was evident that the full surface of each sample had been machined. The material removal rate for these tests, normalised for 100 mm diameter samples, was 0.04 mm^3/min. Tool cut distance for each test was less than 6 Km.

Assessment of the three samples showed greatly different surface morphologies. The zinc sulphide sample exhibited a smooth ductile type surface, but with some limited regions of brittle fracture. These fracture regions were defined by the materials polycrystalline structure. This is clearly shown in the SEM micrographs of Figures 81 and 82. Surface finish measurements on this sample also showed the influence of the material's polycrystalline structure, see Figure 83. The silicon sample which was of the single crystal <111> type showed much higher percentage of surface fracture than found on the zinc sulphide sample, as shown in Figure 84. Some regions did however exhibit a ductile appearance. The BK7 glass sample exhibited solely brittle fracture. No evidence of ductile removal could be seen.

5.4 General Discussion of Diamond Turning Investigations

5.4.1 Diamond Turning of Optical Germanium

The investigations described in section 5.1 established a number of important aspects regarding the production of smooth optical surfaces in germanium. Firstly, tool edge condition, defined by cut distance has a major influence on % surface fracture and induces surface stress when feedrate is greater than 4 μm/rev. This being the case for tools having 0.5 mm and 2 mm radius, and -5° and -25° top rake angles.

At feedrates greater than 4μm/rev, increased tool cut distance increases the level of compressive stress induced into the machined surface and increases the level of % surface fracture. When germanium is cut such that its appearance is ductile, the surface roughness follows equation 2.2, developed from the turning of soft metals. Therefore machine quality ultimately dictates the achievable surface quality.

Also for feedrates above 4μm/rev tool life (for 0.5 mm and 2 mm radii tools) as defined as that which can produce a ductile surface, is <3 Km. The associated material removal rate for a 100 mm diameter optic would be 3.77 mm^3/min and tool life would provide a volumetric removal of up to 40 mm^3.

Application of white spirit coolant was seen to reduce % surface fracture and induced surface stress. The results suggest this coolant prolongs tool life.

Crystal orientation was not seen to have a major influence on % surface fracture or surface stress. The <111> orientation generally gave slightly lower levels of both surface stress and fracture.

At feedrates greater than 4μm/rev the degradation of cutting performance of a diamond tool is critical. Tool cut length will principally effect surface morphology and stress state. Depth of cut is shown to effect the level of % surface fracture.

With a feedrate of 1μm/rev a 2 mm radius tool has a tool life, again that which produces a ductile surface in <110> germanium, greater than 11.2 Km's. With a depth of cut of 10μm, material removal rate for a 100 mm optic is 1.8 mm^3/min. Tool life provides 112 mm^3 volumetric removal. Little degradation of cutting performance is suggested by the constant value of Twyman distortion. An increase of the spindle speed from 600 rpm to 1200 rpm had no noticeable effect on the surface quality at these feedrates. Depth of cut in the 2-10 μm range had little effect on surface quality / condition. The process of diamond turning optical germanium appears repeatable at this operating rate.

The tool life trial carried out on germanium and discussed in section 5.2 test (3) further established that a 0.5 mm radius tool operating at 1μm/rev feedrate would produce surfaces free of brittle fracture for at least 11 Km of cutting length. Furthermore; the consistent level of induced surface stress indicated by the Tywman distortion and the constant level of machining forces suggest that the 1.8 mm^3/min removal rate could be maintained over significantly longer cut distances than the distance of test, 11 Km. This tool life test did also show that a 1.5 μm/rev feedrate would not yield surfaces free from fracture. Therefore, f_{max} is less than 1.5 μm/rev for germanium with these machining conditions and tool type..

Measurement of the machining forces was not found to give an indication of whether brittle fracture would be found on the machined surface. This fact indicates that the

combination of brittle fracture and ductile removal mechanism's proposed by Scattergood and shown in Figure 20 complicates the prediction of brittle fracture on the machined surface by measurement of cutting forces alone.

Diamond turning of optical surfaces in germanium will not generally induce surface stresses which cause significant distortion to the elements other optical surface. It is advisable to take relatively large depths of cut with low feedrates to maximise material removal rate whilst maintaining surface quality.

5.4.2 Diamond Turning of Silicon

The diamond turning trials carried out on the silicon samples identified two very important aspects regarding the machining of optical surfaces in silicon.

An important first point is that from the material mechanical properties standpoint, silicon should be more easily diamond turned without causing brittle fracture than optical germanium. This point is shown theoretically using Lawn's equation for calculating critical penetration depth, equation 2.8.

$$d_c = \Psi\left[\frac{E}{H}\right]\left[\frac{K_c}{H}\right]^2 \quad \text{[Eqn 2.8]}$$

If the indentor constant ψ, is set at unity, the value of d_c for silicon and germanium will be 0.057m and 0.037m respectively. From Figure 21 it can be seen that feedrate is the machining parameter which most influences chip thickness, which can be likened to the penetration depth, d_c in Lawn's equation. The tool life turning test carried out on silicon showed that a 0.5 mm radius tool, in an as new condition, can produce a surface free of brittle fracture with a 2 μm/rev feedrate. The same test carried out on germanium produced a surface having 5% brittle fracture. In fact feedrate had to be reduced to 1μm/rev to attain surfaces free of brittle fracture.

The ratio of d_c for silicon and germanium obtained from equation 2.8 and their mechanical properties is 1.54. Whilst, f_{max} was only truly ascertained for silicon after the tool had cut for 12 Km, the ratio of the feedrates which gave fracture free surfaces on the two materials would be less than 2 and greater than 1.33. Therefore, the findings of the machining trials closely align to that calculated using equation 2.8, and this corroborates Scattergood's work [112].

However, the fact that tool wear is significantly higher for silicon than germanium means that silicon is much more difficult and expensive to diamond turn optical surfaces in silicon as compared to germanium. The machining force F_n, which most closely simulates that of an indentor, can range from 0.04 - 0.7 N and still yield surfaces which are free of any brittle fracture, i.e. ductile like. It is therefore difficult to see how the measurements of machining force obtained in the machining trials can be put to any useful purpose for prediction of brittle fracture occurring, at or beyond the cut plane. Lawn's and Hagan's, indentation developed, equation's, 2.3 and 2.5 indicate fracture occurs with applied forces lower by one and two orders of magnitude than the 0.7 N measured in these diamond turning trials. The reason for this discrepancy is that diamond turning of ductile like surfaces at reasonable material removal rates, ~ 1-2 mm^3/minute involves significant brittle fracture. The fact that micro-fractures often do not propagate beyond the cut plane means the machining force is not limited to that predicted by Lawn's and Hagan's indentation work. The direction and depth of brittle fracture's caused during diamond turning are dependant on the tool geometry, machining rates, but most importantly the edge condition at the nose of the diamond tool, the region of the tool which produces the cut plane.

The magnitude of Tywman distortion did appear to increase with machining force. Hence any diamond turned silicon surface will have a surface stress condition dependant not only on machining parameters but also, and critically on the tool cut distance. Significant spherical distortion can be expected through induced surface stress.

5.4.3 Diamond Turning of BK7, Silicon and Zinc Sulphide

The objective of cutting these three materials in exactly the same manner was to establish the relative difficulty of producing surfaces which are free of brittle fracture. The findings have shown that for a given tool shape / condition and the low level machining parameters used, zinc sulphide is the easiest to cut with limited levels of brittle fracture. Both silicon and BK7 glass were found to have significant levels of brittle fracture. The silicon surface did however exhibit some regions which appeared free of brittle fracture.

To help understand why zinc sulphide is easier to machine without causing brittle fracture than the cases of silicon and BK7 the use of equation 2.3, 2.4 and 2.8 is necessary together with the materials mechanical properties given in Table 3. Since the turning tests discussed in section 5.3 where carried out with exactly tool and machining conditions it is fair to assume the geometric constant over the 3 materials

be the same. If the constant in each of the three equations stated above is made unity, and the calculated values are normalised to zinc sulphide the following table can be developed.

From Table 25 it can be seen that zinc sulphide has relatively large P* and dc values. These are obtained through the materials lower hardness level and higher fracture toughness, and account for this material being the easiest to machine without inducing brittle fracture.

It is somewhat less easy to explain the fact silicon is easier to cut without inducing brittle fracture into the cut surface than is the case for BK7 glass. The main reason for the glass being more difficult is the associated large crack length value. Scattergood has shown that the production of optical surfaces in silicon by diamond turning is through a combination of brittle and ductile material removal mechanisms. Therefore the relatively large C* value for the glass means that the fractures propagate further and beyond the cut plane surface. Whilst silicon has a smaller dc and P* value than BK7 glass, by approximately a factor of 20, the relative value of C* for the two materials differs by a factor of 30.

Figure 85 schematically shows the fractures caused when machining the three materials using a round tool. 85a shows the case of zinc sulphide, 85b shows the case of silicon and 85c is the case for BK7.

It is also thought that the crystalline nature of the silicon material means the direction of the brittle fractures are more in-line with the major direction of cut, i.e. the feed direction, than is the case for the amorphous glass.

Further investigations are needed to establish clearly the mechanics behind the propagation of fractures when diamond turning these brittle materials. However the comparative tests here further reinforce the difficulty of diamond turning optical surfaces into amorphous glass materials even at low material removal rates.

CHAPTER 6

Diamond Grinding Investigations

This chapter presents and discusses the results from the diamond grinding trials outline in sections 3.3.4 and 3.3.5. A detailed discussion of the results is given in section 6.3.

6.1 Diamond Grinding Investigation (1)

Diamond Grinding of BK7, SF10 and LaSFN30 Glasses
Influence of Machining Parameters on Surface Morphology / Sub-Surface Damage

Initial grinding trials were carried out solely on BK7 and SF10 glass samples. The intention was to establish the levels which permitted these glasses to be ground to optical quality without causing significant surface damage. Subsequent tests evaluated the comparative ease of grinding BK7 and LaSFN30 glasses.

In order to ensure that the grinding wheels were in the same condition before each test a well established method for wheel dressing was adhered to. The grinding wheels were formed such that a small angle was produced on the periphery of the wheel. This forming operation ensured that a set width across the grinding wheel was actually used in removing the glass material. Figure 86 shows the shape of the grinding wheel used. It was understood through Namba's work [88] that the number of active grains which actually carried out the overall material removal would have a large effect on the surfaces produced. Precisely forming the small angle on the grinding wheel permitted calculation of the theoretical number of "active" grains involved and therefore permitted the material removal and depth of penetration, grain depth of cut (GDOC), by each individual grain to be estimated..

Table 26 summarises the grinding trials carried out on BK7 and SF10 glasses. This table lists the machining parameters used and measurements of the surface roughness obtained. All grinding tests were carried out using de-ionised water as the grinding coolant. It was found that a single measurement of surface roughness of the ground samples did not reflect the quality of the whole surface obtained. Therefore to gain a more meaningful measure of surface quality, measurements of roughness were taken every 0.25 mm across the radius of the sample. These measurements were plotted on a graph, see Figure 87. The slope on this graph gives an indication of the degradation

of surface roughness from centre to edge of the sample. This slope figure and the roughness measured at 8 mm radius are given in Table 26 to describe overall surface roughness.

6.1.1 Assessment of Grinding Wheel Specification

The influence of wheel grain size on surface roughness of BK7 and SF10 samples is shown in Figure 88. Results are those obtained with resin bond wheels.

The average grain size of the 3-6 μm wheel and the 6-12 μm wheel was 4.06 μm and 9.6 μm respectively. It was found that the larger grain size wheel would only produce surfaces which were formed solely by micro-brittle fractures on both BK7 and SF10 glasses. Even with very low levels of material removal the surfaces were of a very poor quality. The previous work which had shown 6-12 μm to produce nanometric surfaces had been carried out using cup wheel grinding and with only one machine axis of movement. The wheel to work contact area for this type of grinding is much greater than seen in the mode used on the NION machine this is thought to be the main reason for the larger grain wheels poor performance.

The smaller grain size wheel produced surface roughness ranging from 1-10 nm Ra. In some regions roughness was better than 1 nm Ra, see Figure 89. Also significantly high percentage of the ground surfaces appeared to be of a "ductile" nature, see Figure 90. Atomic force probe investigations also suggested the surface was ductile-like in morphology, see Figure 91.

A limited number of tests were undertaken using the 1-2 μm grain size wheels. These wheels were found to be extremely difficult to use with the grinding mode incorporated into the NION machine. Grain "dulling" or premature fall-out was thought to be the main problem. Detailed trials were not continued with these fine grain wheels.

Comparison of the surface roughness produced by the 3-6μm metal and resin wheels is given in Figure 92. It can be seen that both wheel types produced surfaces in the 1-20 nm Ra range. What is not conveyed by Figure 92 is the tendency for the resin bond wheels to cause 'local" scratching. These scratched regions exhibited severe brittle fracture and were found to be up to 10 μm in depth. No noticeable local scratching was seen when using the metal bond wheel and the ELID method.

Since the work discussed in Appendix 1 had previously given a high level of confidence in the cast-iron wheels and the ELID method, all further tests concentrated on the 3-6 μm metal bond wheel.

6.1.2 Assessment of the Mode of Grinding

Two modes of grinding using the NION machine had been proposed. The first method was where the workhead spindle speed was held constant (CRPM) as in the case of the diamond turning trials. The second mode provided a constant surface speed between the test sample and the grinding wheel (CSS) mode. With the CSS mode the workhead spindle speed was increased as the grinding wheel traversed towards the centre of the sample, thereby providing the constant (V_w) speed. The major workpiece feed direction, i.e. workpiece rotation, is held constant in CSS mode whereas it varies across the radius of the sample in the CRPM mode.

It was immediately noticeable that a surface pattern effect existed on some of the ground samples. The pattern shape was different for CSS and CRPM modes. This pattern effect has previously been explained by Franse [73]. The pattern effects for each mode is shown schematically in Figure 93, and is discussed in more detail in section 6.1.5.

From the measurements of surface roughness shown in Table 26 the preferred mode is not clear since both modes can produce roughness of better than 2 nm Ra when measured with the Wyko Topo instrument. The angular velocity of the workhead spindle against the surface roughness obtained at the 8 mm radius position is shown in Figure 94. This graph suggests that slower workhead velocities give better surface quality when using the 3-6 μm wheels.

Figures 95 and 96 show the surface roughness against radial position on samples ground in CSS and CRPM modes respectively. It can be seen that the slope of the graph for the CSS ground sample is higher than that for the CRPM sample. This occurrence should not be to surprising since the workhead rotational speed will be very low whilst grinding the outer regions of the sample. This low rotational speed will give rise to a "cusp" effect. This "cusp" effect is that which is seen in the diamond turning process and is defined by equation 2.1. This equation applies for grinding where tool radius and feed per revolution is much larger.

Surface measurements over larger areas / lengths show the "cusp" effect to influence "waviness" or mid-term slope. The waviness of a CSS ground surface is shown in the Form Talysurf trace illustrated in Figure 97.

6.1.3 Influence of Feedrate (V_l)

The effect of linear feedrate on surface quality when using 3-6μm grain wheels is shown in Figures 98 and 99. Surprisingly, reducing linear feedrate from 0.145 to 0.075 mm per revolution of workhead spindle had very little influence on surface roughness at the 8 mm radius position, or on the slope of Ra against radial position. The linear velocity (V_l) for these tests was 0.025 - 0.1 mm / second.

6.1.4 Influence of Depth of Cut (d)

The effect of depth of cut on surface quality when using 3-6 μm grain wheels is shown in Figures 100 and 101. As with V_l, reducing depth of cut (d) from 0.0015 to 0.0005 mm had very little influence on surface roughness at the 8 mm radius position or on the slope of Ra against radial position. Depths of cut larger than 1.5 μm were not found to be possible. It was noticed that the actual depth of material removed from the samples did not correspond to that applied by the machine motions when depth of cut was larger than 1.5 μm.

6.1.5 Assessment of Surface Wave Velocity of Samples

A number of samples were assessed for their surface wave velocity. Unfortunately, the SF10 glass proved to be difficult to assess using this method since high attenuation of the signal made isolation of the Rayleigh wave difficult. Figures 102 and 103 show radial scan data for a polished and a ground SF10 sample respectively. Little of significance can be deduced from these plots.

BK7 glass was found to be more easily assessed using this acoustic method. A number of BK7 samples was assessed by using radial and azimuthal scans. The samples which were assessed, some important machining data and the average surface wave velocity of the azimuthal scan are listed in Table 27. Azimuthal scans of surface wave velocity were taken at a 12 mm radius. These data are shown in detail in Figure 104.

As discussed in section 2.6.4 the higher the surface wave velocities the less surface and sub-surface damage. From Table 27 and Figure 104 it is clear that the polished surface had the lowest levels of damage. However, it is not clear which is the better grinding mode or which is the better type of wheel bond.

The surface wave velocity measurements taken as radial scans however provided very important information on the influence of the grinding mode.

Figure 105 is a radial scan of sample 17, a sample produced using CRPM grinding mode. With this mode of grinding the material removal rate is highest at the outer regions of the sample. Interestingly the surface wave velocity is lowest in this outer regions of the sample suggesting higher levels of surface and sub-surface damage. Sample 18 was also produced using the CRPM mode. The radial scan of surface wave velocity for this sample is shown in Figure 106. As for sample 17 velocity drops toward the outer regions of the sample.

Figure 107 is a radial scan of sample 15 and it is clear that the surface wave velocity has a larger variation towards the outer regions of the sample. This outer region is that which was produced with a low workhead rotational speed, ~20 rpm, using the CSS grinding mode. The surface wave velocity however does not obviously degrade toward the outer regions as was seen for sample 17. Figure 108 is a radial scan of sample 19 which was also ground using the CSS grinding mode and this scan also shows an increase in variation of surface wave velocity at the outer regions of the sample.

Figure 109 shows the radial scan of surface wave velocity for sample 4. This sample was also ground using the CSS grinding mode. However, a resin bond wheel was used on this sample and again there is a variation of surface wave velocity at the outer regions of the sample. The maximum surface wave velocity is higher for this sample as compared to samples 15 and 19 which were ground with a metal bond grinding wheel and ELID dressing method.

Figure 110 is a radial scan of a polished surface of BK7 which shows the surface wave velocity to be similar to that measured on sample 4. However, the velocity is more consistent across the radius of the sample, within + / - 1 m s^{-1}.

6.1.6 Assessment of Etched Surfaces using Optical Microscopy

To obtain some information on the near-surface regions a number of the BK7 samples had half of their ground surface etched. Protection was applied to half the surface to permit any subsequent analysis. The unprotected half was etched in ammonia bifluoride, see section 3.4.5 for details. The etching process removed approximately 250 nm from the surface, see Figure 111.

The influence of the choice of grinding mode, CRPM and CSS, was made more obvious after etching.

Figures 112 and 113 shows the newly exposed surface of sample 17 observed using a low magnification (x 86) optical microscope. The etching revealed noticeable levels of sub-surface micro-cracking which were previously not evident. The severity of the fracture differed with respect to radial position. Observations of increased micro-fracture with the radius across the ground surface correlated well with reduction of the measured values of surface wave velocity shown in Figure 105.

Figures 114 shows the newly exposed surface of sample 15 and it can be seen that this surface had lower levels of micro-fracture when compared to the same regions on sample 17. It can also been seen in Figure 107 that a higher surface wave velocity is measured. Figures 115 and 116 show the etched surface of sample 19 and again less micro-fracture was measured on this sample when compared to sample 17. Interestingly, the prominent brittle fracture regions toward the outer diameter of the sample appear in "bands". This "band" effect was not at a frequency equal to the linear feedrate per revolution of the workhead spindle and therefore was not a function of the "cusp" effect defined by equation 2.1.

Sample 4 was ground using the CSS mode of grinding but with a resin bond wheel. The surface wave velocity measured on this sample was higher than for samples 15 and 19. Figures 117 and 118 show that Sample 4 also had lower levels of micro-fracture beneath its surface. In fact very little brittle fracture was apparent up to a radius of 15 mm. A number of small scratches were however evident.

Sample 14 was ground in the same manner as sample 4 but using a metal bond wheel, Figures 119 and 120 show that low levels of brittle fracture can be obtained using the metal bond wheel. A possible difference in the tests carried out on samples 14 and 19 is the quality of dynamic balance. It can be seen however that there is a significant difference in the severity of sub-surface micro-fracture.

6.1.7 Comparison of Grinding BK7 and LaSFN30 Glasses

The relative difficulty in producing surfaces in glass materials that are free of any brittle fracture is thought to be influenced by both the material mechanical and chemical properties. The mechanical properties infer critical depths, d_c of : SF10 at 81nm, BK7 at 39 nm and LaSFN30 at 30 nm as calculated using equation 2.9.

The grinding trials carried out on BK7 and SF10 glasses and discussed in Appendix 1 indicated that the SF10 was the easier glass to grind without inducing surface apparent brittle fracture. This work was supported by the findings of the limited work discussed in section 6.1.1 on SF10.

The chemical characteristics of BK7 and SF10 are similar, see Table 5. However; LaSFN30 is a glass which has mechanical properties which indicate that it should be more difficult to grind without inducing micro-fracture than BK7 as demonstrated by the smaller value of d_c, but has chemical properties which indicate it more likely to generate a softened hydrated surface layer. The work of Izumitani [19] indicated that Lanthanum based glasses have higher polishing rates due to a rapid generation of a hydrated surface layer which has a much lower hardness than the bulk glass.

A limited number of grinding trials were carried out on samples of LaSFN30, the grinding parameters used were those which had previously produced some levels of surface brittle fracture when grinding BK7. The limited findings strongly suggest that LaSFN30 glass is considerably easier to grind without causing noticeable "surface apparent" brittle fracture. Figure 121 is a SEM photomicrograph of a ground surface of LaSFN30 and little fracture can be seen even at this outer diameter position. The surface roughness obtained on this material was in the range 3-6 nm Ra.

Whilst these initial findings obtained on the LaSFN30 are only qualitative they do strongly suggest that the process of ductile mode grinding is significantly dependant on chemical removal aspects as is known to be the case for the polishing process.

6.2 Diamond Grinding Investigation (2)

Diamond Grinding of Zerodur™

Influence of "Ductile Mode" Grinding on Surface Morphology and Residual Stress Levels

6.2.1 Stress State of Prepared Zerodur Samples

The specially prepared Zerodur™ samples differed in a number of ways from the glass samples used in grinding investigation (1). These ceramic samples were thinner than had previously been used, diameter 32 mm and thickness 3 mm. The Zerodur samples were prepared such that both sides were finely polished. These polished surfaces were flat to approximately $\lambda/4$ and had surface roughness ~ 1 nm Ra. Since one of the objectives of this investigation was to establish that fixed abrasive "ductile mode"

grinding induces only limited levels of residual surface stress it was important to establish that the prepared samples were in a stress-free condition prior to testing.

To ensure the samples were in a "stress-free" state, six samples were etched on one surface in an ammonium bifluoride solution for 5 minutes. The sample's other surface, which was protected during etching, was measured for flatness before and after etching. The etching process removed approximately 0.5 μm from the sample.

Any distortion of the unetched surface would indicate that the so-called "stress-free" samples had surface stress prior to grinding. Table 28 shows the level of distortion of the protected surface for each of the six samples. The accuracy of using the "difference" function on the Zygo / Wyko interferometer was limited by the repositioning accuracy of the sample. It was found that the error associated with repositioning was +/- 50 nm P-V.

Change in flatness of the protected surface was less than 150 nm. The protected surface became more convex indicating its stressed state relative to the etched surface was more compressive. This indicates the etched surface had some compressive surface stress released during etching. The magnitude of this change of stress state is given by equation 2.12.

$$\sigma = dH \cdot \frac{T^2}{D^2}\left[\frac{E}{3(1-\nu)}\right] \qquad \text{[Eqn 2.12]}$$

where, D = $32\text{x}10^{-3}$m, T= $3.02\text{x}10^{-3}$m, ν = 0.243, E = $90.3\text{x}10^{9}$ N/mm^{-2} with a change of flatness dH of 127 x 10^{-9} m, maximum longitudinal surface stress σ equates to 53 N/m. Therefore any distortion of the ground samples above 150 nm, equivalent to a longitudinal surface stress of 53 N/m, would be a function of the ductile mode grinding.

6.2.2 Grinding of Zerodur Samples

All of the Zerodur samples were ground using the fixed grinding parameters set out in Table 12. Initially, six samples were ground, 30 μm was removed from one surface. Additionally, a single sample was machined using the same grinding parameters, however after a certain amount of material was removed from the sample it was assessed for Twyman distortion and surface roughness. This machining and then measurement procedure was repeated to gain information of the surface stress associated with depth of material removed.

6.2.3 Surface Roughness of Ground Zerodur Samples

The surface roughness of the Zerodur samples was much more consistent across their smaller radius when compared to the surfaces produced on the BK7. Surface roughness measured 1.5-3.0 nm Ra across the full 16 mm radius, see Figure 122. Little degradation of surface roughness was measured towards the outer regions of the samples. Consistency of surface roughness from sample to sample was within 3 nm Ra.

6.2.4 Twyman Distortion

The Twyman distortion of the mounting surface for each of the six ground samples which had 30 micron removed is given in Table 29. The distortion is highly spherical in shape giving confidence when calculating surface stress, see Figure 123. The calculated change in surface stress of the ductile ground surface is also given in Table 29. Consistency of Twyman distortion across the six samples was within 160 nm P-V. The polished mounting surfaces consistently became more concave indicating that the ductile ground surface was in a more compressive state than when polished. The longitudinal surface stress of the ductile ground samples was 136 N/m (+/- 45 N/m). This level of surface stress is 250% greater than that induced during fine pitch polishing.

The increase of Twyman distortion as a consequence of the depth of material removed was assessed on a single Zerodur sample. The Twyman distortion measured after varying depths were removed from the polished surface is given in Figure 124. It can be seen that the distortion increases during the first 12 μm of material removal, after which point little increase in Twyman distortion is seen. This suggests that the level of surface stress induced by this form of ductile mode grinding is discernible and consistent. After a 60 μm depth was removed from the sample the change of surface stress state, from the polished condition, was ~160 N/m.

6.2.5 Comparison of Surface Wave Velocity

The surface wave velocity of a ductile mode ground Zerodur sample was compared against a fine pitch polished surface. Figures 125 and 126 show radial scans of surface wave velocity for polished and ductile mode ground surfaces respectively. These figures show that the surface wave velocity of the polished surface was 3476 m s^{-1} and constant to + / - 1 m s^{-1} over the radius of the sample. The ductile ground sample exhibited a surface wave velocity of 3475 m s^{-1} at the outer diameter, down to 3469 m s^{-1} near the central regions of the sample. In comparison to the measurements

taken on the BK7 glass samples the difference between polished and ductile ground surfaces is less for the Zerodur samples.

6.2.6 Comparison of Nano-indentation Hardness

Three Zerodur samples were assessed for their surface hardness with the aim of gaining additional information regarding surface stress . Nano-indentation tests were carried out at 0.5, 2 and 10 mN applied load. Table 30 gives the mean hardness for each of the three samples.

Sample 50 was in the polished condition, sample 4 was ductile ground having 60 μm removed from its surface using the standardised grinding parameters. Sample 10 had 30 μm removed from its surface using the standardised grinding conditions.

The average penetration depth for each loading level is also given in Table 30 and it can be seen that this ranges from 60 nm - 300 nm. The suggestion from these hardness tests is that there is no statistical difference in mean hardness of the three samples. This suggests that the residual stress induced by the grinding was either, not significant enough to increase the measured hardness when measured by nano-indentation or that the induced residual stress is concentrated within a very thin layer, i.e. less than 60 nm.

6.2.7 Depth Assessment of Surface Stressed Layer

The ground surface of a Zerodur sample, which had 30 μm ductile ground from its polished surface, was etched in dilute aqueous ammonium bifluoride for 30 seconds. The surface removal rate of this mild etching operation had previously been calibrated and found to be 100 nm per minute. Therefore the etching operation removed approximately 50 nm.. The flatness of the unetched mounting surface was then re-assessed. It was found that the spherical distortion caused by the ductile grinding had been completely removed through the etching operation, indicating that the stressed surface layer was less than 50 nm in depth.

6.2.8 Observation of Sub-Surface Regions

To assess the depth which any sub-surface micro-fractures extended below the ground surface a sample was repeatedly polished, etched and observed using an optical microscope. The depth of material removal was calculated by measuring the change of mass of the sample before and after polishing.

It was found that the majority of the sub-surface fractures extended to a depth of less than 1.5 μm, see Figure 127. This optical micrograph shows little evidence of brittle fractures. However, less frequent micro-fractures were apparent up to a depth of 10 μm. This deeper but less widely distributed damage can be seen in Figure 128. The pattern effect of the damage supports the view that the dynamics of the NION machine motions have some influence.

6.3 Discussion of Ductile Mode Grinding

6.3.1 Roughness Quality of Ductile Mode Ground Surfaces

The most influential parameter on surface roughness was abrasive grain size. It was found that only brittle fractured surfaces having poor surface roughness could be obtained with the 6-12 μm grain size wheel. Whilst Namba has claimed to have used a wheel of this grain size to produce a ductile-like surface, his work used a cup wheel grinding mode and on relatively soft glasses.

The 3-6 μm grain size wheel produced good quality surfaces having ductile-like appearance. This grain size was that selected by Ball et al [87] as being the most useful since it produced good surface quality and offered a reasonable material removal rate. The material removal rate associated with the 1-2 μm grain size wheel was considered too low for the mode of grinding under assessment.

Ductile type surfaces were produced with both metal and resin bond grinding wheels of 3-6 μm grain size. Long term stability was better when using the metal bond wheel and the ELID dressing method.

The importance of depth of cut (d) in the range 0.5 - 1.5 μm was not significant. It was considered that a 1.5 μm depth of cut was the maximum for the 3-6 μm wheel since actual depth removed did not correspond to that applied to the machine when cuts larger than 1.5 μm were taken .

The importance of linear feedrate (V_l) in the range 0.025-0.1 mm s^{-1} was also not significant. Workhead velocity (V_w) was however an important parameter and strongly influenced the obtained surface roughness. V_w was most strongly effected by the grinding mode used, CSS or CRPM.

Grain size strongly influences the number of active grains in the grinding wheel and therefore controls the grain depth of cut, GDOC. The forming of the grinding wheel to have a shallow angle was do so to ensure that GDOC remained under the critical

depth suggested by Bifano's [75] work. The importance of the taper angle on the grinding wheel and its influence on GDOC is illustrated schematically in Figure 129.

Calculation of the number of active grains in the grinding wheel can be achieved by dividing the theoretical number of grains in the wheel by an active volume where a constant distribution of cube shape grains is assumed. In practice, however the amount of active grains at the surface of a "dressed" grinding wheel is significantly lower than that calculated. This lower level of active grains was established by assessing the surface of grinding wheels after dressing and grinding, see Appendix 1.

The angle chosen for the grinding trials carried out with the 3-6 μm grain size wheel was 0.24° providing a GDOC of approximately 25 nm, see Figure 129. As this wheel profile angle becomes smaller then a larger contact area is invoked between the wheel and workpiece. Larger contact regions lead to higher forces and therefore the permissible grinding force will need to be balanced against the GDOC value.

Achievable surface roughness on the optical glasses and the Zerodur was in the 1-3 nm Ra range. Surface roughness did however degrade towards the outer regions of the larger BK7 glass samples. This degradation towards the outer diameter was qualified by the slope of a graph of roughness against radial position and was in the 0.03-0.1 nm mm^{-1} range.

6.3.2 Material Removal Rates Available

The material removal rates for the ductile mode grinding of the optical glasses and Zerodur, when normalised for a 100 mm optic, were in the 0.75-1.5 mm^3 min^{-1} range. This value is for producing 1-3 nm Ra quality surface roughness and is close to that achieved by the polishing process working flat surfaces.

Optimisation of the chemical removal mechanisms of the ductile mode grinding technique could significantly increase the removal rate which has been achieved in these tests. Investigation of optimising the chemo-mechanical effects of ductile mode grinding is presently being investigated by Bifano.

A removal rate of $1mm^3$ min^{-1} can however be obtained using a grinding mode suitable for producing aspheric lens forms and with the application of water as a grinding fluid.

6.3.3 Induced Surface Stresses

The induced surface stress found on ductile mode ground Zerodur samples was limited to approximately 135 N/m as measured as a longitudinal surface stress. The depth of the surface stress is limited to approximately 50 nm. This very thin layer of surface stress is in-line with the findings of Golini and suggests rapid cooling of the surface causes contraction and hence stress at the surface. The material removal rate which gave rise to this stressed condition, normalised for a 100 mm optic, was 0.8 $mm^3\ min^{-1}$

For most optical aspheric lenses having diameter to thickness values of below 15-1, the level of residual surface stress induced would not cause significant form accuracy problems.

Nano-indentation tests did not provide useful information for surface stress assessment.

6.3.4 Sub-Surface Quality / Depth

The sub-surface quality of all the ground surfaces was not sufficiently high enough for their direct use as high quality visible wavelength optical elements. Whilst the surface roughness of ground samples was measured in the 1-3 nm Ra region, the regular pattern effect induced by the grinding process means that the surfaces would require some amount of post polishing. The pattern or machining 'lay" effects would in themselves only necessitate approximately 50 nm to be removed off the ground surface. However, the sub-surface micro-cracking extends between 2-10 μm. Therefore in order to make these ground surfaces acceptable as high quality optics this depth of material must be removed from the surface, using a low damaging polishing process.

The sub-surface micro-cracking is not a straight forward geometric function of the wheel and workpiece interface. The pattern of the sub-surface defects suggests that it is greatly influenced by the dynamic behaviour of the NION machine motions. Since the available GDOC value is limited to the 50 - 100 nm range is it important that the machines axes are very stable at the higher frequencies at which the grinding spindle operates. The operational frequency of the grinding spindle during these tests was 100 Hz, or 6000 rpm. Every effort went into balancing the grinding spindle using both, an accelerometer based dynamic analyser and the laser history from the NION machine's lasers. The stability of the linear axis of the machine was however in the 25-50 nm region at 100 Hz.

6.3.5 Conclusion of "ductile" Mode Grinding Glasses

A method of ductile mode grinding, using fixed abrasives on an ultra precision machine tool, can produce surface roughness qualities approaching that achieved with the polishing process i.e., 1-2 nm Ra. The associated material removal rate available using this technique is 0.75 - 1.5 mm^3 min^{-1} for a range of optical glasses.

The residual surface stress caused by this level of grinding compared to polishing is about 3 fold higher. The depth of this stressed layer is less than 50 nm, and should not preclude the use of ductile mode grinding in the production of optical surfaces.

The sub-surface conditions of the ductile ground surfaces were not comparable to high quality polished optical surfaces. In order to improve the functional quality of the ductile ground surfaces upwards of 2 microns would need to be removed using a less damaging process such as free-abrasive polishing.

The patterns which are created by the sub-surface micro-fractures, seen beneath the ductile ground surface, strongly suggest that the machine tool's dynamic behaviour is critical in determining the extend and amount of sub-surface micro-fractures.

The chemical removal methods associated with this process are of importance and optimisation through the use of different coolant media could increase the material removal rate and reduce the sub-surface damage.

CHAPTER 7

Conclusions and Recommendations for Further Work

7.1 NION Machine

The NION machine has a 10-12 nm P-V asynchronous error motion which permits surfaces of 8-10 nm P-V (~1 nm Ra) roughness to be diamond turned. This error motion is insensitive to workhead spindle speed and therefore this quality of surface roughness is readily achieved.

The high level of thermal control and the precision of machine motions permits form accuracy of ~100 nm to be achieved. The major contribution toward form error originates from the precision of the workhead spindle, principally through its level of synchronous axial error motion. The achievable form accuracy is however dependant on the operational speed of the workhead spindle. The NION machine's performance would be improved if a higher precision workhead spindle could be developed and fitted.

Static loop stiffness of the NION machine, in diamond turning mode, is 25% higher than any other diamond turning machine for which data are available. The dynamic stability of the machine's linear motions was influenced by the rotational speed of the workhead spindle. When in a grinding mode the stability of the Z axis carriage was influenced by the operation of the grinding spindle. This was the case even after the grinding spindle was balanced using an accelerometer to < 0.02 μm level.

To gain a better understanding of the NION machine's performance it would be useful to establish the static loop stiffness of the NION machine whilst set up in a grinding mode. More importantly, a detailed investigation of the dynamic stiffness / performance of the NION machine in both a diamond turning and grinding mode would allow the interaction of the sub-surface micro-cracking found in the machined samples and the NION machine's dynamic behaviour to be more clearly understood.

7.2 Diamond Turning Optical Surfaces in Brittle Materials

Diamond turning of optical surfaces directly into germanium has been found to be a viable process. The most influential machining parameter was feedrate. Tool cut distance was found to influence strongly the maximum feedrate which can be used to provide high quality surfaces which are free of noticeable surface fractures.

The term "ductile" mode turning when applied to cost effective machining of IR materials is somewhat mis-leading, since the generation and propagation of micro-fractures is a major mechanism in the overall material removal process. Material removal at the nose of diamond tools is by a mechanism which is thought not to be based on brittle mode fracture.

Application of a hydrocarbon based coolant improved tool life when cutting germanium. Material removal rates in the 2-4 mm/min range can be obtained when diamond turning germanium optics of 100 mm diameter. Tool life for producing optical surfaces at this machining rate is over 12 Km. Tool cut distance influenced both the induced surface residual stress and percentage of brittle fracture found on the machined surface. Crystal orientation prominently showed itself through the pattern made by the fractured regions on some machined samples. When useful IR optical surfaces are machined there is little practical influence of crystal orientation. Samples of germanium aligned to the <1 1 1> plane did indicate slightly lower levels of surface residual stress through lower amounts of Twyman distortion. Achievable surface roughness when diamond turning germanium is controlled by the machine tool performance, in the case of the NION machine surface roughness of below 1 nm Ra was obtained when assessed over 0.25 mm^2.

Diamond turning of silicon, to produce optical surfaces useful for IR elements, has also been shown to be possible. The maximum feedrate which can be employed is higher for silicon than for germanium when a new sharp tool is used. Tool wear associated with diamond turning silicon is much higher than that found on germanium. Tool wear takes place at the nose of diamond tools and this causes brittle fractures to propagate into the cut plane.

Twyman distortion associated with diamond turning silicon was found to be closely linked to both the measured tool forces and tool cut distance. Tool life was found to be less than 8 Km and available removal rates of 2-4 mm^3/min were obtained. Roughness quality was found to be the same as for germanium, ~1 nm Ra.

Diamond turning of zinc sulphide can produce functional optical surfaces to operate at IR wave-lengths. The polycrystalline nature of this material limits the achievable surface roughness to approximately 4 nm Ra. This material is more easily diamond turned to this quality than silicon or germanium permitting higher material removal

rates. Recent work has shown tool life to be higher for this material than associated with silicon and germanium.

Diamond turning of optical surfaces in glass materials for use at visible wave-lengths has not been shown to be commercially viable. The propagation of micro-fracture into the cut plane persisted even at very low material removal levels, i.e. low feedrates. Ductile mode removal of optical glass may well be possible, although this was not indicated during the investigations discussed in this thesis. However the available material removal rate will not be high enough for practical use to produce optical elements.

Diamond turning of aspheric and hybrid type IR optics has been demonstrated [113]. The tool costs for producing IR lenses made in zinc sulphide and optical germanium is found to be in the range 5-15 % of the overall cost of manufacture, for silicon however this is 25-35%.

The improved performance of the NION machine permits functional IR optics to be diamond turned to higher levels of precision than has previously been reported. The available material removal rate for diamond turning IR materials is in-line with that reported elsewhere.

To improve the process of diamond turning IR optics it is necessary to look more closely at the machining procedures that are employed. Using separate tools for bulk material removal, machining of base aspheric profiles and machining diffractive profiles should be considered. More rapid material removal rates could be offered when using larger tool radius particularly on zinc sulphide and germanium. Newly devised tool setting systems [114] permit tools to be precisely referenced with respect to each other, making it practical to have more than one tool employed in the machining sequence of a complex shape hybrid optic. Significant reductions in machining time will be available through reassessment of machining practices..

Investigation of the sub-surface qualities associated with diamond turned IR materials would prove useful to aid the optimisation of this process. Investigation of tool wear characteristics, particularly when diamond turning silicon, could lead to a reduction of the significant tooling costs. Assessment of the influence of different coolants / lubricants could prove important and be useful not only for machining of IR elements but also for the much larger "silicon" micro-electronics industry..

7.3 Diamond Grinding Optical Surfaces in Brittle Materials

The achievable surface roughness when diamond grinding optical glasses, using a fixed abrasive grinding technique that is suitable for the production of aspheric optics, is in the 1-3 nm Ra range. This quality of surface is determined by both the grinding process and the machine tool performance. The grinding parameter which was found to be most influential on the surface quality obtained was wheel grain size. Wheels containing grains smaller than 3-6 μm provided smooth ductile-like surfaces.

Surface assessments made of "ductile" ground glass did not reveal any indication of brittle micro-fracture. However, etching and polishing of ground Zerodur samples clearly showed that sub-surface fractures were present. The extent of the depth of sub-surface micro-fractures were in the range of 1-10 μm. The majority of micro-fracture extended to a depth of 1-2 μm. Less frequent micro-fractures where seen to extend up to 10 μm. These deeper fractures are considered to be associated with the NION machine's dynamic behaviour. Assessment of surface wave velocity gave useful information on the magnitude of sub-surface damage in the 1 - 10 μm range. This acoustic method is less painstaking than etching and polishing methods and is also non destructive.

The available material removal rate for 100 mm diameter optics was 0.5-1.5 mm^3/min when grinding BK7 glass. Limited grinding trials carried out on the less chemically durable LaSFN30 glass strongly suggest that the formation of a hydrated layer is highly influential in this "ductile" mode grinding process.

Limited levels of induced residual stress were found in samples of Zerodur ground to a 1 - 3 nm Ra roughness level. The majority of this surface stress was found to be contained in a surface layer of less than 50 nm.

Overall the quality of the "ductile" ground surfaces was not high enough for direct application to elements for use in high precision visible systems. For such systems post polishing methods would be needed removing a minimum of 2 μm and as much as 10 μm to remove all sub-surface defects.

The tooling costs of the ductile grinding process are considerably lower than those incurred by diamond turning. In the case of producing silicon IR optics, where surface roughness requirement is 20 nm Ra, diamond grinding could offer lower overall production costs. The direct grinding of IR silicon asphere and "hybrid" optics is now being pursued.

There is much research needed to optimise the direct grinding of optical surfaces. Establishing the level of sub-surface micro-fracture which is associated with the process of "ductile" grinding for a given grinding mode is very important. The optimum mode of grinding must be established. This will allow the true usefulness of the process for manufacturing optics and other components to be established. Defining the machine tool characteristics necessary to achieve this "process dictated" level of sub-surface damage is key to a more complete understanding.

Development of machines having higher dynamic stiffness than the NION machine but which have the same profiling motions is needed. Clearly, the NION machine's dynamic characteristics must firstly be clearly established.

The strong effect which chemical resistance of glass type has on the ductile mode grinding process needs further investigation. It is suggested by the limited grinding work on LaSFN30 glass that chemical mechanisms for forming hydrated layers, as found in polishing, have a significant influence. Selection of the optimum coolant fluid may have dramatic effects on the achievable material removal rates and the associated level of sub-surface damage. Further work in this particular area is continuing by both Bifano and Golini.

Developing a post polishing method to remove 1-2 microns from the surface of a "ductile" ground aspheric glass surfaces would reduce the cost of manufacturing such optics. This work is actively being pursued in industry .

Development of a quick, non destructive and low cost methods for assessing the extent of sub-surface micro-fracture in optical glasses would also be desirable.

REFERENCES

1 W. J. Smith, Modern Optical Engineering : The Design of Optical Systems, McGraw - Hill Inc. Printed USA 1966.

2 Zygo Precision Optics Catalogue 1986

3 Melles Griot Precision Optics Catalogue 1989

4 J. A. Clarke, Designing Optical Lenses to Exploit Available Asphere Technology, SPIE, Vol. 237, 1980, P184-188

5 A. Mann, Infrared Zoom Lenses in the 1990's, Optical Engineering, Jan 1994, Vol. 33 No.1, P109-115

6 A. I. Erko, et al , Fabrication and Tests of Multilayer Bragg-Fresnel X Ray Lenes, J Micro-Electronic Engineering, Vol 13 No.1-4, 1991, P335-338.

7 M. J. Riedl, Pre-design of Diamond Turned Refractive / Diffractive Elements for IR Objectives, SPIE, Critical Review, Vol. CR 41 08.

8 M. J. Riedl, J.T.McCann, Analysis and Performance Limits of Diamond Turned Diffractive Lenses for the 3-5 Micrometer Regions, SPIE, Critical Review, Vol. CR 38, April 1991.

9 W. Zschommler, Precision Optical Glass Working, SPIE, Vol. 472, 1984, P20.

10 D. F. Horne, Optical Production Technology, Adam Hilger, London, 1972.

11 E. Koike, et al, High Precision Machining of Aspheric Mirrors, 4th Biennial Nanotechnology Symposium, Warwick, Sept 1994.

12 S. Murakami, Development of Ultra-precision Grinding Machine for non-axisymmetric aspheric mirrors, 4th Biennial Nanotechnology Symposium, Warwick, Sept 1994.

13 G. F. Chapman, Recent Developments in the Generation of Glass Aspherical Surfaces, SPIE, Vol. 1015, 1988, P36-44.

14 K. Carlisle, P. Shore, Experiences in the Development of Ultra Stiff Aspheric Generators for "ductile" Mode Grinding Brittle Materials, Proc 6th IPES 1991, Springer-Verlag, P85-93.

15 Moore Machine Tool Co. Precision Turning and Grinding Machine Catalogue 1988.

16 Cranfield Precision Engineering Ltd. Nanocentre Machine Catalogue 1993.

17 M. T. Gale, Fabrication of Continuous-relief Micro-optical Elements by Direct Laser Writing in Photoresist, Optical Engineering, Vol. 33, 1994, P3556-3566

18 Personnel Dialogue, Cost Estimates Provided by Pilkington Optronics Ltd, Sept 1993.

19 T. Izumitani, Polishing, Lapping and Diamond Grinding, in Treatise on Material Sci and Tech, Vol 17, P115-170 Acad Press, New York 1979.

20 F. W. Preston, Journal of Society of Glasses, Vol 11, 1927, P214

21 L. M. Cook, Chemical Processes in Glass Polishing, Journal of Non-crystalline solids, Vol. 120, No. 1, P152-171

22 L. Holland. The Properties of Glass Surfaces, Chapman and Hall, London, 1966, P38-50.

23 LOH, Syncro-Speed Machine Catalogue, Frankfurt, Gremany, 1993.

24 Personnel Dialogue, Details Provided by Pilkington Optronics Ltd, Sept 1993.

25 R. E. Parks, Fabrication of infrared Optics, Optical Engineering, March 1994, Vol. 33 No.3, P685-691

26 Schott Glaswerke, Complete Glass Catalogue, 1989.

27 Schott Glaswerke, Zerodur "Precision from Glass Ceramics, 1992.

28 M. Weck, et al, Limits of Workpiece Accuracy Caused by Geometrical and Dynamic Behaviour of Ultra Precision Diamond Turning Machines, Proc UPT Conf. May 1988, P153-169.

29 D. H. Youden, Diamond Turning Achieves Nanometer Smoothness, Laser Focus World, Feb 1990,P105-115.

30 J. K. Myler, et al, High Quality Diamond Turning, SPIE, Vol 1333, 1990, P58-79.

31 J. B. Bryan, International Status of Thermal Error Research, Proc CIRP, Michigan, Sept 1967.

32 J. B. Bryan, Practical Solution to the Thermal Stability Problem in Machine Tools, Proc SME Pub #MR72-138, Int Conf Chicago, April 1972.

33 Y. Namba, et al, Ultra-precision Surface Grinder having a Glass-Ceramic Spindle of Zero Thermal Expansion, Annals of CIRP, Vol 38/1, P331, 1989.

34 G. Spur, et al, Thermal Behaviour Optimisation of Machine Tools, Annals of CIRP, Vol 37/1, P401, 1988

35 E. R. McClure, et al, Thermal Effects in Dimensional Metrology, ASME Report 65 Prod 13, July 1965

36 P. Shore, Design and Development of Precision Machine Tool Spindle, MSc thesis, Cranfield Institute of Technology, 1986.

37 ANSI / ASME, Doc B89.3.4M, Axis of Rotation. Methods for Specifying and Testing, 1985, and Annals of CIRP, Vol. 25/2, 1979

38 J.B. Bryan, Spindle Accuracy, American Machinist, Dec 1967, P149-164

39 W. B. Rowe, Hydrostatic & Hybrid Bearing Design, Butterworth, London, 1983, P136-138

40 M. Weck, Measurement and Evaluation Techniques for Machine Performance Testing, Tutorial notes, UME 3, Aarchen, Germany, May 1994.

41 Pioneer PDG 500/110 Series Capacitance Probe Operator Manual.

42 R. Donaldson, Simple methods for separating spindle error from test ball roundness errors, CIRP, Vol 21/1, 1987.

43 General Tests for Machine Tools Pt2, Statistical Methods of Determination of Accuracy and Repeatability of M/C Tools, BS3800, 1991.

44 W. J. Wills-Moren, et al, Some Aspects of the Design and Development of a Large CNC Diamond Turning Machine, Annals of CIRP, Vol. 31/1, P409, 1982.

45 K. Ueda, et al, Machining High Precision Mirrors using a Newly Developed CNC Machine, Annals of CIRP, Vol. 40/1, P555, 1991

46 W. J. Wills-Moren, The Design and Manufacture of a Large CNC Grinding Machine for Off axis Mirror Segments, CIRP Vol. 38/1/, 1989, P529-532.

47 J. Franse, et al, Dynamic Characteristics of the LLNL Precision Engineering Lathe, Proc ASPE, Atlanta, August 1988.

48 D. Thompson, Tighter Tolerances at Lower Costs, Mechanical Eng. September 1988, P36-42

49 Optoform 50 Product brochure, RTH Ltd, Leicester, England.

50 B. Kearney, Surface Replication, 3M Today Mag, Vol. 11, No7, 1994.

51 A. Kobayashi, Observation of Chip Producing Behaviour in Ultra-Precision Diamond Machining and Study of Mirror-like Surface Generating Mechanism, Precision Eng,Vol. 12 No.3, July 1990, P137

52 M. E. Merchant, Mechanics of the Metal Cutting Process, Applied Physics, Vol. 16,1945, P267-318

53 M. C. Gerchman, The effects of Fundamental Axial Spindle Motion on the Optical Performance of Diamond Turned Surfaces, Proc ASPE, Oct 1991, P74.

54 R.F.J. Read, SERC Report GR/C88450, R&D of Single Point Mono-crystal Diamond Tools and Diamond Machined Parts, 1986.

55 K. Carlisle, et al, Review of the Ultra-Precision Machining Research Facility, the "NION" machine, Proc UME3, May 1994, P89-93.

56 P. Hannah, D. Roaer, Basics of Diamond Turning, Proc One Day Workshop held Cranfield University 10th Oct 1988.

57 J. B. Bryan, LLNL, Report No. UCRL 92682 1985,Berkely, California.

58 A. E. Gee, Single Point Form Finishing of Glasses and Other Macroscopically Brittle Materials, SPIE Vol. 1573, 1991

59 M. C. Gerchman, B. E. McLain, Investigation of the Effects of Diamond Machining Germanium for Optical Applications, SPIE, Vol. 929, 1988, P94-96.

60 W. S. Blackley, R. O. Scattergood, Diamond Turning Brittle Materials, Proc. IPES 5, Sept 1989, P252-255.

61 P. N. Blake, R. O. Scattergood, Ductile Regime Machining of Germanium and Silicon, Journal Am.Ceram Soc, Vol 73, 1990, P949-957.

62 M. Tidwell, R. O. Scattergood, Analysis and Modelling of Diamond Turning of Brittle Materials, Proc. ASPE, 1991, P108-111.

63 D. A. Lucca, et al, Orthognal Ultra Precision Machining of Single Crystal Germanium, Proc ASPE, 1992, P211-213.

64 K. E. Puttick, et al, Single Point Diamond Machining of Glasses, Proc. R. Soc. London, A426, 1989, P19-30.

65 M. G. Schinker, Plasticity and Fracture Induced by Scratching Optical Glasses at High Speed, from "Strength of Inorganic Glass", Pub. Plenum, 1985, P115-132.

66 Y. Tani, et al, Optimisation of Single Point Turning of Optical Glass, SERC (UK) Report No. G/C 94544.

67 C. L. Chao, A. E. Gee, Material Removal Mechanisms in the Single Point Turning of Brittle Materials, Proc ASPE, 1992, P112-115.

68 D. B. Marshall, et al, The Nature of Machining Damage in Brittle Materials, Proc. R. Soc. London, A385, 1983, P461-475

69 B. R. Lawn, Measurement of Thin-Layer Surface Stress by Indentation Fracture, Journal Material Sci, Vol. 19, 1984, P4061-4067.

70 B. R. Lawn, Hardness, Toughness and Brittleness: An Indentation Analysis, Journal Am. Ceram Soc, Vol. 62, 1979, P347-349

71 B. R. Lawn, et al, A Model for Craack Initiation in Elastic/Plastic Indentation Fields, Journal Material Sci, Vol. 12, 1977, P2195-2199.

72 J. T. Hagan, Journal Material Sci, Vol. 15, 1980, P1417.

73 J. Franse, Aspects of Precision Grinding, PhD Thesis, 1991, University of Eindhoven.

74 S. S. Smith, et al, Fracture Toughness of Glass using the Indentation Fracture Technique, ASTM, 1981, P33-45

75 T. Bifano, Ductile-regime Grinding of Brittle Materials : Experimental Results and the Development of a Model, SPIE Vol. 966, 1988.

76 S. R. Saunders, et al, Proc. Workshop on Surface Hardness and Metrology, Eindhoven, 1994.

77 Y. Hara, et al, New Micro-Cutting Device with High Stiffness and Resolution, Annals of CIRP, August 1990.

78 H. Mairlot, The Texture of Ground Glass Surfaces, IDR, Feb 72, 61-68.

79 M. Miyashita, et al, Surface Grinding with a Newly Developed Grinding Machine, SME, MR82-930, 1982.

80 N. Brown, et al, Shear Mode Grinding, 43rd Sym on Freq Control, 1989.

81 K. L. Blaedel, et al, Ductile Grinding of Glass, OE Report, Dec 1990.

82 Y. Namba, et al, Ultra Precision Grinding of Inorganic Non-linear Crystals, JSPE, Vol 28 No.1 1994, P39-40.

83 T. Nakano, et al, Newly Developed Dressing Technology for Cutting Sialon Ceramics, Annals of CIRP, Vol. 38/1, 1989.

84 H. Ohmori, Electrolytic In-Process Dressing Grinding Technique for Ultra Precision Mirror Surface Machining, JSPE, Vol. 26, No. 4, Dec 1992.

85 A. Buttner, Electrolytic Dressing of Diamond Wheels for use in Steel Grinding, IDR, Nov 1969, P205-208.

86 M. Walter, ELID Dressing of Grinding Wheels, Proc.ASPE, 1993, P205-208.

87 M. J. Ball, N. Murphy, P.Shore, Electrolytically Assisted "Ductile" Mode Diamond Grinding of BK7 and SF10 Optical Glasses, SPIE, Vol. 1573, 1991, P30-38.

88 Y. Namba, et al, Ultra-Precision Surface Grinder Having a Glass Ceramic Spindle of Zero-Thermal Expansion, Annals of CIRP, Vol 38/1/1983.

89 P. Shore, State of the Art "Damage free" Grinding of Advanced Engineering Ceramics, British Ceramics Proc, Vol.46, 1990, P189-200.

90 J.Boettger, et al, Influence of Ductile Mode Grinding on the Strength of Silicon Based Ceramics, NIST Pub 847, July 1993, P353-358

91 I. Inasaki, Grinding of Hard and Brittle Materials, Annals of CIRP, Vol. 36 / 3, 1987.

92 M. K. Ker, The Strength Enhancement of Conventionally Ground Silicon Nitride Ceramics, PhD Thesis, Cranfield University, 1992.

93 D. Golini, Transition between Brittle and Ductile Mode in Loose Abrasive Grinding, SPIE, 1990, P80-91

94 D. G. Chetwynd, S. T. Smith, High Precision Stylus Profilometry, in From Instrumentation to Nanotechnology, J. W. Gardner and H. T. Hingle (eds) Gordon and Breach, London, 1991, 273-299.

95 K. Creath, Phase Shifting Interferometry Techniques, Prog in Optics, Elsevier Science, 1988, P357-373.

96 Nanostep Instrument, Precision1 Handbook, RTH Ltd, Leicester, England, 1993, P126

97 Digital Instruments, "Nanovations" Magazine, 1994, Vol. 1, No. 1.

98 A. J. Dalladay, Some Measurements of the Stress Produced at the Surfaces of Glass by Grinding with Loose Abrasives, Trans Opt Soc, London, Vol. 23, 170-173, 1922.

99 D. K. Bowen, Sub-Surface Damage, Assessment of Sub-Surface Damage for Nanotechnological Processing, Link DTI (UK) Report, July 1992.

100 Nanotest 500 product brochure, Micro-Materials Ltd, Wrexham,Wales

101 R. G. Sparks, M. A. Paesler, Micro-Raman Analysis of Stress in Machined Silicon and Germanium, Precision Eng.10 (4), 1988, P191.

102 Renishaw Raman Imaging Microscope brochure, Gloucester, Engand.

103 R. G. Sparks, et al, Microbeam Analysis, 1989, P149

104 K. E. Puttick, et al, Surface Damage in Nanoground Silicon, IMECHE, Tribology Seminar,10th April 1992.

105 K. E. Puttick, et al, Transmission Electron Microscopy of Nano-machined Silicon Crystals, Philosophical Mag, Vol. 69, No.1, 1994, P91-103.

106 A. Briggs, An Introduction to Scanning Acoustic Microscopy, Royal Microscopical Soc. Handbook 12, Oxford Press, 1985.

107 ~~A. Brigg~~s, et al, Non-Destructive Testing of Ceramics by Acoustic Microscopy, Br. Ceram Trans Vol. 88, 1989, P127-132.

108 P. Morantz, et al, Application of a Nanometric Resolution Optical Tool Setting System for Aspheric Generating, Proc. 7th IPES, May 1993, P314-317.

109 G. Box, S. Bisgaard, The Scientific Context of Quality Improvement, Quality Progress June 1987, P54-61.

110 D. DeBra, Design of Laminar Flow Restrictors for Damping Pneumatic Vibration Isolators, Annals of CIRP, Vol. 33/1, 1984.

111 W.S. Blackley, R. O.Scattergood, Crystal Orientation Dependence of Machining Damage- A Stress Model, Unpublished work.

112 W. S. Blackley, R. O. Scattergood, Ductile -Regime Machining Model for Diamond Turning of Brittle Materials, Precision Eng. Butterworth-Heinemann, 1991, P95-103.

113 P. Shore, Assessment of the Precision and Cost Effectiveness of Direct Machining "hybrid" Type Optical Surfaces for IR Applications, SPIE, Int Conf on Optical Fabrication, June 1995, Tokyo.

114 P. Morantz, A Nanometric Precision Non-Contacting Toolsetting System, Proc ASPE, October 1992.

Table 1 : Relative Cost of Advanced Optical Surfaces

(Costs obtained through [18])

Optical Surface	Estimated Cost (£)	Relative Cost (%)
Flat	250	100
Spheric	500	200
Asphere	1,250	500
Hybrid (diffractive)	5,000	2000

Table 2 : Removal Rates and Surface Quality for BK7 Glass

Process	Volumetric Removal Rate (mm^3/min)	Depth Removal Rate (mm/min)	Typical Processing Time (min)	Resulting Surface Finish (nm Ra)
Polishing (from lapped)	2	0.0003	30	0.5
Lapping	117	0.015	1	300

Table 3 : Properties of Important IR materials

(Cost is based on 50 mm diameter lenses, batch size of 5)

Material	Hardness Vickers GPa	Density g/cm^3	Young's Modulus GPa	Fracture Toughness x 10^6 $N/m^{3/2}$	Approx. Cost £/cm3
Germanium (mono)	9	5.32	128	0.46	7.85
Silicon+ (mono)	10	2.32	159	0.6	2.25
Zinc Sulphide* (clear)	1.9	4.08	74.5	0.8	8.60
Zinc Selenide*	1.1	5.27	67.2	0.5	8.30

Table 4 : Mechanical and Optical Properties of Some Important Glass and Ceramic materials

(Cost is based on 50 mm diameter lenses, batch size of 5)

Material	Hardness Vickers GPa	Density g/cm^3	Young's Modulus GPa	Fracture Toughness $x\ 10^6$ $N/m^{3/2}$	Approx. Cost £/cm3
BK7	6.7	2.51	81	1.0	0.65
SF10	4.57	4.28	64	~ 0.9	1.25
LaSFN30	7.9	4.46	124	~ 0.9	0.72
Zerodur	6.3	2.53	90.3	1.0	1.95

Table 5 : Thermal and Chemical Properties of Important Glass/Ceramic materials

[Data obtained from Schott]

Material	Thermal Co. Expansion $10^{-6}/K$	Softening Temp. C^o	Acid Resistance class (SR)	Water Resistance class (CR)
BK7	7.7	559	1	2
SF10	7.5	454	1	1
LaSFN30	5.9	599	4	1
Zerodur	0.02	515	1	1

Table 6 : Calculated Critical Depth (d_c) According to Equation 2.9 for Some Optical Glasses & Zerodur

Material Type	Critical Depth ($\mathbf{d_c}$) nm
BK 7	39
SF 10	81
LaSFN30	30
Zerodur	54

Table 7 : Theorectical Rayleigh Wave Velocities

Material Type	Rayleigh Wave Velocity Vr (m/second)
BK 7	3334
SF 10	2463
Zerodur	3789

Table 8 : Test samples for Diamond Turning Trials

Material	Crystal Structure	Supplier	Sample size
Optical Germanium	mono <111,100,110>	Eagle Picher	∅32mm x 3mm
Silicon	mono <111>	Eagle Picher	∅32 mm x 3mm
Silicon	polycrystalline	Lattice	∅32 mm x 3mm
Zinc Sulphide	polycrystalline	Lattice	∅ 32mm x 10mm
BK7 glass	amorphous	Pilkington	∅ 32mm x 25mm

Table 9 : Test samples for Diamond Grinding Trials

Material	Material Structure	Supplier	Sample size
BK7	Amorphous	Pilkington	∅50mm x 25mm
SF10	Amorphous	Pilkington	∅50 mm x 25mm
LaSFN30	Amorphous	Schott	∅50 mm x 25mm
Zerodur	polycrystalline	Schott	∅32mm x 3mm

Table 10 : Grinding Wheel Specifications

Grain size (μm)	Bond Type	Concentration
1-2	Resin	40
3-6	Cast Iron	75
6-12		

Table 11 : Machining Parameters for Glass Grinding Tests

Depth of Cut (d) µm	X axis Feed rate (V_r) µm/sec	Workspindle Speed (V_w)
0.5, 1, 1.5, 2	25, 50,75, 100	25, 50, 100 mm/sec (css)
		62 & 125 rpm (crpm)

Table 12 : Fixed Machining Parameters for Grinding Zerodur™

Depth of Cut (d)	0.0015mm
Feedrate (Vf)	0.075 mm/second
Workspindle Speed (Vw)	62 rpm (constant rpm mode)
Grinding Wheel Type	D3-6 C75 N4
Grinding Speed (Vs)	40 metres / second
Dressing Type	ELID

Table 13 : Machine Synchronous Axial Error Motion / Workhead Speed

Workhead Spindle Speed (rpm)	Synchronous Axial Error (nm)	Movement of Z axis to base (nm)
500	100	40
600	60	25
750	160	100
800	80	30
1000	85	35

Table 14 : Machine Asynchronous Axial Error Motion / Workhead Speed

Workhead Spindle Speed (rpm)	Asynchronous Axial Error (nm)
500	20
600	12
750	20
800	15
1000	15

Table 15 : Results of Matrix 1 Optical Germanium, 111 orientation. Surface Roughness, % Surface Fracture and Distortion

Sample No.	Feed µm/rev	Tool Rad (mm)	Coolant	Surface Texture Ra [p-v] nm	% Surface Fracture	Tool Cut Distance (Km)	Twyman Distortion (nm)
1	12	0.5	on	8.53 [59.3]	25	1.27	+150
3	4	0.5	on	3.74 [21.7]	-	6.57	-338
4	4	0.5	off	5.50 [76.7]	75	8.98	-356
6	4	2	on	2.66 [15.6]	2	2.08	+100
7	12	2	off	8.15 [56.0]	60	5.16	-250
8	12	2	on	7.89 [52.0]	70	5.49	-259

Table 16 : Results of Matrix 1 Optical Germanium, 100 orientation. Surface Roughness, % Surface Fracture and Distortion

Sample No.	Feed µm/rev	Tool Rad (mm)	Coolant	Surface Texture Ra [p-v] nm	% Surface Fracture	Tool Cut Distance (Km)	Twyman Distortion (nm)
1	4	0.5	on	2.24 [12.0]	5	2.48	-50
2	12	0.5	on	13.0 [74.2]	45	5.16	-612
3	4	0.5	off	11.2 [66.7]	-	8.98	-681
5	12	2	on	3.15 [26.2]	5	2.68	+97
6	4	2	on	13.2 [85.3]	50	3.48	-262
7	12	2	off	10.4 [89.6]	60	3.82	-440
8	12	2	on	9.55 [67.6]	50	4.15	-336

Table 17 : Results of Matrix 2 Optical Germanium, 111 orientation. Surface Roughness, % Surface Fracture and Distortion

Sample No.	Depth of Cut (μm)	Tool Radius (mm)	Top Rake deg°	Surface Texture Ra [p-v] nm	% Surface Fracture	Tool Cut Distance (Km)	Twyman Distortion (nm)
11	2.5	0.5	-25	4.89 [83.5]	30	3.48	-205
3	5	0.5	-25	3.74 [21.7]	-	6.57	-338
5	2.5	2	-25	0.92 [5.85]	0	1.27	+217
6	5	2	-25	2.66 [15.6]	2	2.08	+100
9	2.5	0.5	-5	7.49 [53.0]	55	2.01	+172
10	5	2	-5	4.78 [41.7]	20	2.01	+360

Table 18 : Results of Matrix 2 Optical Germanium, 100 orientation. Surface Roughness, % Surface Fracture and Distortion

Sample No.	Depth of Cut (μm)	Tool Radius (mm)	Top Rake deg °	Surface Texture Ra [p-v] nm	% Surface Fracture	Tool Cut Distance (Km)	Twyman Distortion (nm)
6	5	2	-25	13.2 [85.3]	50	3.48	-262
1	5	0.5	-25	2.24 [12.0]	5	2.48	-50
9	2.5	0.5	-5	7.32 [58.1]	20	1.01	+117
10	5	2	-5	1.64 [8.69]	0	1.01	+315
4	2.5	0.5	-25	11.3 [79.6]	55	10.18	- 821

Table 19 : Results of Matrix 3 Optical Germanium, 111 orientation. Surface Roughness, % Surface Fracture and Distortion

Sample No.	Top Rake deg °	Depth of Cut (μm)	Work Speed (RPM)	Surface Texture Ra [p-v] nm	% Surface Fracture	Tool Cut Distance (Km)	Twyman Distortion (nm)
12	-5	5	600	7.68 [49.1]	20	4.02	+290
13	-25	10	600	6.95 [58.7]	30	2.21	-392
14 -	-25	5	600	11.3 [81.3]	40	5.03	-454
10	-5	5	1200	4.78 [41.7]	20	2.01	+360
6	-25	5	1200	2.66 [15.6]	2	2.08	+100

Table 20 : Results of Matrix 3 Optical Germanium, 100 orientation. Surface Roughness, % Surface Fracture and Distortion

Sample No.	Top Rake deg °	Depth of Cut (μm)	Work Speed (RPM)	Surface Texture Ra [p-v] nm	% Surface Fracture	Tool Cut Distance (Km)	Twyman Distortion (nm)
13	-25	5	600	12.1 [88.7]	65	3.22	-432
12	-25	10	600	9.21 [57.5]	70	1.21	-413
11	-5	5	600	2.97 [17.1]	5	3.02	+217
10	-5	5	1200	1.64 [8.69]	0	1.01	+315
6	-25	5	1200	13.2 [85.3]	50	3.48	-262

Table 21 : Results of Optical Germanium, 110 orientation.
Surface Roughness, % Surface Fracture and Distortion

Sample No.	Feed µm/rev (mm/min)	Depth of Cut (µm)	Surface Texture Ra [p-v] nm	% Surface Fracture	Tool Cut Distance (Km)	Twyman Distortion nm
1	2 (2.4)	2.5	2.16 (8.76)	0	1.9	+120
2	2 (2.4)	1	1.41 (6.54)	0	4.28	+80
-3	1 (1.2)	1	1.91 (8.45)	0	8.63	-
4	1 (1.2)	10	1.82 (8.47)	0	11.71	+100

Table 22 : Results of Silicon Sample 1, 111 orientation.
Machining Forces, % Surface Fracture and Distortion

Assessment No.	% Surface Fracture	Tool Cut Distance (Km)	Twyman Distortion (nm)	Normal Force Fn (Newton)	Cutting Force Fc (Newton)
1	0	1.6	-50	0.11	0.12
2	0	2.8	-	0.23	0.13
3	0	3.7	-180	0.42	0.15
4	0	5.8	-250	0.73	0.16
5	5	8.2	-270	1.19	0.2

Table 23 : Results of Silicon Sample 2, 111 orientation.
Machining Forces, % Surface Fracture and Distortion

Assessment No.	% Surface Fracture	Tool Cut Distance (Km)	Twyman Distortion (nm)	Normal Force Fn (Newton)	Cutting Force Fc (Newton)
1	0	0.53	-100	0.04	0.02
2	0	2.39	-	0.1	0.04
3	0	6.58	-350	0.3	0.12
4	0	9.58	-	0.46	0.12
5	5	12.10	-1330	0.77	0.17

Table 24 : Results of Germanium Sample 1, 111 orientation.
Machining Forces, % Surface Fracture and Distortion

Assessment No.	% Surface Fracture	Tool Cut Distance (Km)	Twyman Distortion (nm)	Normal Force Fn (Newton)	Cutting Force Fc (Newton)
1	5	1.2	+180	0.03	0.02
2	5	2.4	+195	0.045	0.03
3	5	3.6	+190	0.045	0.03
4	5	4.8	+217	0.05	0.035
5	5	6.8	+208	0.05	0.035
6 (*)	0	8.4	+220	0.045	0.03
7 (**)	3	9.6	+220	0.045	0.03
8 (*)	0	11.2	+225	0.055	0.04

Table 25 : Comparison Relative Level of Critical Parameters
(Normalised to Zinc Sulphide)

Material.	P* critical applied load	C* critical crack length	dc critical penetration depth
Zinc Sulphide	1	1	1
BK7 glass	0.02	1.02	0.165
Silicon	0.002	0.03	0.008

TEST	SAMPLE	GRIT SIZE (μm)	CONCEN-TRATION	BOND	WORK SPEED	FEEDRATE (μm/sec)	DEPTH OF CUT (μm)	Ra at 8mm (nm)	Ra Slope (nm/mm)
1	SF10 1	6 - 12	40	RESIN	50mm/s CSS	50	2	1050	-
2	SF10 2	6 - 12	40	RESIN	50mm/s CSS	25	2	870	-
3	SF10 3	6 - 12	40	RESIN	50mm/s CSS	25	1	930	-
4	SF10 4	3 - 6	75	METAL	25mm/s CSS	50	1	4.08	0.1679
5	DEDF 1	3 - 6	75	METAL	25mm/s CSS	50	1	4.05	0.1333
6	BK7 1	6 - 12	40	RESIN	50mm/s CSS	50	2	1510	-
7	BK7 2	6 - 12	40	RESIN	50mm/s CSS	25	1	550	-
8	BK7 3	3 - 6	75	METAL	25mm/s CSS	50	1	-	-
9	BK7 4	3 - 6	75	RESIN	25mm/s CSS	75	1	3.16	0.1008
10	BK7 5	3 - 6	75	RESIN	100mm/s CSS	75	1	1.59	0.0971
11	BK7 6	3 - 6	75	RESIN	100mm/s CSS	100	1	-	-
12	BK7 7	3 - 6	75	RESIN	100mm/s CSS	75	1	-	-
13	BK7 8	3 - 6	75	RESIN	100mm/s CSS	75	1	-	-
14	BK7 9	3 - 6	40	RESIN	25mm/s CSS	50	1	-	-
15	BK7 10	3 - 6	40	RESIN	25mm/s CSS	75	1	2.5	0.1384
16	BK7 12	3 - 6	40	RESIN	125rpm CRPM	75	1	-	-
17	BK7 13	3 - 6	40	RESIN	125rpm CRPM	75	1	-	-
18	BK7 14	3 - 6	75	METAL	25mm/s CSS	100	2	2.79	-
19	BK7 15	3 - 6	75	METAL	25mm/s CSS	75	1	1.87	0.1811
20	BK7 16	3 - 6	75	METAL	125rpm CRPM	75	1	8.69	0.4742
21	BK7 17	3 - 6	75	METAL	125rpm CRPM	75	1	5.58	0.4535
22	BK7 18	3 - 6	75	METAL	125rpm CRPM	100	1	7.40	0.4459
23	BK7 19	3 - 6	75	METAL	25mm/s CSS	75	1	6.42	0.9806
24	BK7 20	3 - 6	75	METAL	62rpm CRPM	75	1	-	-
25	BK7 21	3 - 6	75	METAL	62rpm CRPM	75	1.5	2.57	0.0546
26	BK7 22	3 - 6	75	METAL	62rpm CRPM	75	1.5	1.82	0.0540
27	BK7 23	3 - 6	75	METAL	62rpm CRPM	75	1.5	-	-
28	BK7 25	3 - 6	75	METAL	62rpm CRPM	75	1.5	-	-

CSS : constant surface speed → V_w = constant
CRPM : constant workhead spindle speed

Table 26 : Machining Parameters and Surface Roughness
Grinding of BK7 and SF10 Glasses

Table 27 : Grinding Mode, Wheel Bond and Surface Wave Velocity of Ground BK7 Glass Samples

Sample No.	Wheel Bond	Grinding Mode	Average Azimuthal Velocity (m/s)
BK7 # 4	Resin	CSS	3357.5
BK7 # 14	Metal	CSS	3356.0
BK7 # 15	Metal	CSS	3355.5
BK7 # 17	Metal	CRPM	3355.0
BK7 # 18	Metal	CRPM	3353.0
BK7 # 19	Metal	CSS	3362.0
BK7 # 28	-	Polished	3368.0

Table 28 : Twyman Distortion / Longitudinal Surface Stress of Etched Zerodur

Sample	Distortion (nm) P-V	Longitudinal Surface Stress N/m
101	-101	35.6
102	-116	40.9
103	-140	49.4
104	111	-39.1
105	-127	44.8
106	-130	45.8

Table 29 : Twyman Distortion / Longitudinal Surface Stress of "Ductile" Ground Zerodur

Sample	Distortion (nm) P-V	Longitudinal Surface Stress N/m
31	-516	182
32	-376	132
33	-352	124
34	-349	132
35	-375	142
36	-475	180

Table 30: Nano-indentation Hardness Results on Ductile Ground and Polished Zerodur

Sample	Load mN	Hardness GPa	σ	Mean Penetration nm
4 (ground)	2	6.92	0.26	150
	10	6.27	0.23	325
10 (ground)	0.5	7.23	0.62	60
	2	6.90	0.57	150
	10	6.52	0.38	325
50 (polished)	0.5	8.02	0.92	60
	2	7.04	0.25	150
	10	6.62	0.62	325

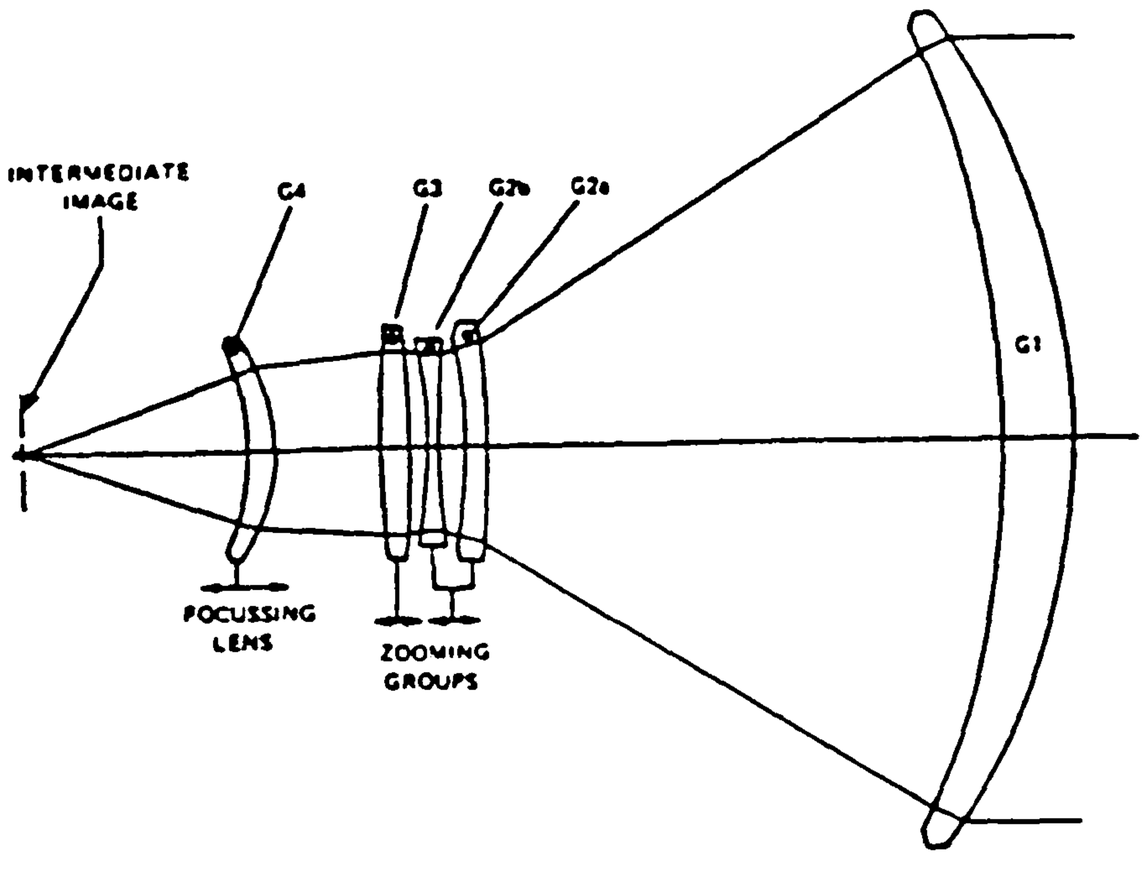

Figure 1 : Schematic of Aspheric Element Based Optical System [5]

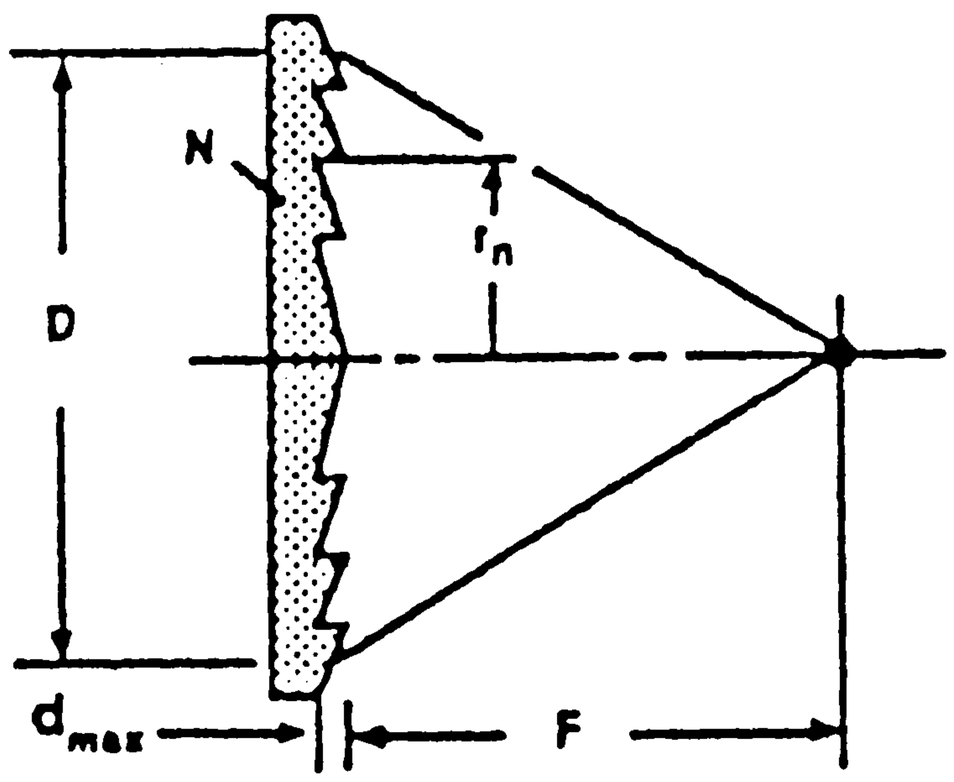

Figure 2 : Schematic of Diffractive "Binary" Element

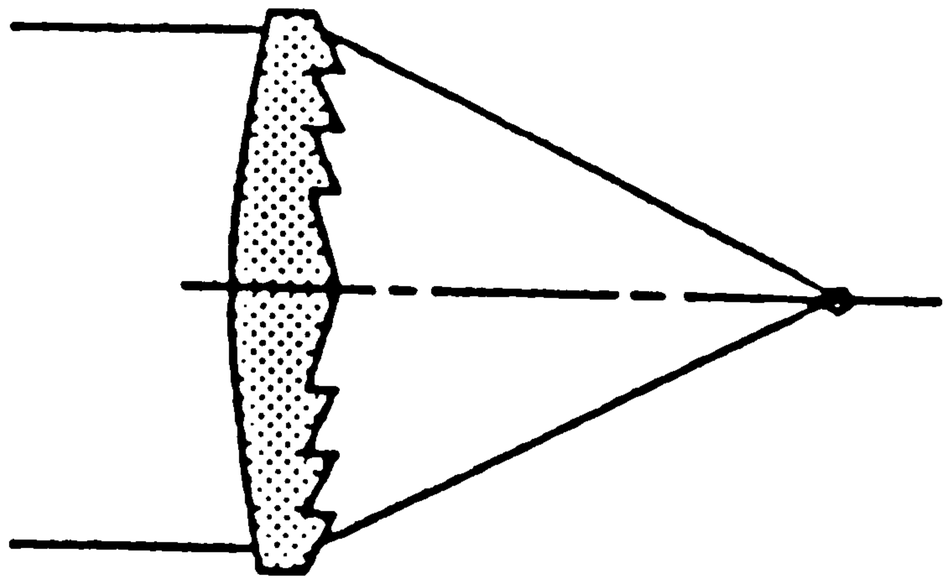

Figure 3 : Schematic of "Hybrid" Type Optic

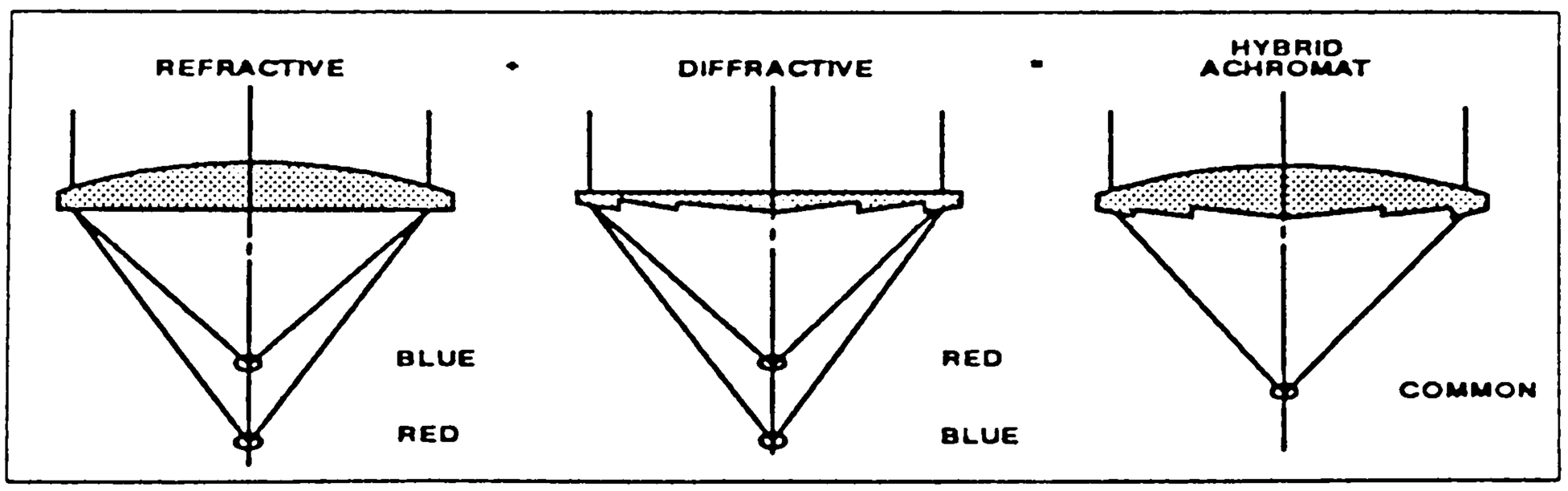

Figure 4 : Chromatic Correction using Diffractive and Refractive Surfaces [7]

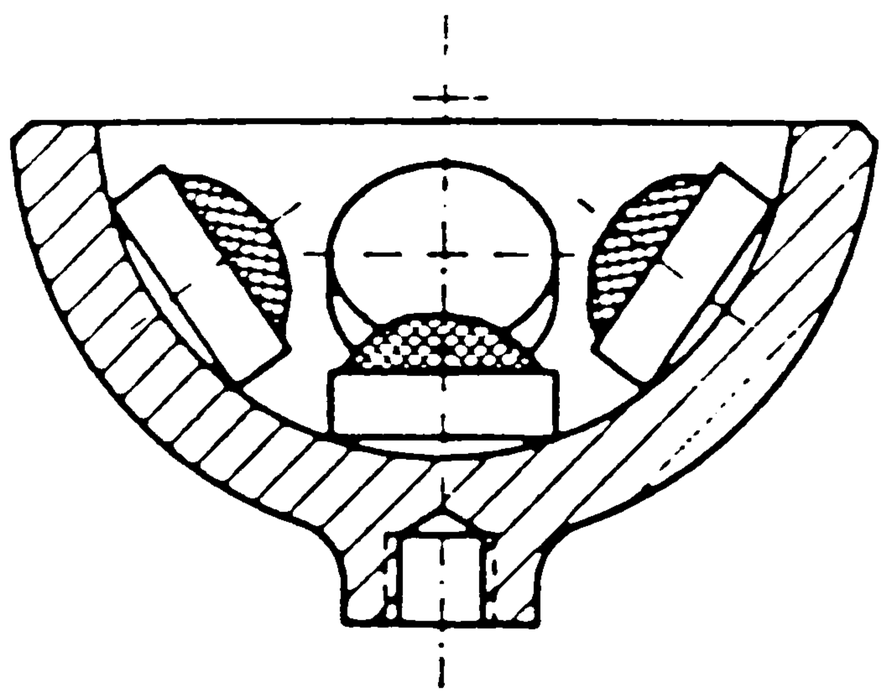

Figure 5 : Schematic of "Laying in" Shell

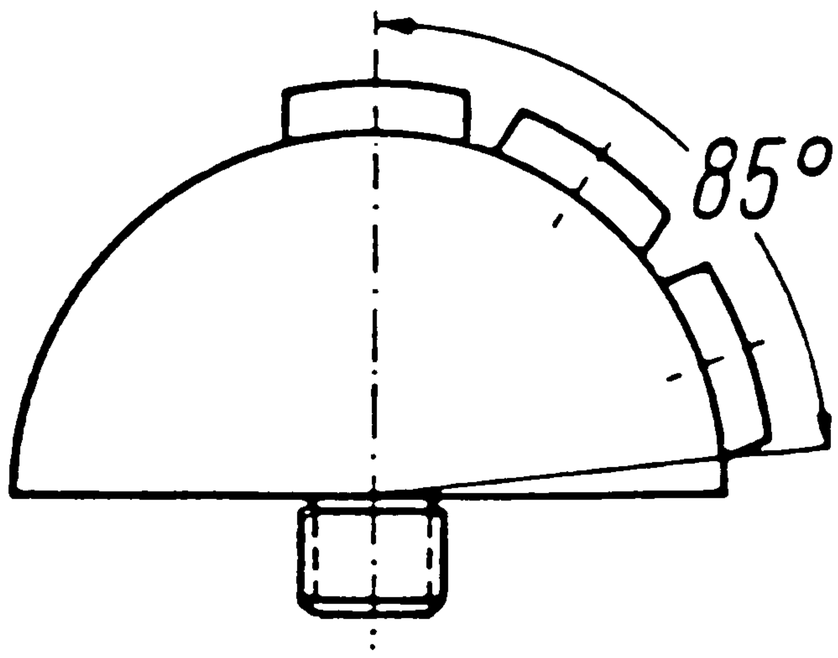

Figure 6 : Schematic of Blockholder

Figure 7 : "Lever Arm" Polishing Machine [10]

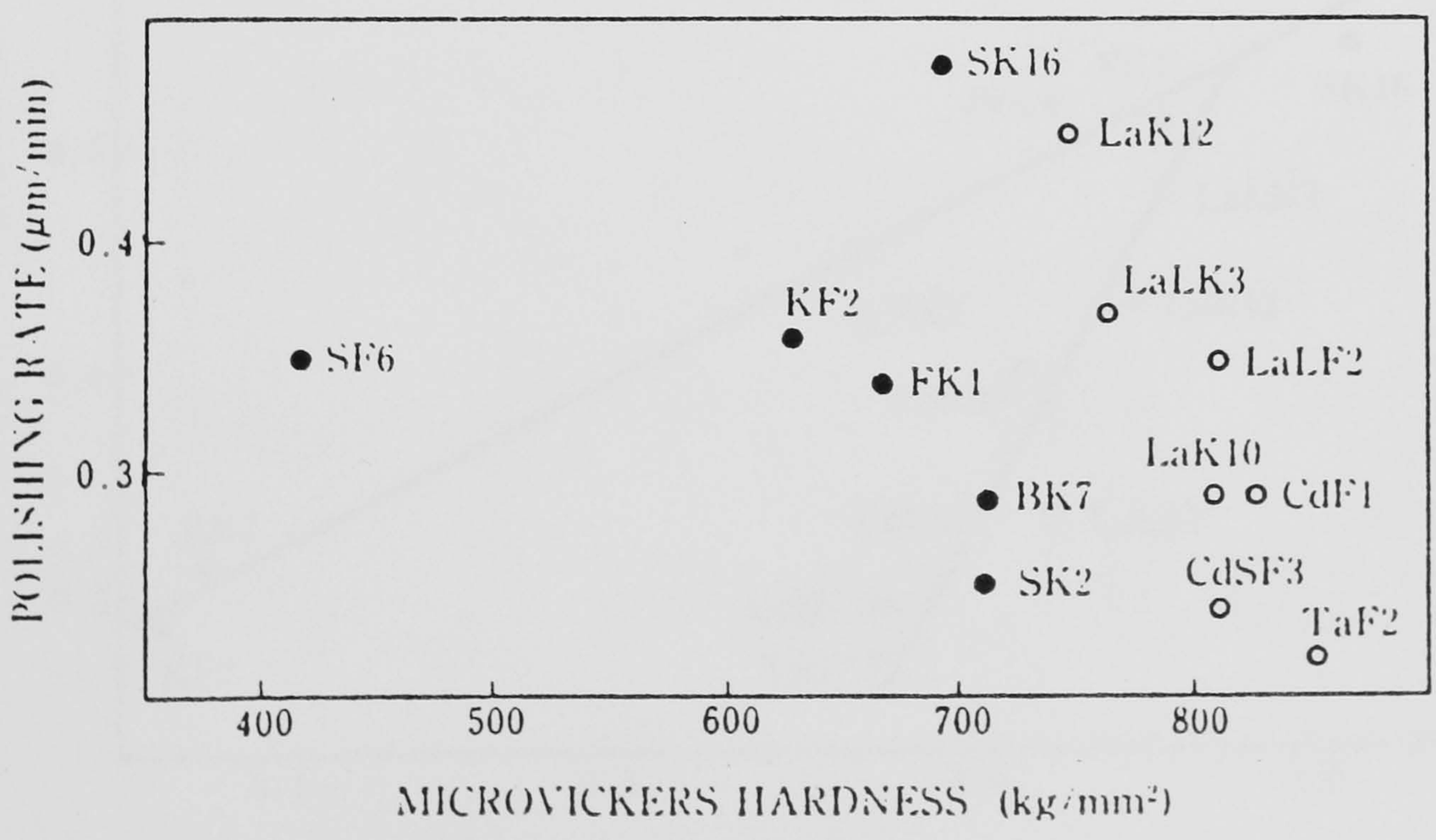

Figure 8 : Hardness / Polishing Rate Graph [19]

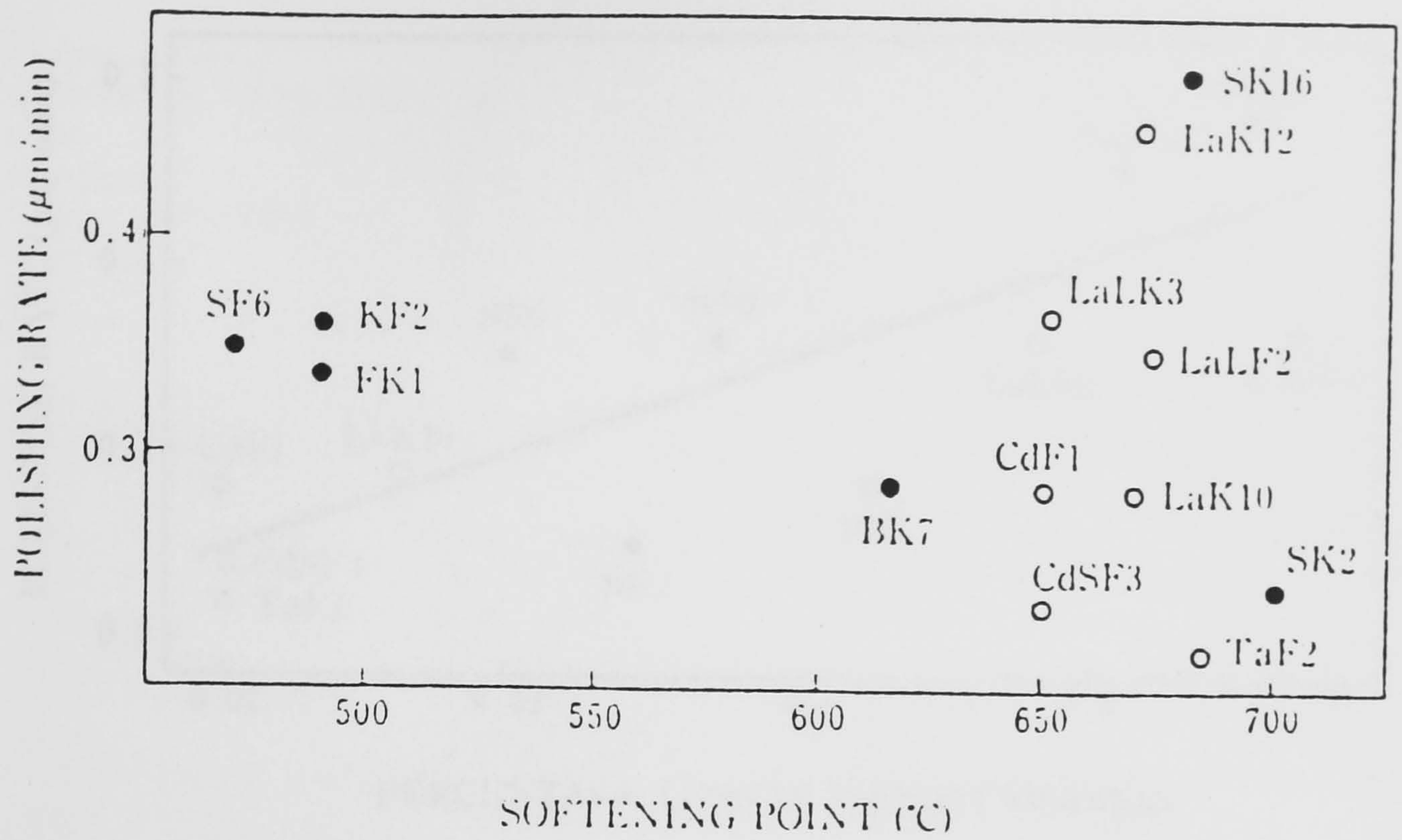

Figure 9 : Softening Temperature / Polishing Rate Graph [19]

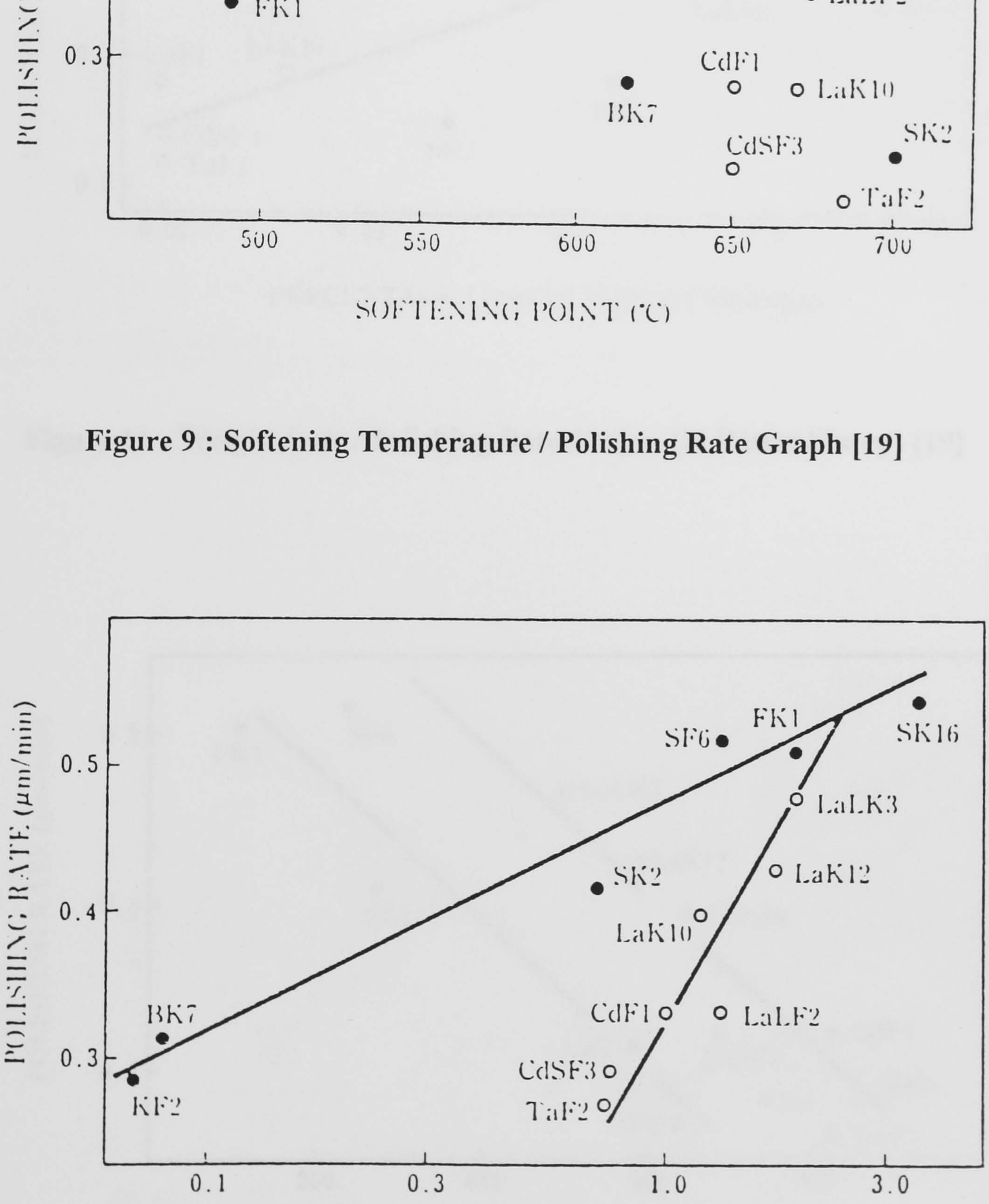

Figure 10 : Weight Loss / Polishing Rate Graph (in Nitric Acid) [19]

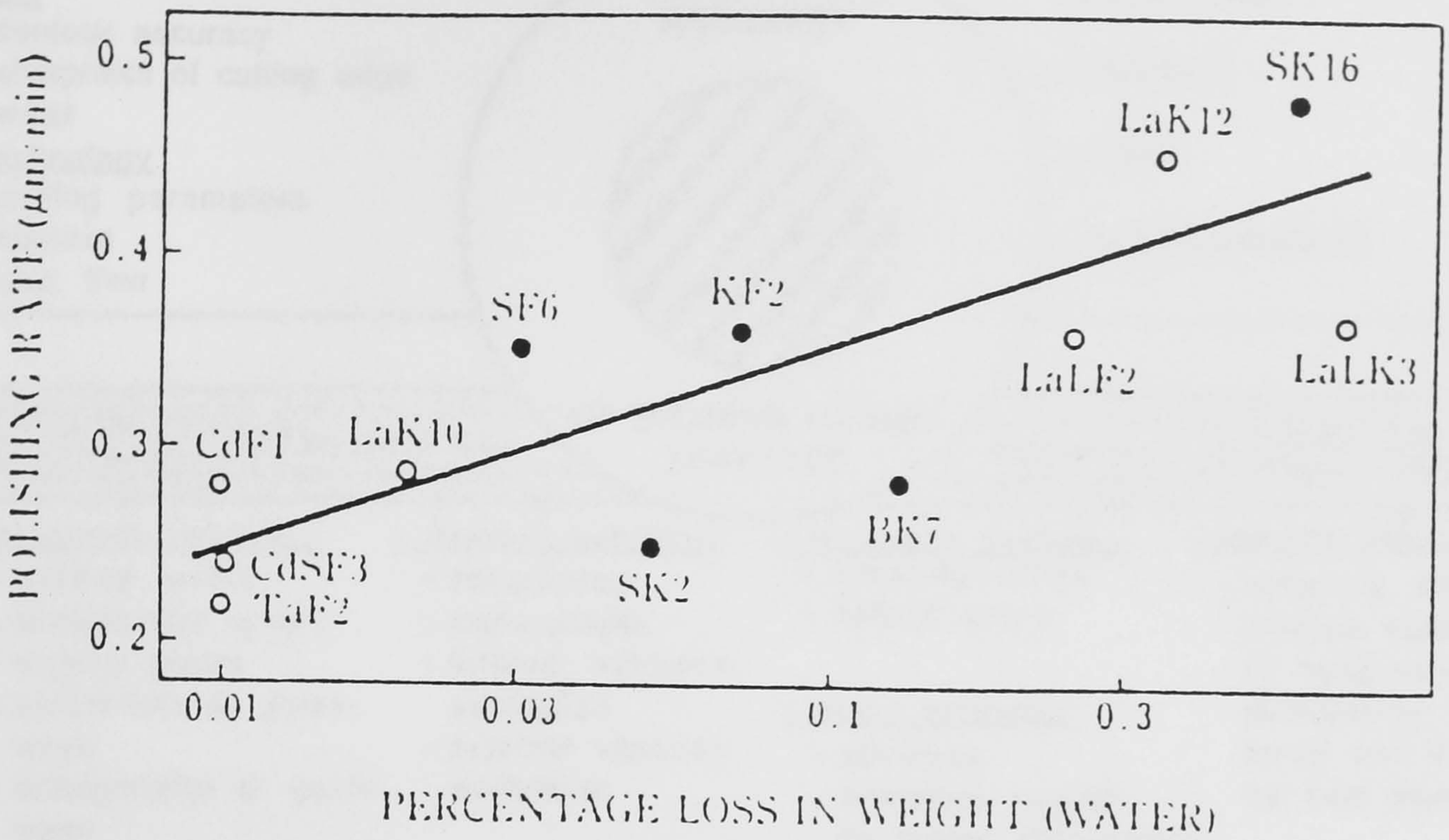

Figure 11 : Weight Loss / Polishing Rate Graph (in Water Slurry) [19]

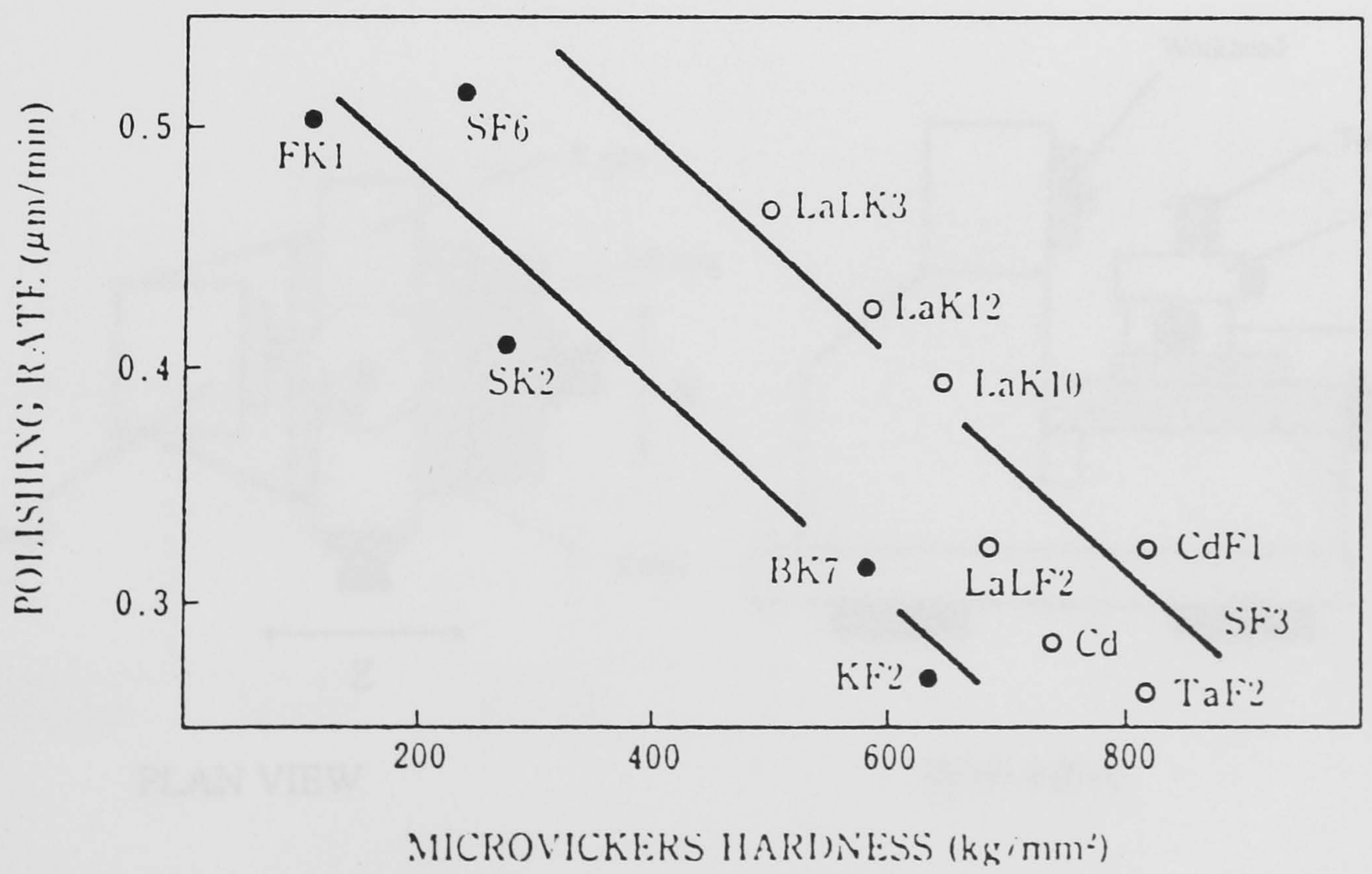

Figure 12 : Hardness of "Hydrated" Layer / Polishing Rate [19]

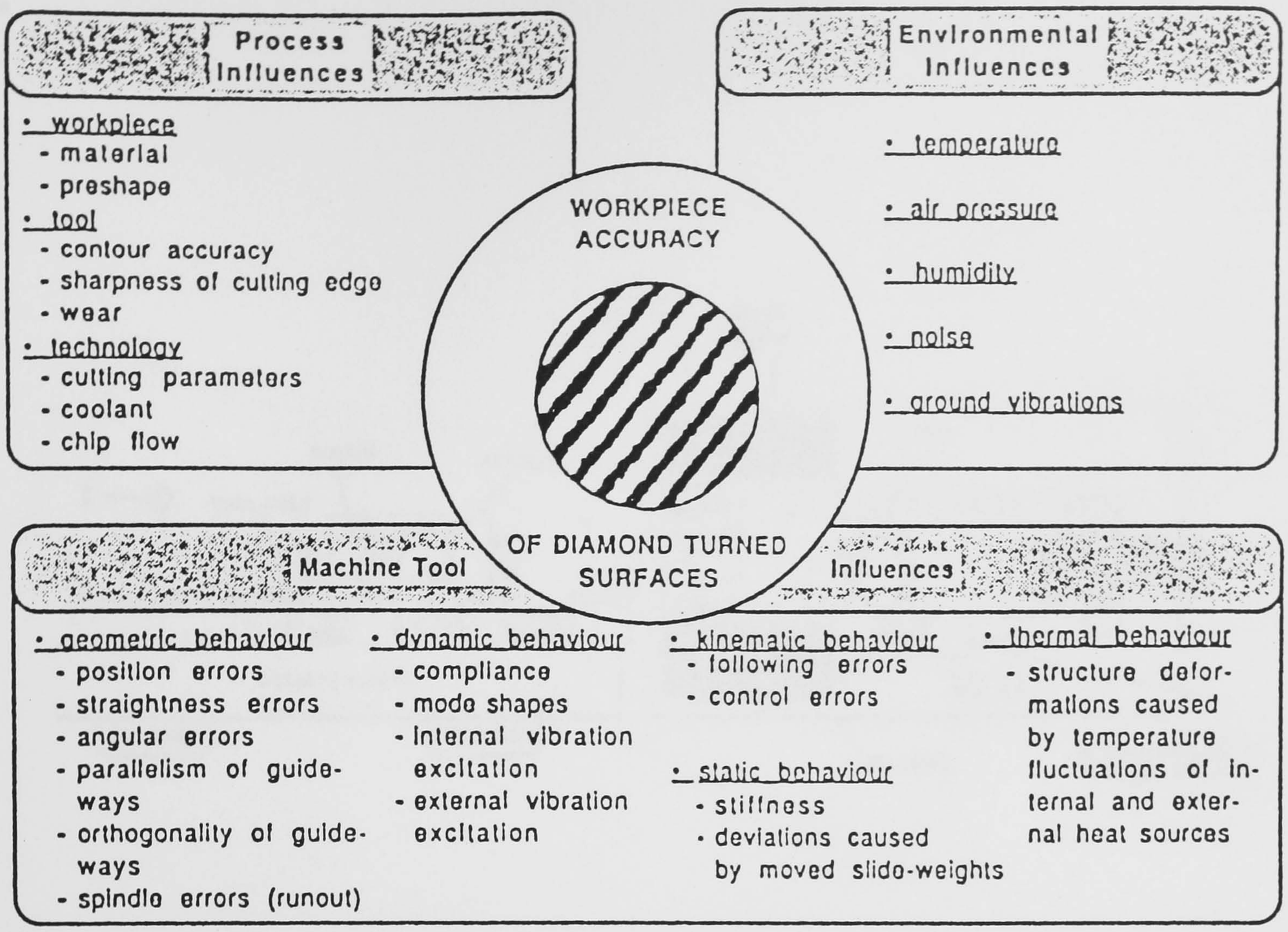

Figure 13 : Influences on Component Quality [28]

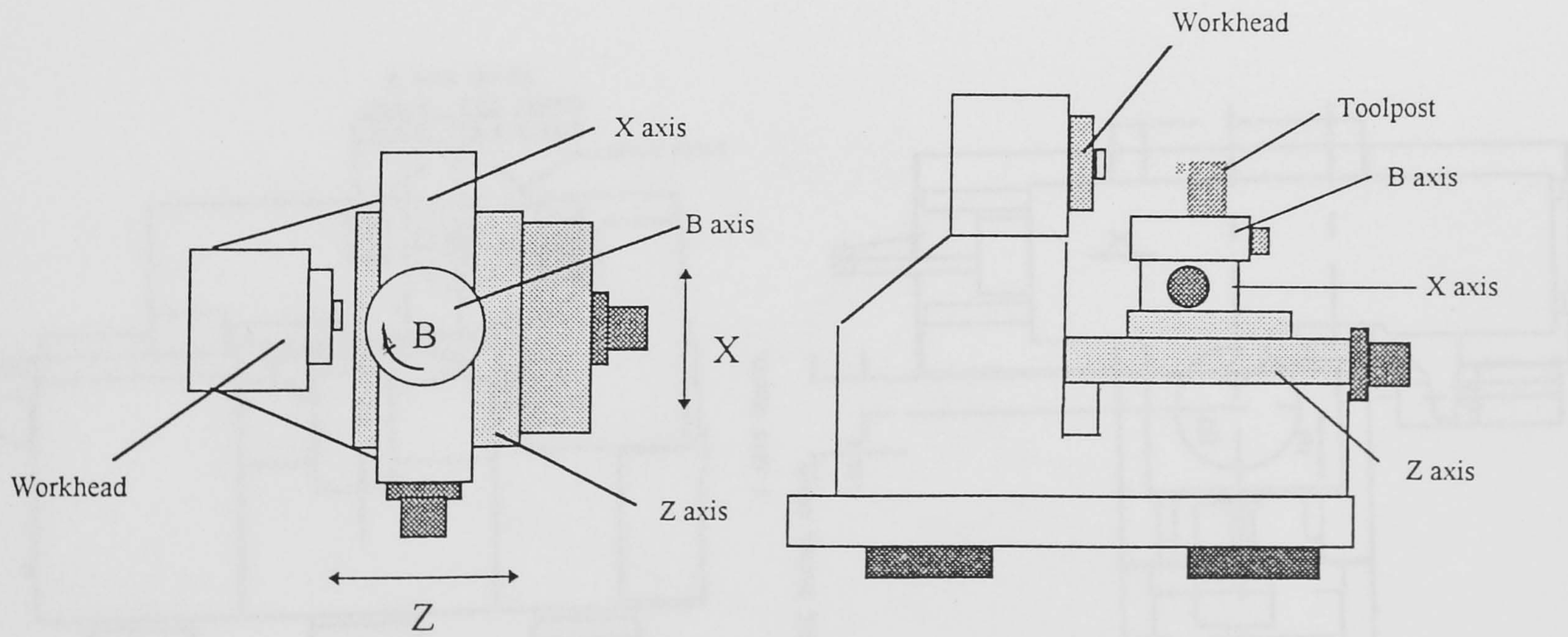

Figure 14a : Various Lay Out's of Aspheric Generators

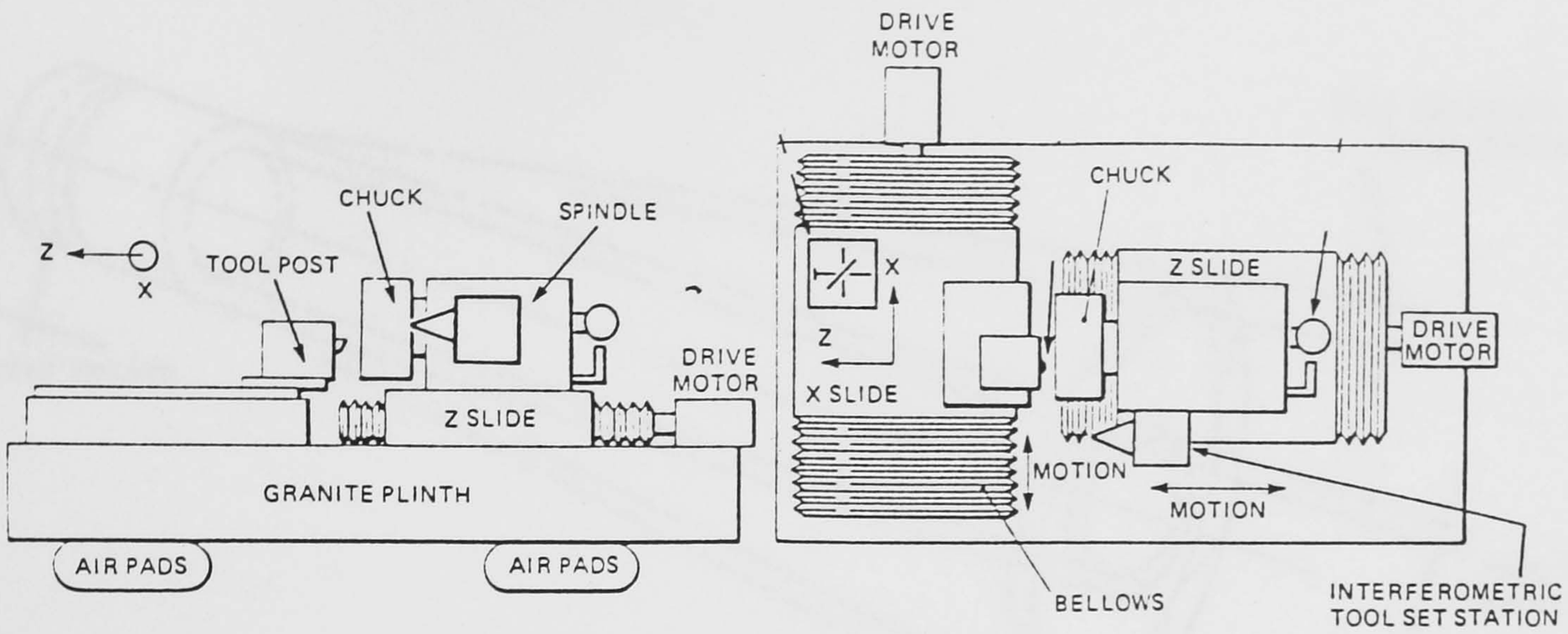

Figure 14b : Various Lay Out's of Aspheric Generators

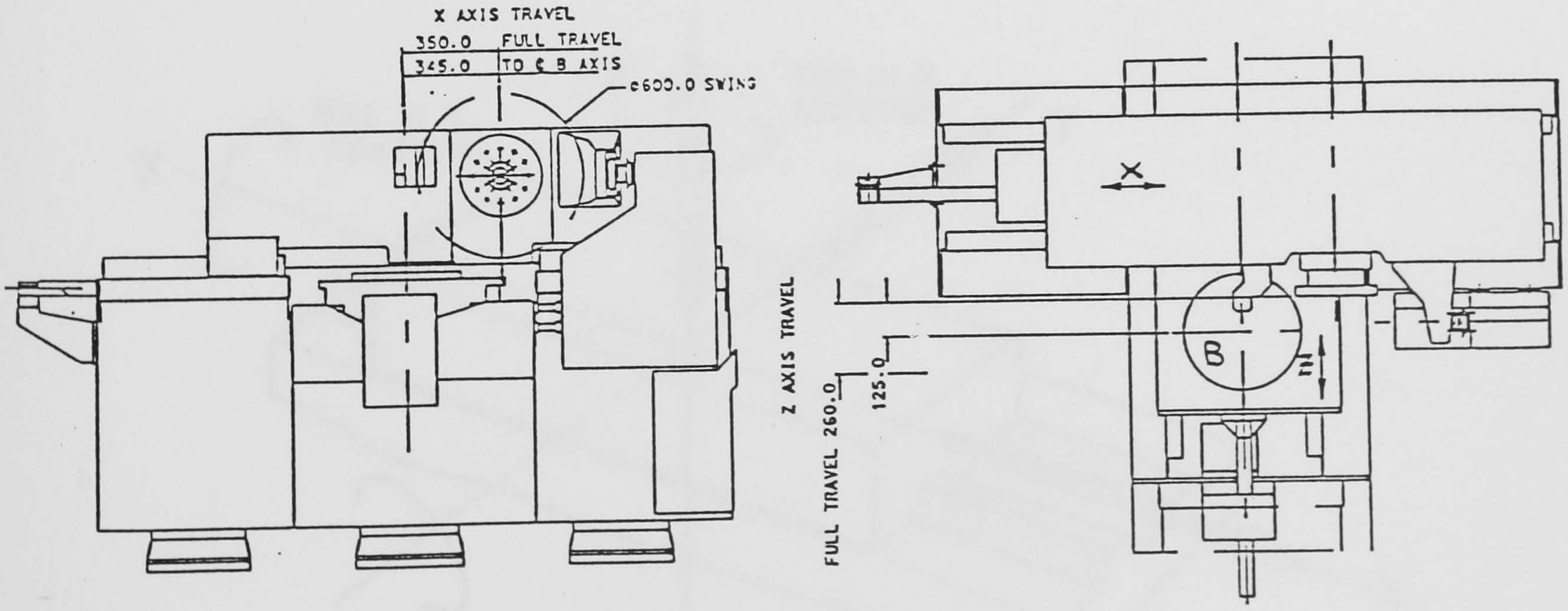

Figure 14c : Various Lay Out's of Aspheric Generators

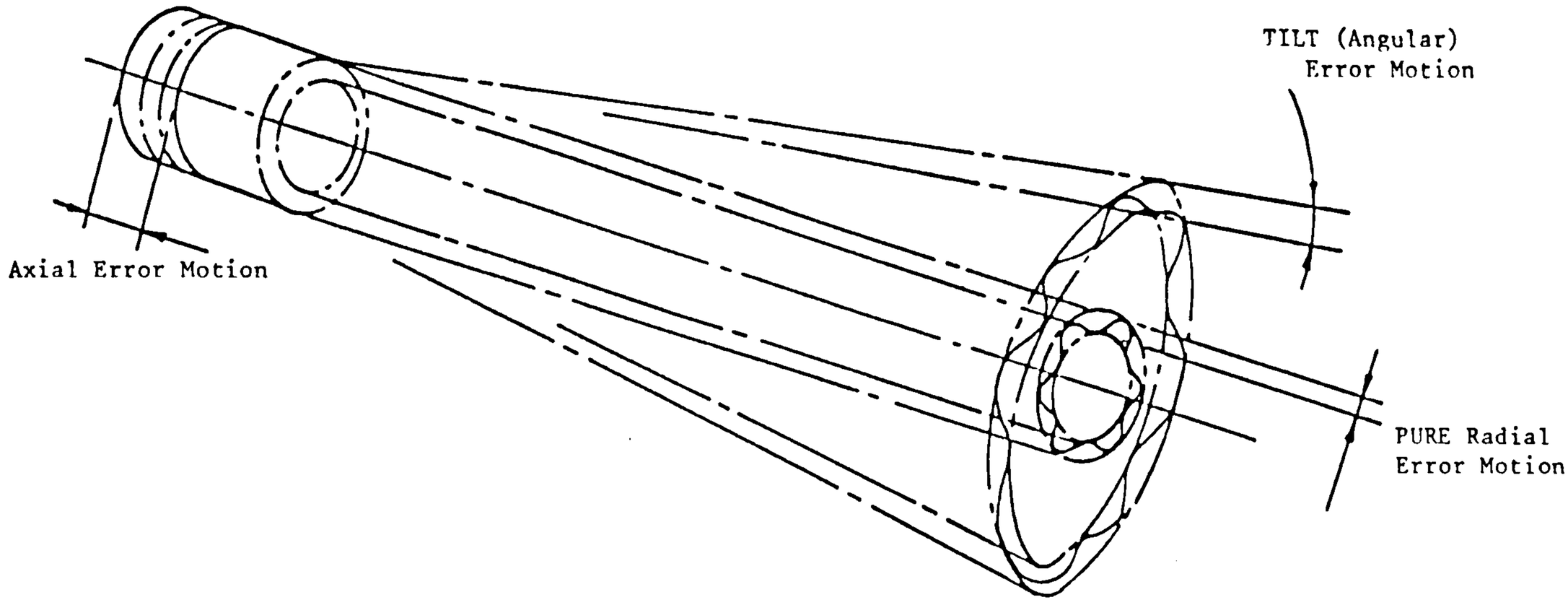

Figure 15 : Errors of Axis of Rotation [38]

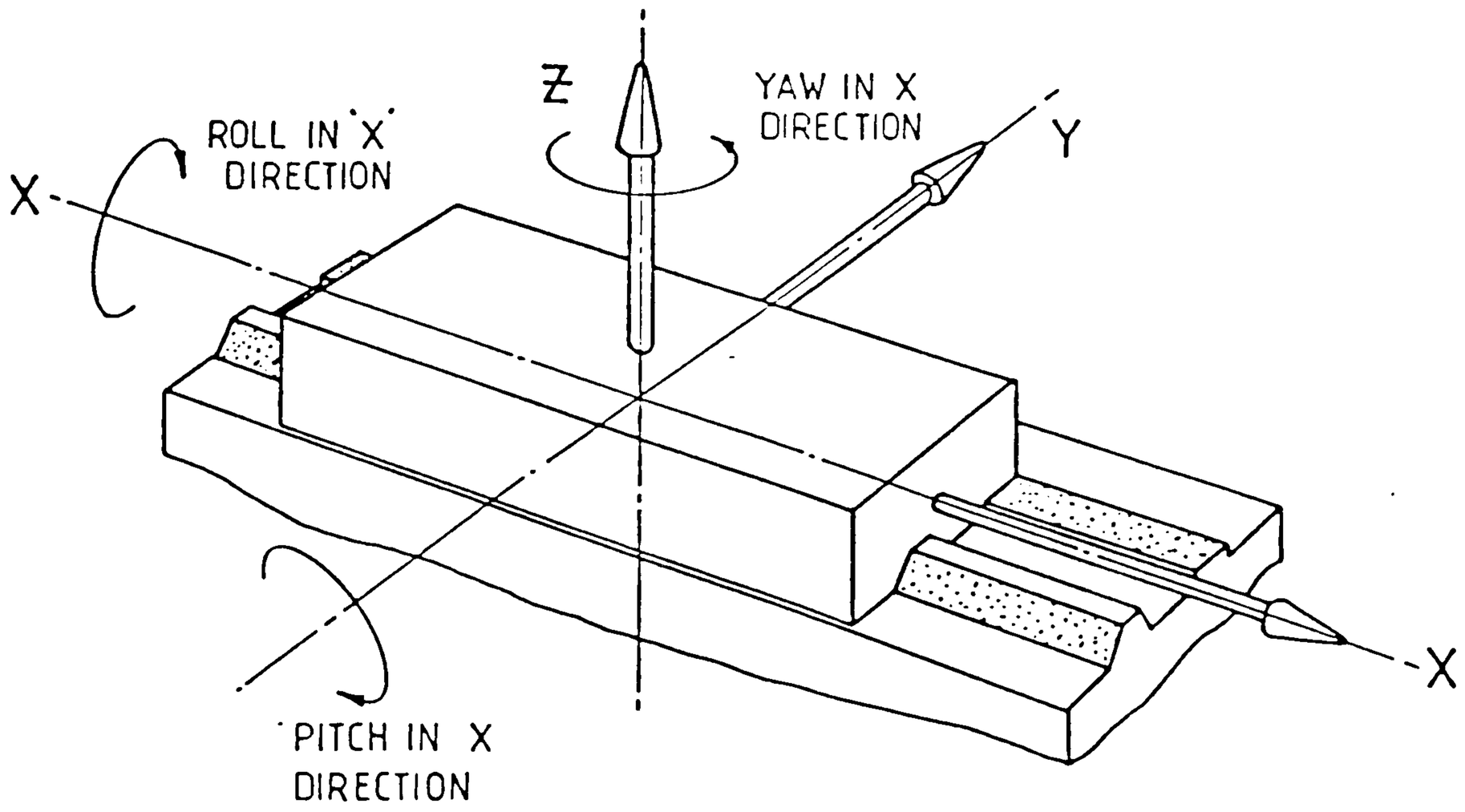

Figure 16 : Six Degrees of Freedom of a Linear Slideway [40]

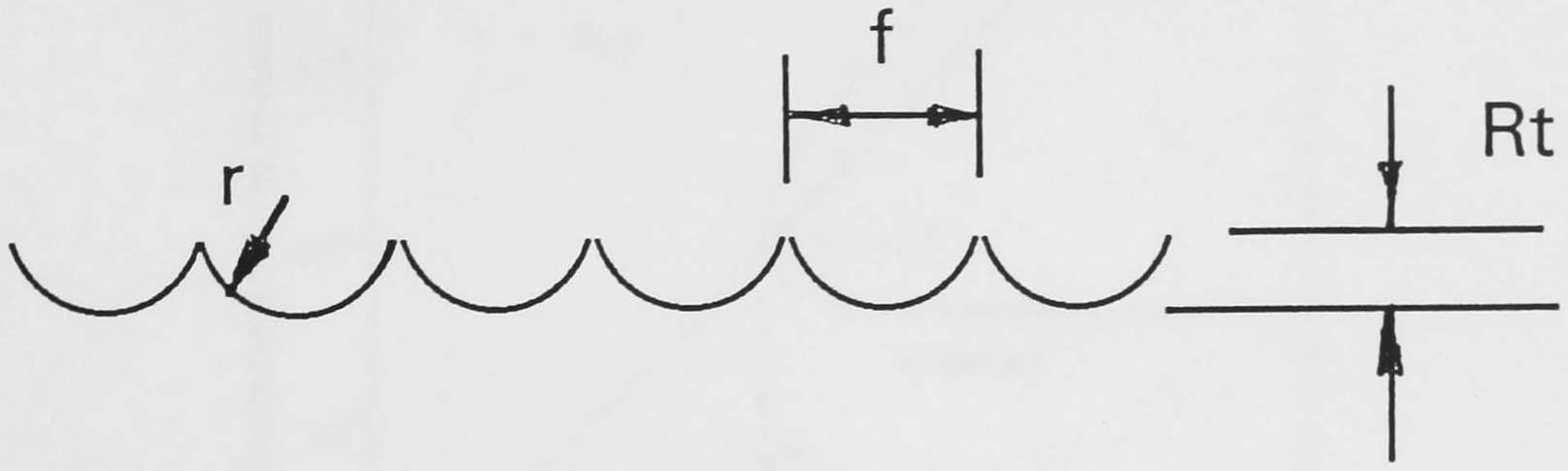

Figure 17 : Geometric Surface Roughness of Diamond Turned Surfaces

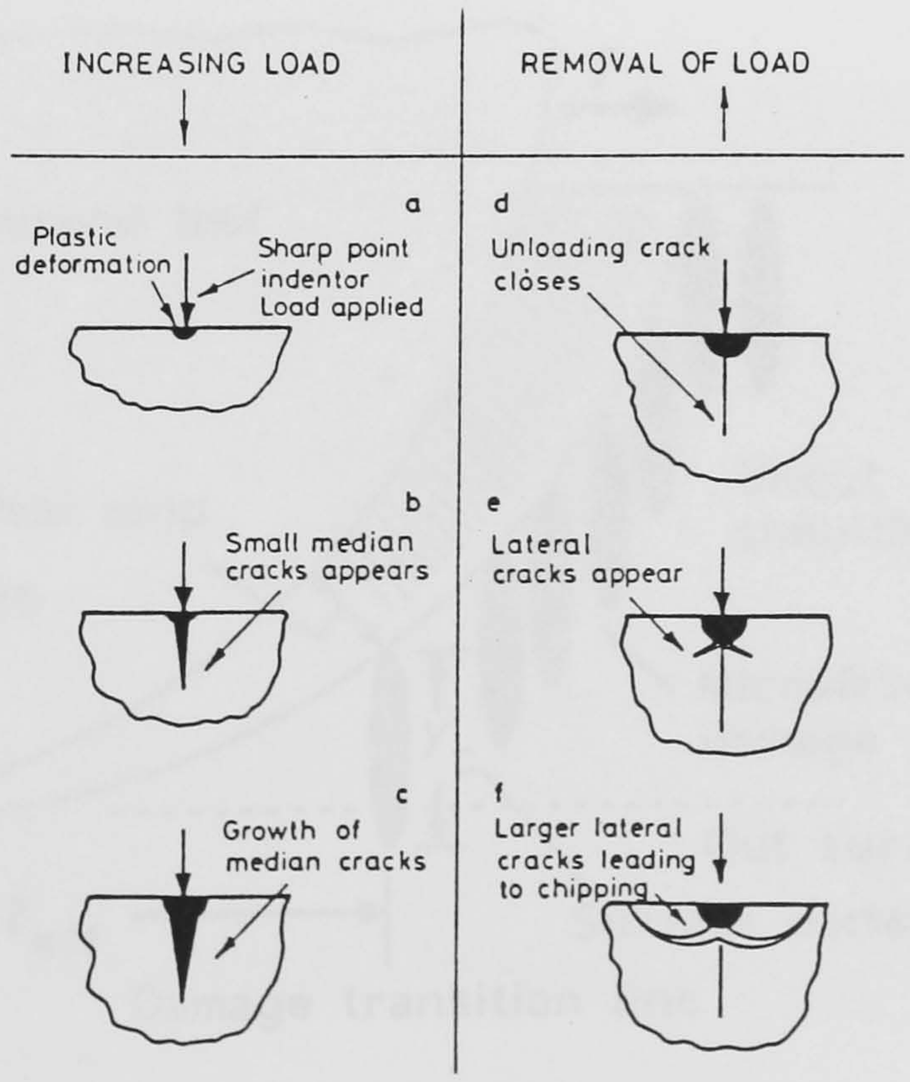

Figure 18 : Formation of Plastic / Fracture Under Sharp Point Indentor [71]

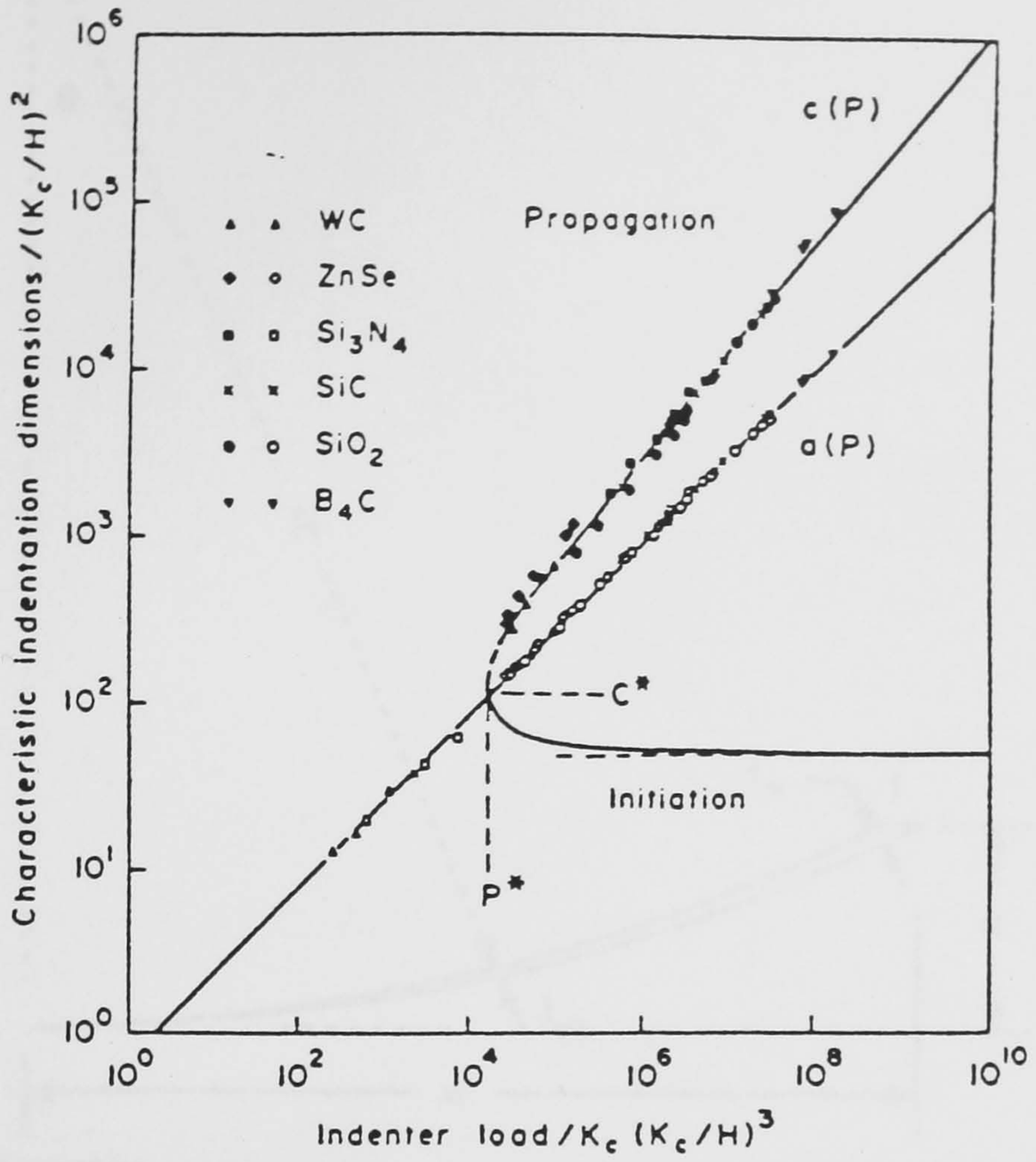

Figure 19 : Universal Deformation / Fracture Diagram [70]

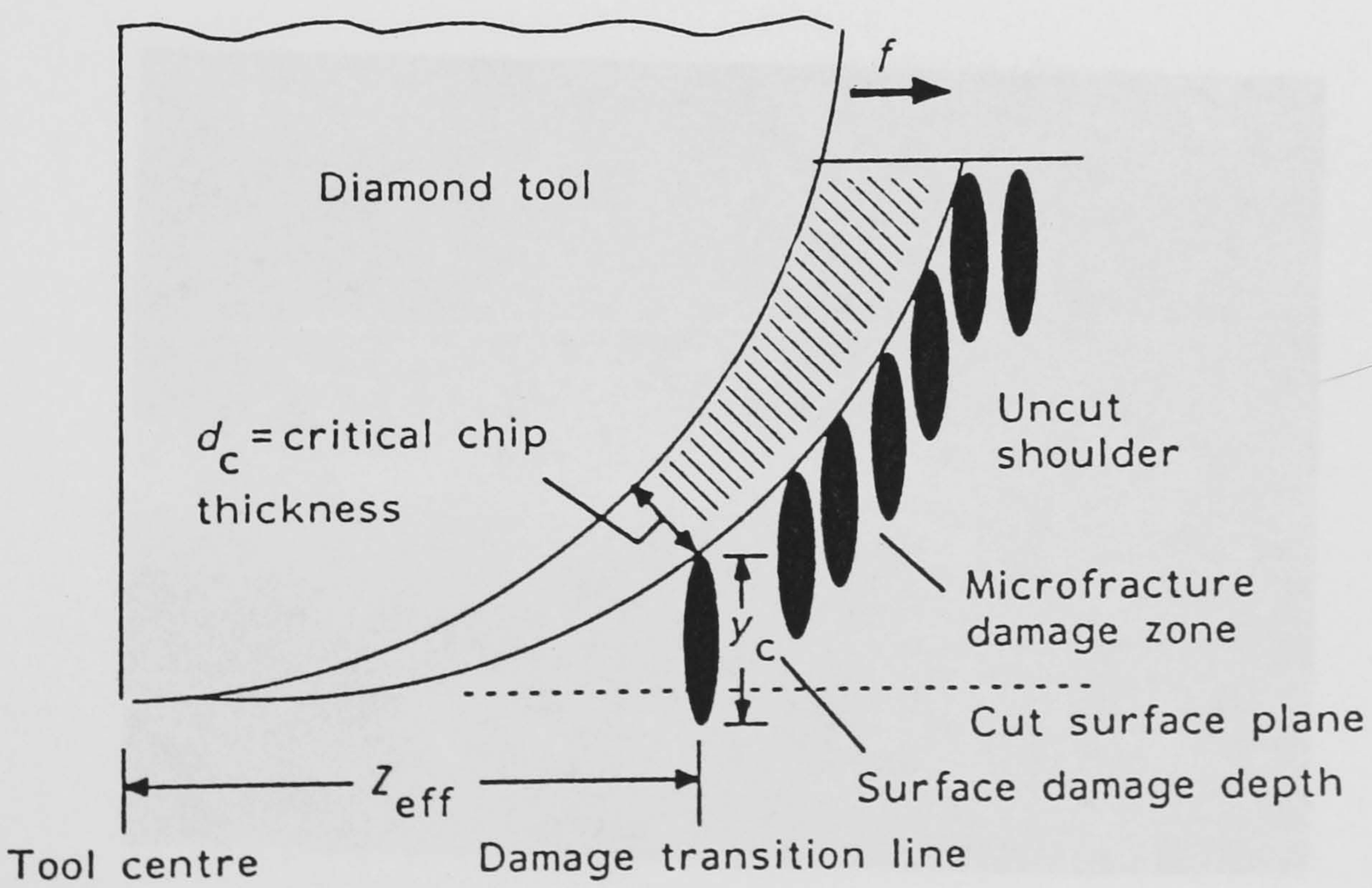

Figure 20 : Schematic of Brittle / Ductile Removal by Diamond Turning [61]

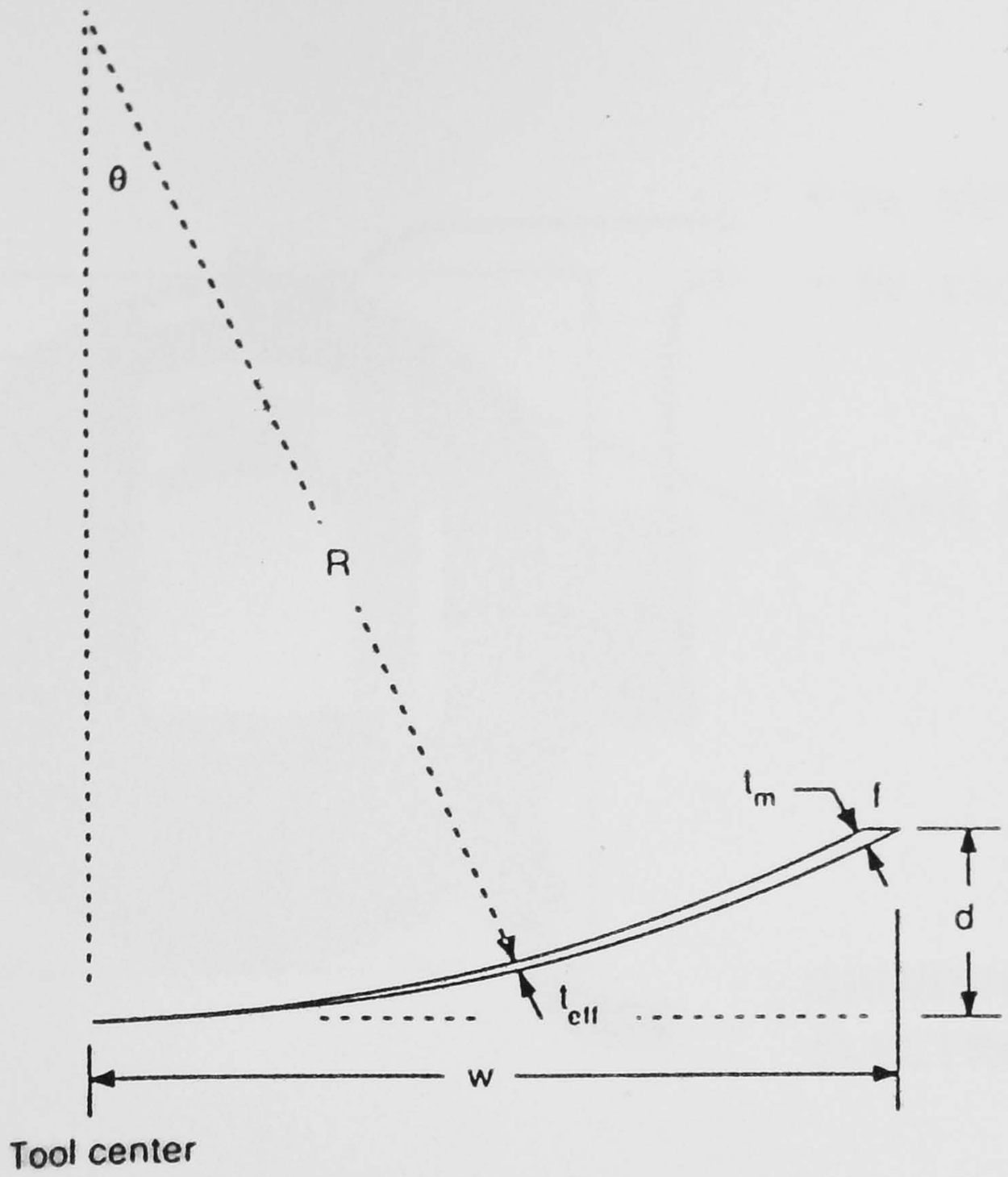

Figure 21 : Scale Drawing of Uncut Chip Thickness

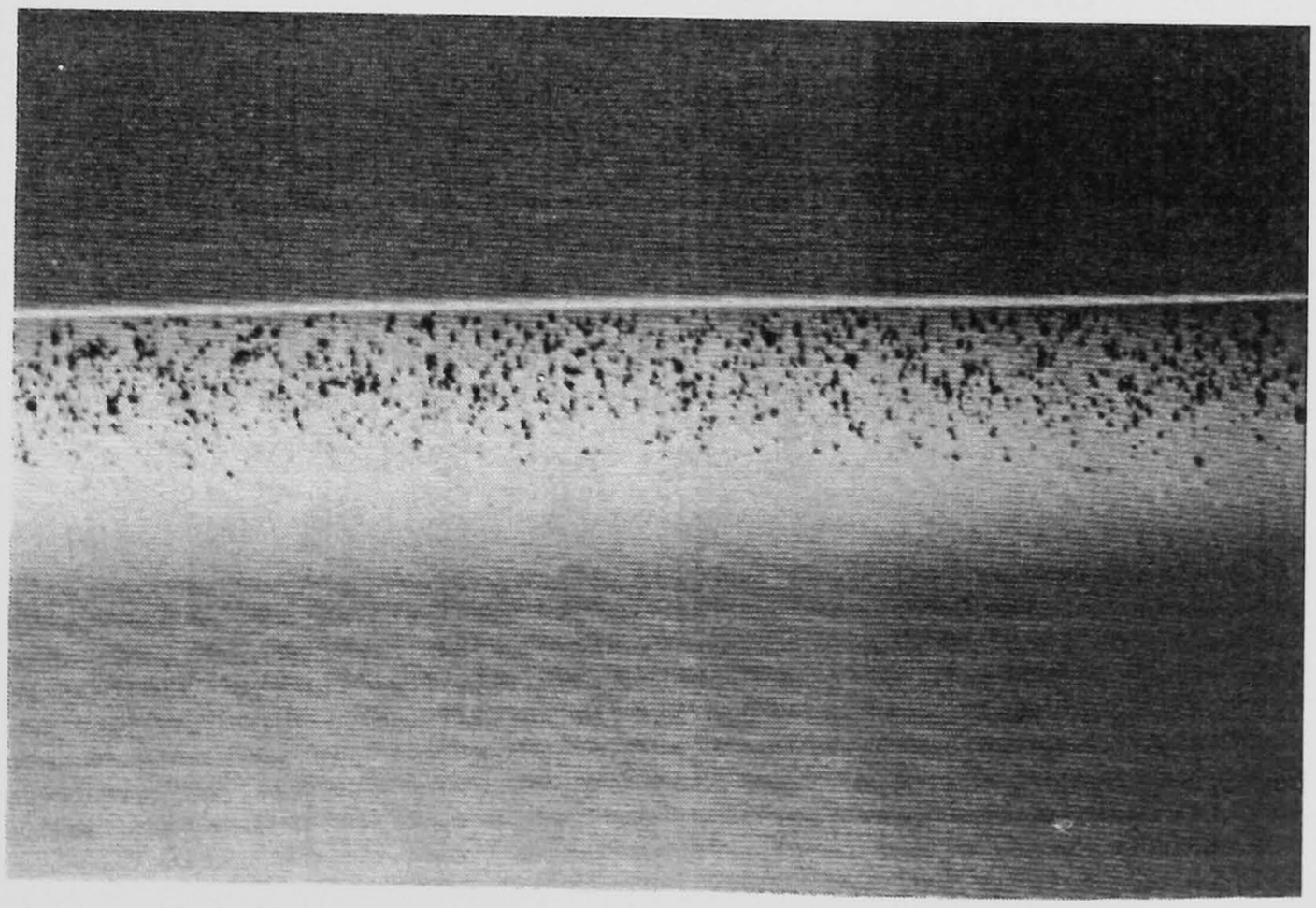

Figure 22 : Micro-photograph of "Uncut" Brittle / Ductile Shoulder [61]

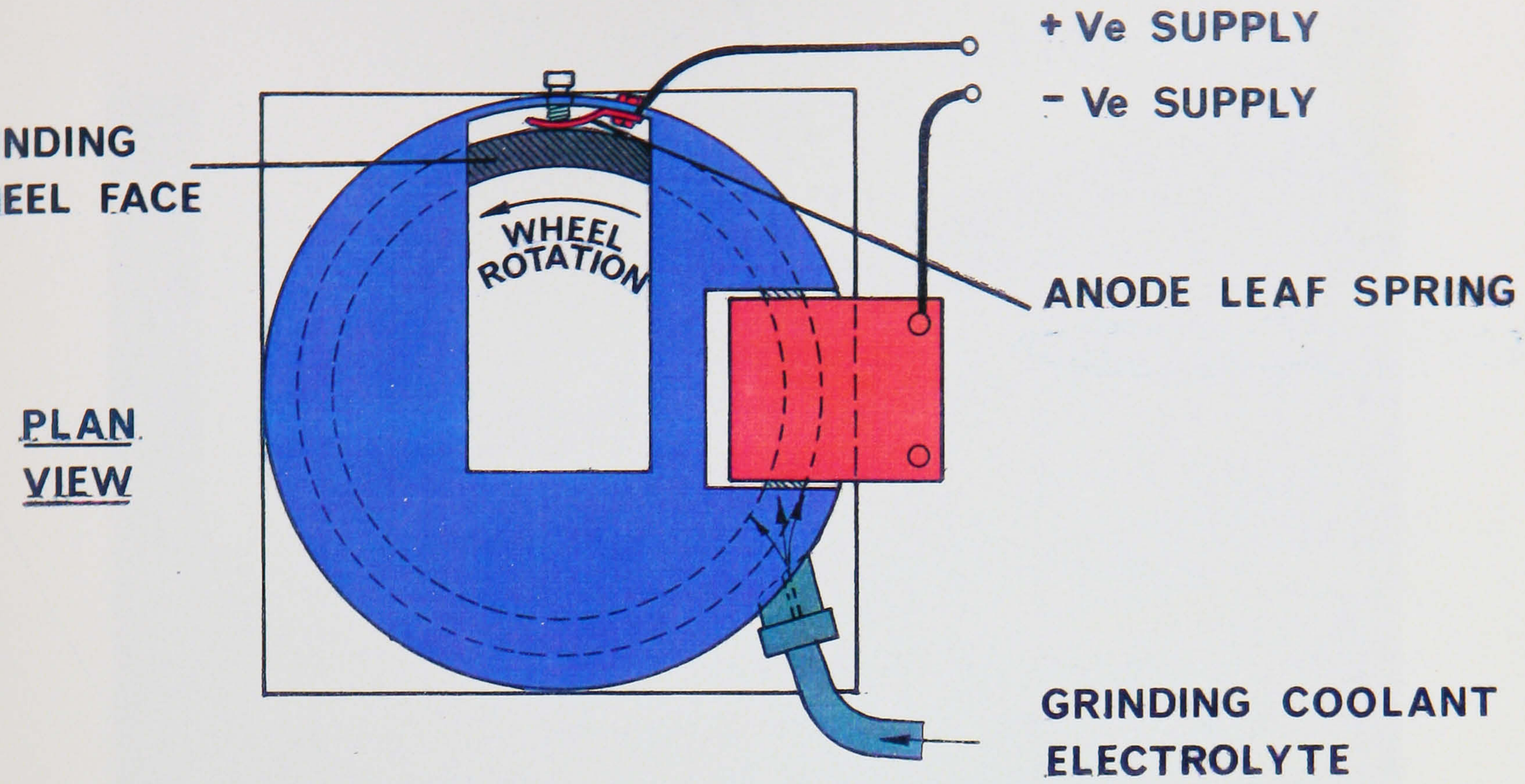

Figure 23 : Schematic of ELID Cup Wheel Set-Up

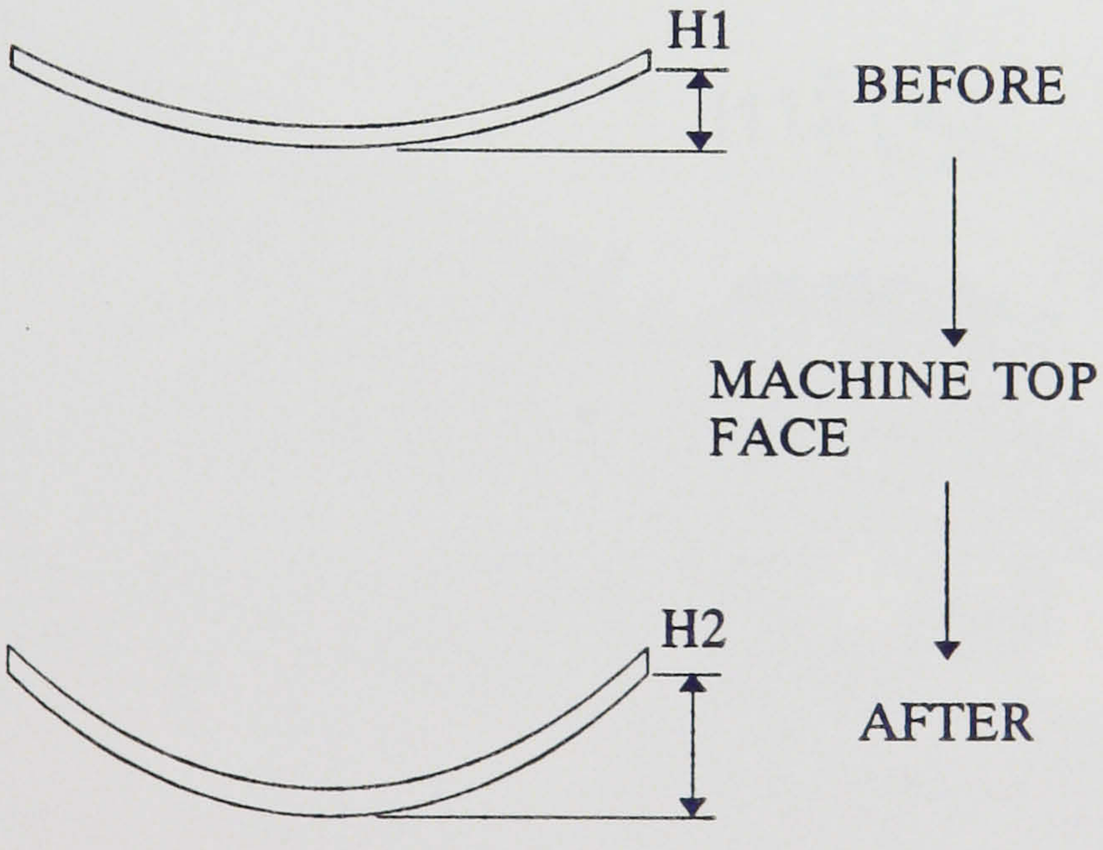

$$dH = H2 - H1$$

Figure 24 : Twyman Effect

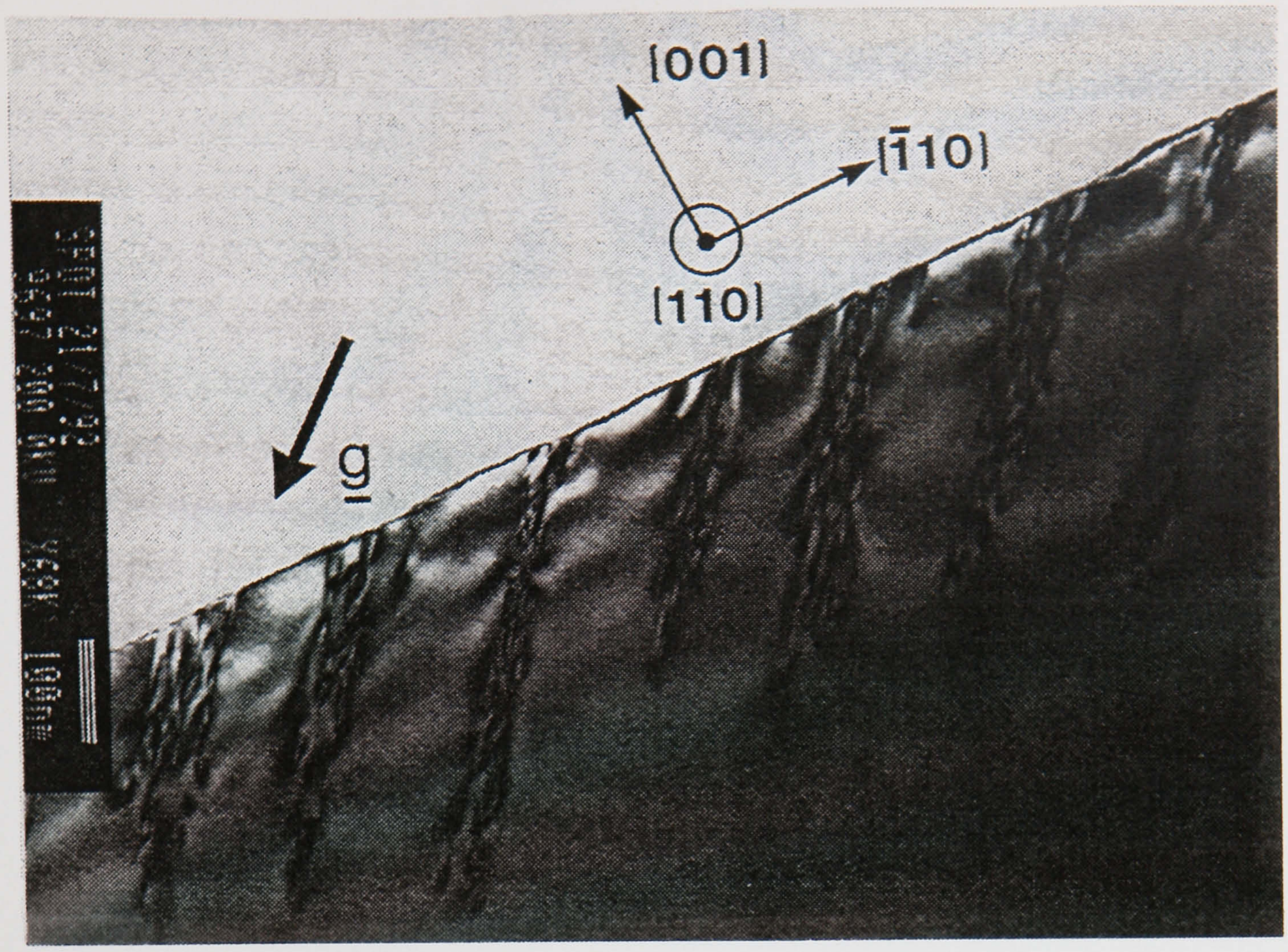

Figure 25 : Cross Sectional T.E.M. of Turned Silicon [105]

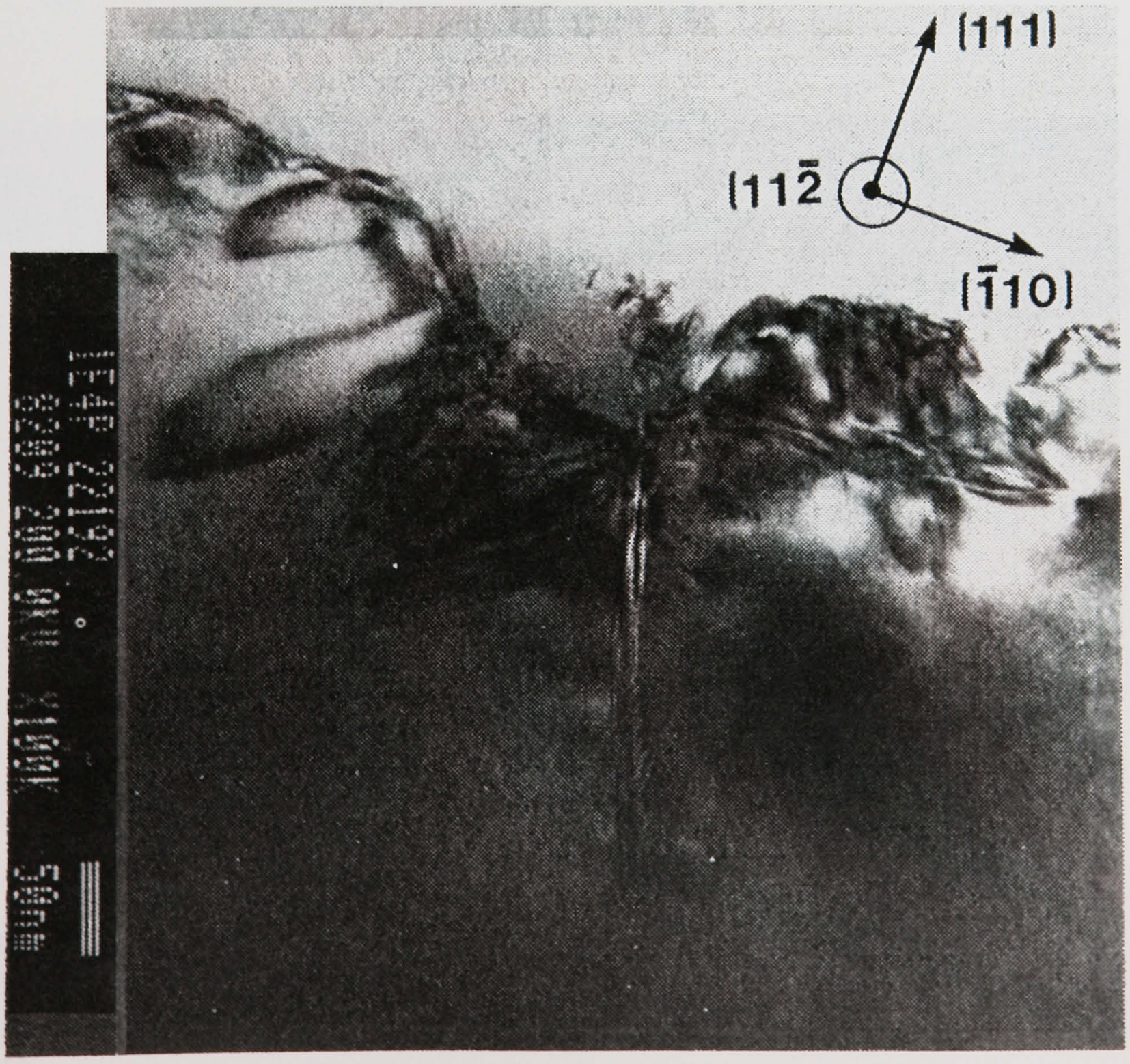

Figure 26 : Cross Sectional T.E.M. of Ground Silicon [105]

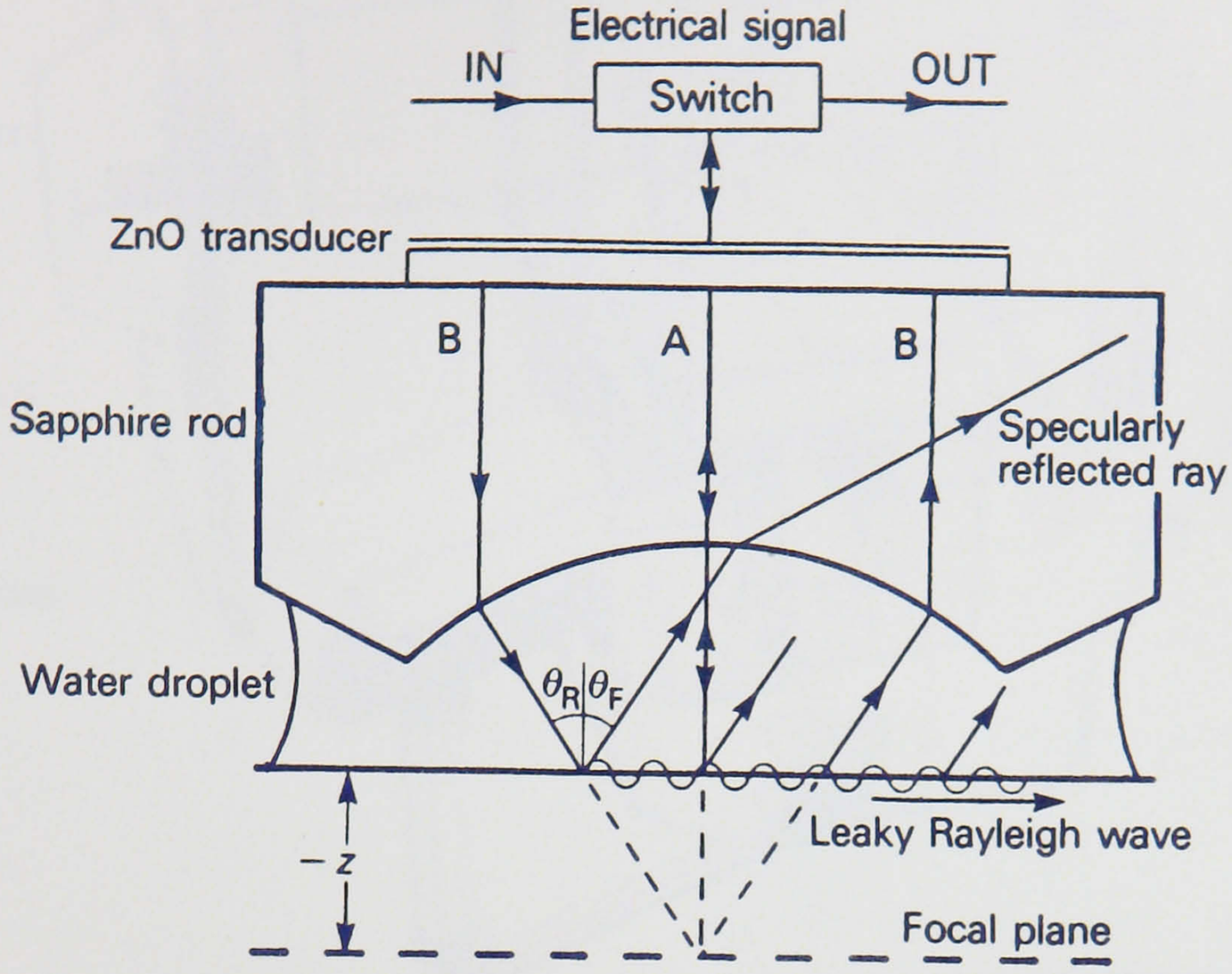

Figure 27 : Schematic of Rayleigh Surface Wave and Generation [106]

Figure 28 : The NION Machine

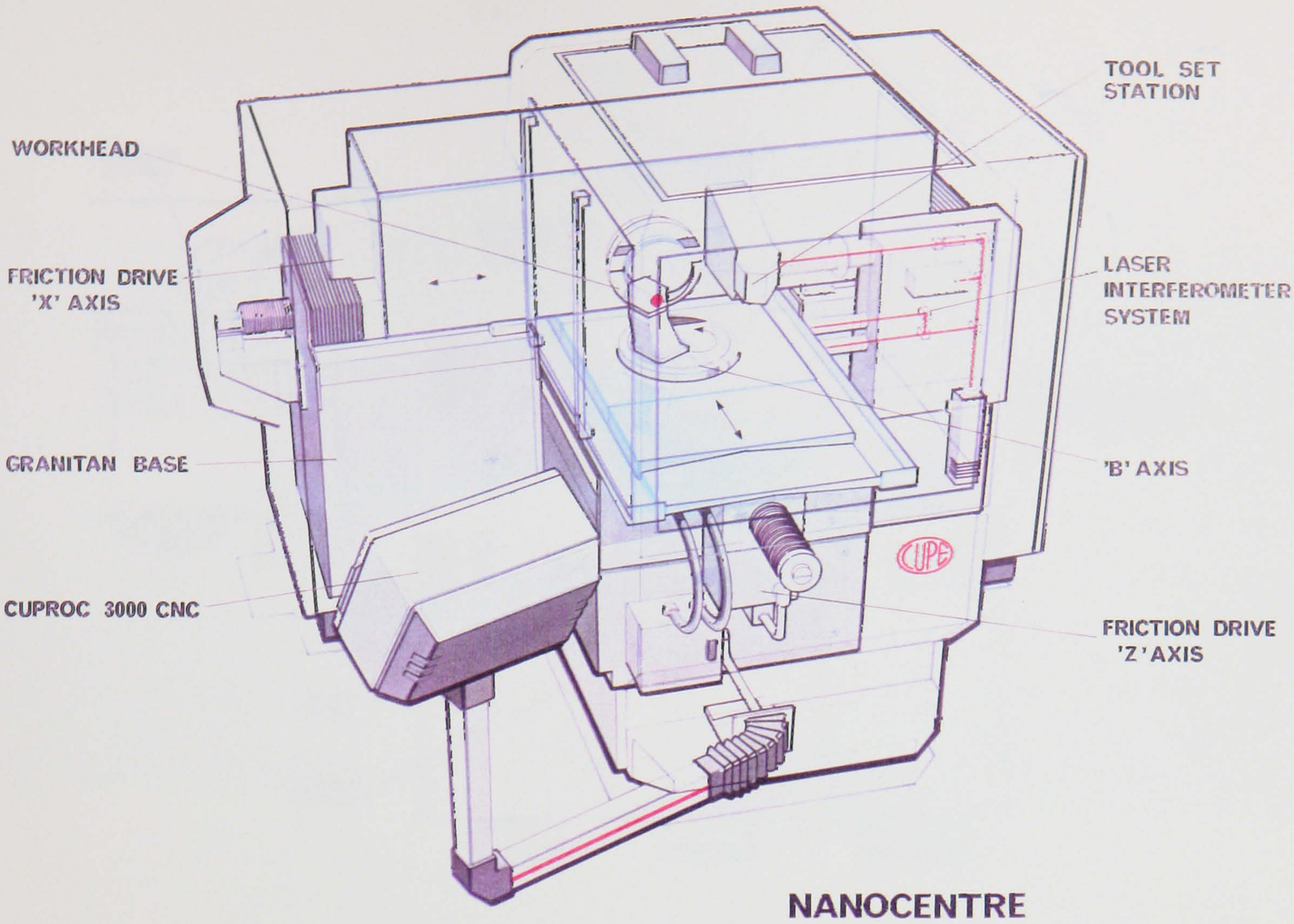

Figure 29 : Schematic of Nanocentre Machine

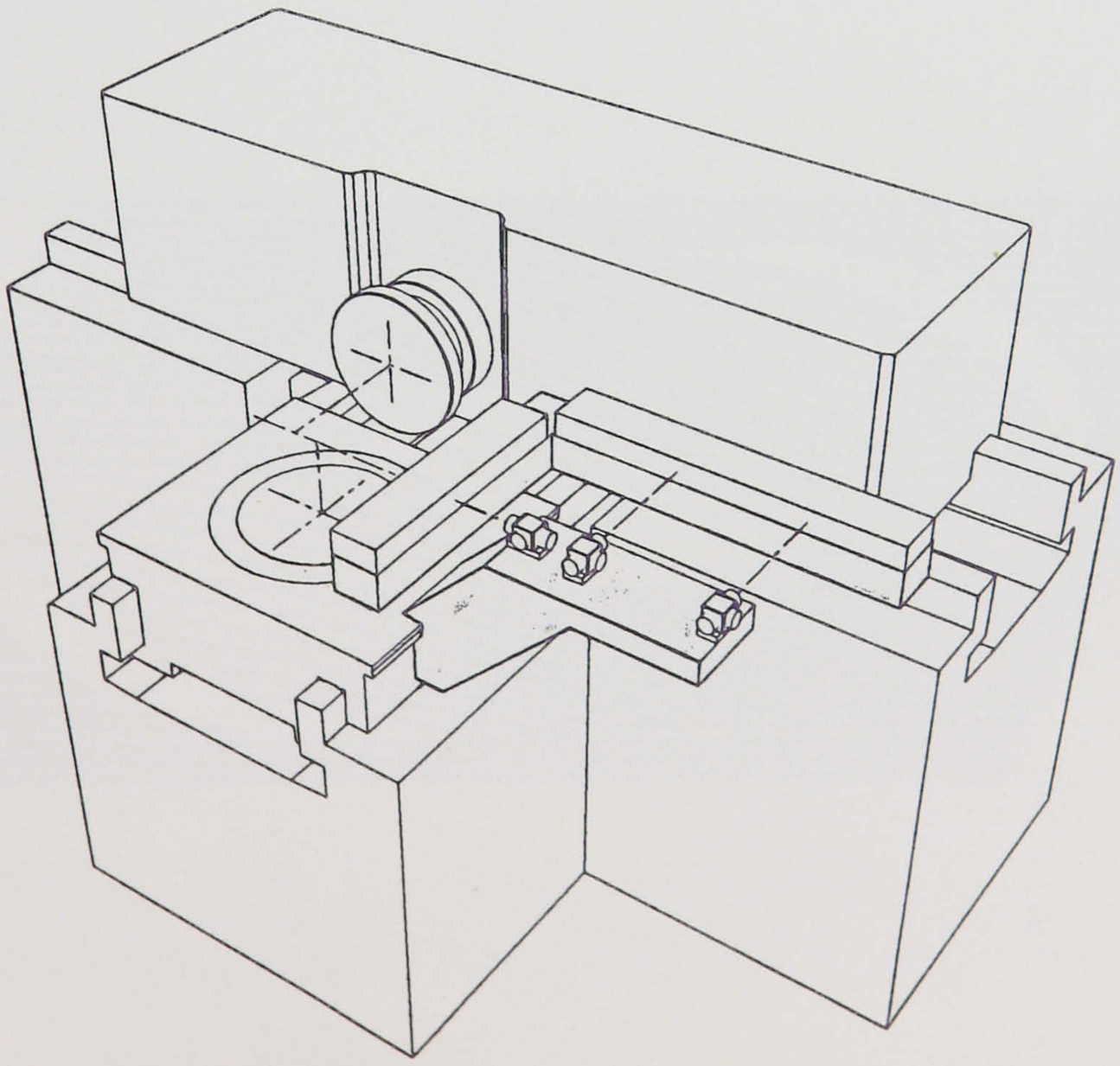

Figure 30 : Schematic of Metrology Frame

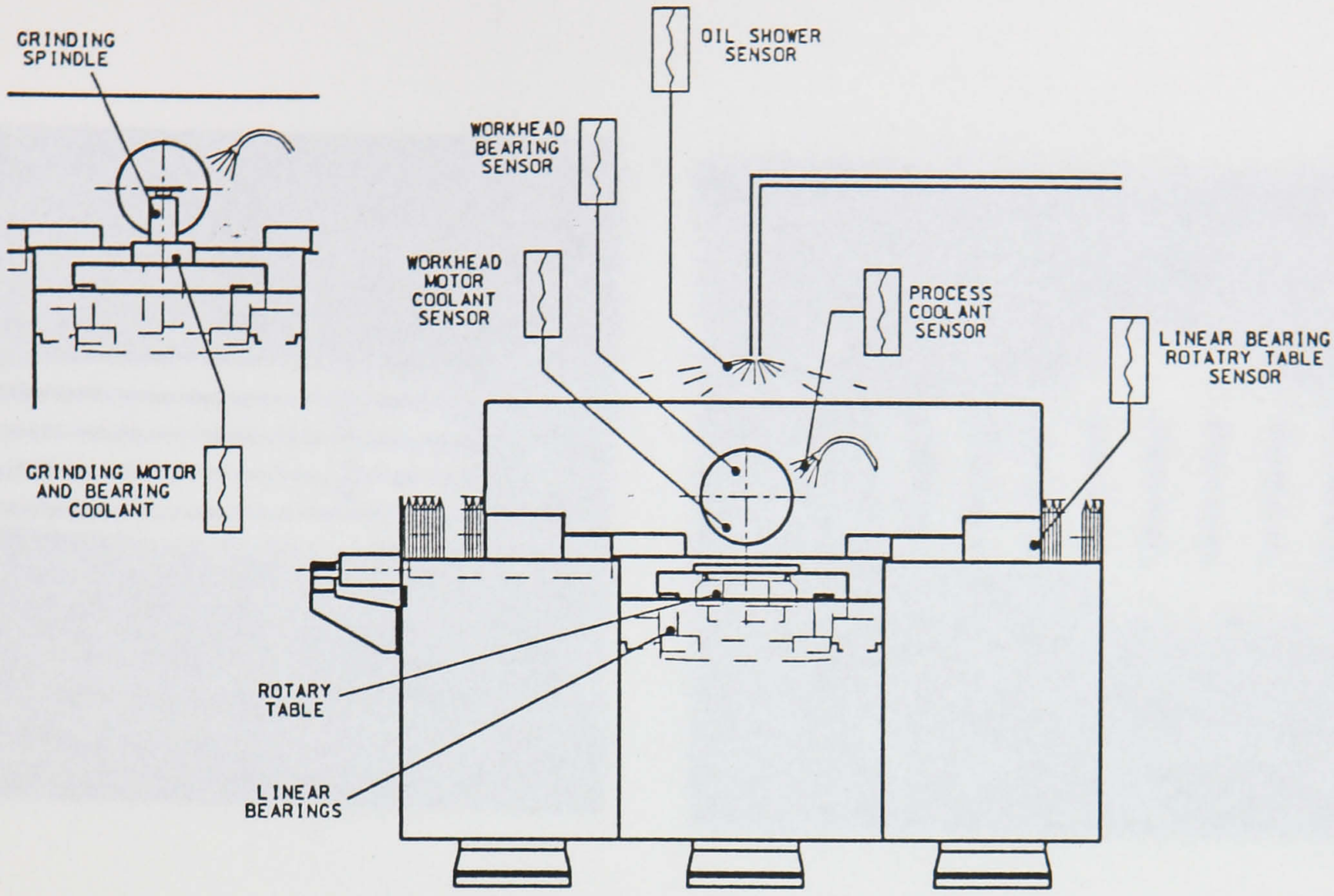

Figure 31 : Schematic of the NION Machines Temperature Control Systems

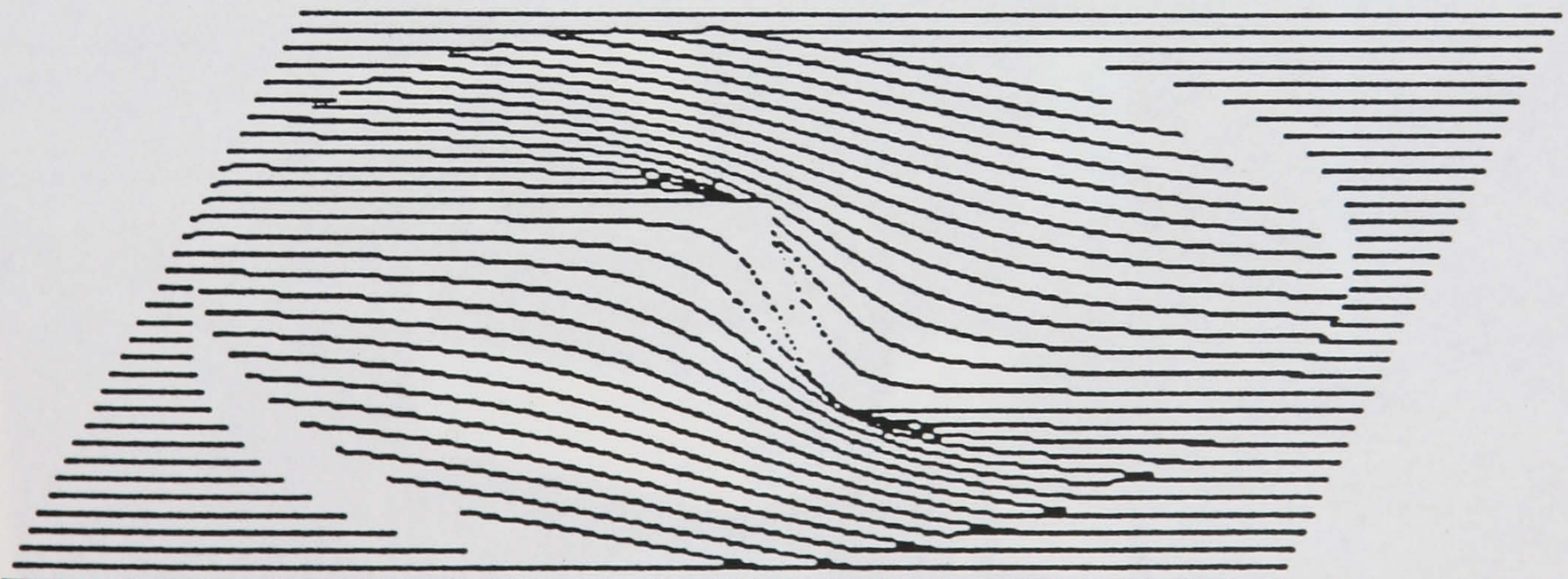

Figure 32 : Schematic of Figure Error Produced by Synchronous Axial Error

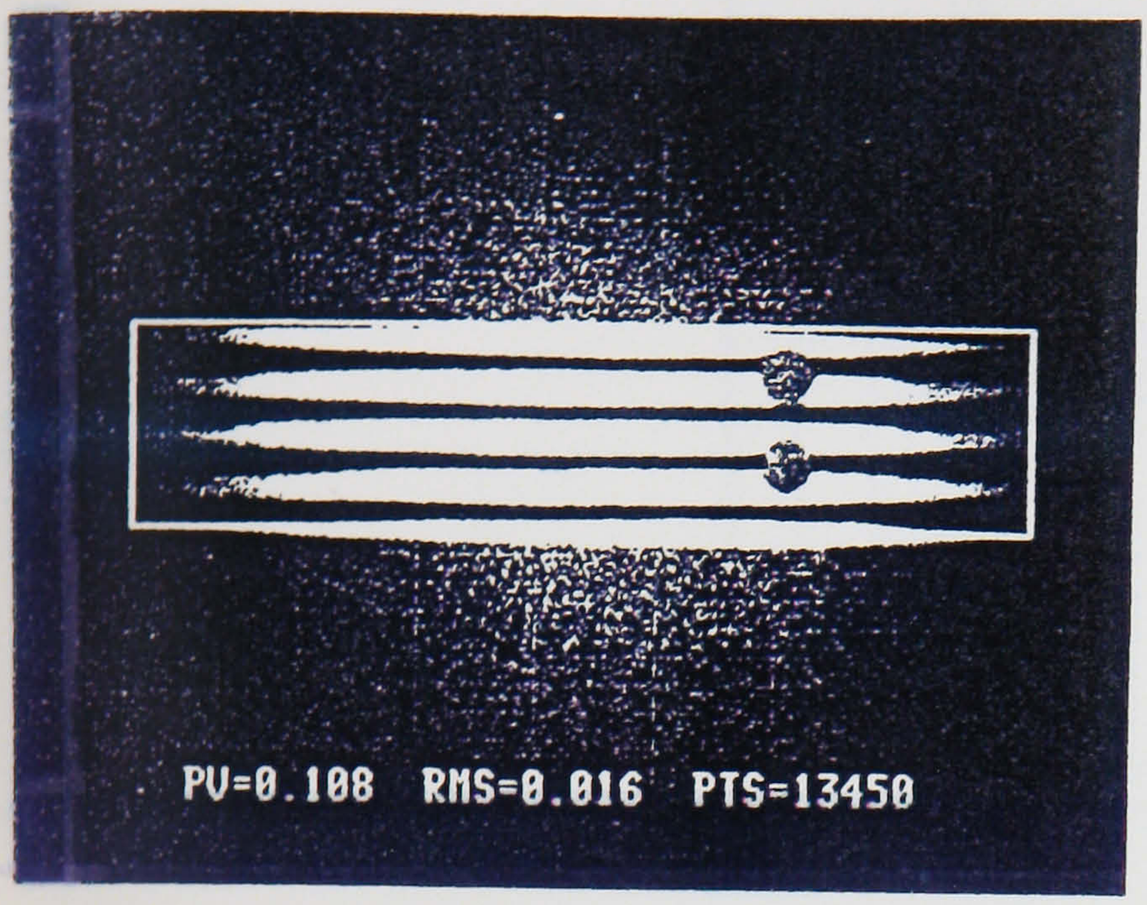

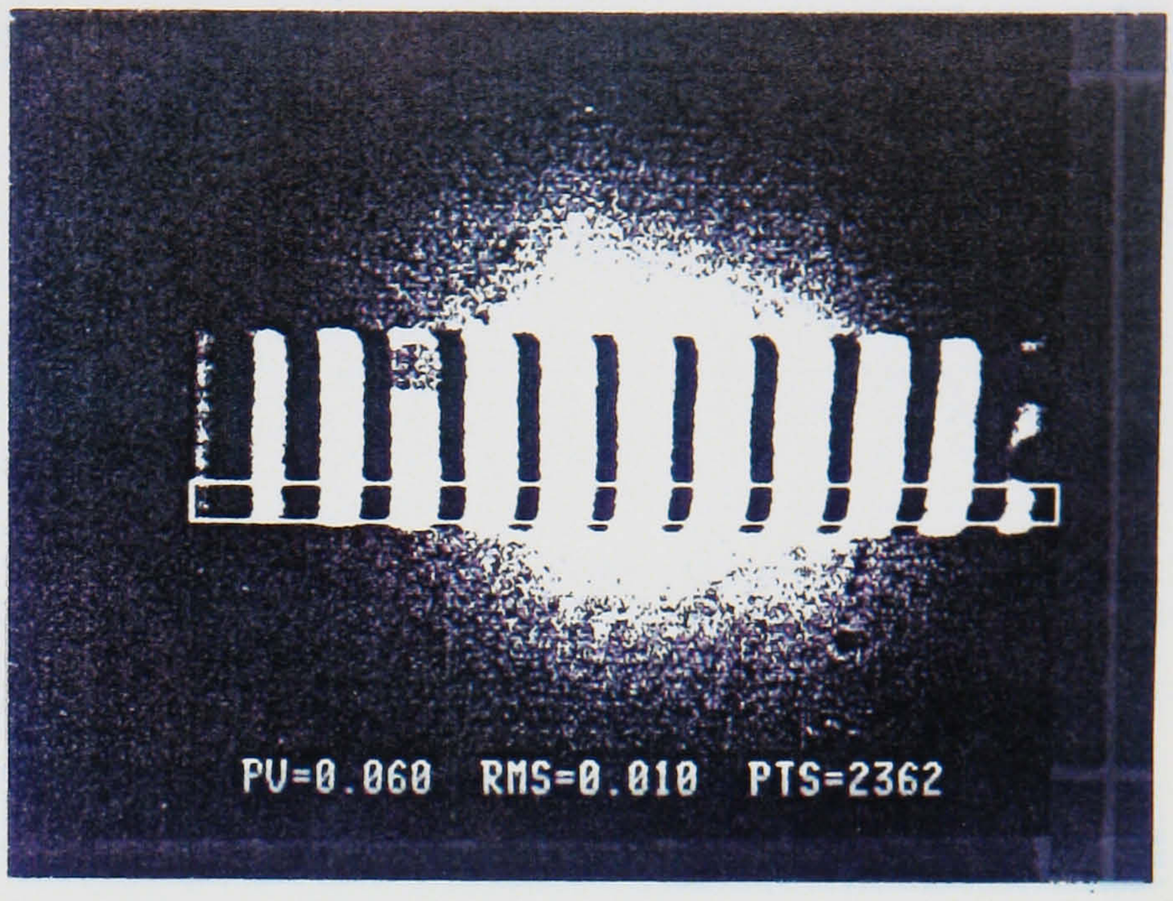

Figure 33 : Flatness of NION Metrology Frame Straight Edges

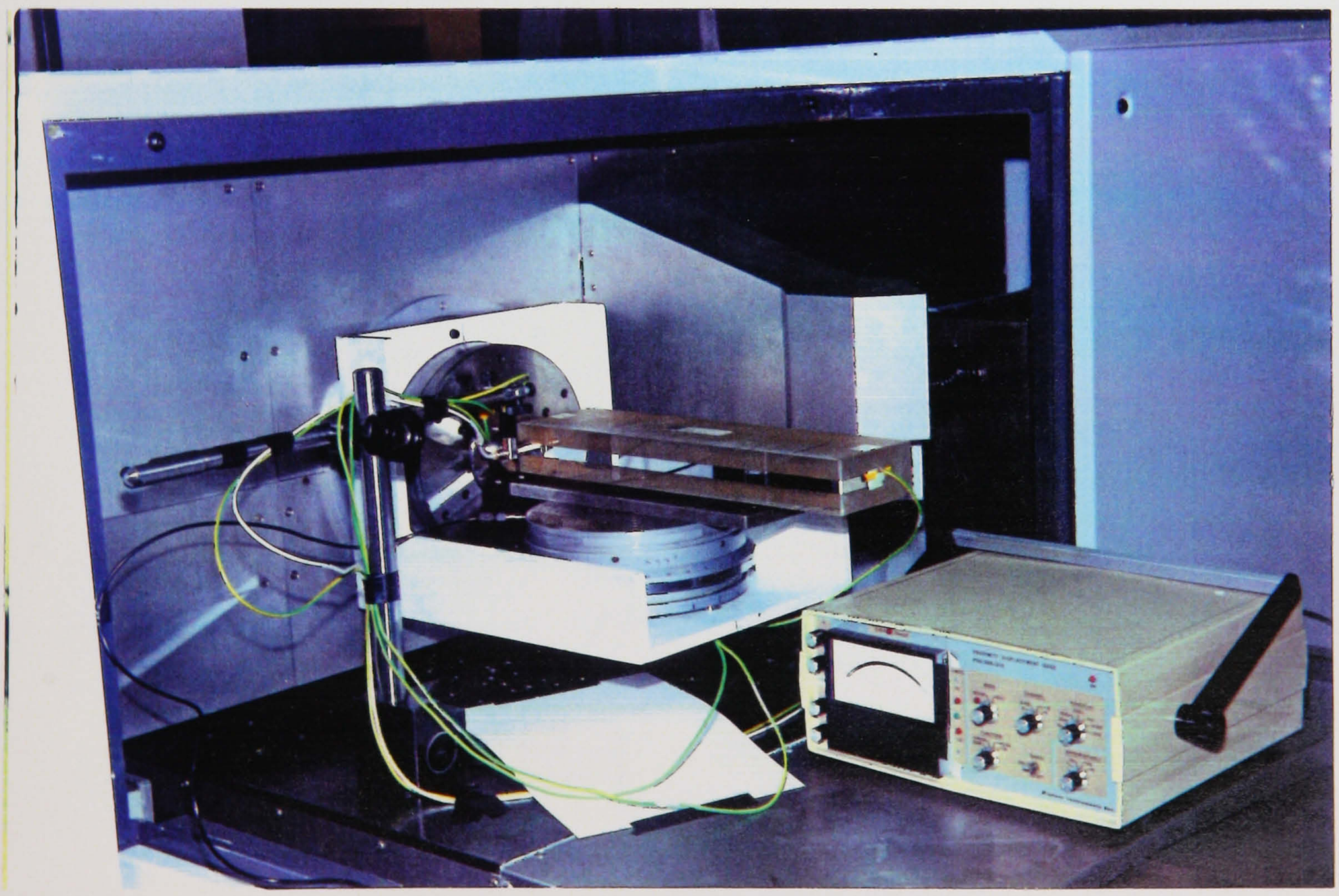

Figure 34 : Photograph of Set Up for Checking NION Machine Z Axis Straightness

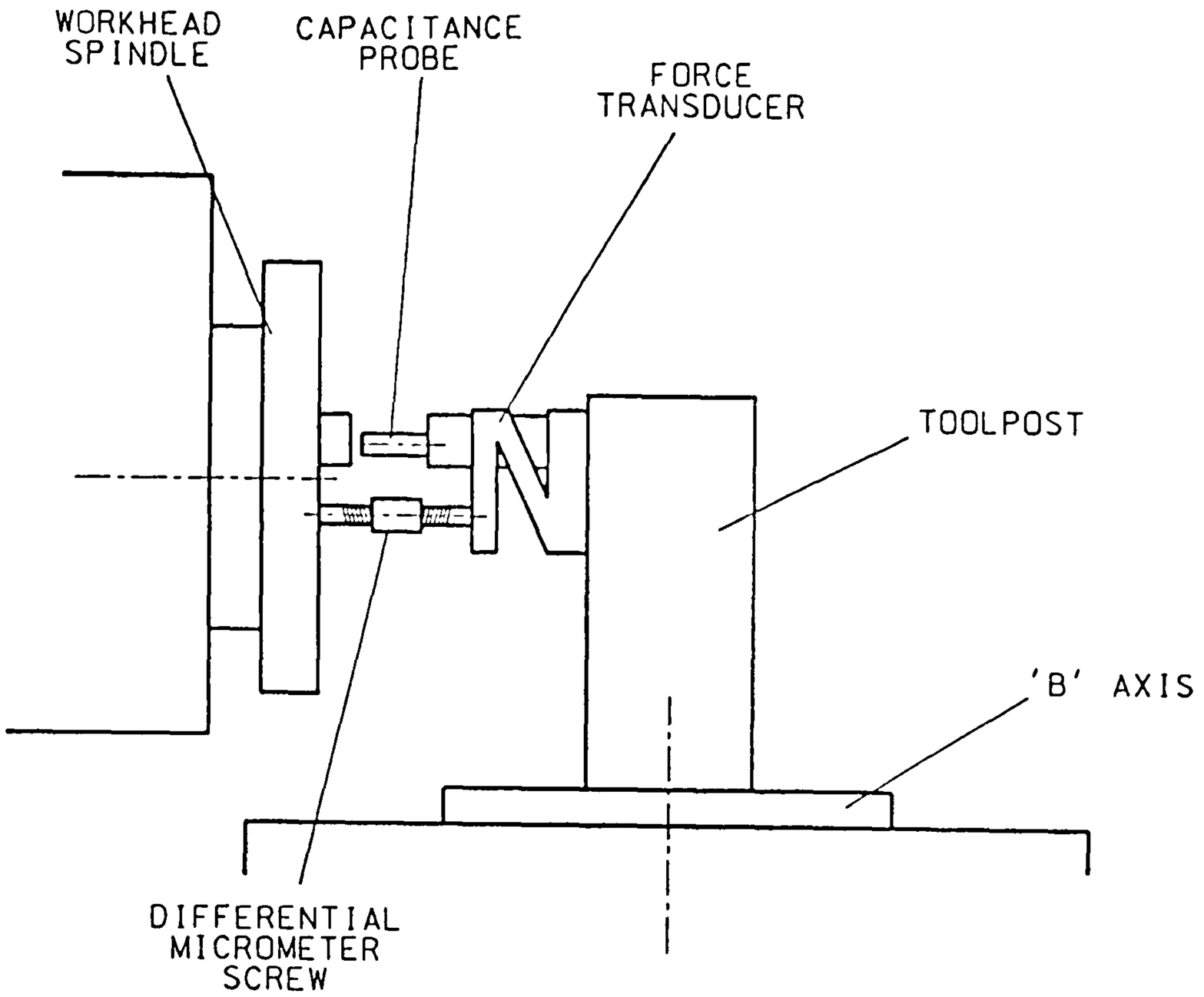

Figure 35 : Schematic of "Loop" Stiffness Check Set Up

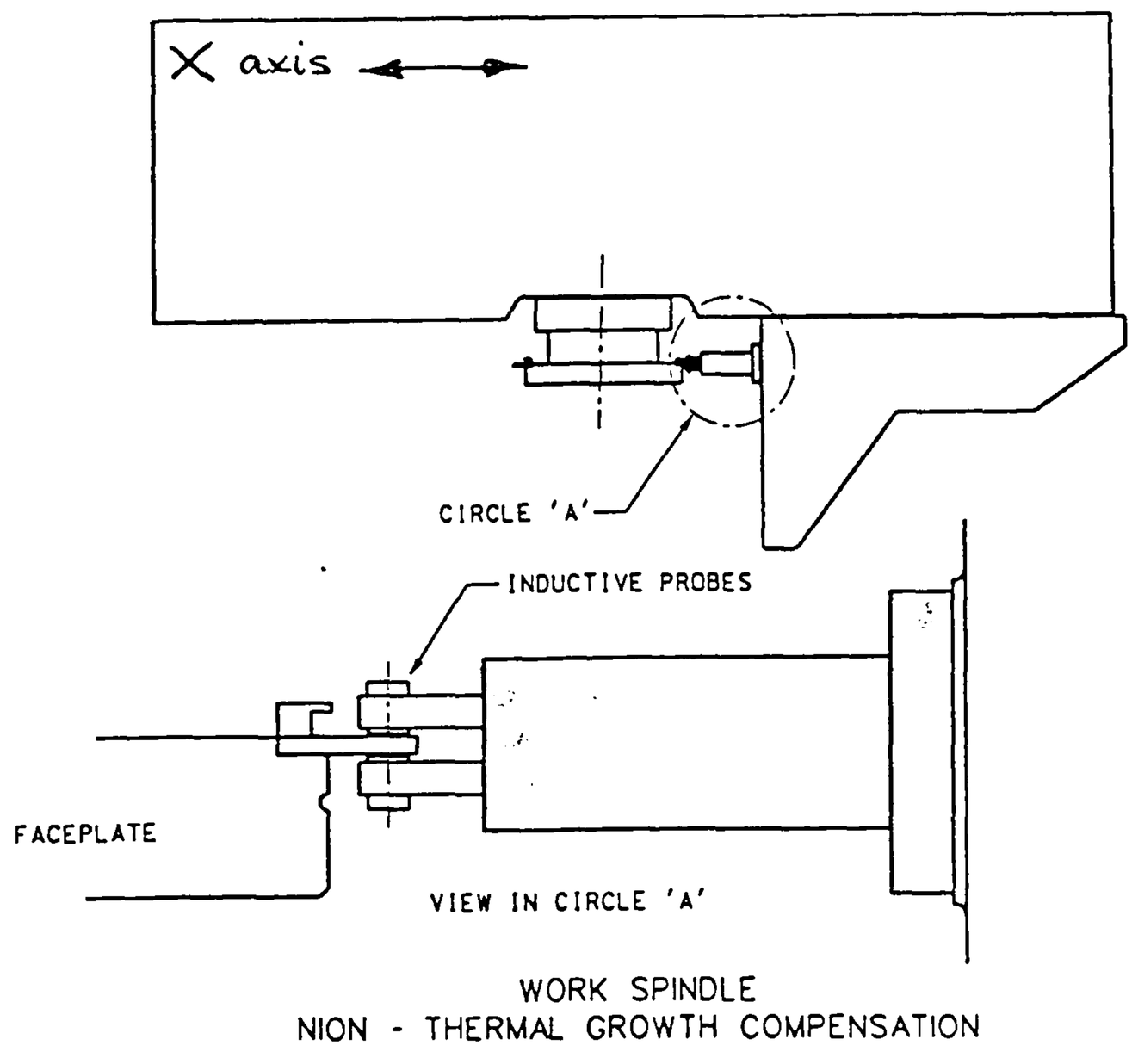

Figure 36 : Schematic of Workhead Thermal Growth Compensation System

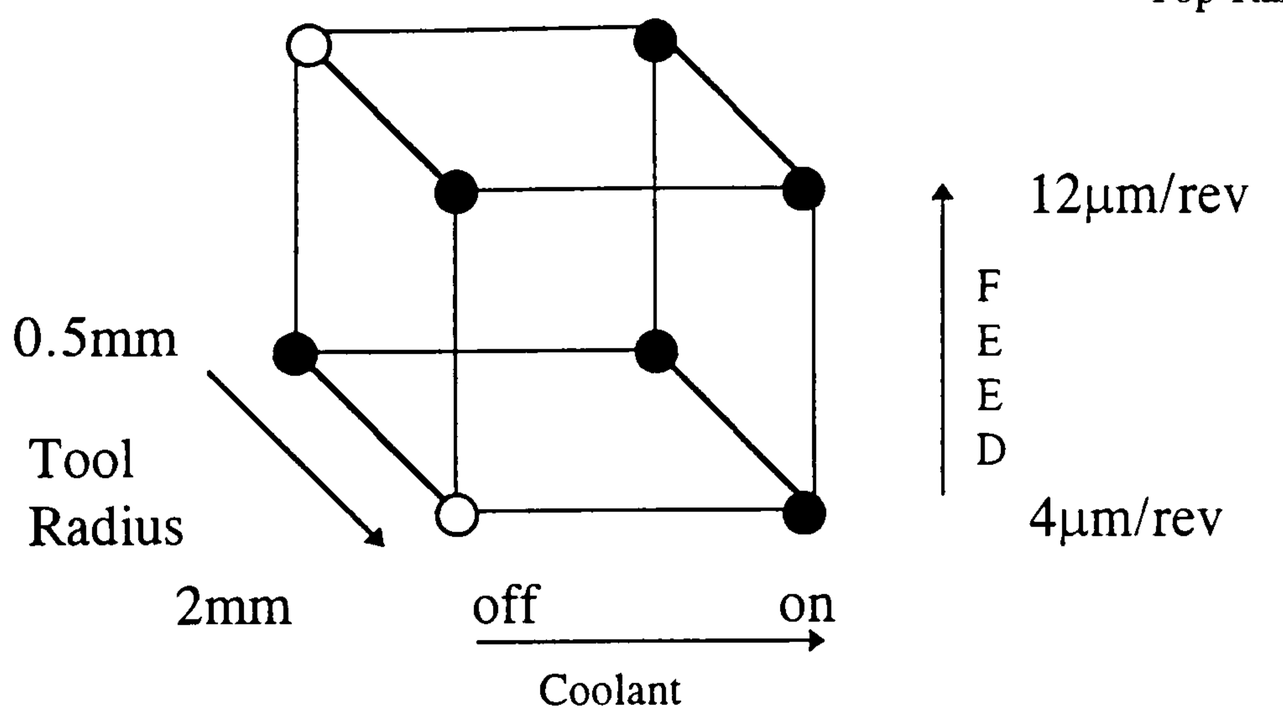

Figure 37 : Experimental Design Matrix 1, Diamond Turning of Germanium

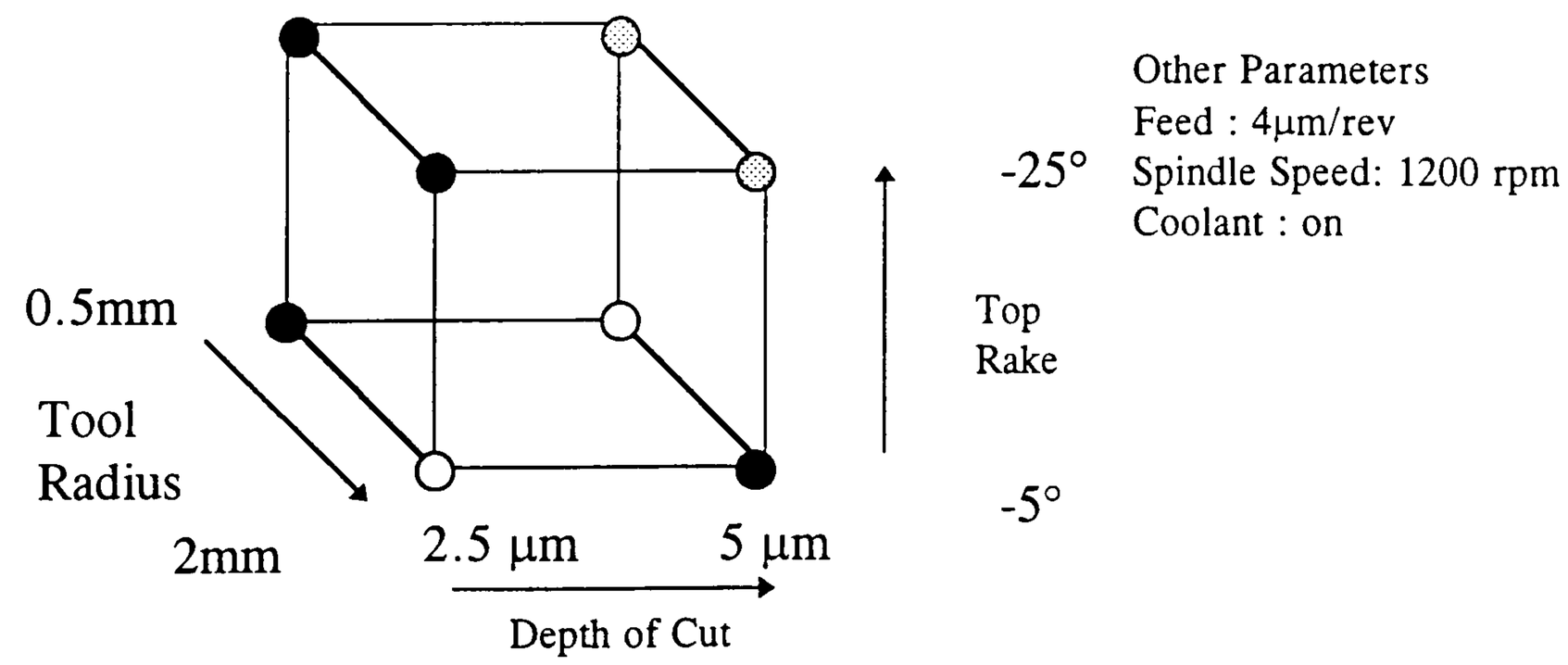

Figure 38 : Experimental Design Matrix 2, Diamond Turning of Germanium

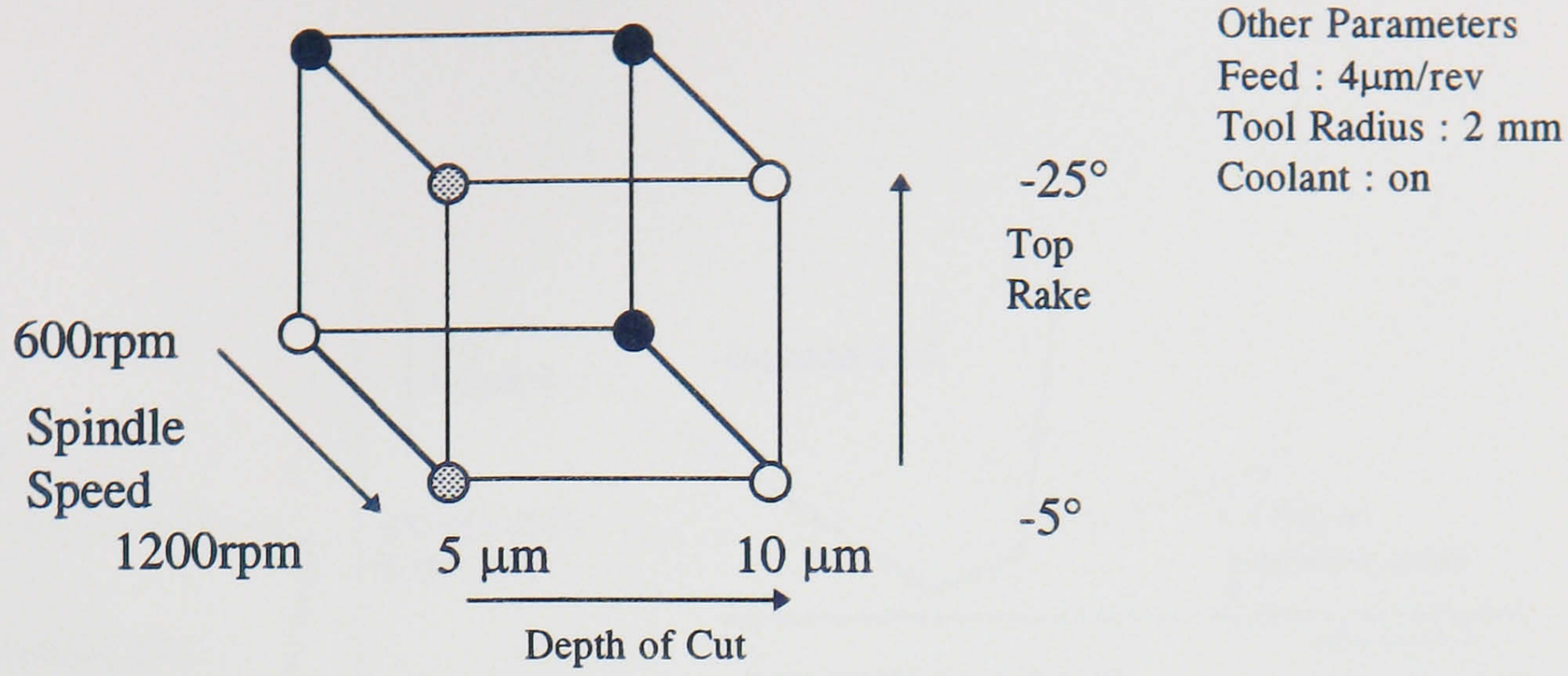

Figure 39 : Experimental Design Matrix 3, Diamond Turning of Germanium

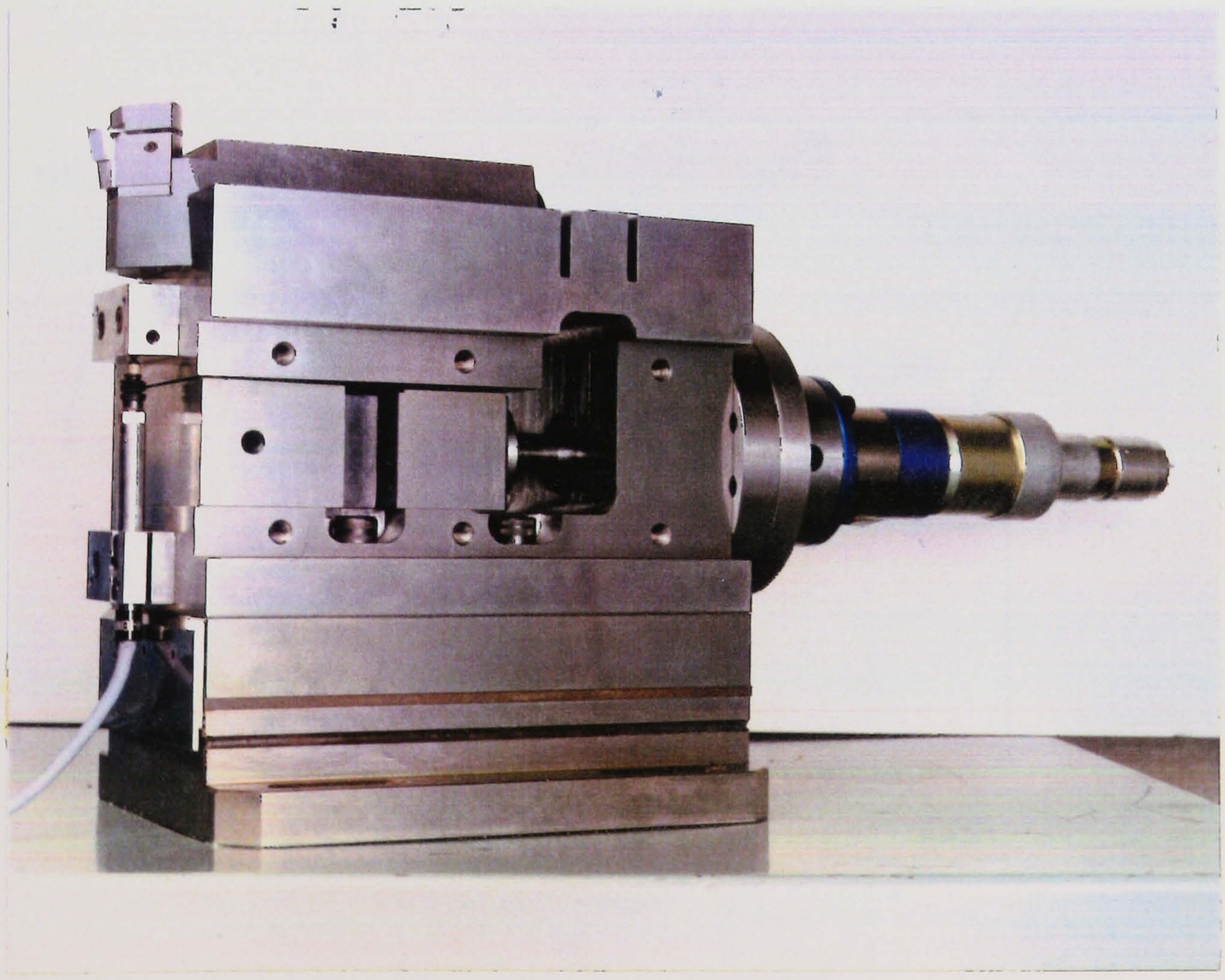

Figure 40 : Photograph of Motorised Toolpost with In-situ Dynamometer

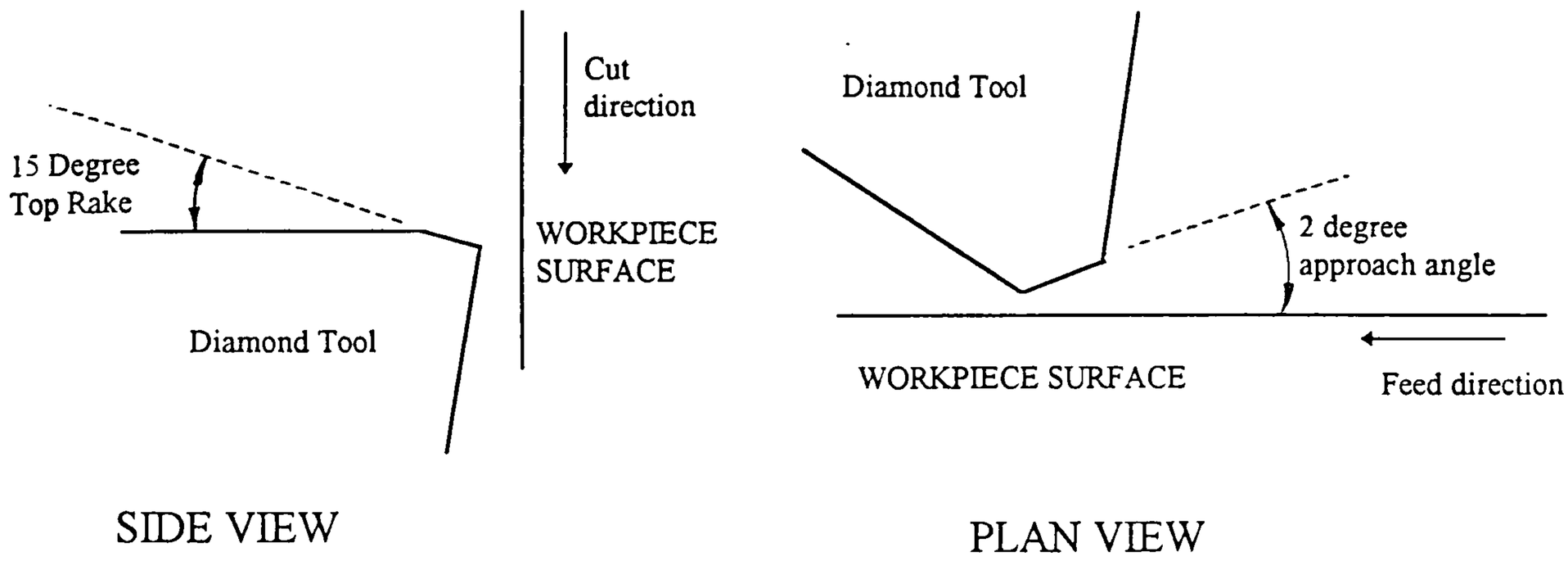

Figure 41 : Schematic Showing Orientation of Flat Nose Tool to Cut Plane

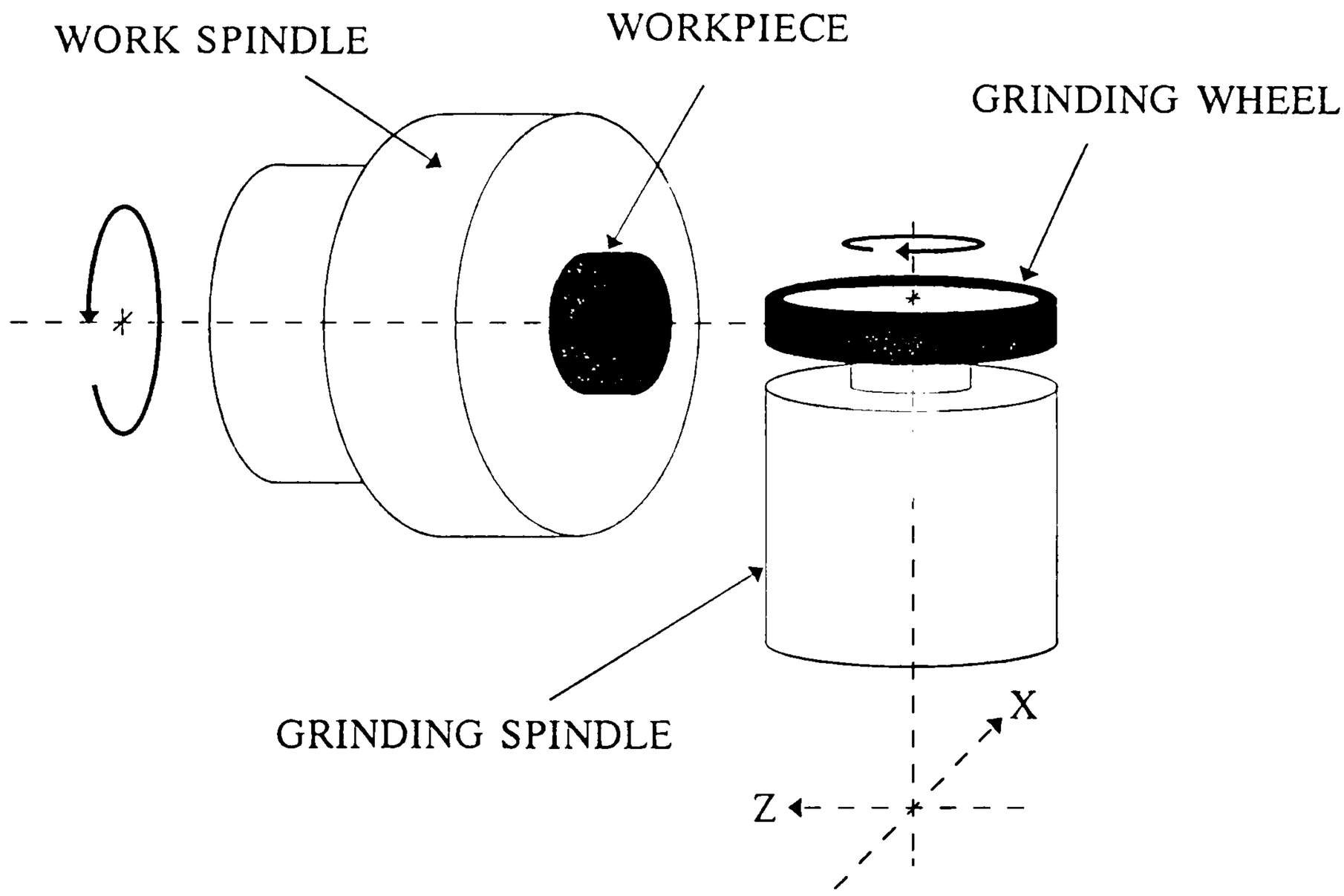

Figure 42 : Schematic of NION Machine Grinding Mode

Figure 43 : Photograph of Wyko & Zygo Phase Shift Interferometers

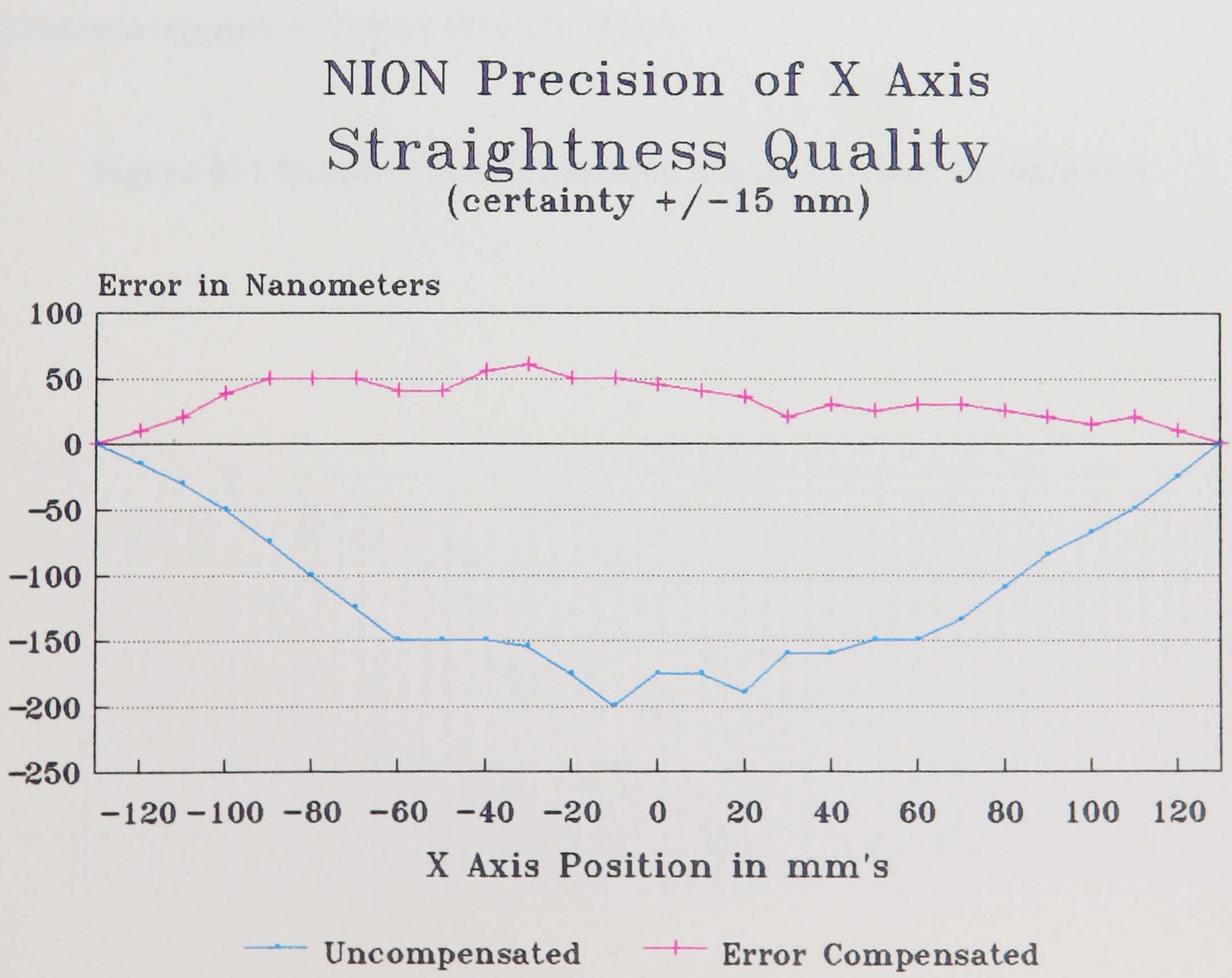

Figure 44 : Graph of NION Machine X Axis Carriage Straightness

Figure 45 : Graph of NION Machine Z Axis Carriage Straightness

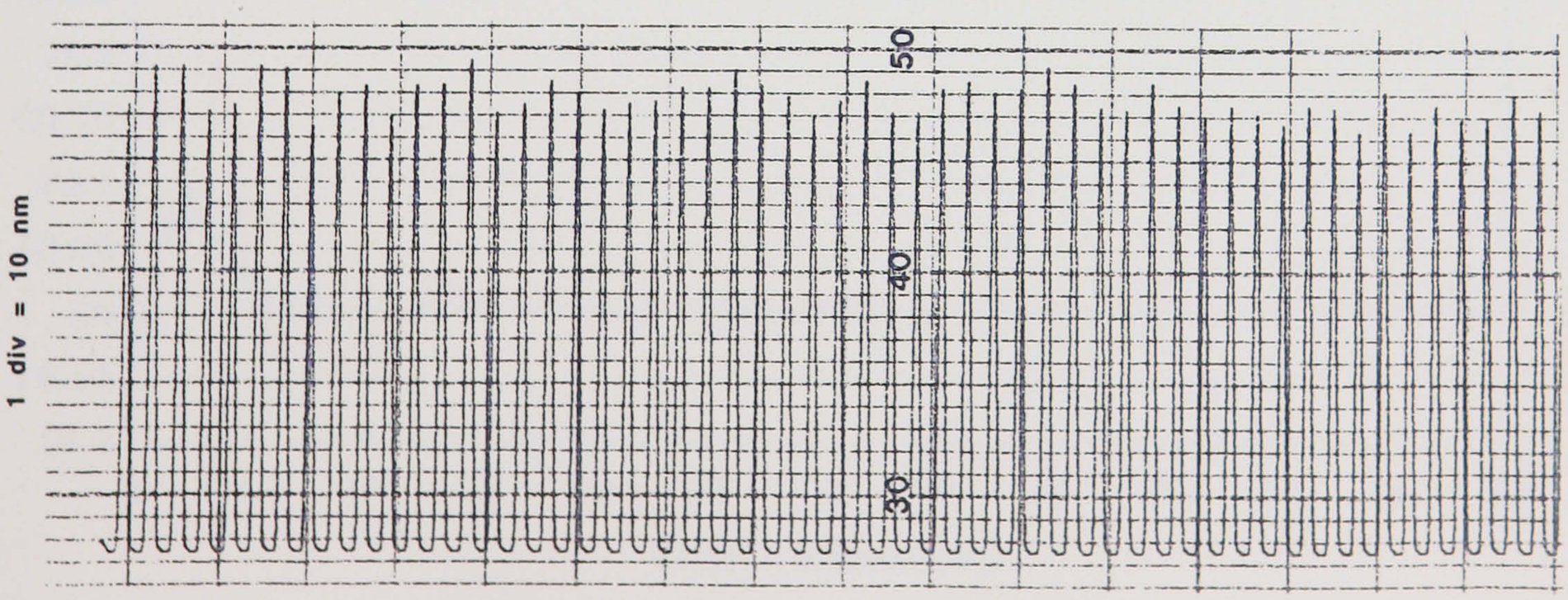

Figure 46 : Graph of Radial Asynchronous Error Motion

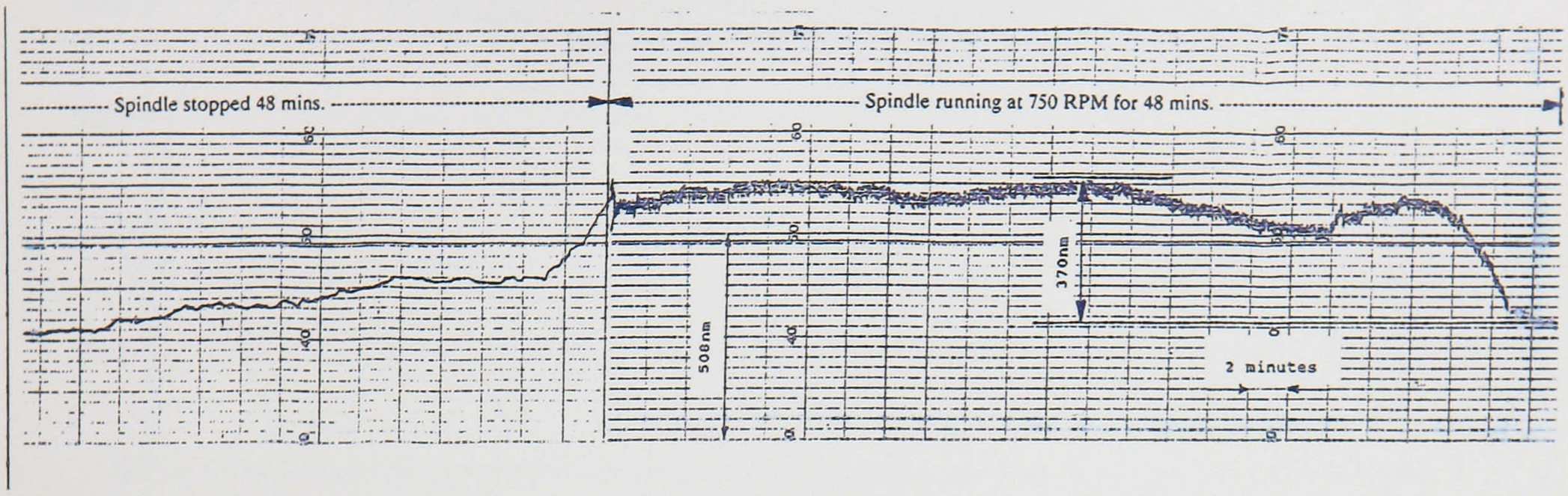

Figure 47 : Graph of Axial Thermal Growth

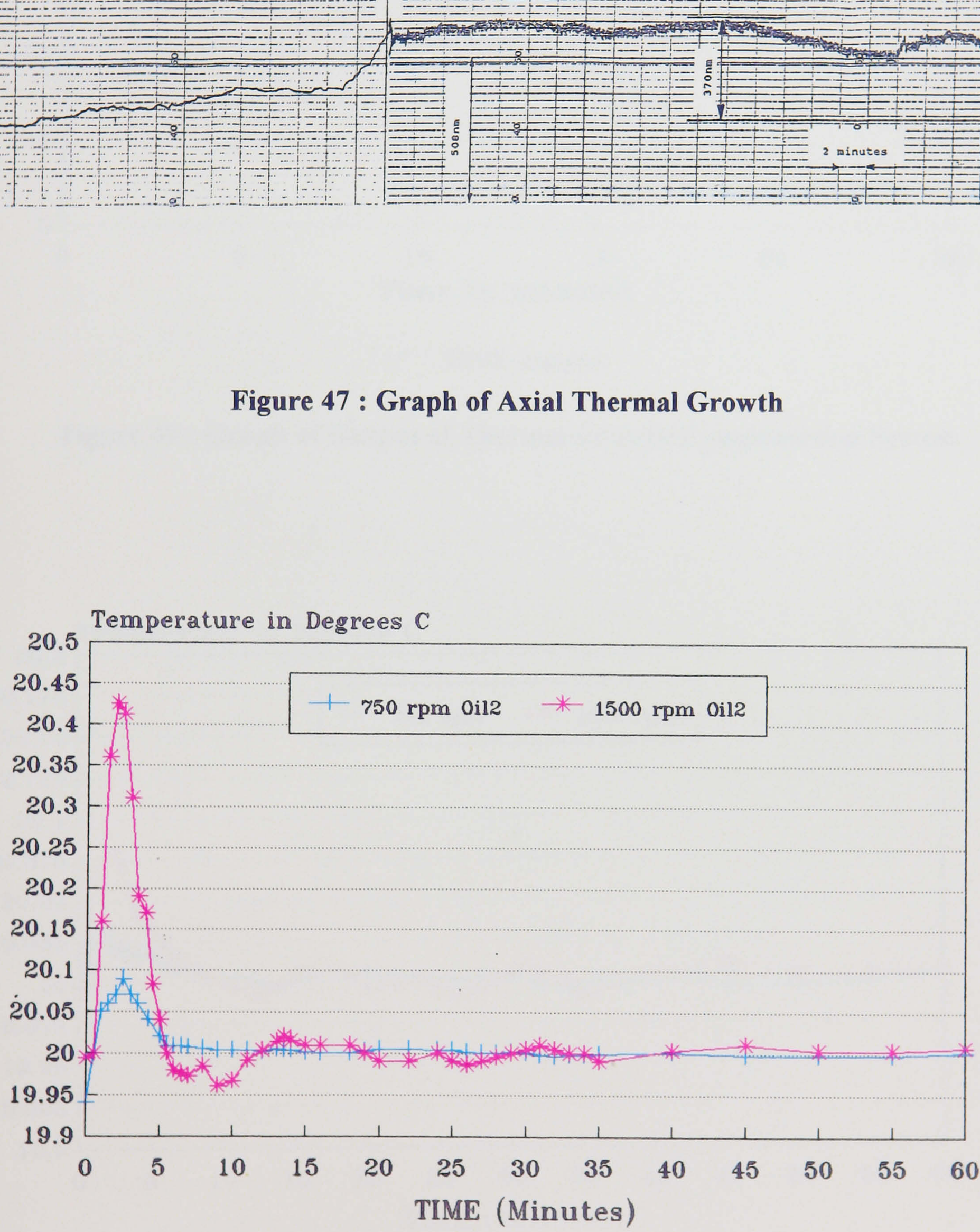

Figure 48 : Graph of Temperature Control of Workhead Spindle Bearing Fluid

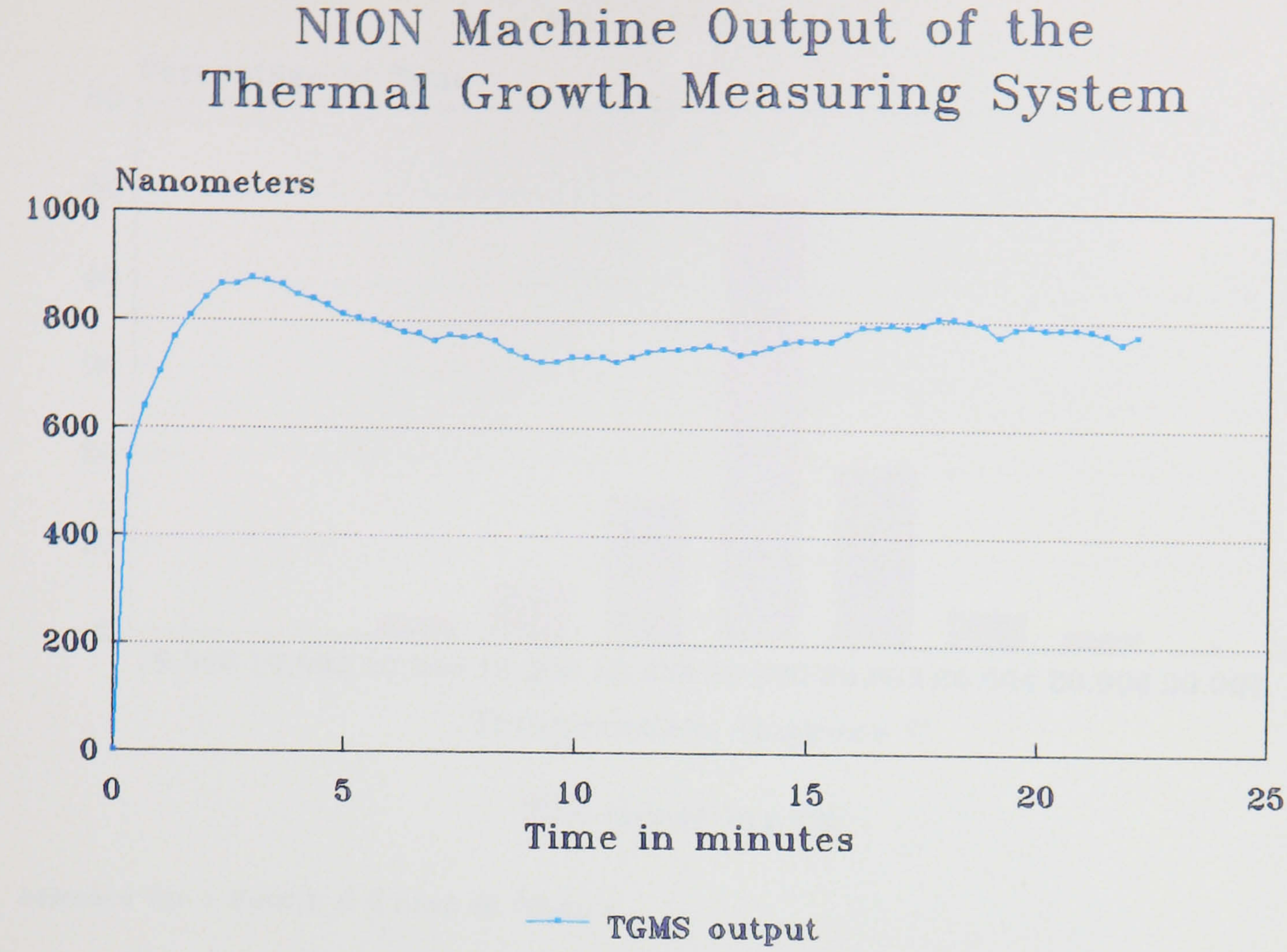

Figure 49 : Graph of Output of Thermal Growth Compensation System

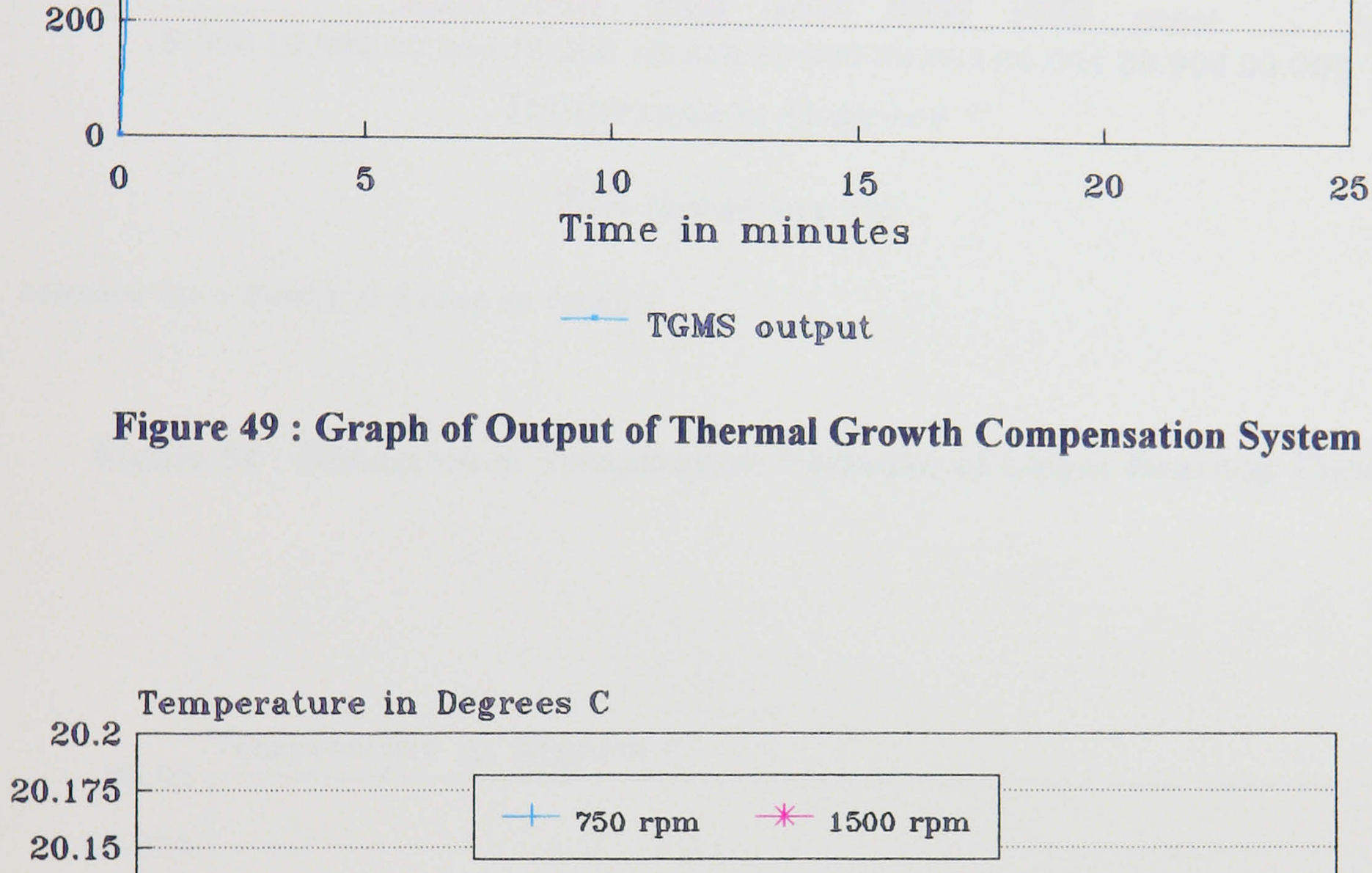

Figure 50 : Graph of Temperature Control of Workhead Spindle Motor Coolant

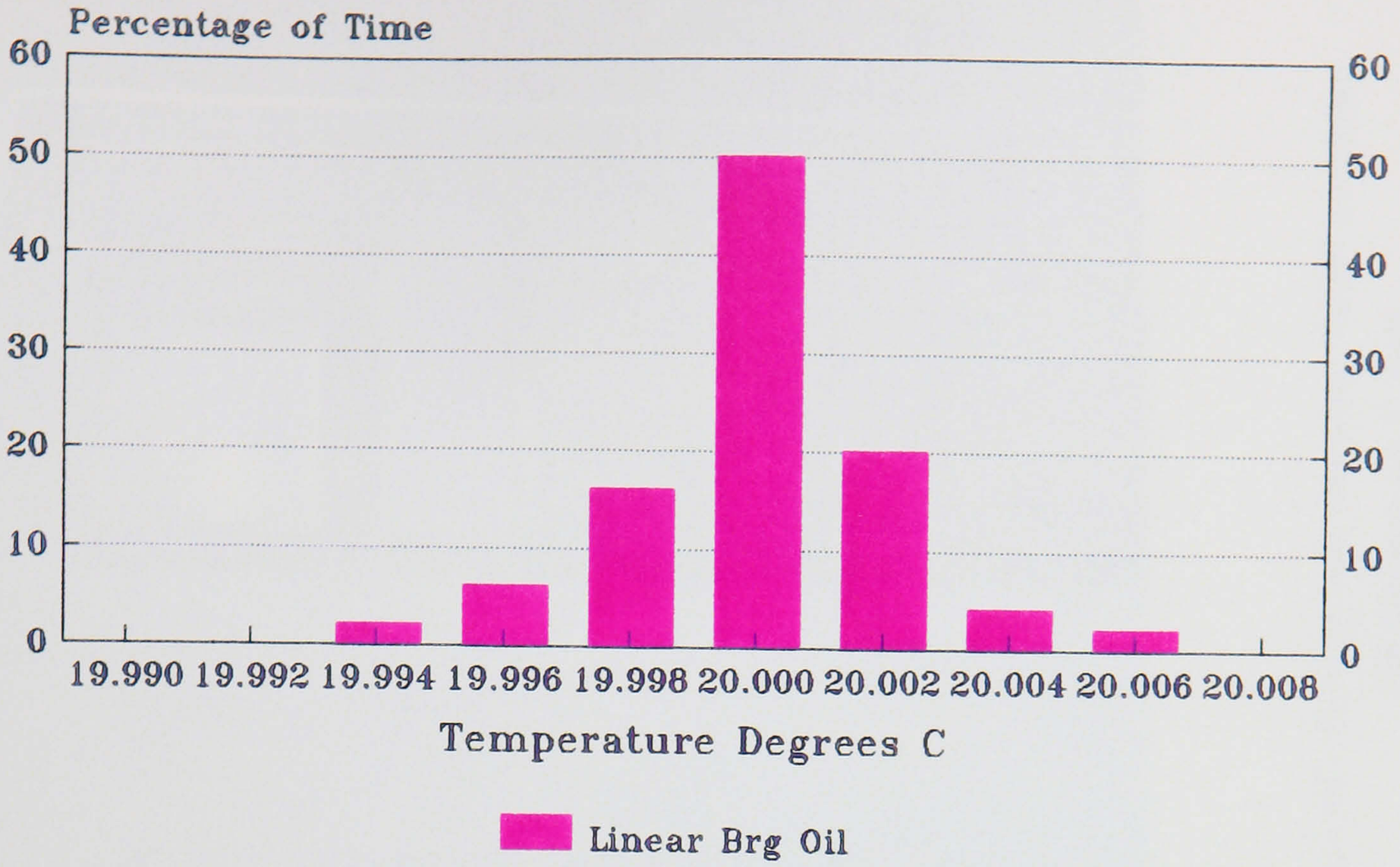

Assessed for 1 hour,X & Z axes at 5mm/s

Figure 51 : Histogram of Temperature Variation of Linear Bearings Fluid

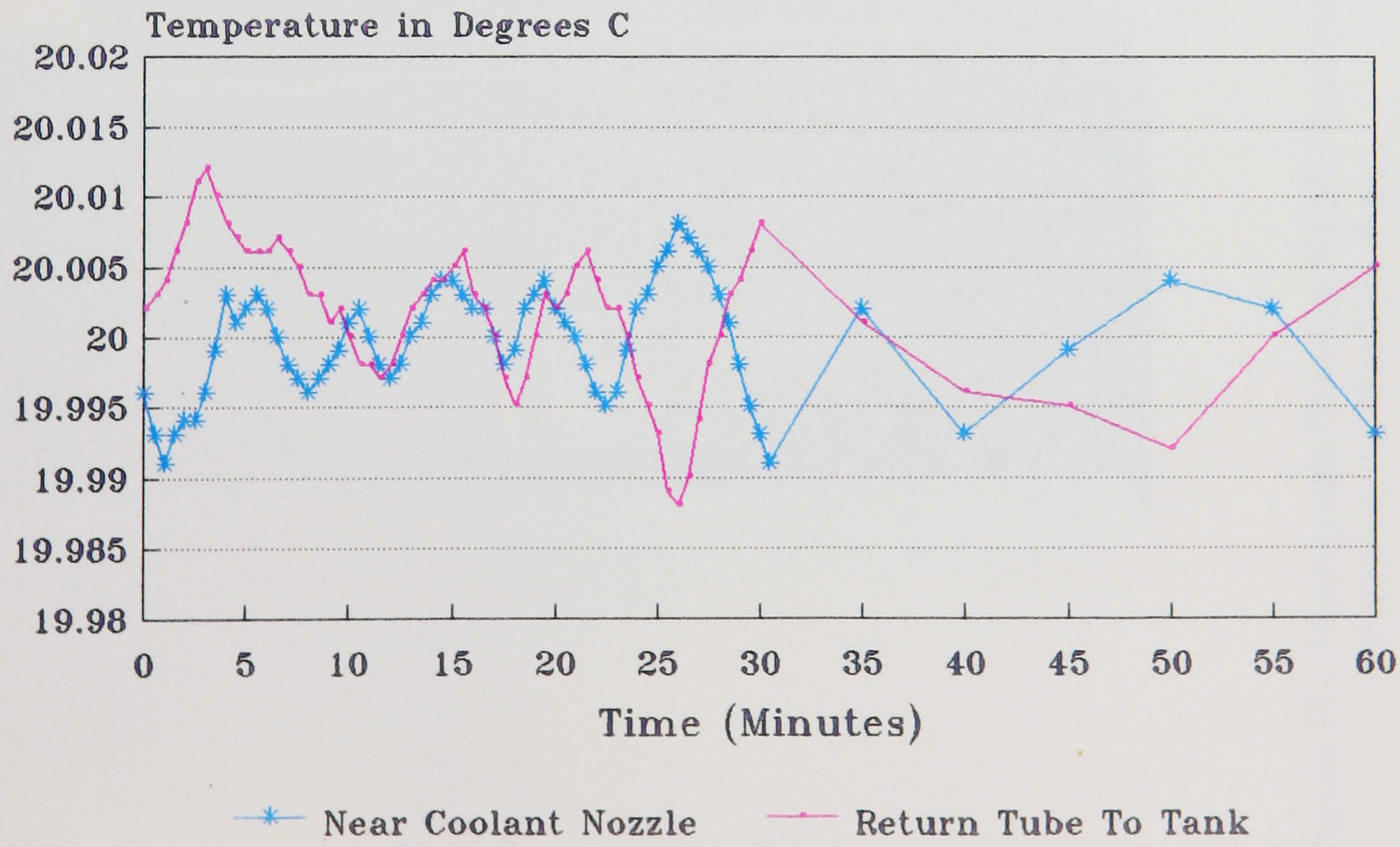

Figure 52 : Graph of Temperature Control of Grinding Coolant

Figure 53 : Photograph Showing NION Machine Oil Shower on Machine Base

Figure 54 : Photograph Showing NION Machine Oil Shower on X Axis

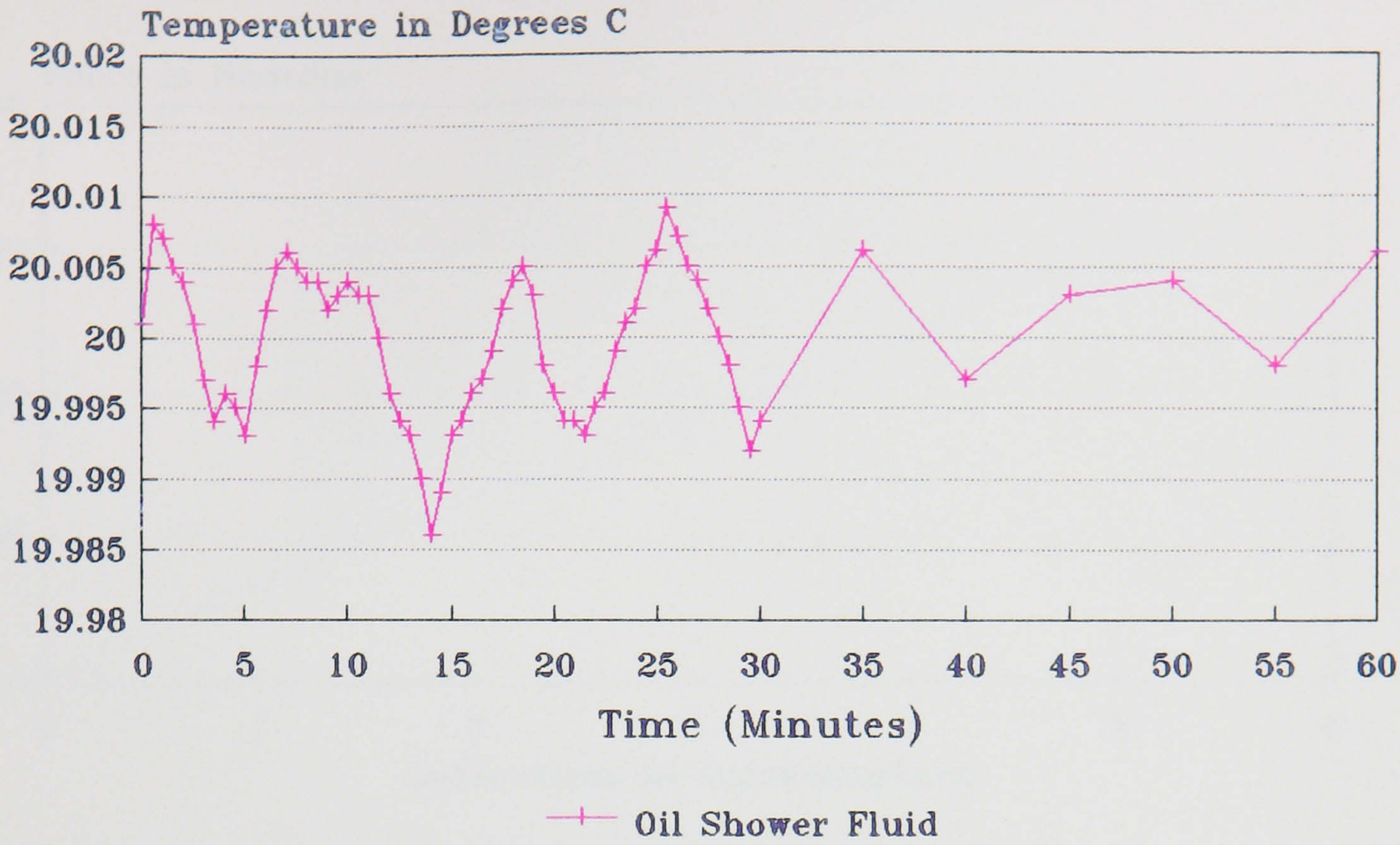

C, X, Z and B Axes all moving

Figure 55 : Graph of Temperature Control of Oil Shower Fluid

(Spindle stopped after 54 minutes)

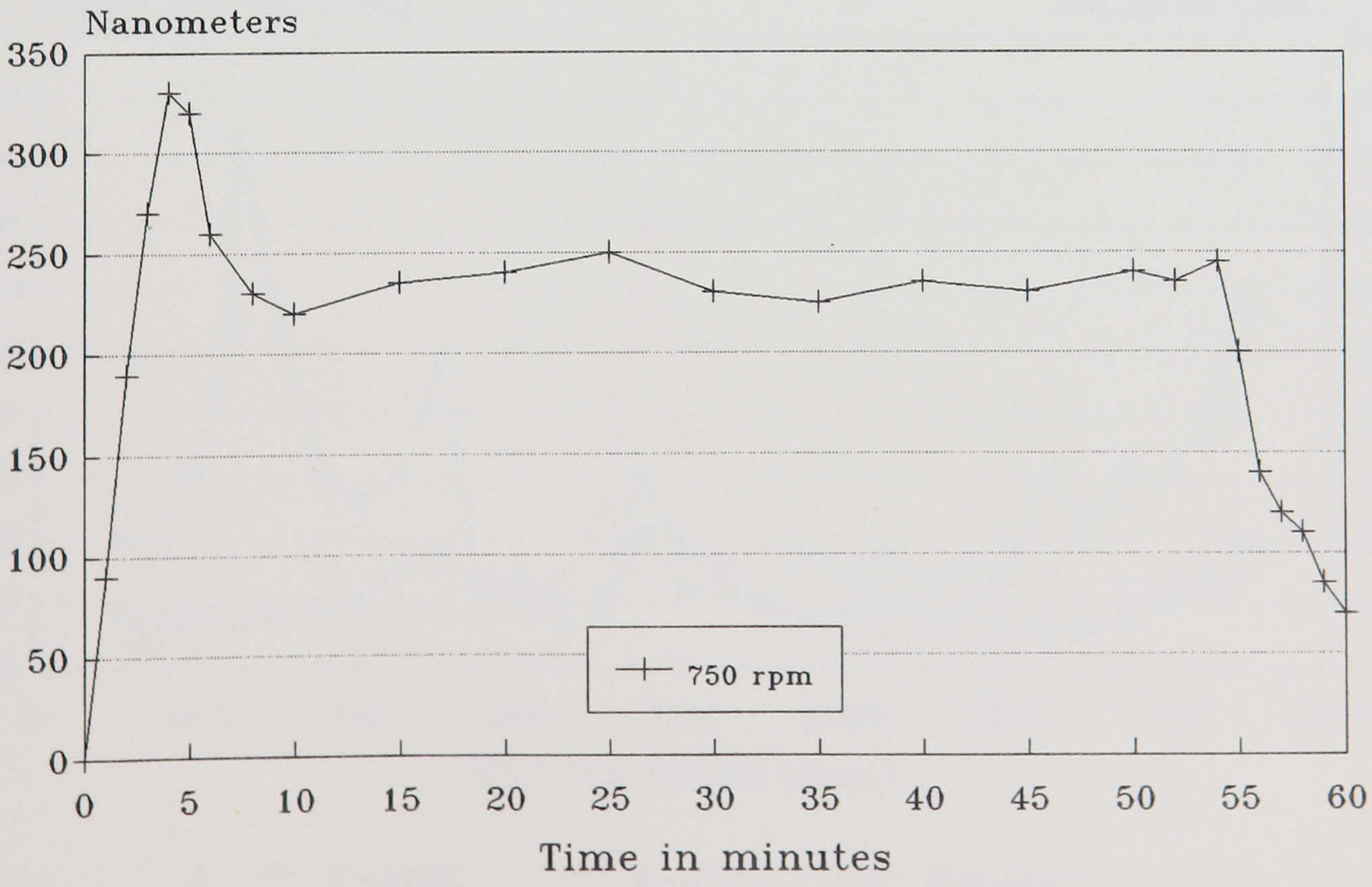

Figure 56 : Graph of Thermal Stability of NION Machine

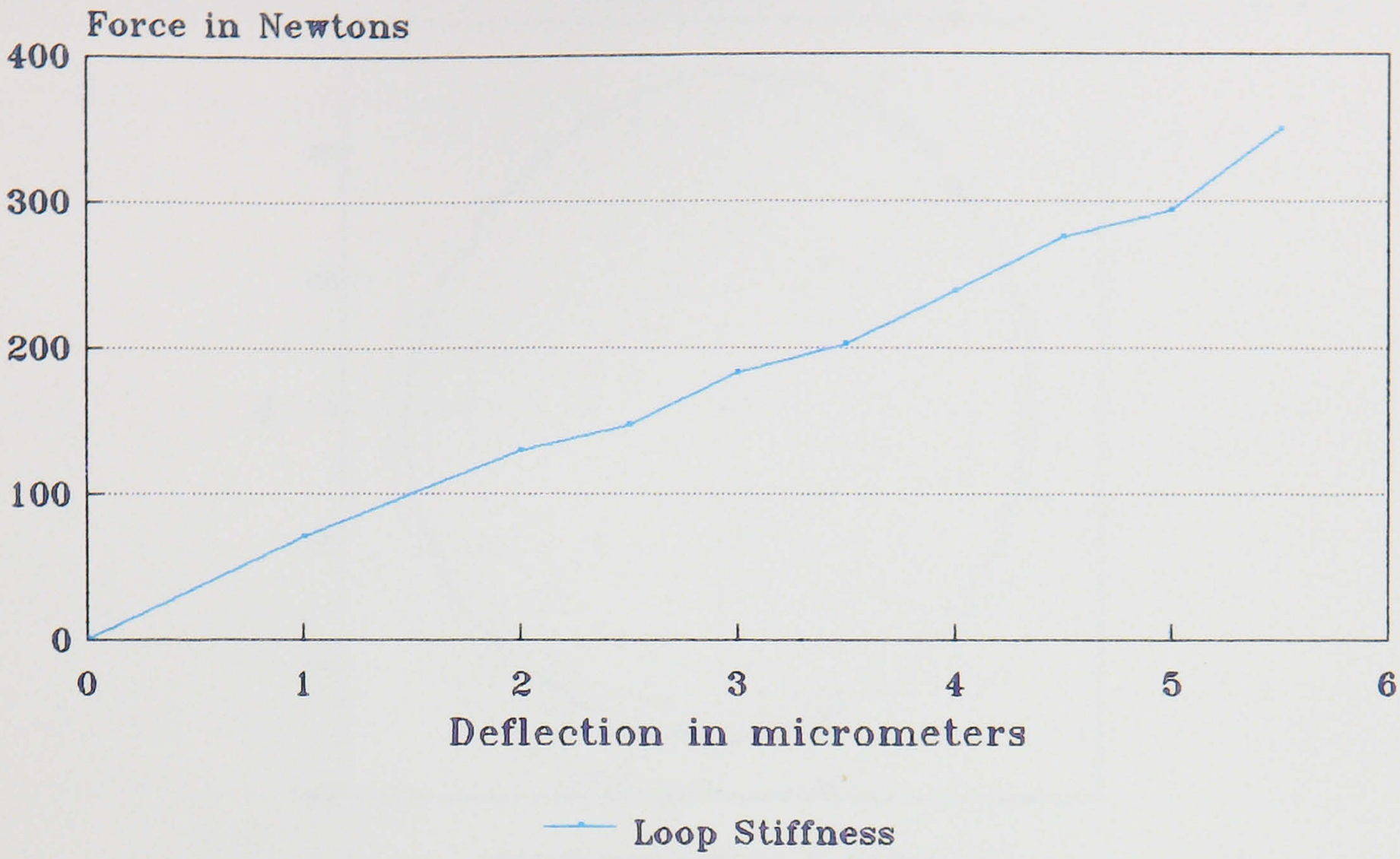

Figure 57 : Graph of NION Machine Static Loop Stiffness

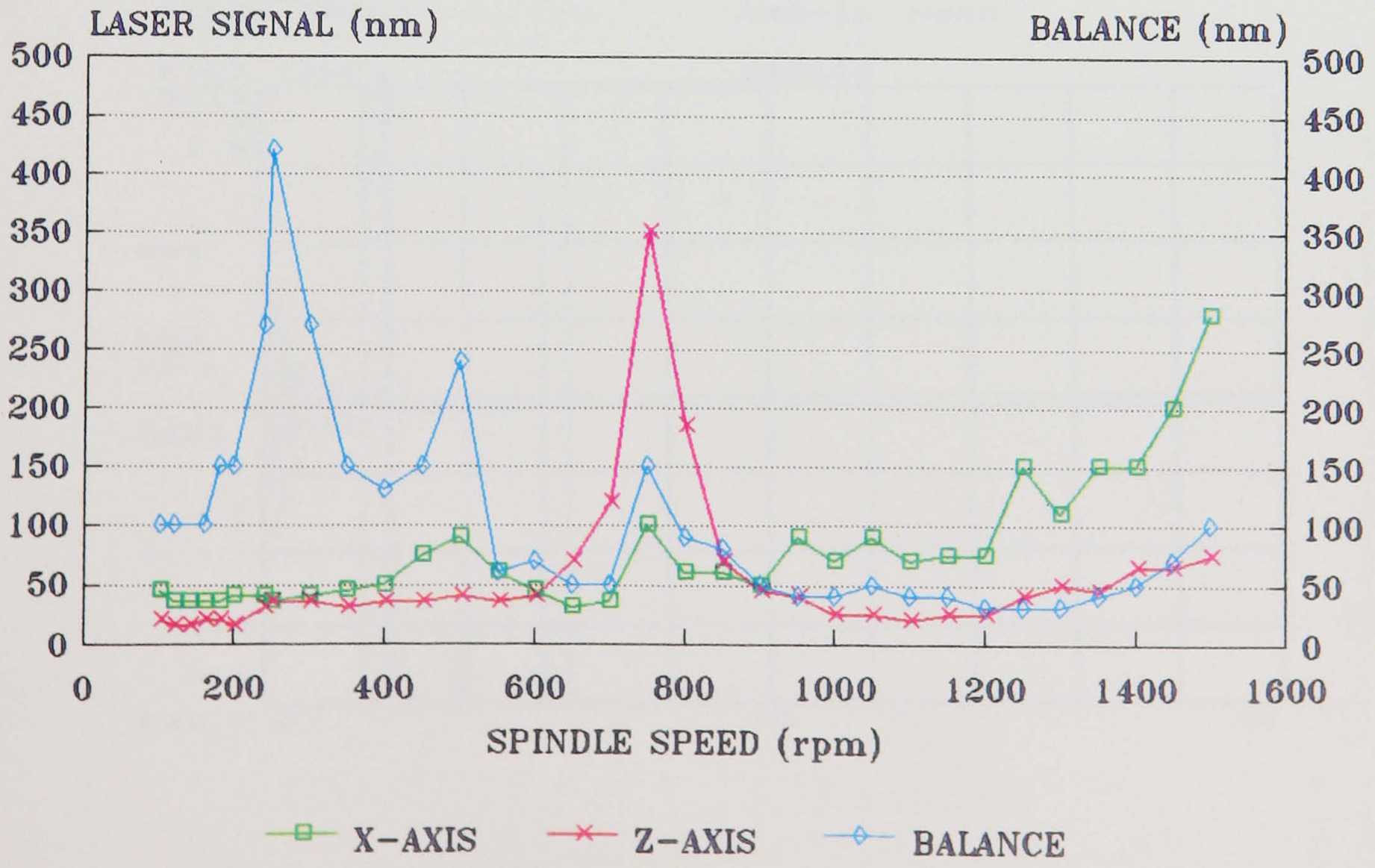

Figure 58 : Graph of NION Machine Laser Noise / Workhead Spindle Speed

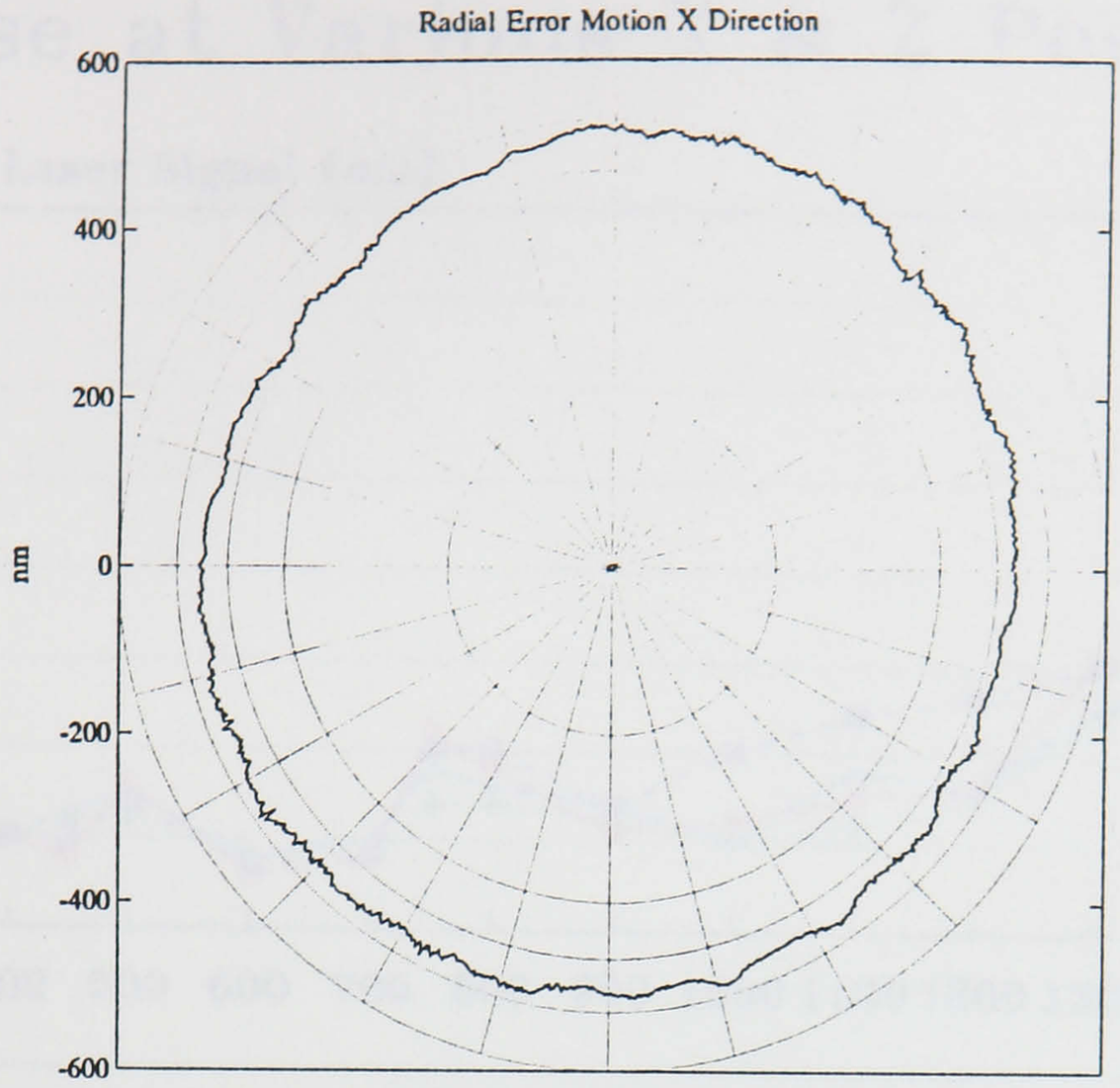

Figure 59 : Graph of Radial Error Motion of NION Workhead Spindle

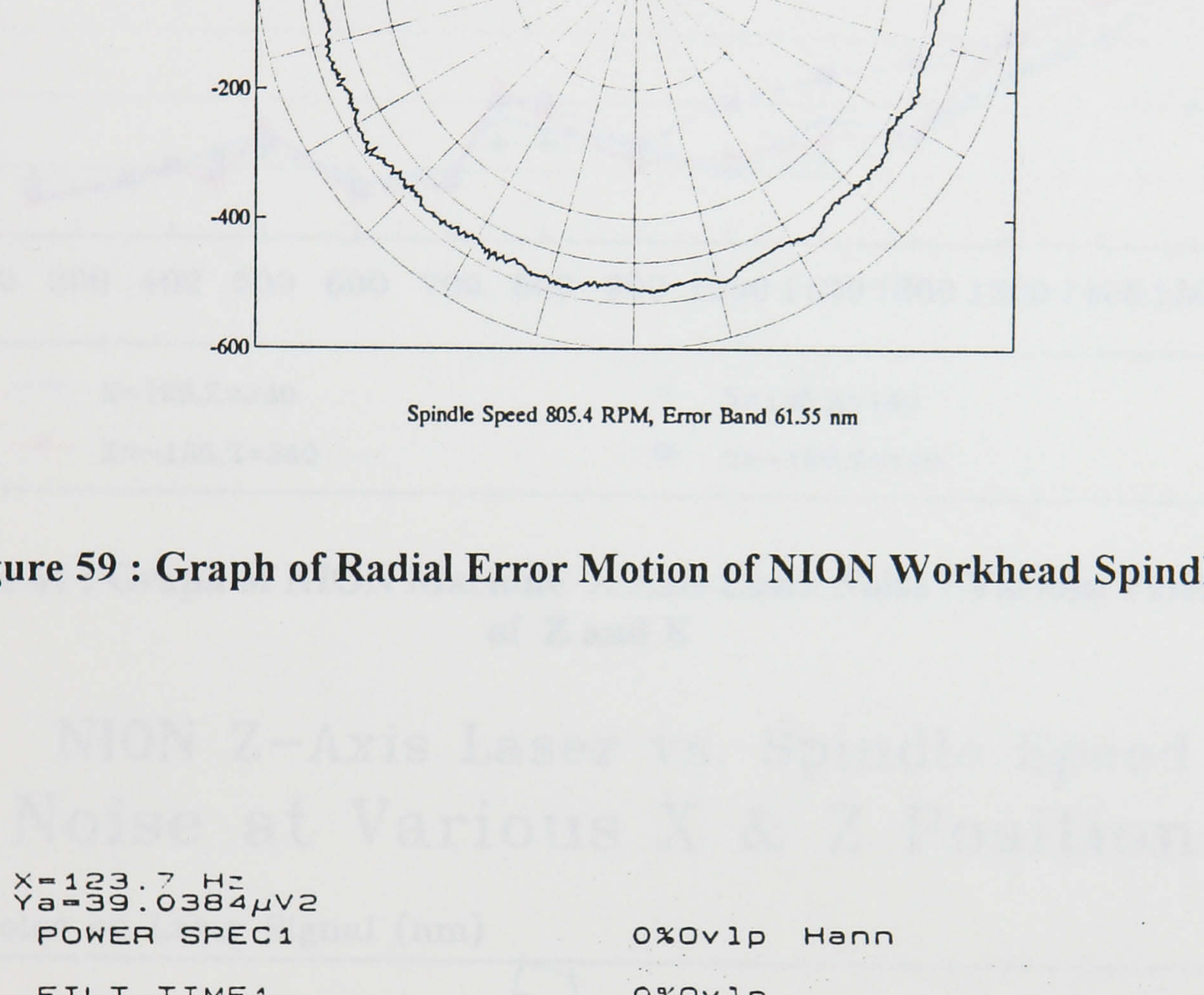

Figure 60 : Graph of NION Machine Metrology Frame Frequency Response

NION X-Axis Laser vs. Spindle Speed
Noise at Various X & Z Positions

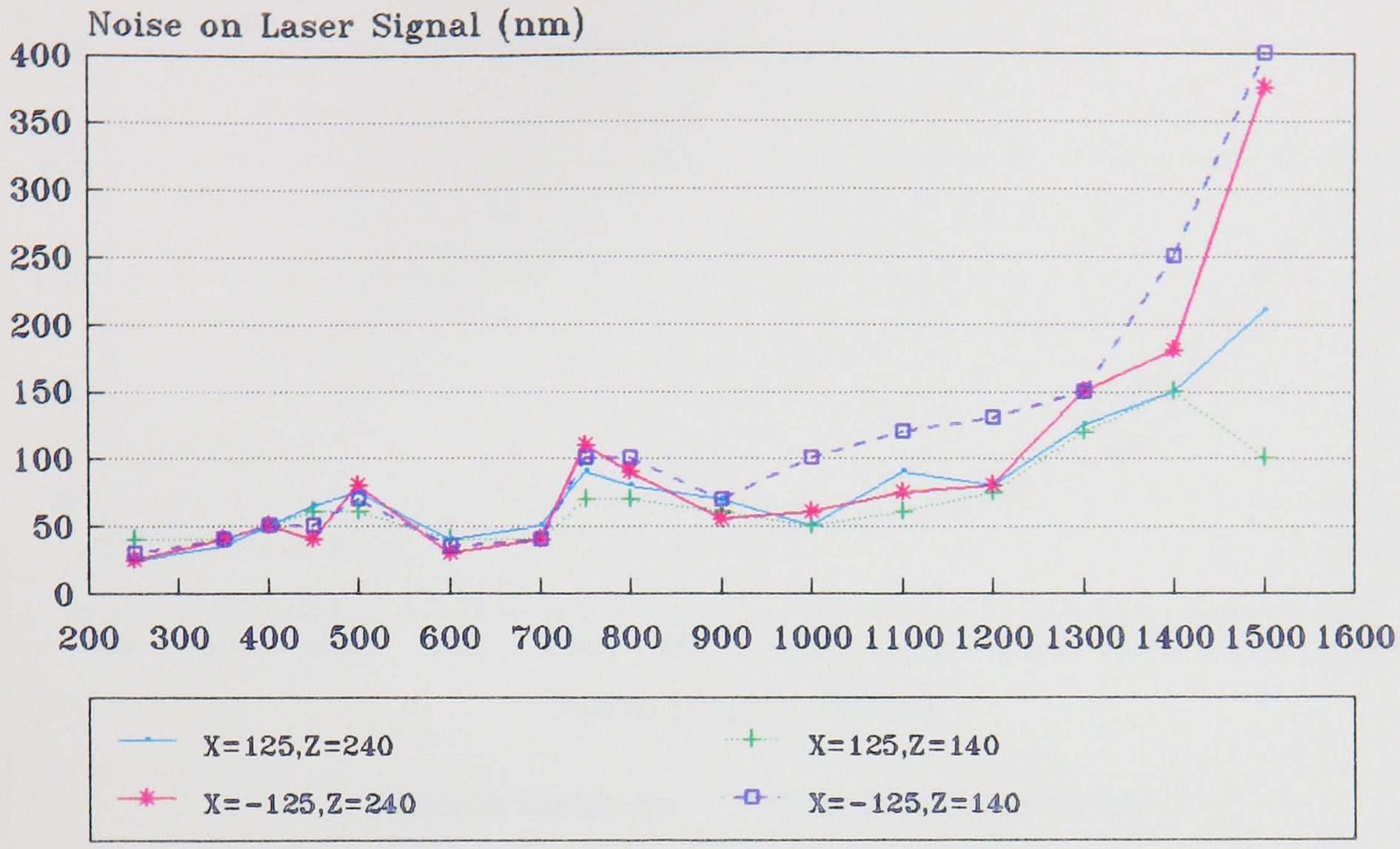

Figure 61 : Graph of NION Machine X Axis Laser Noise / Various Positions of Z and X

NION Z-Axis Laser vs. Spindle Speed
Noise at Various X & Z Positions

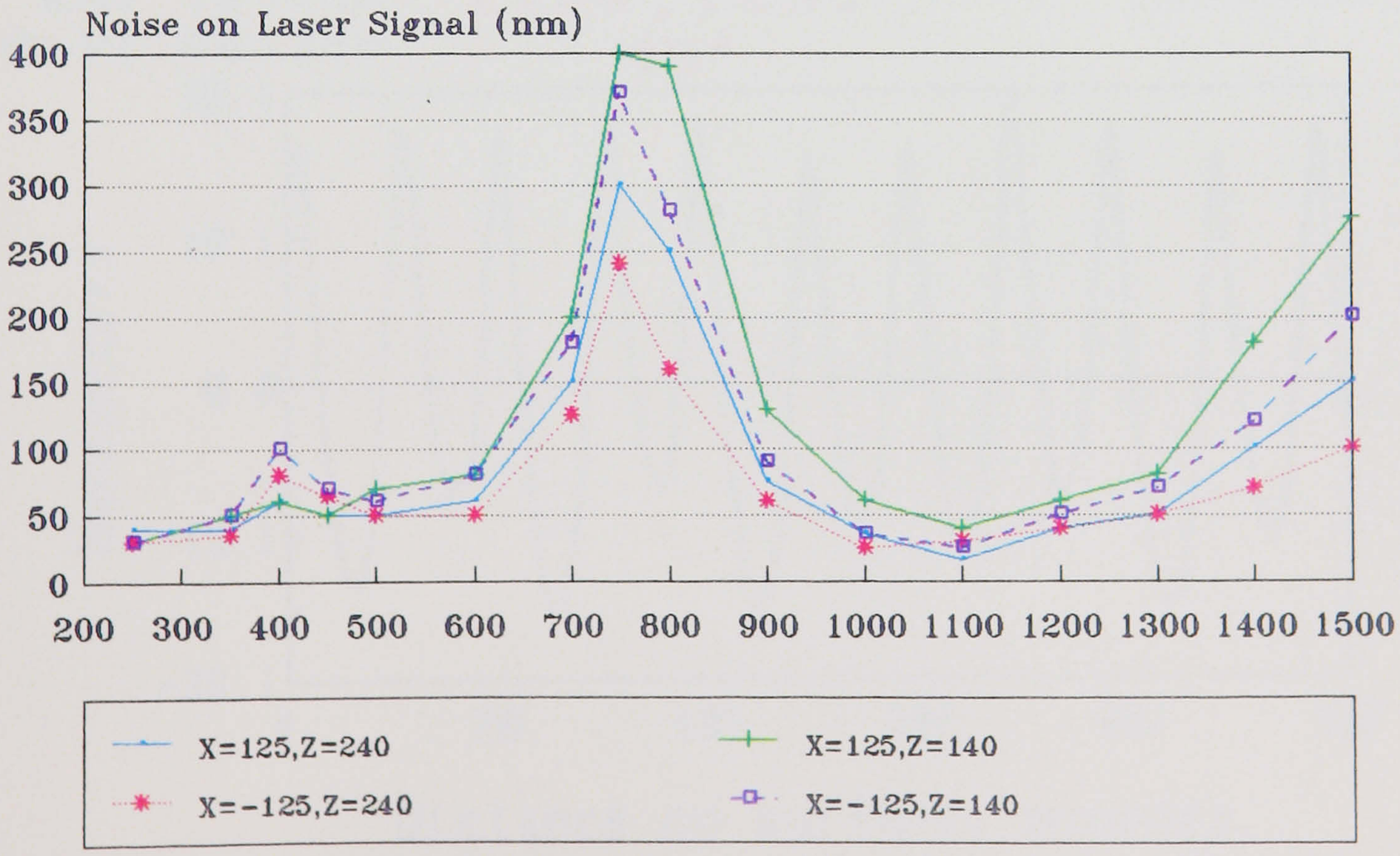

Figure 62 : Graph of NION Machine Z Axis Laser Noise / Various Positions of Z and X

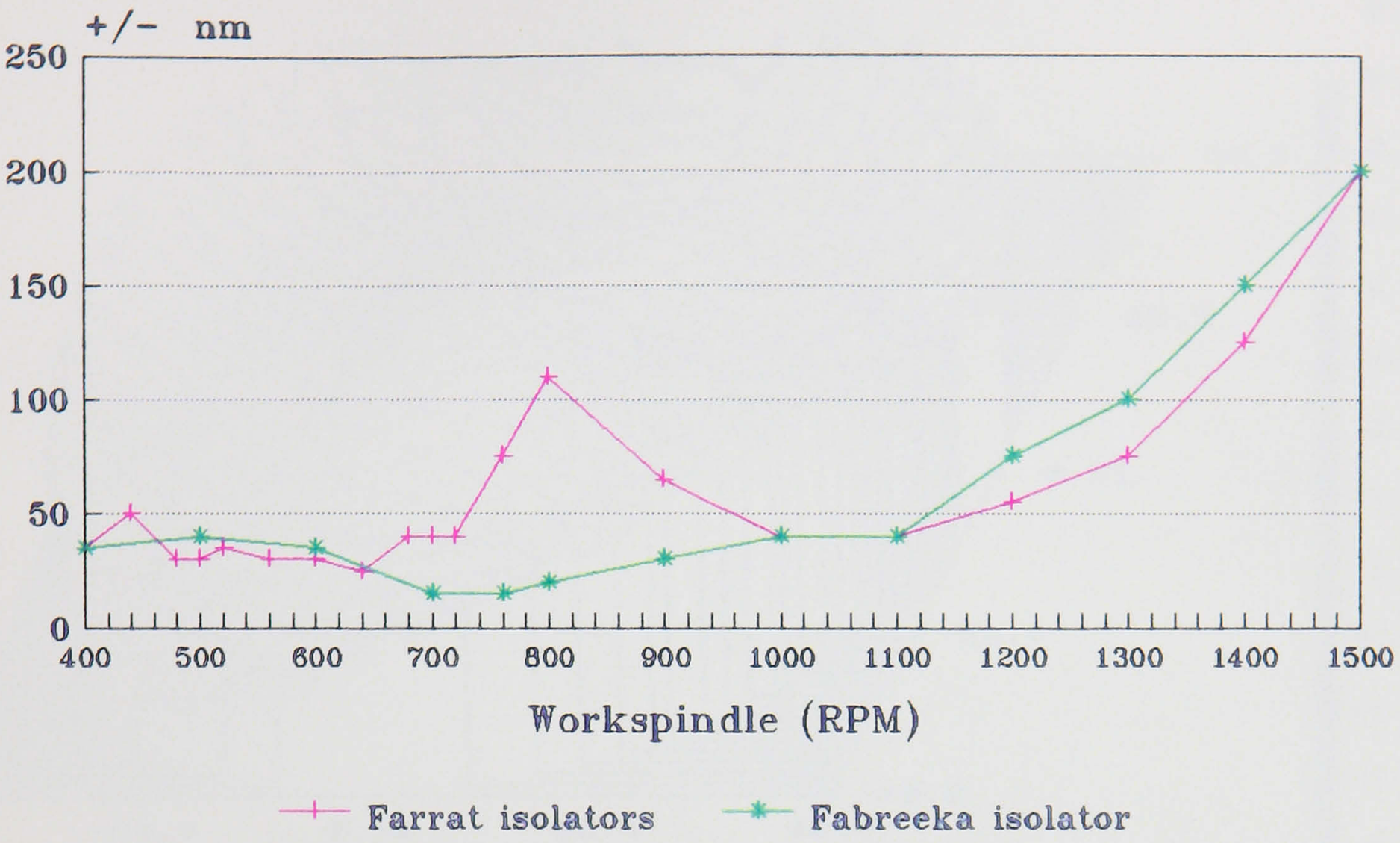

Figure 63 : Graph of NION Machine Laser Noise / Various Isolation Feet

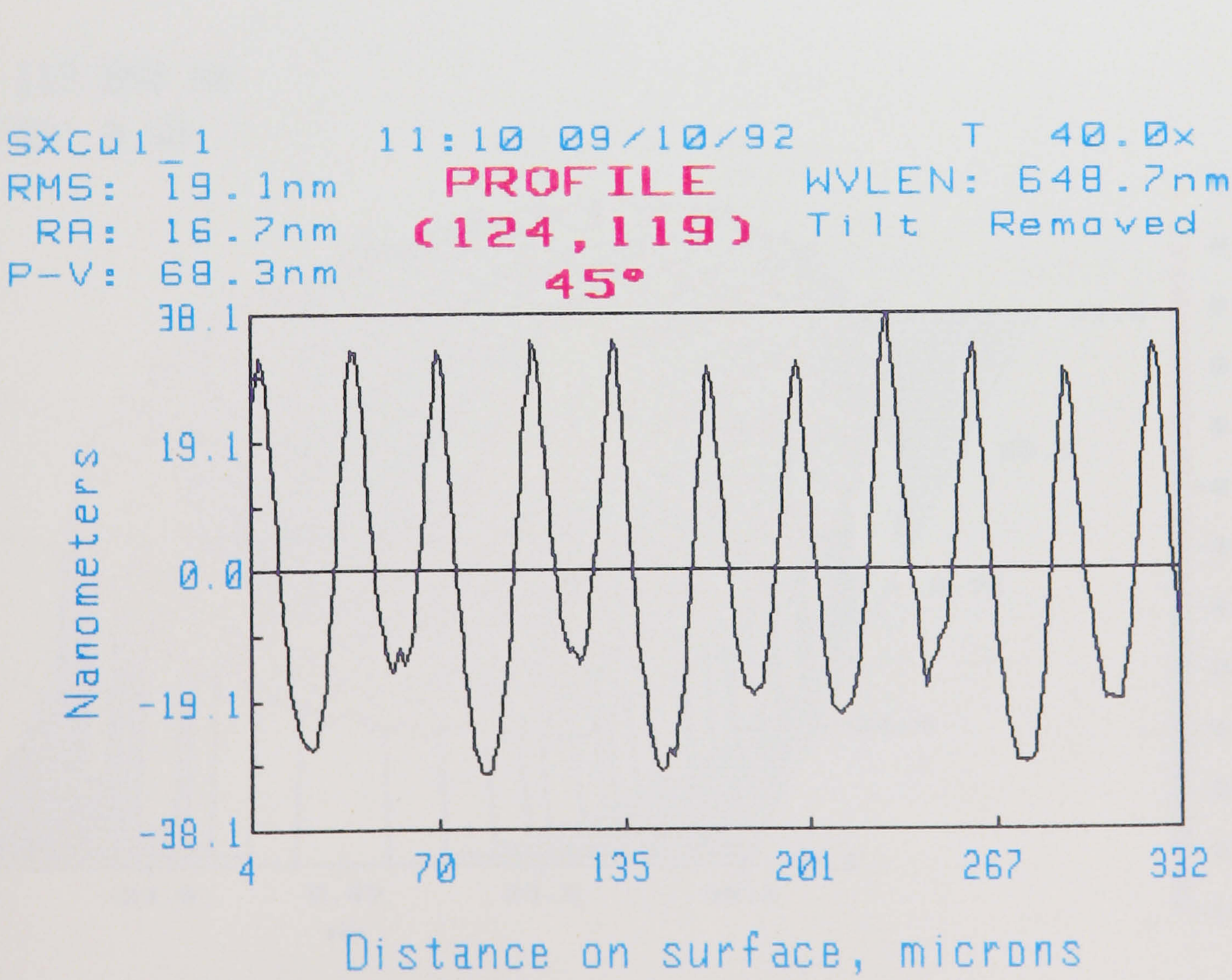

Figure 64 : Wyko 2D Surface Roughness Trace of Diamond Turned Copper

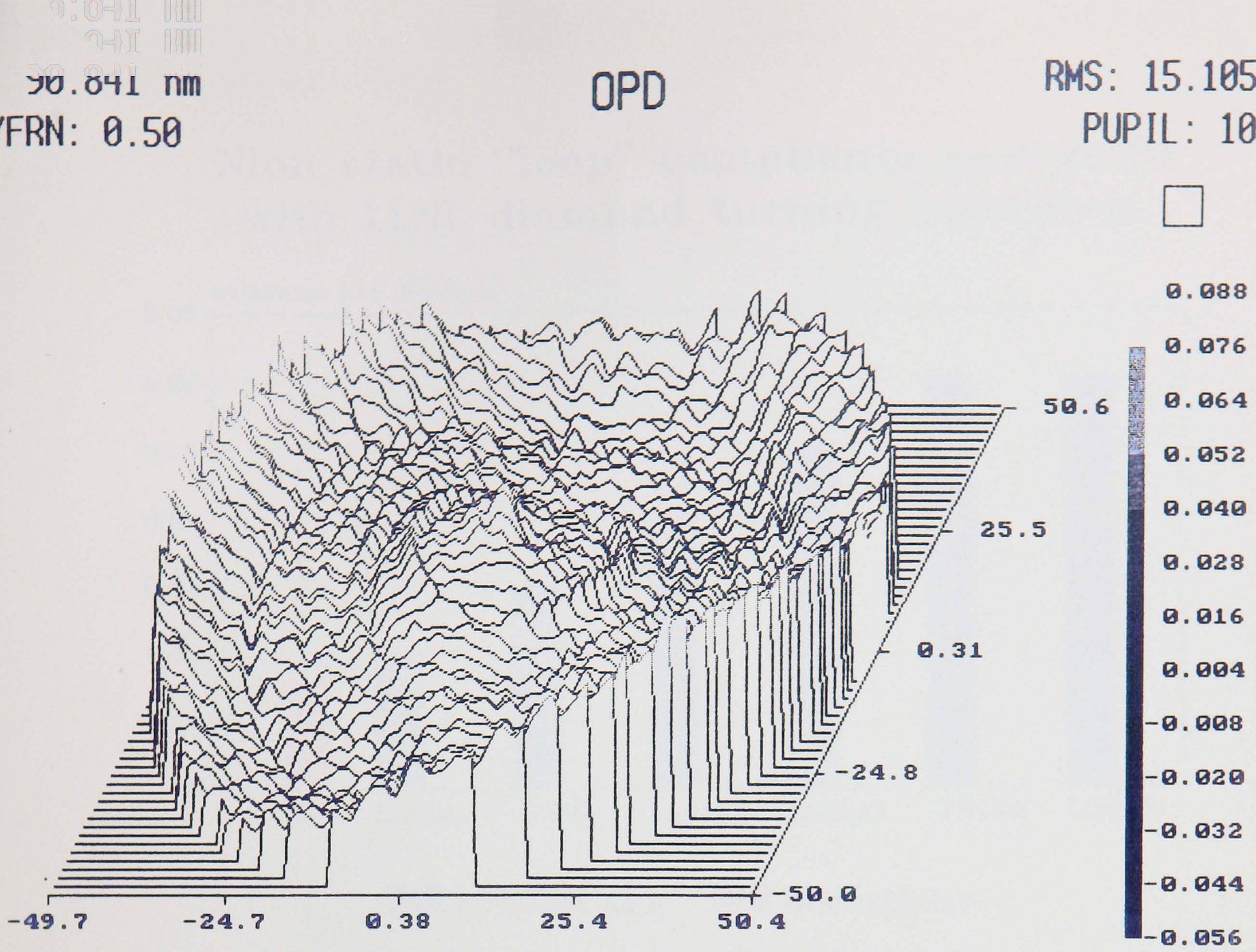

Figure 65 : Wyko 3D Surface Form Plot of 100 mm Diameter Aluminium Flat

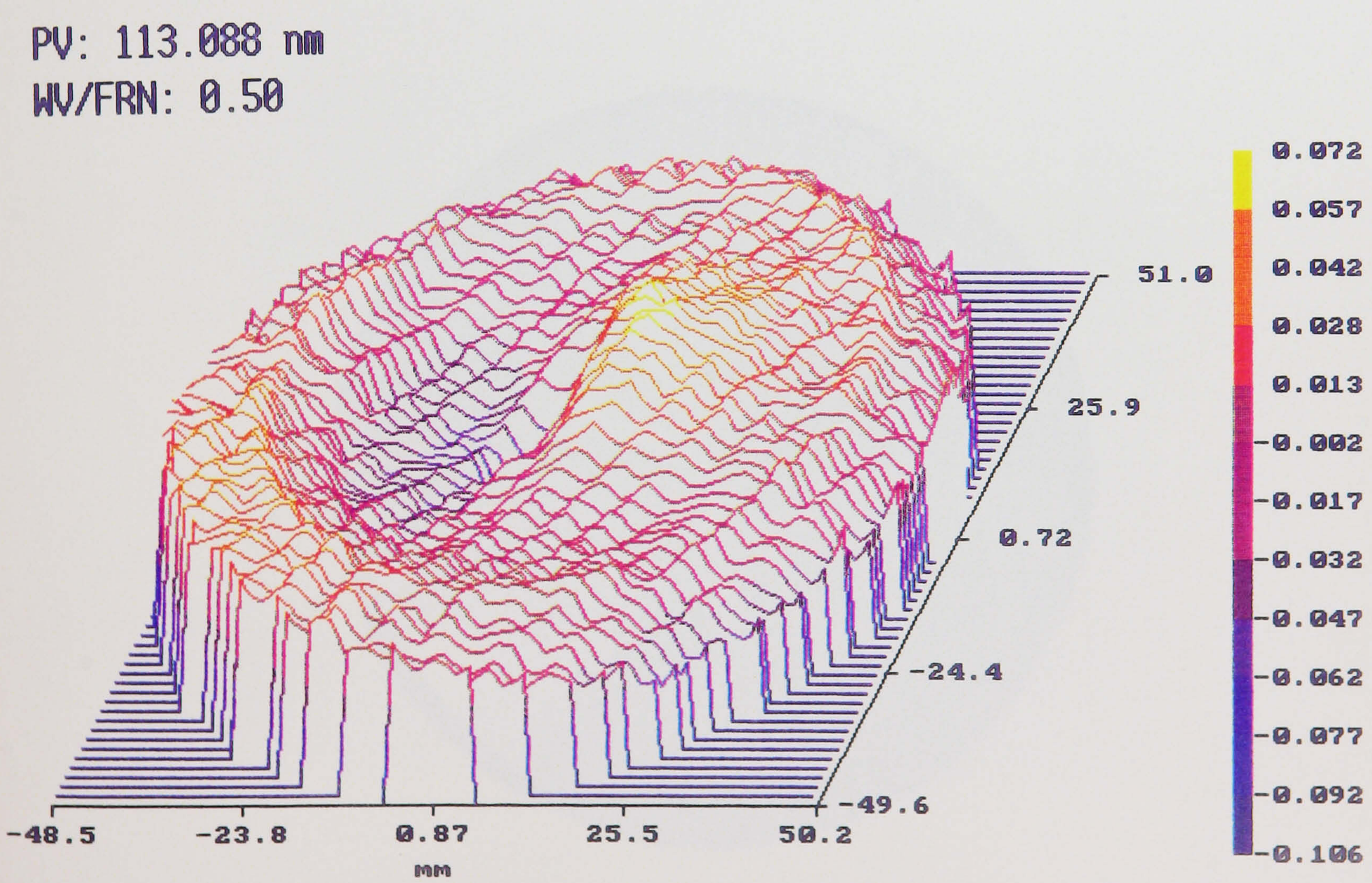

Figure 66 : Wyko 3D Surface Form Plot of Concave Spherical Aluminium Mirror

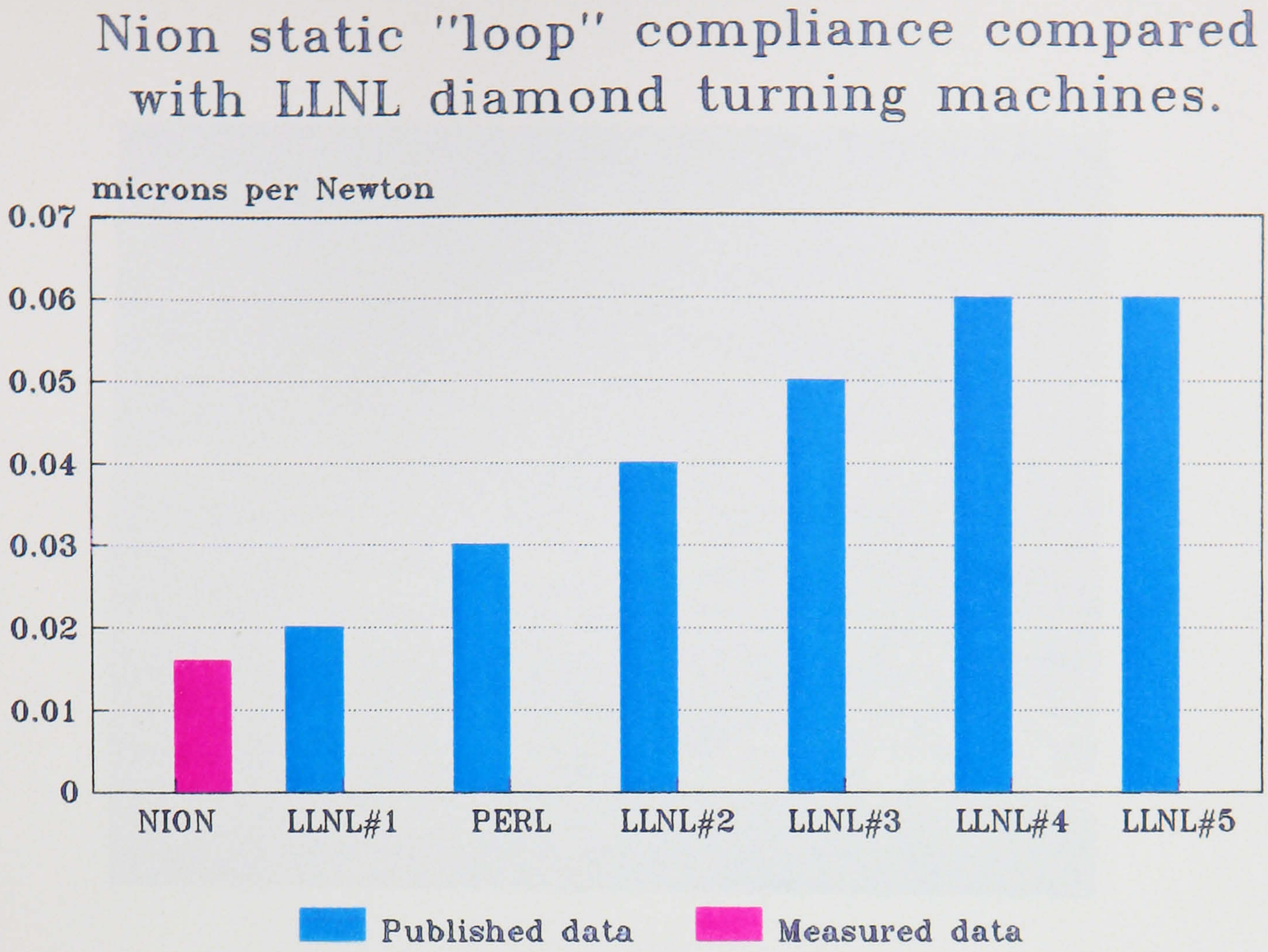

Figure 67 : Histogram showing Loop Compliance of Various Diamond Turning Machines

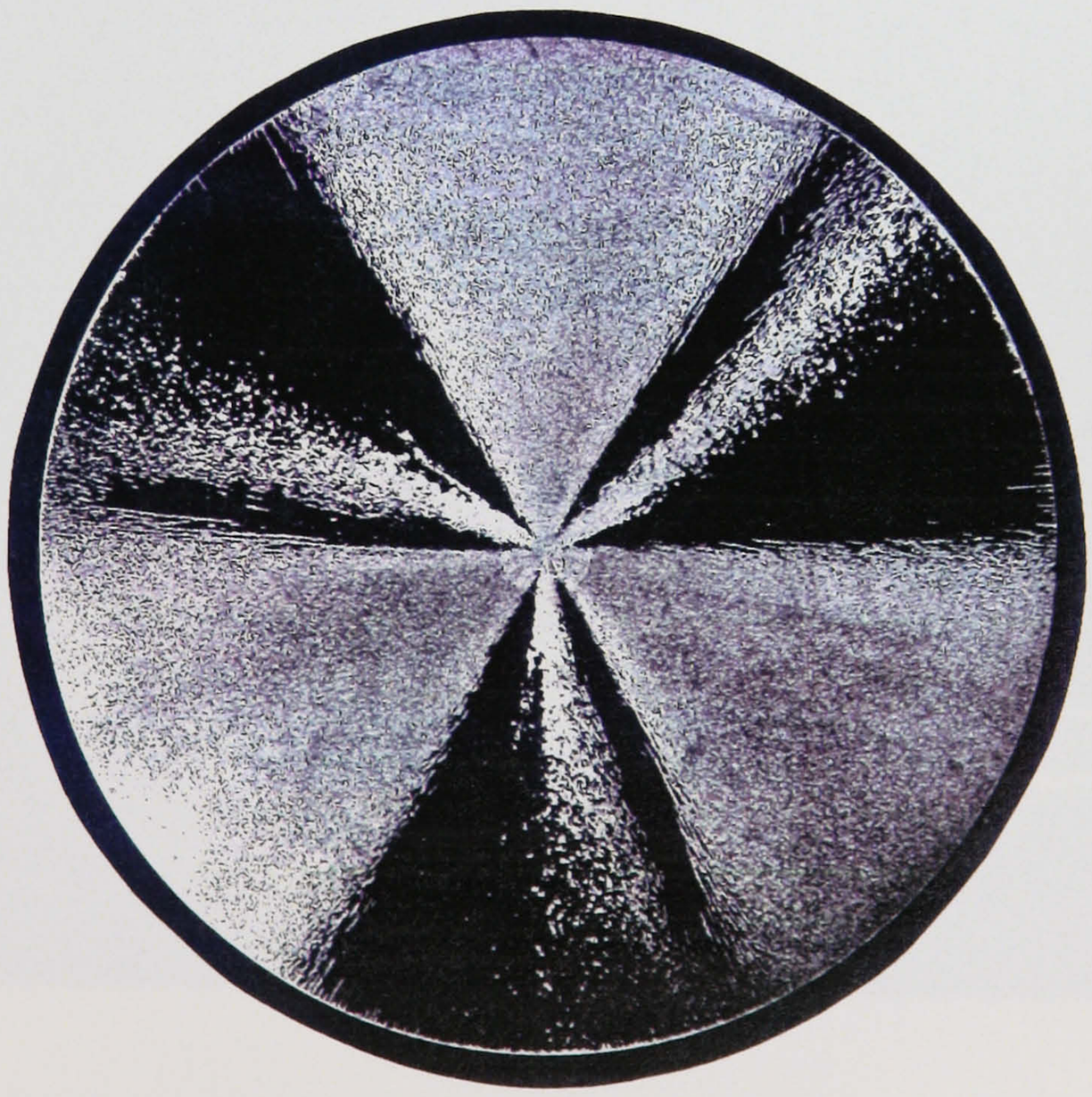

Figure 68 : Photomicrograph of Diamond Turned Germanium, Sample 4 <111> Orientation

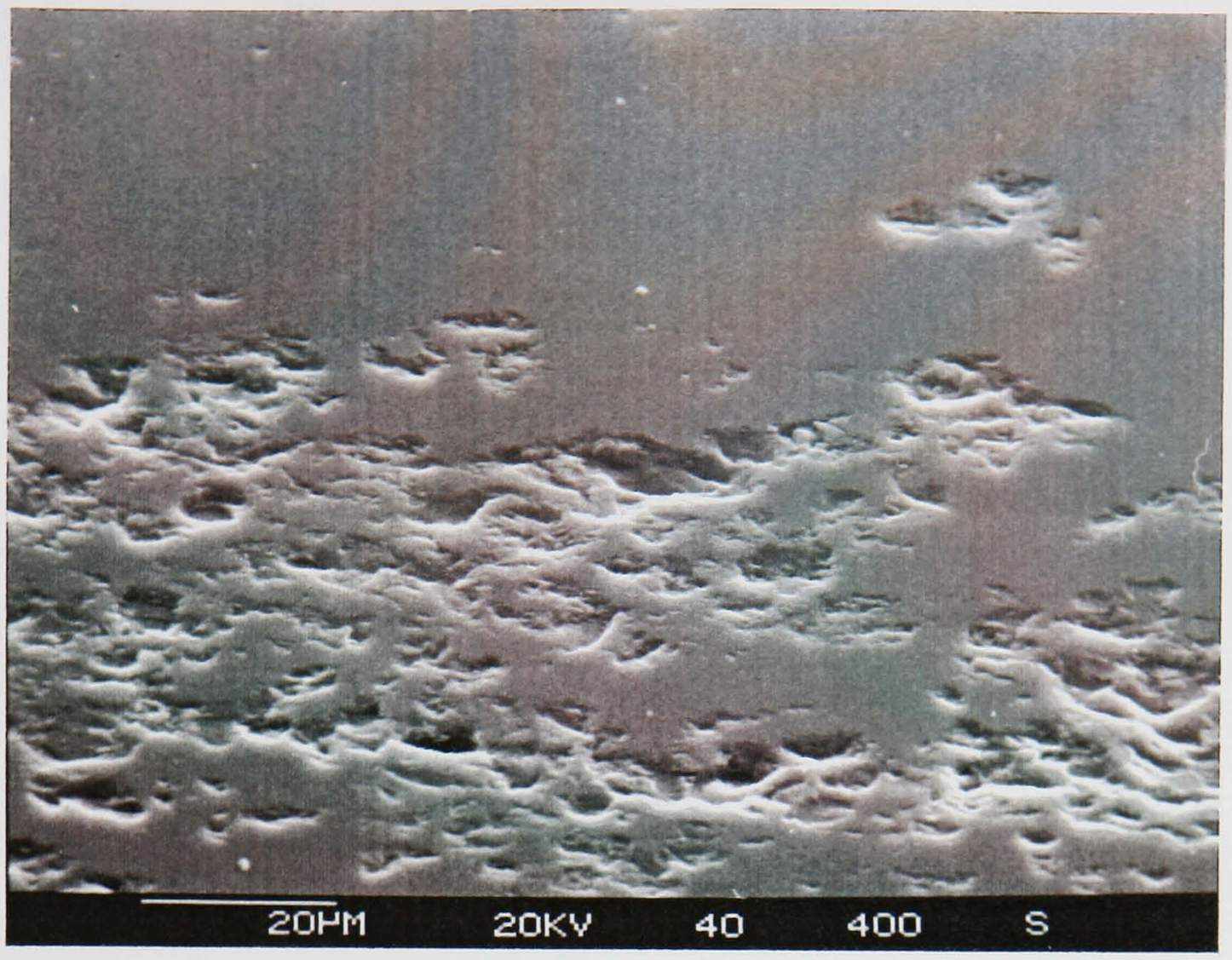

Figure 69 : S.E.M. Micrograph showing Detail of Diamond Turned Germanium, Sample 4 <111> Orientation

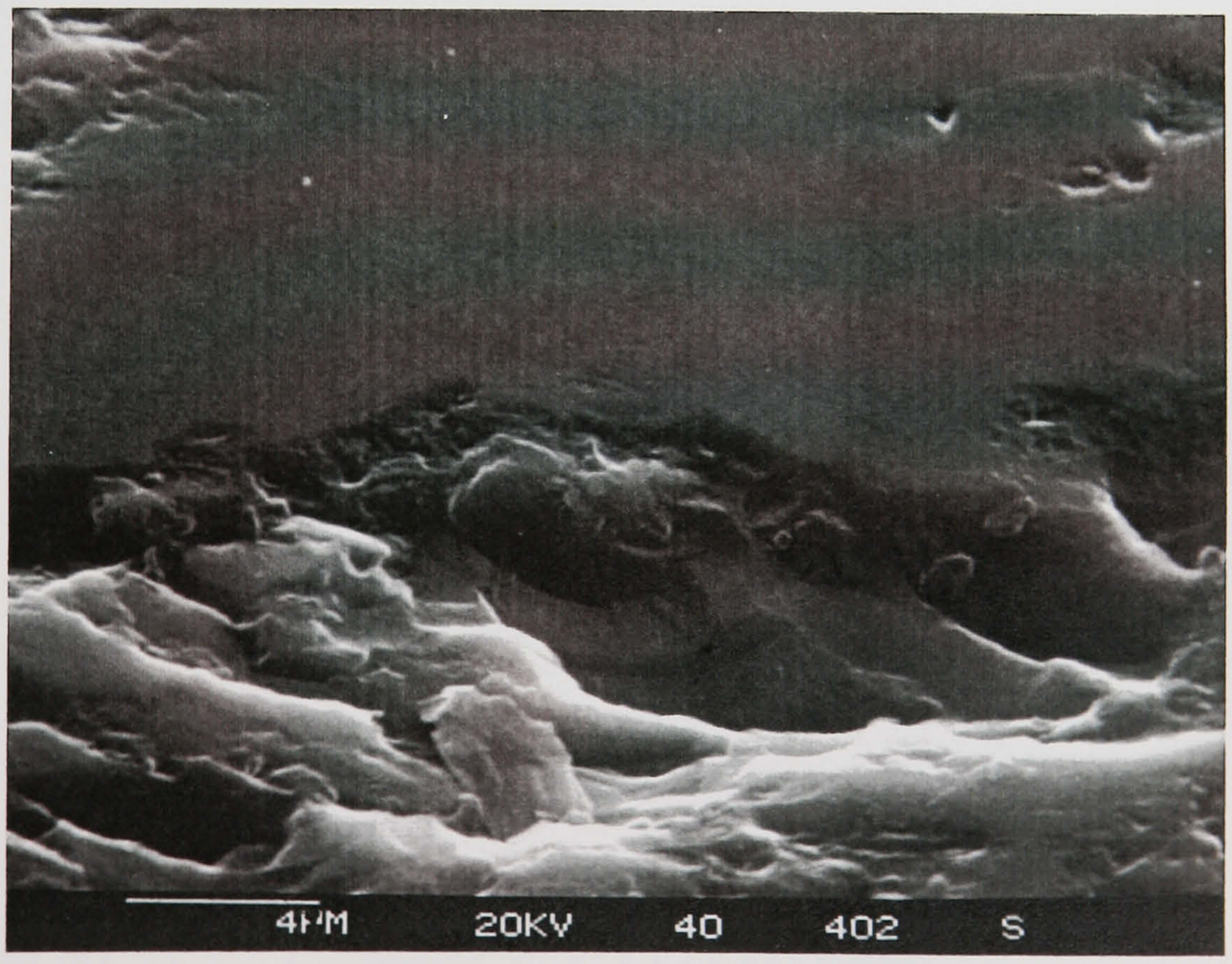

Figure 70 : S.E.M. Micrograph showing Detail of Diamond Turned Germanium, Sample 4 <111> Orientation

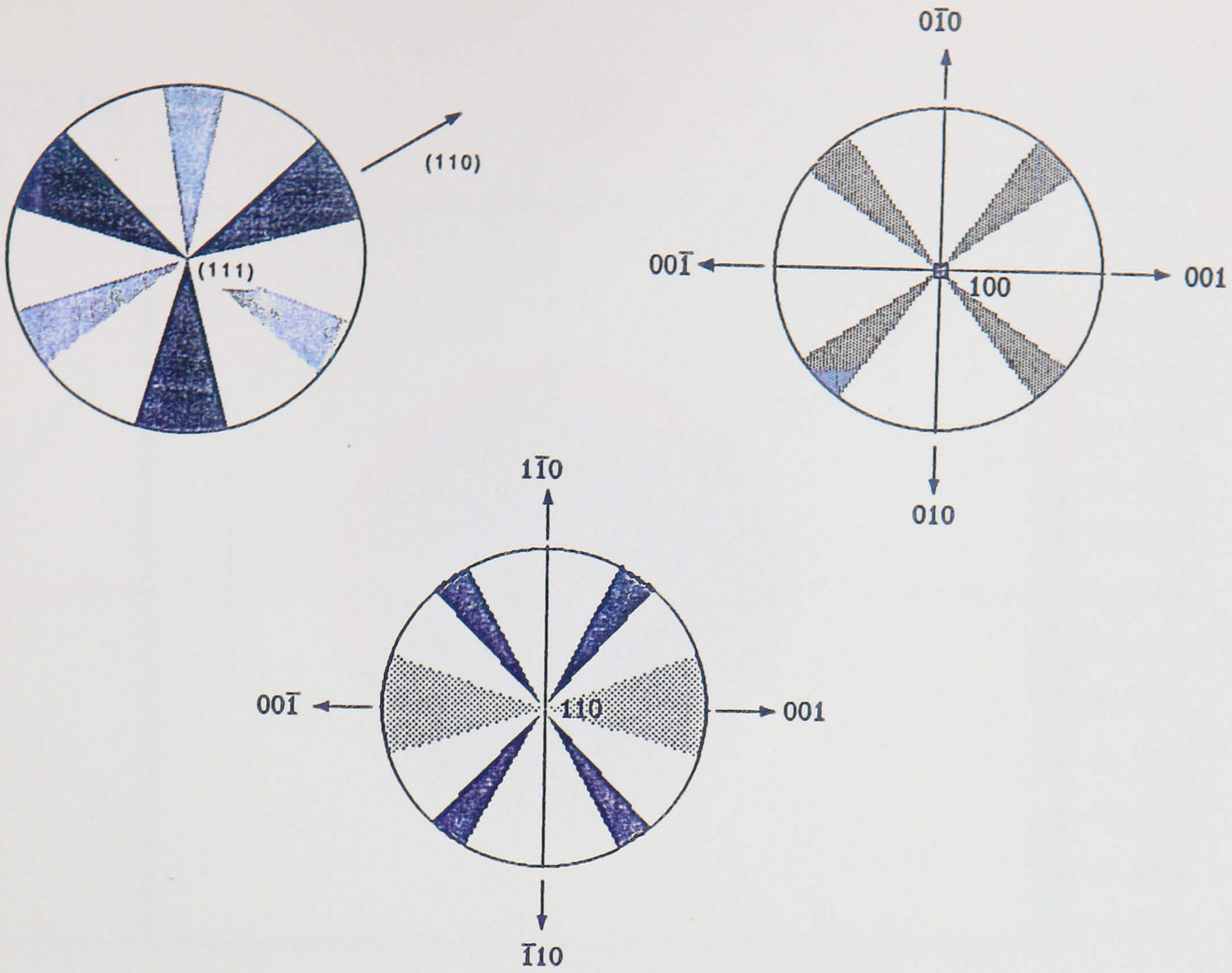

Figure 71 : Schematic of Fracture Patterns for Various Crystal Orientations

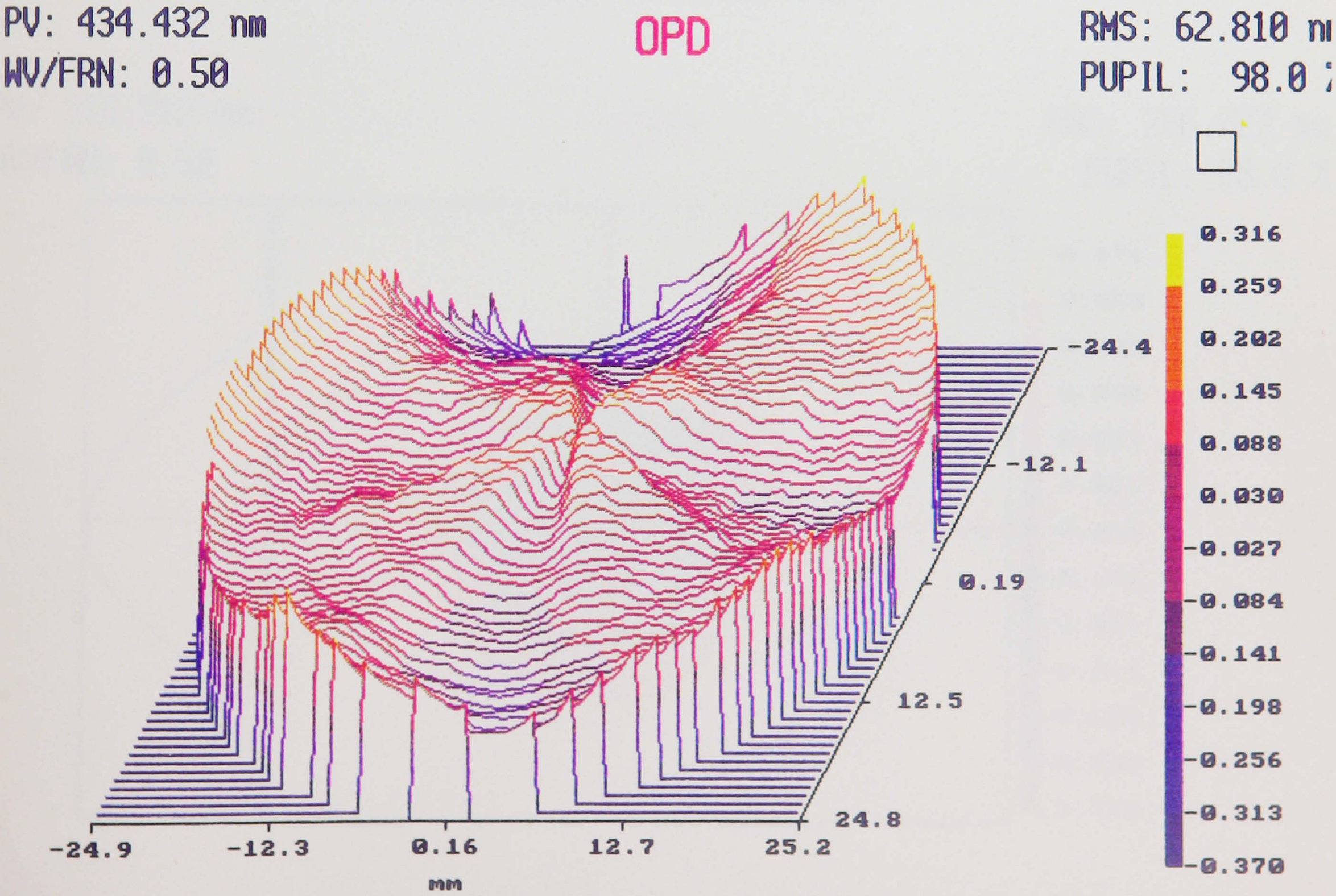

Figure 72 : Wyko 3D Surface Form Plot of Diamond Turned Germanium

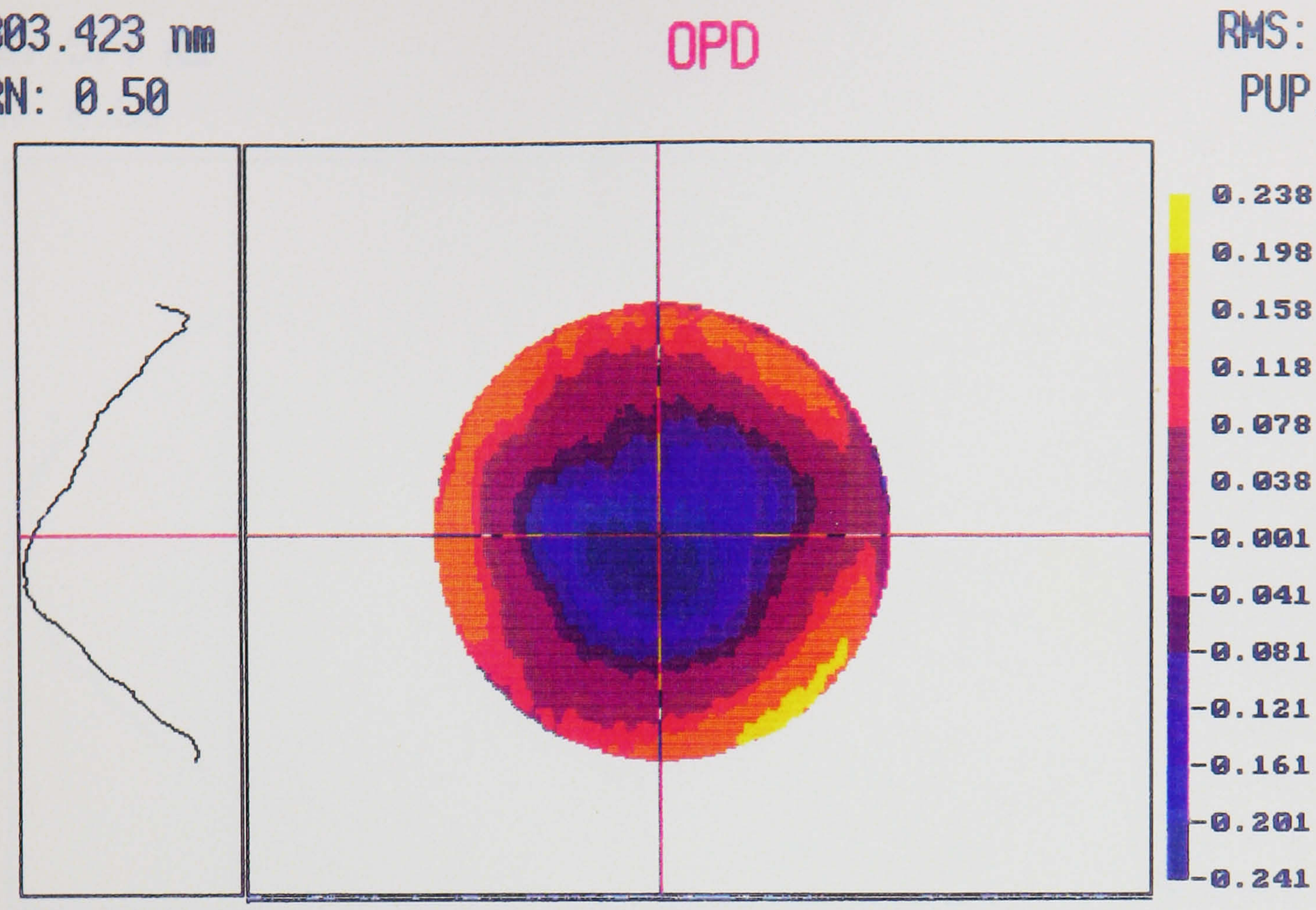

Figure 73 : Wyko 3D Surface Form Plot of Opt Germanium 3 <111> Mounting Face (before turning)

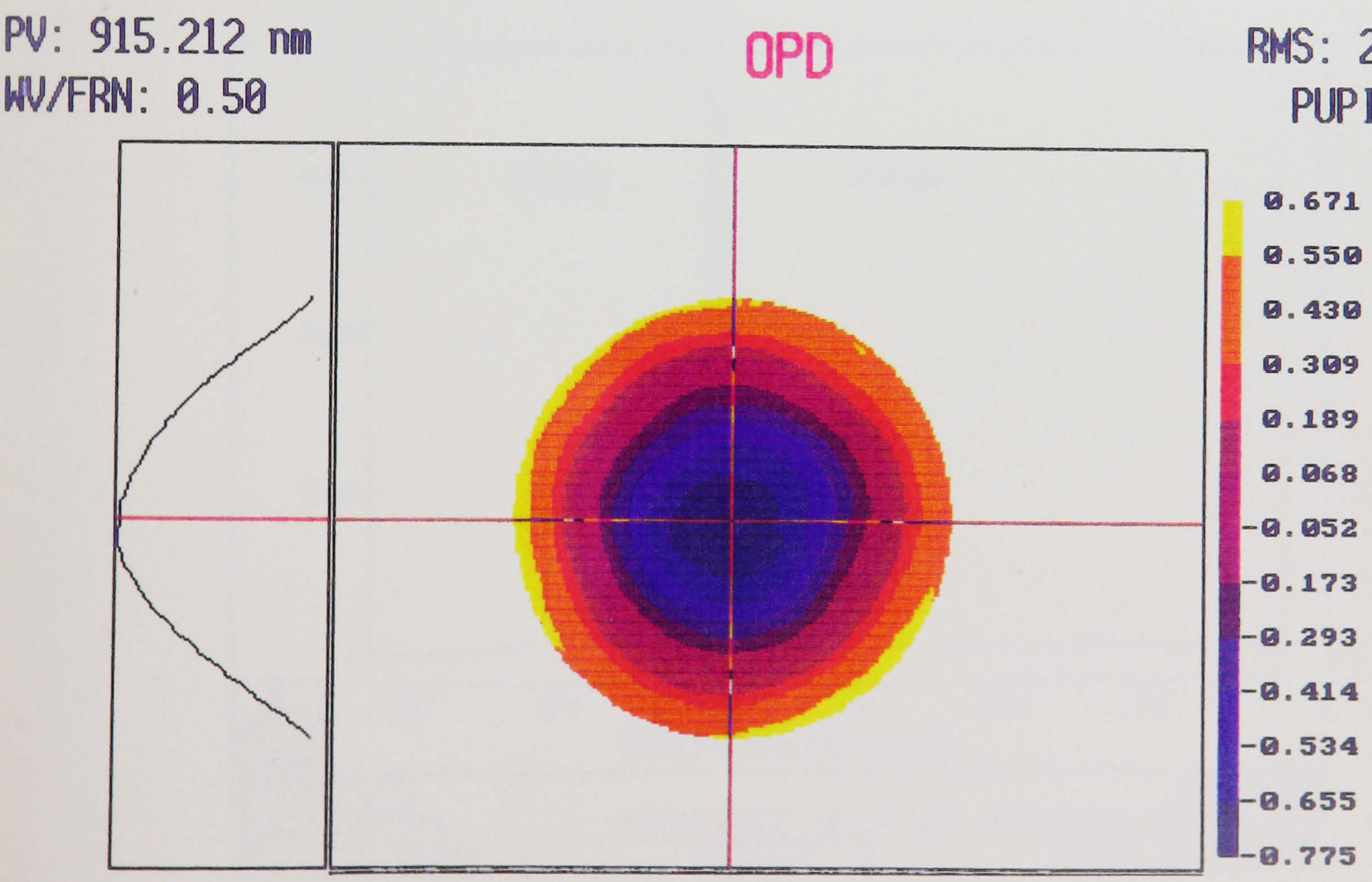

Figure 74 : Wyko 3D Surface Form Plot of Opt Germanium 3 <111> Mounting Face (after turning)

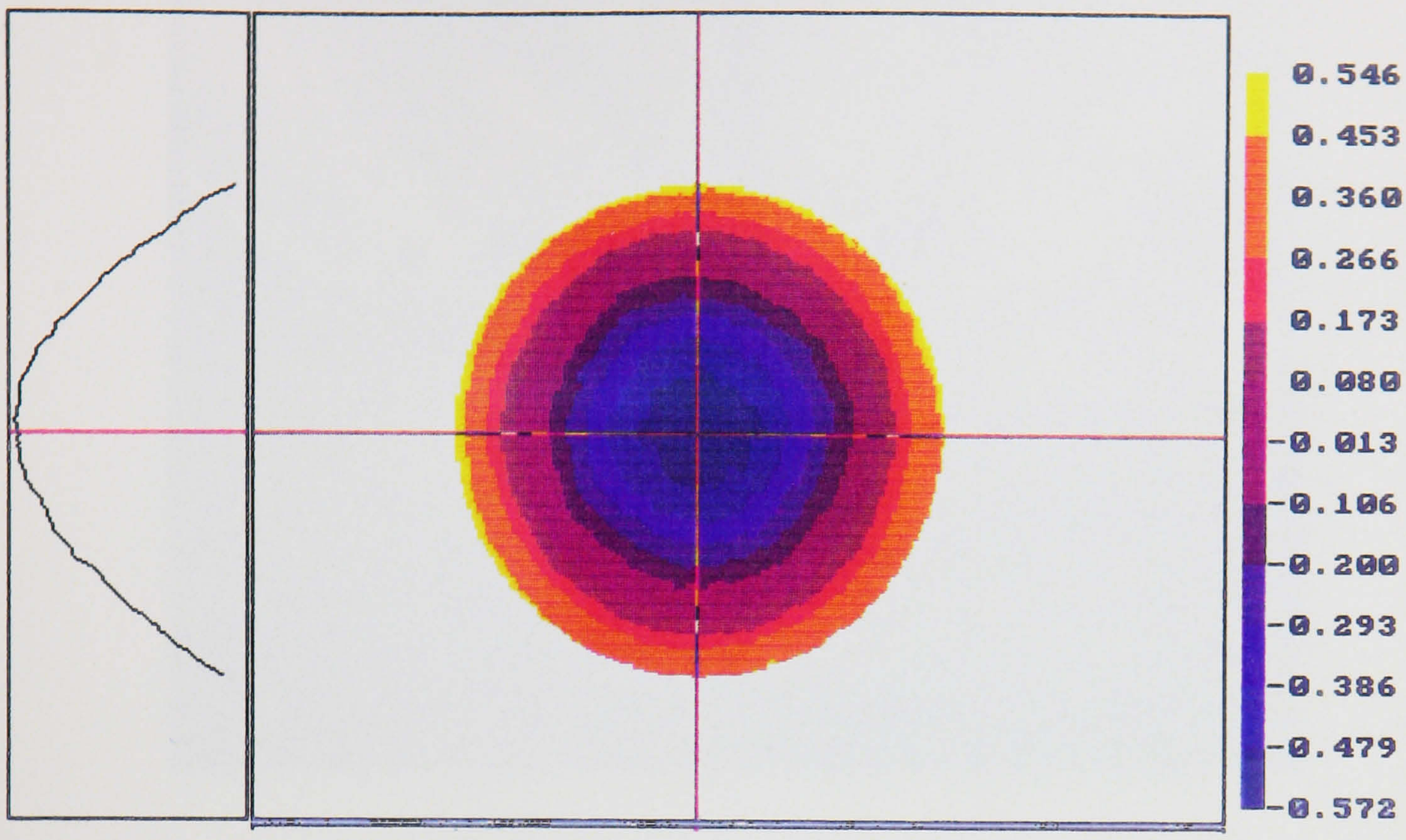

Figure 75 : Wyko 3D Surface Form Plot of Opt Germanium 3 <111>
Difference of Mounting Face Flatness (before & after turning)

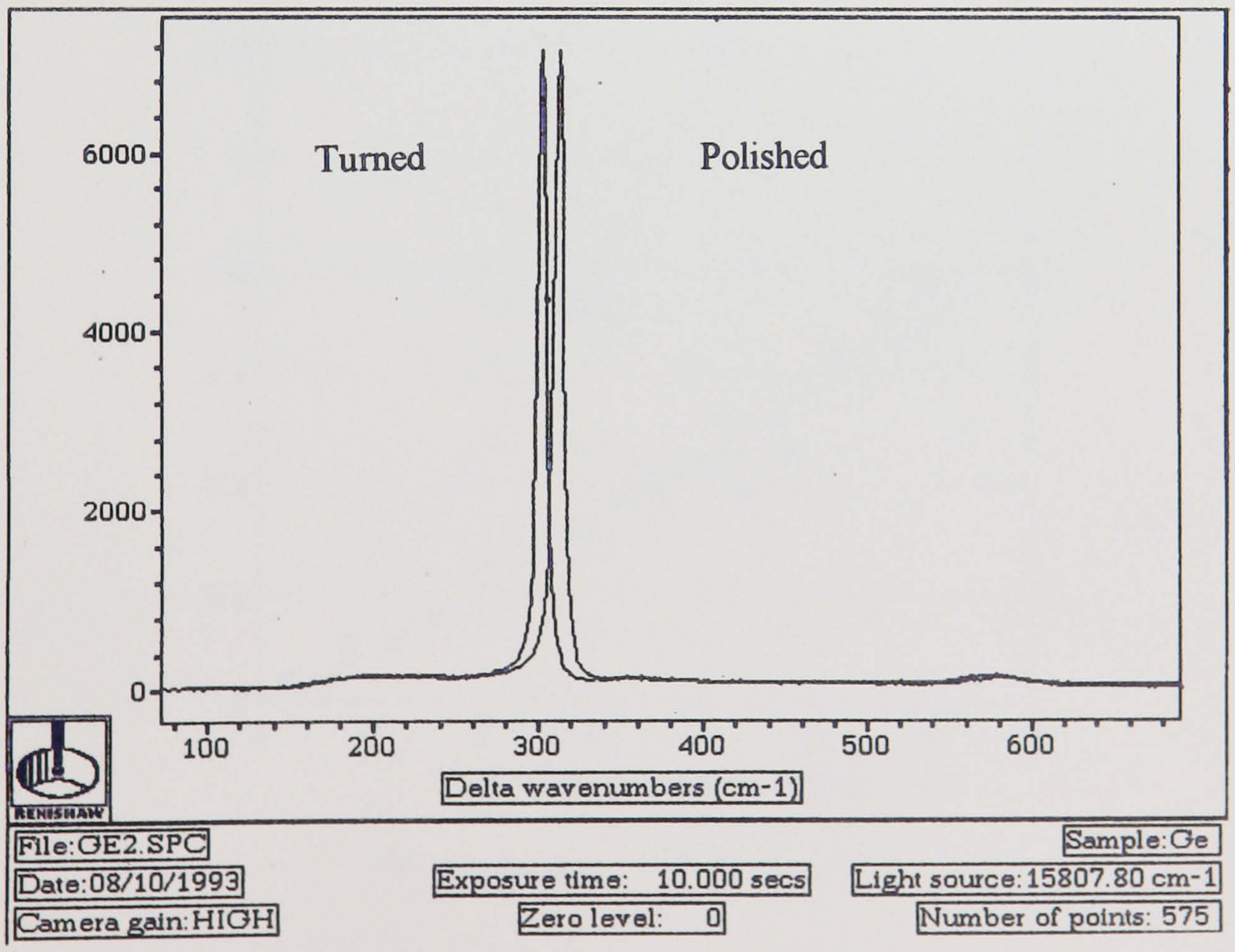

Figure 76 : Graph Showing Shift in Raman Spectra
(polished and turned germanium surfaces)

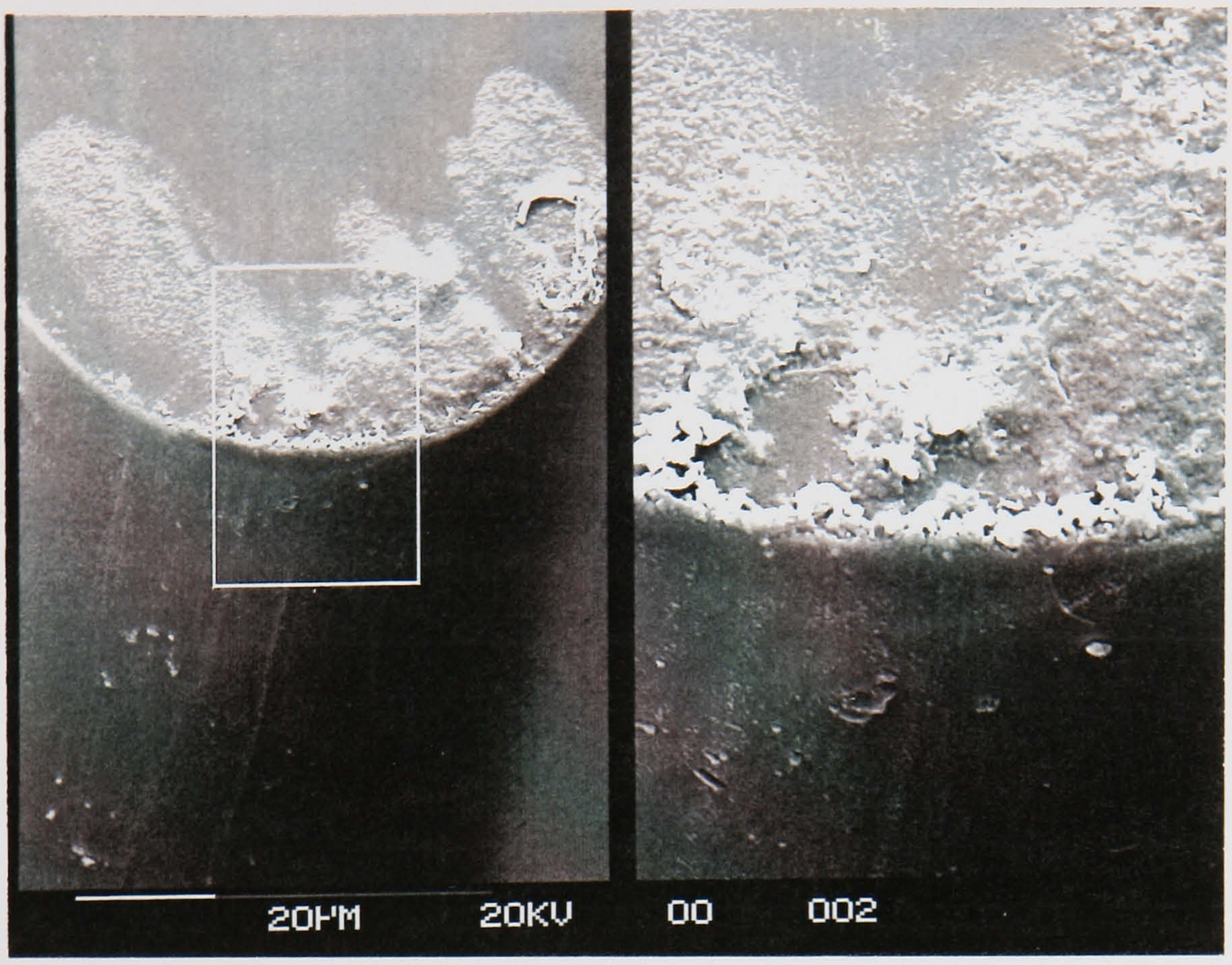

Figure 77 : S.E.M. Micrograph showing Tool Wear on Diamond Tool

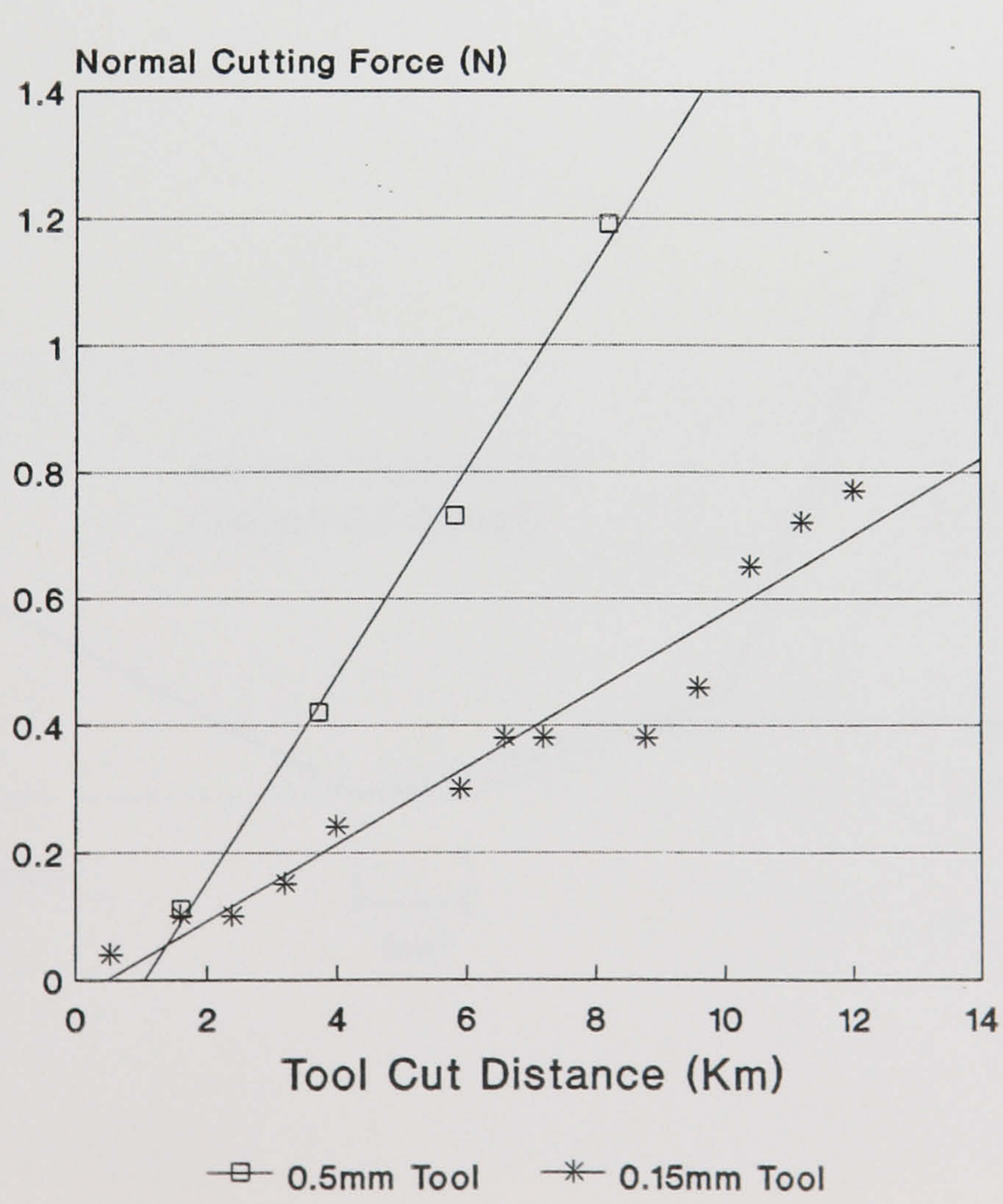

Figure 78 : Graph showing Increased Cutting Force / Tool Cut Distance (Diamond turning of Silicon)

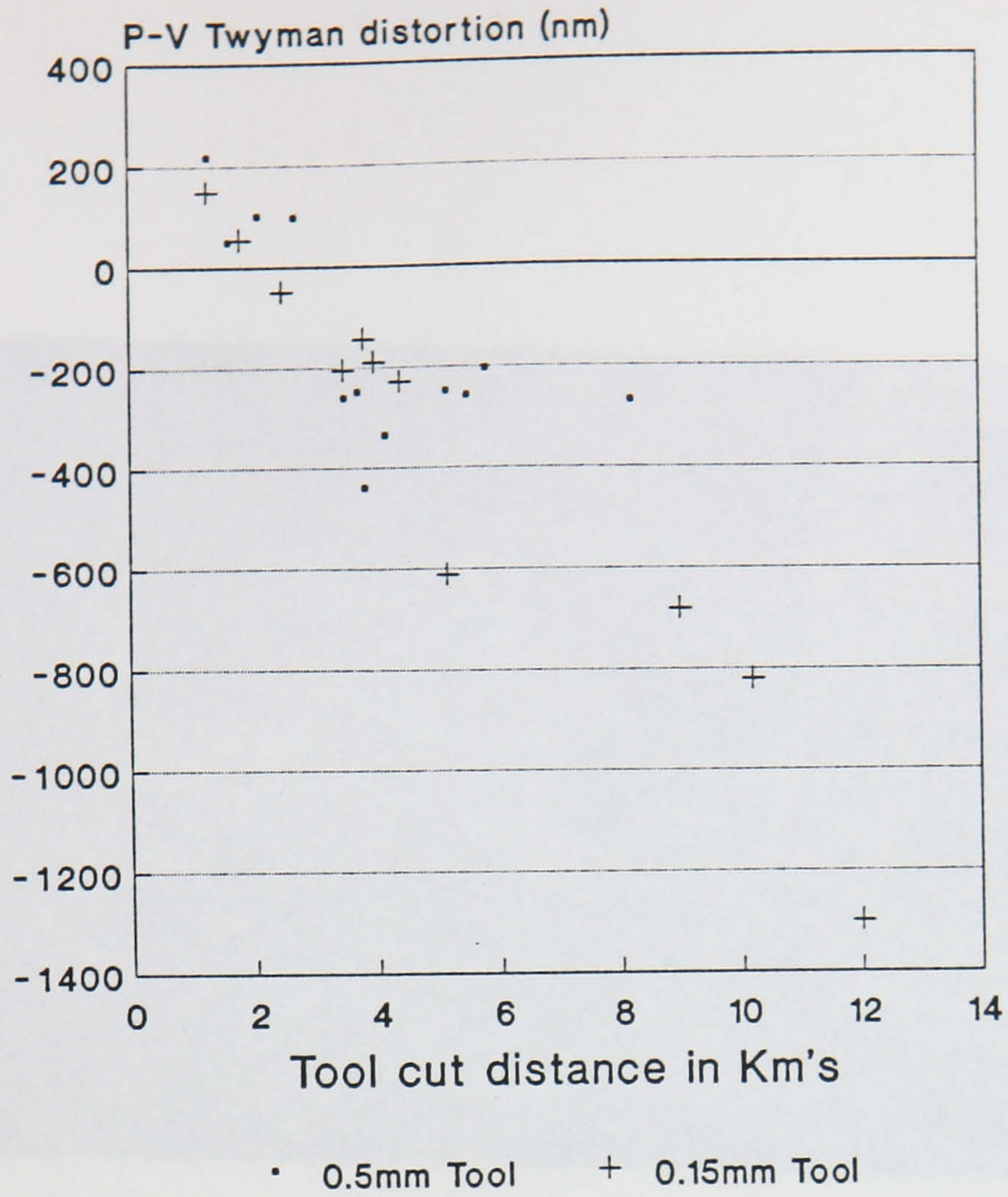

Figure 79 : Graph showing Increased Twyman Distortion / Tool Cut Distance

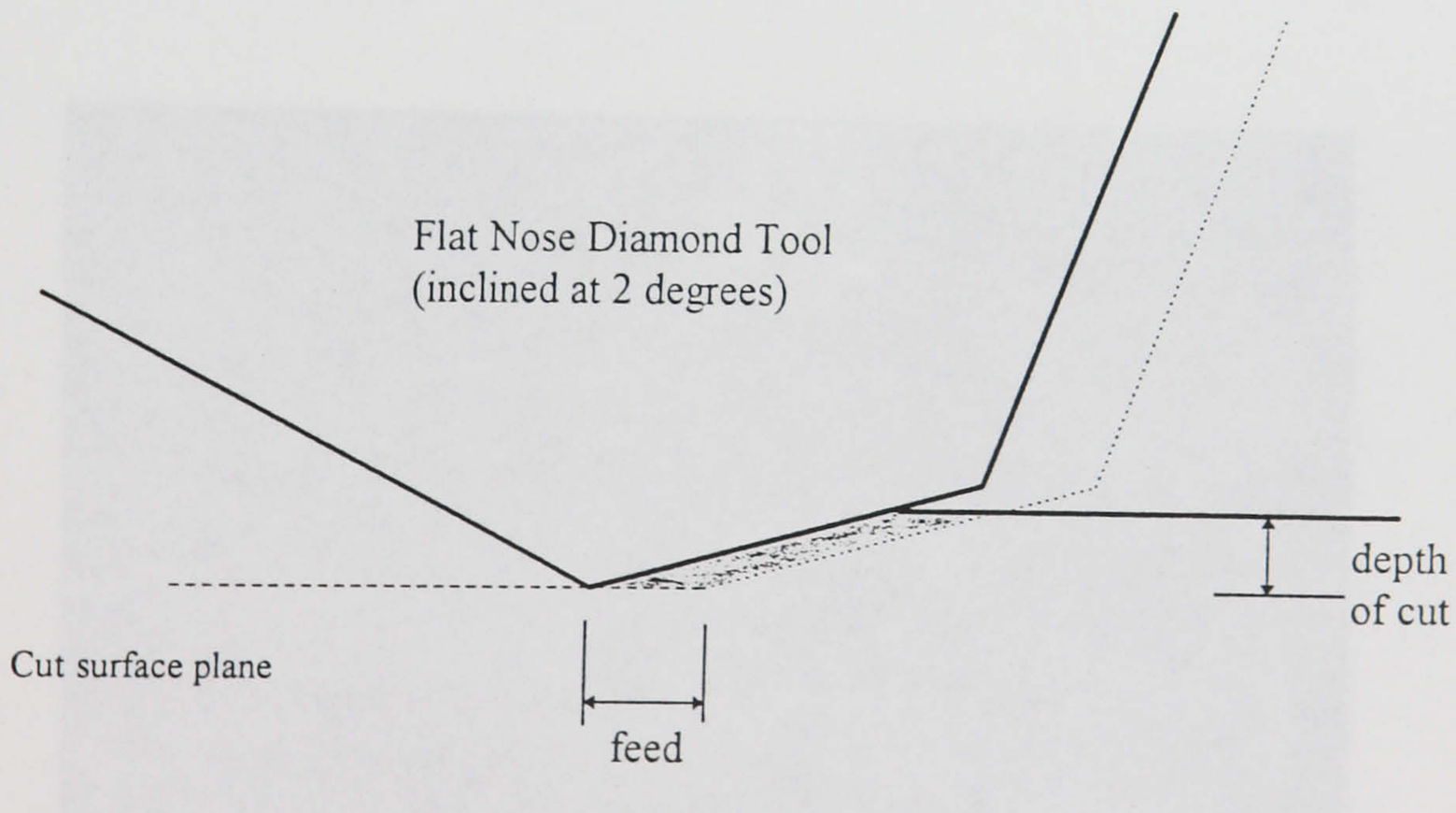

Figure 80 : Chip Geometry for Flat Nose Tool

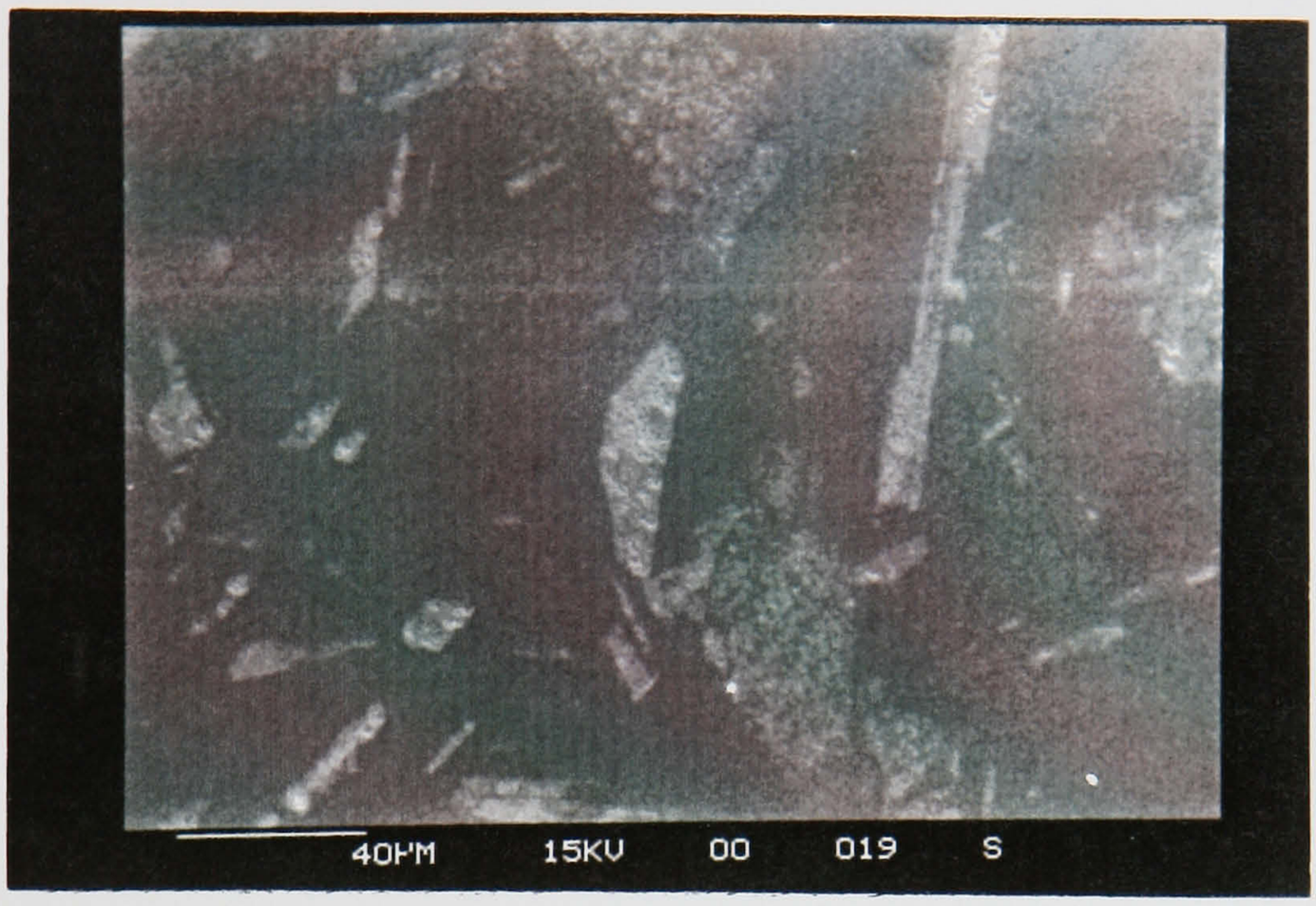

Figure 81 : S.E.M. Micrograph of Diamond Turned Zinc Sulphide

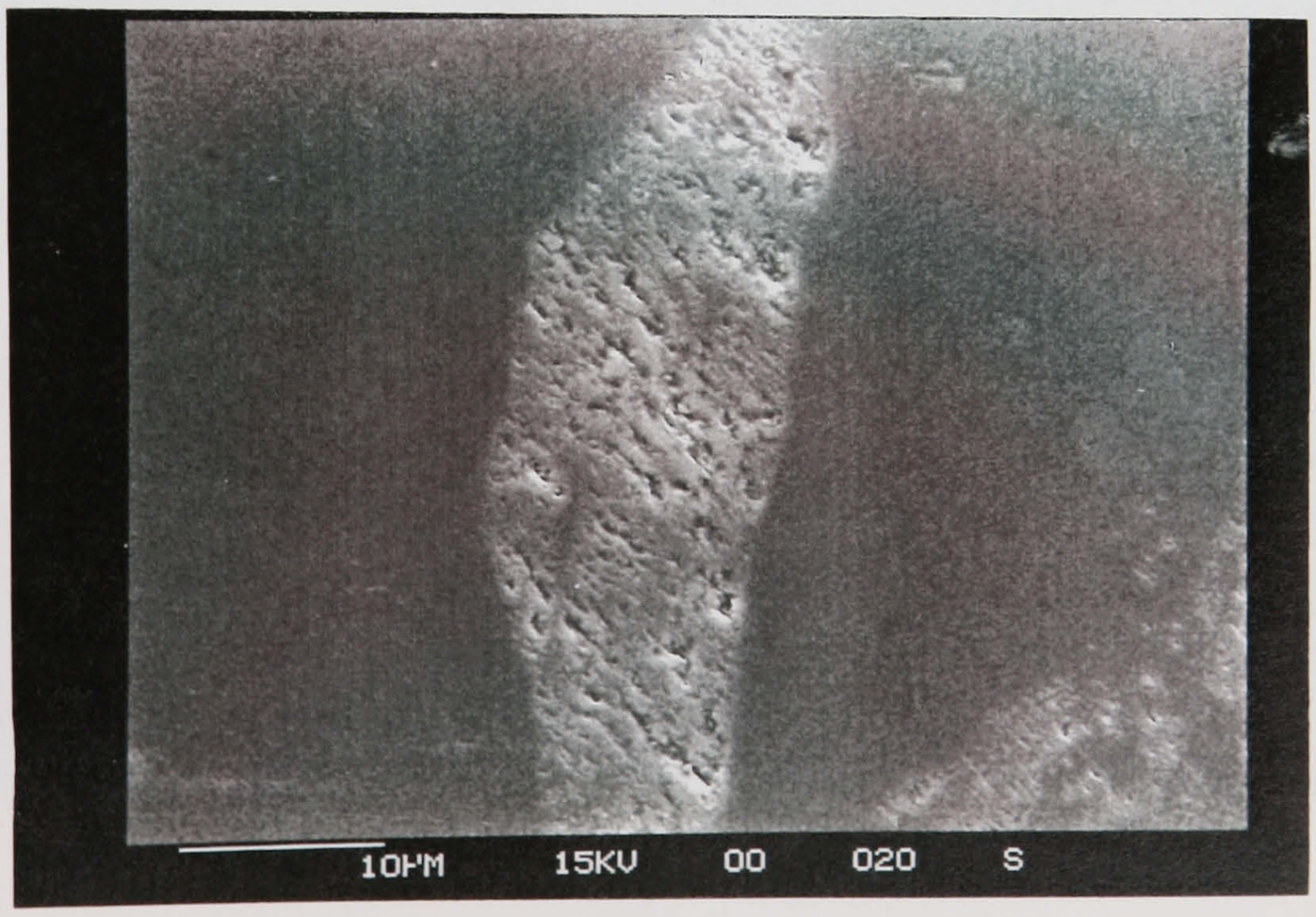

Figure 82 : S.E.M. Micrograph of Diamond Turned Zinc Sulphide (close up)

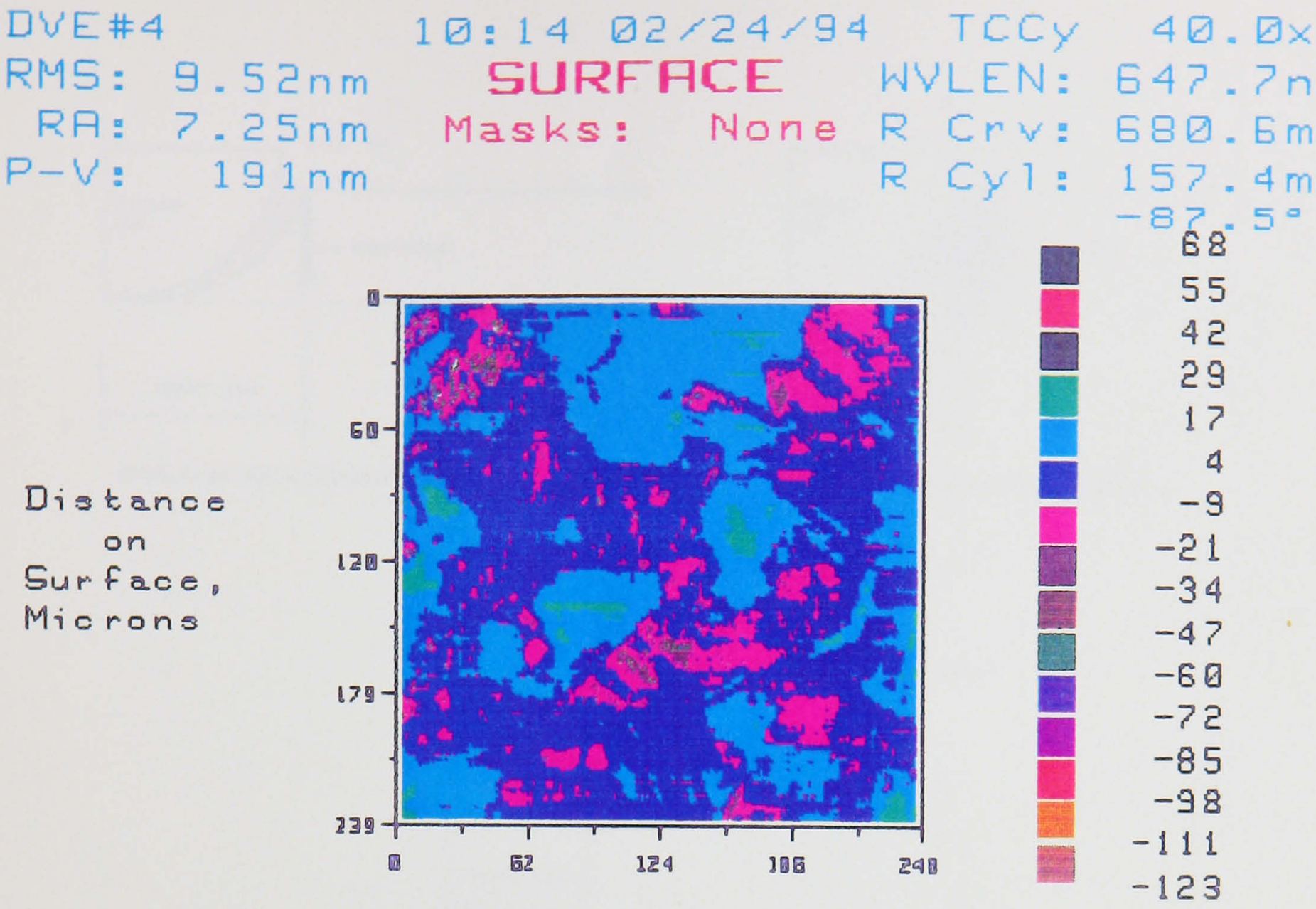

Figure 83 : Wyko 3D Surface Roughness Plot of Diamond Turned Zinc Sulphide

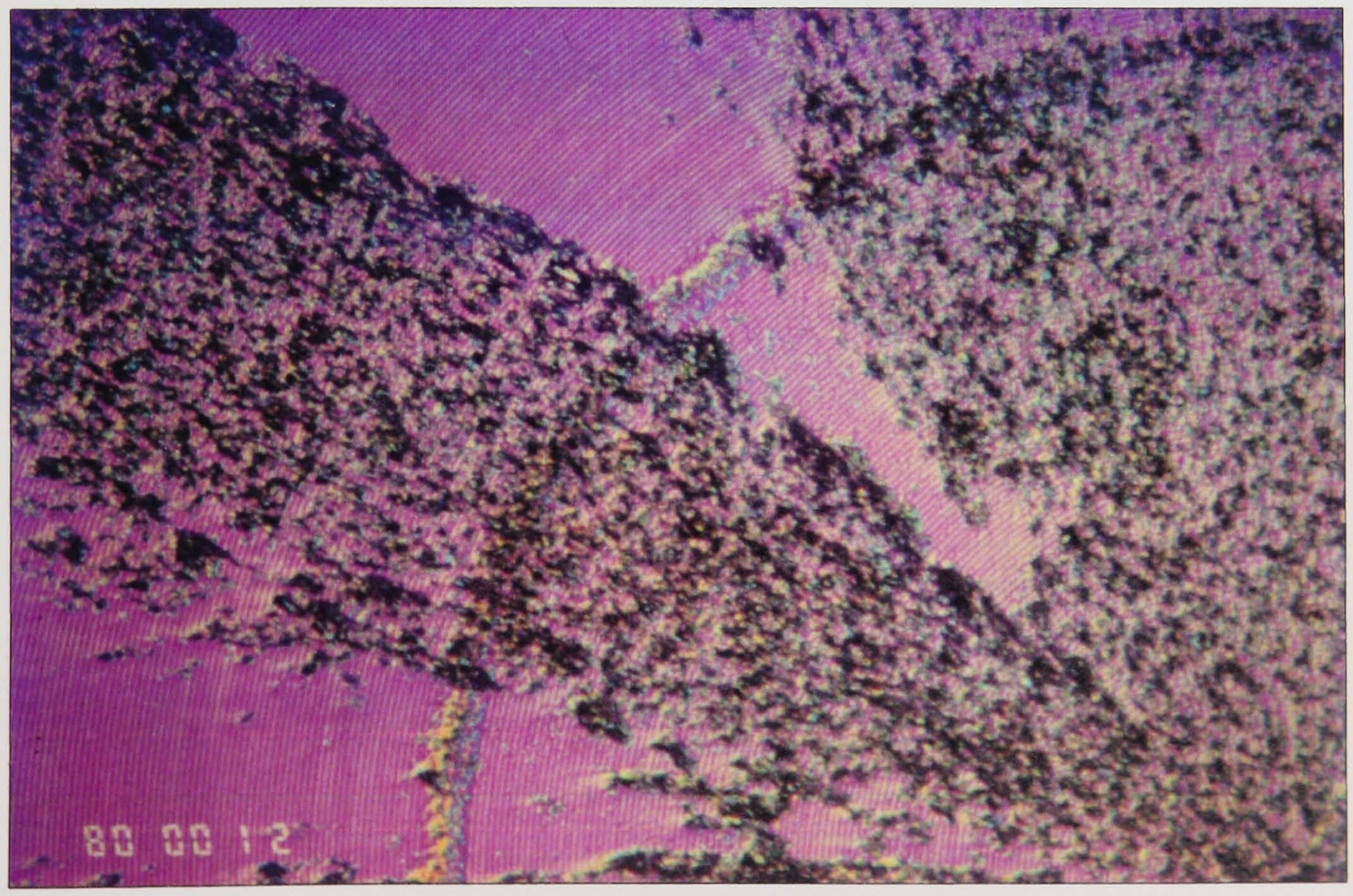

Figure 84 : Photomicrograph of Diamond Turned Silicon

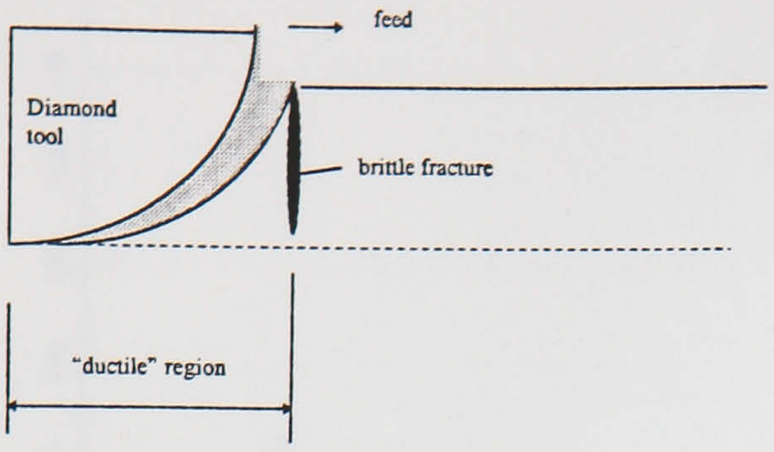

Schematic for Diamond Turning Zinc Sulphide

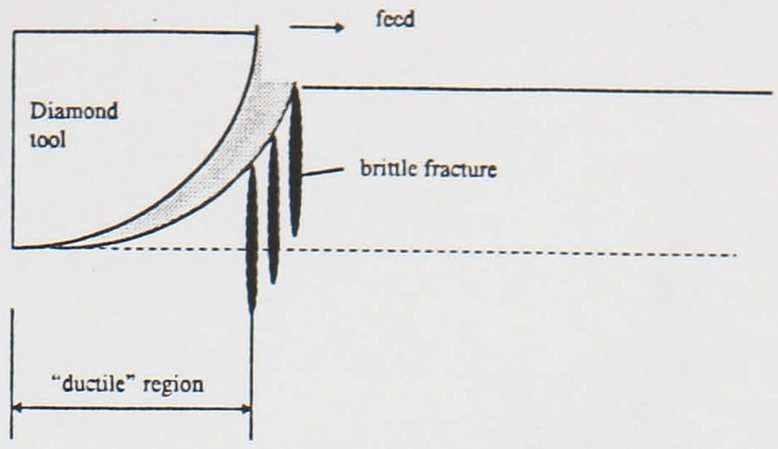

Schematic for Diamond Turning BK7 Glass

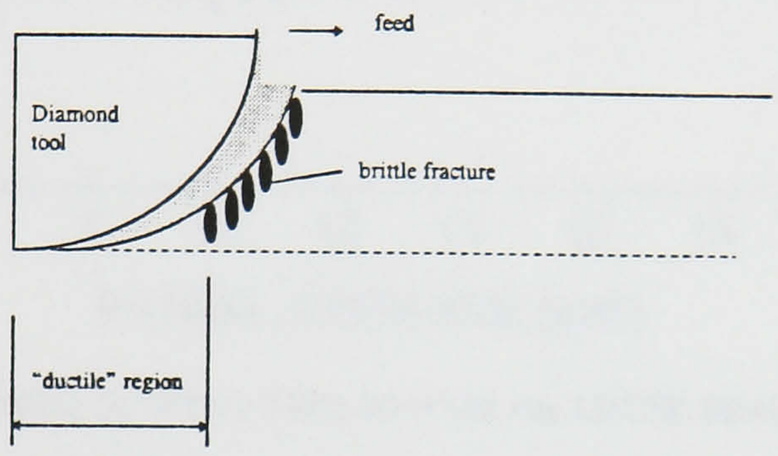

Schematic for Diamond Turning Silicon

Figure 85 : Schematic of Brittle / Ductile Fracture at Tool Interface (various materials)

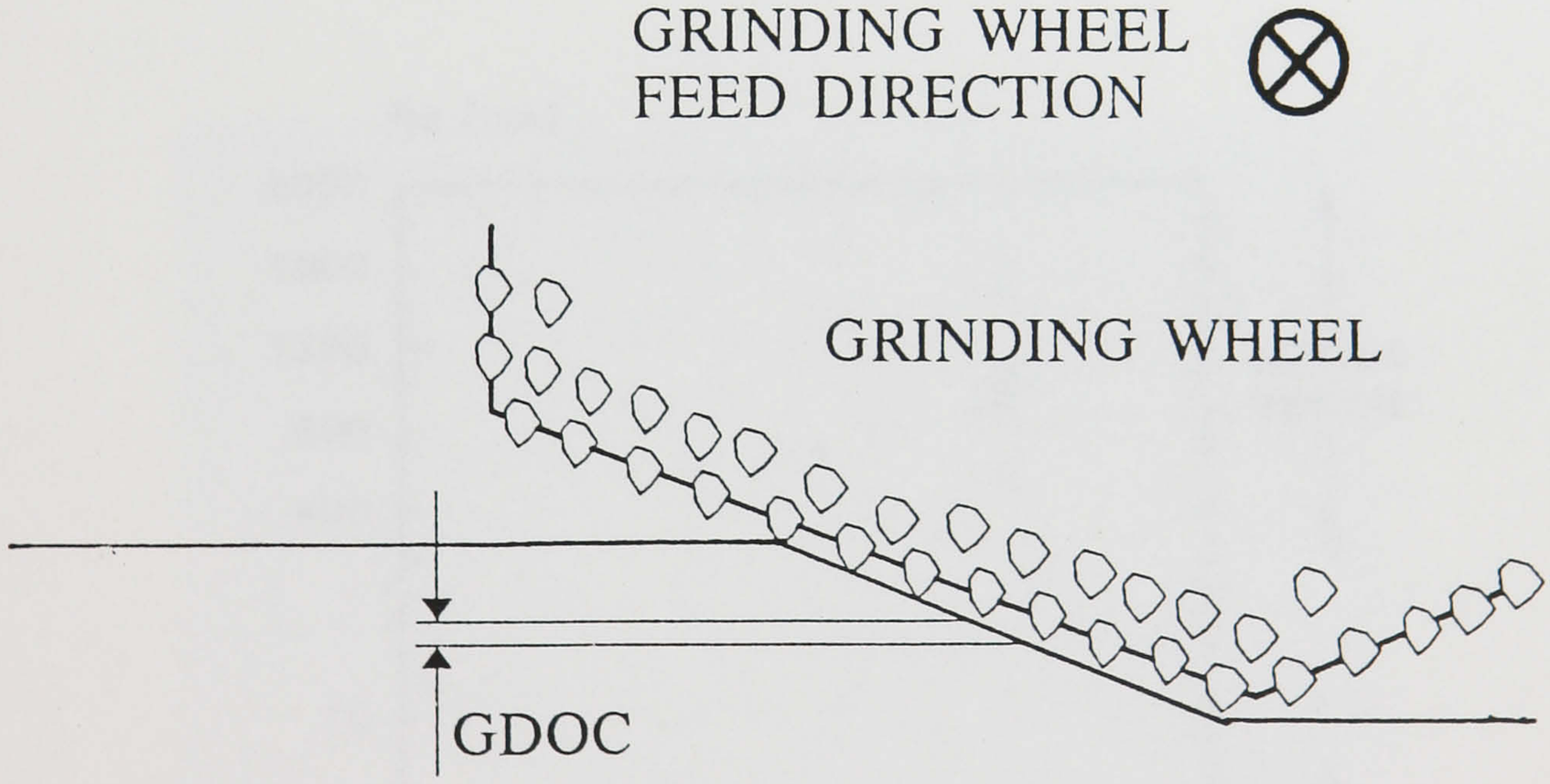

Figure 86 : Schematic of Grinding Wheel Cross Sectional Profile

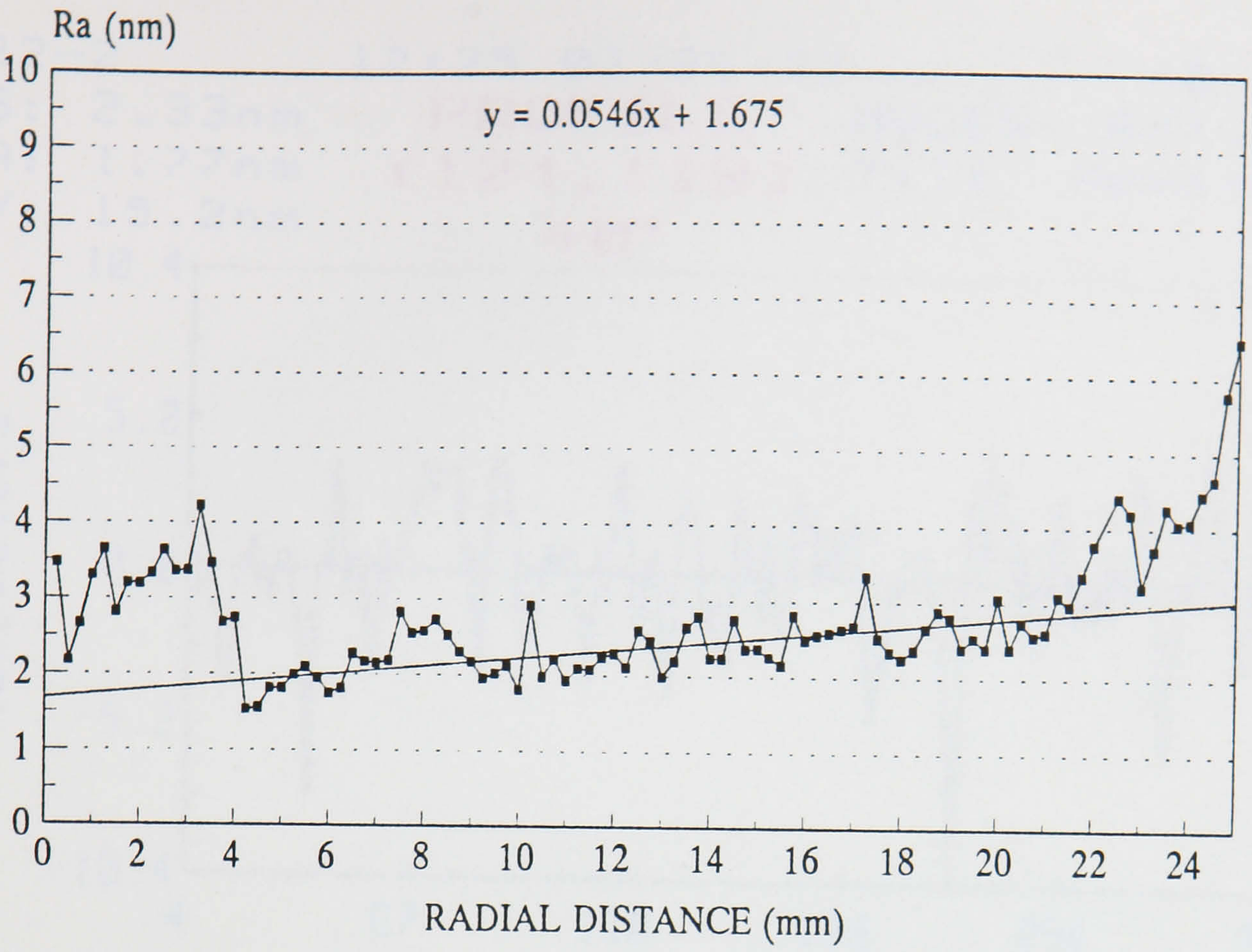

MEASURED ON WYKO TOPO-3D WITH 40x LINNIK HEAD

Figure 87 : Graph showing Surface Roughness / Radial Position

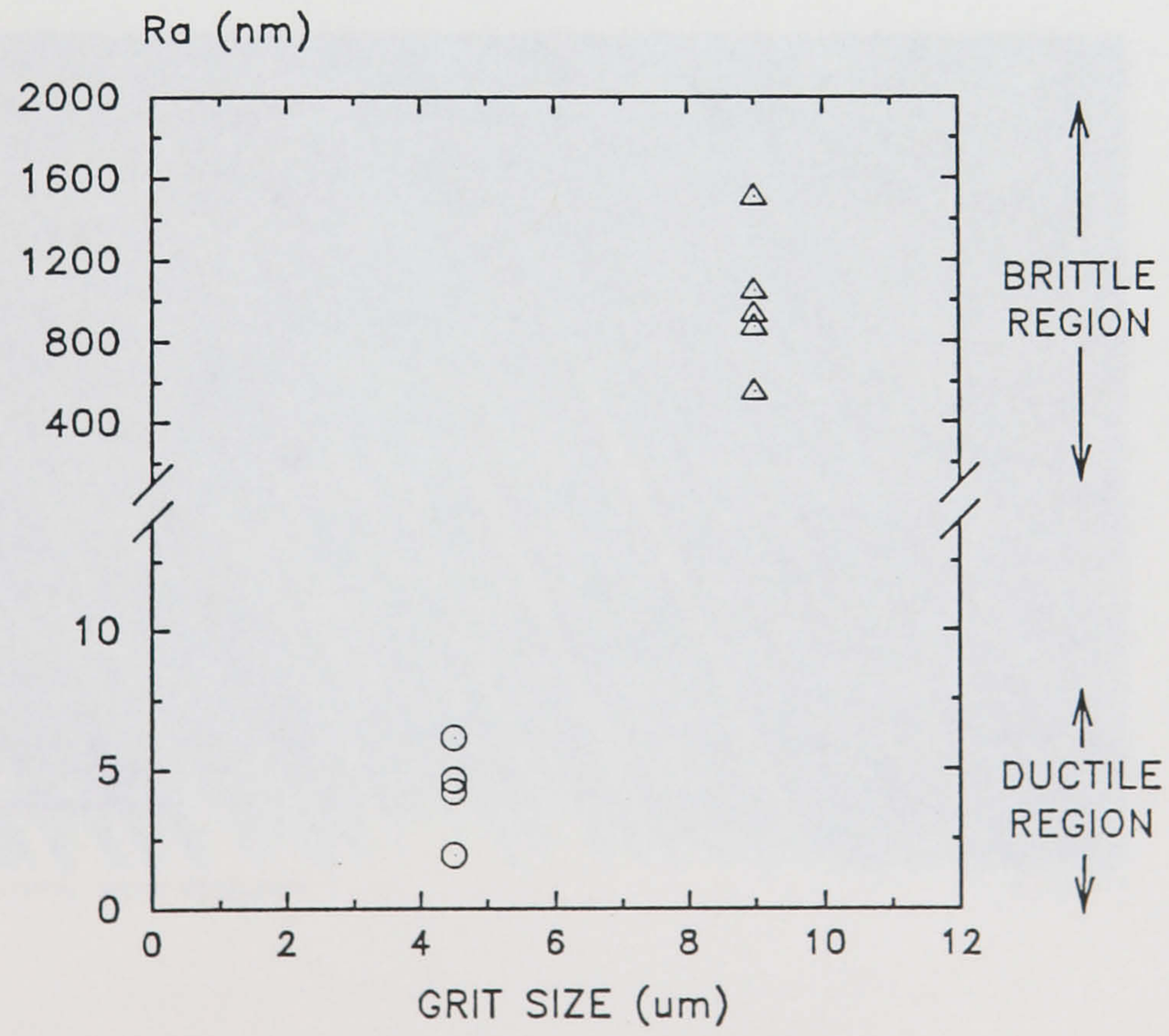

Figure 88 : Graph showing Influence of Grain Size on Surface Roughness

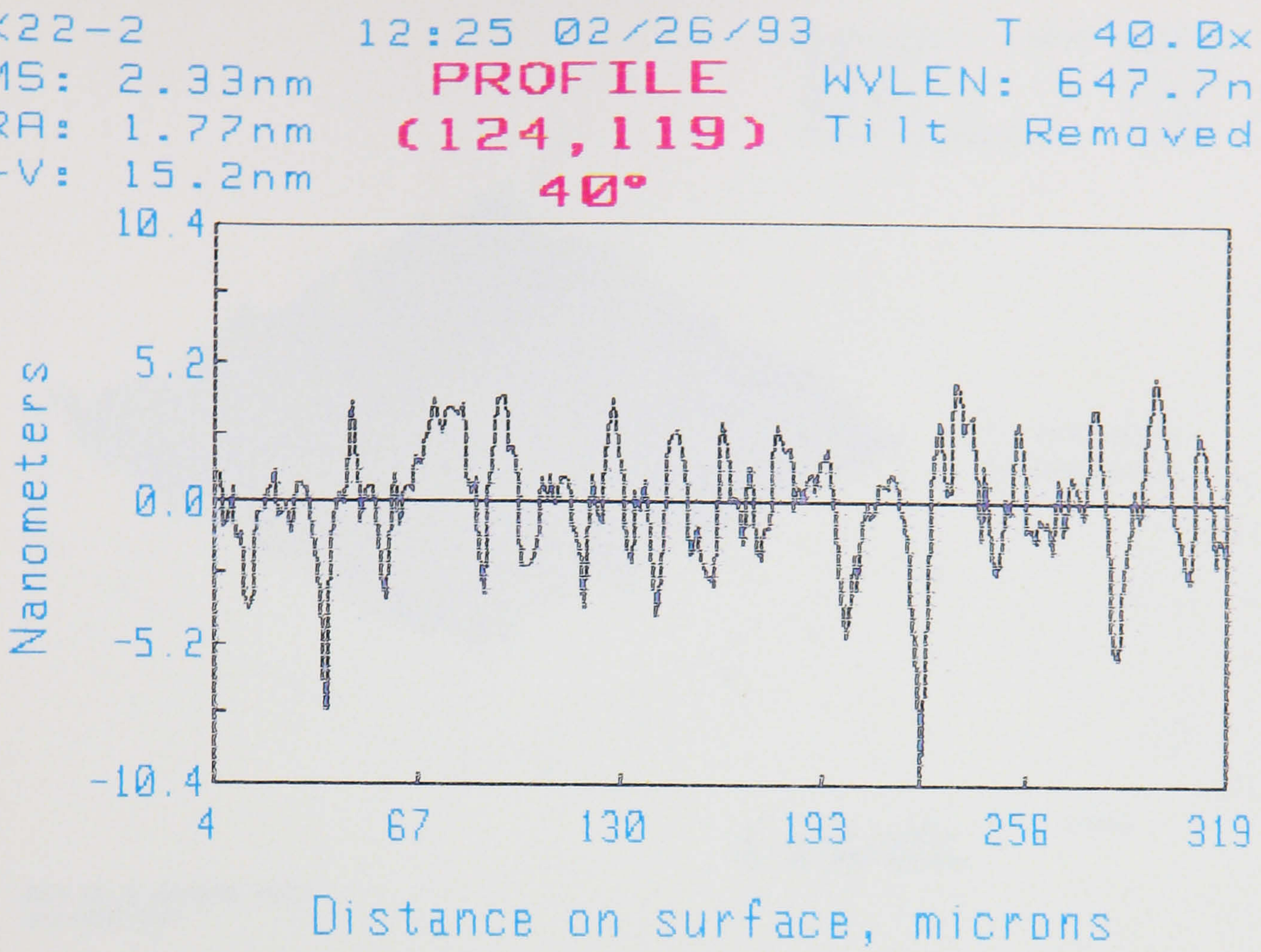

Figure 89 : Wyko 2D Surface Roughness Plot of Ground BK7 Glass

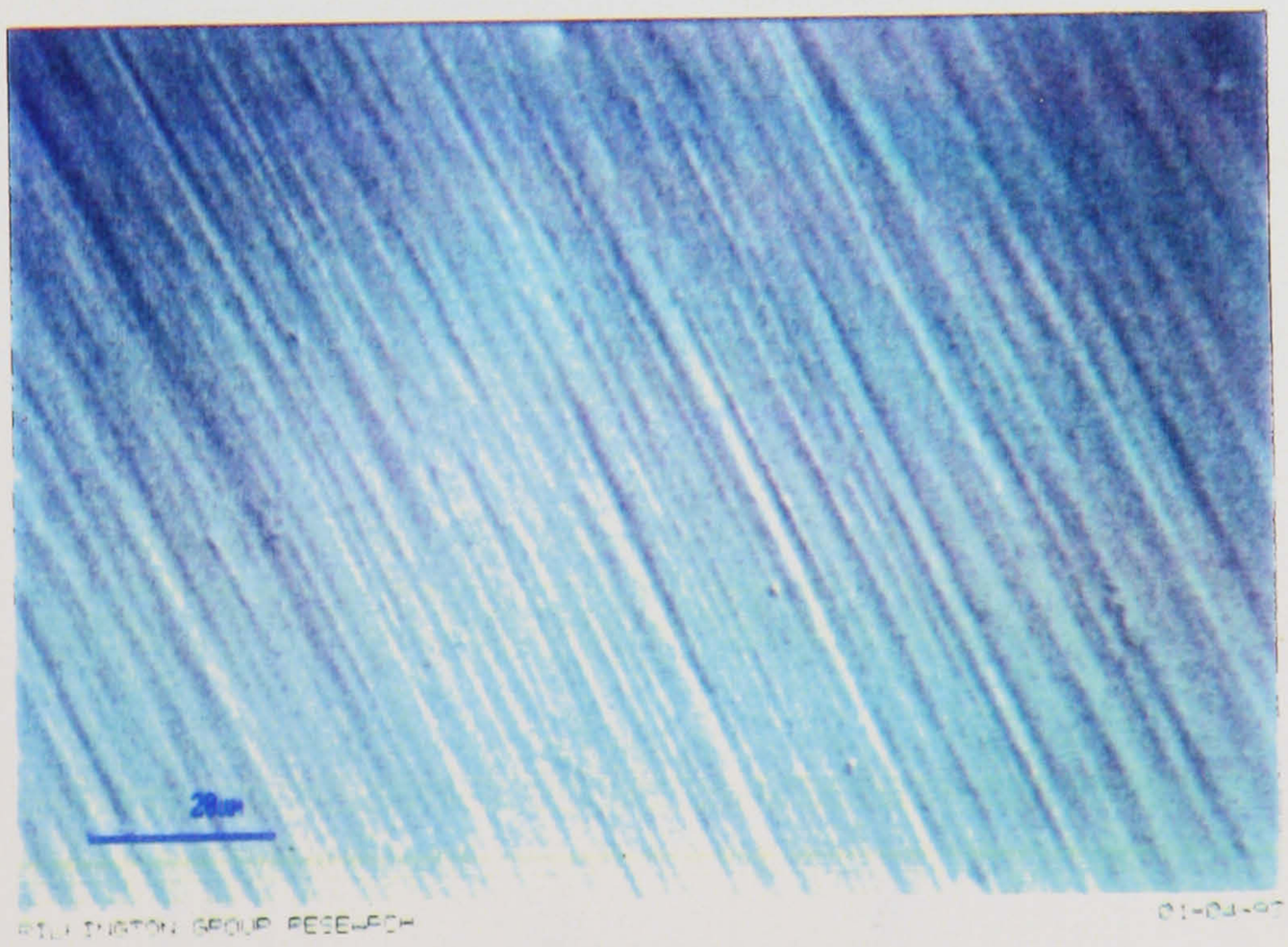

Figure 90 : S.E.M. Micrograph showing Ductile Ground BK7

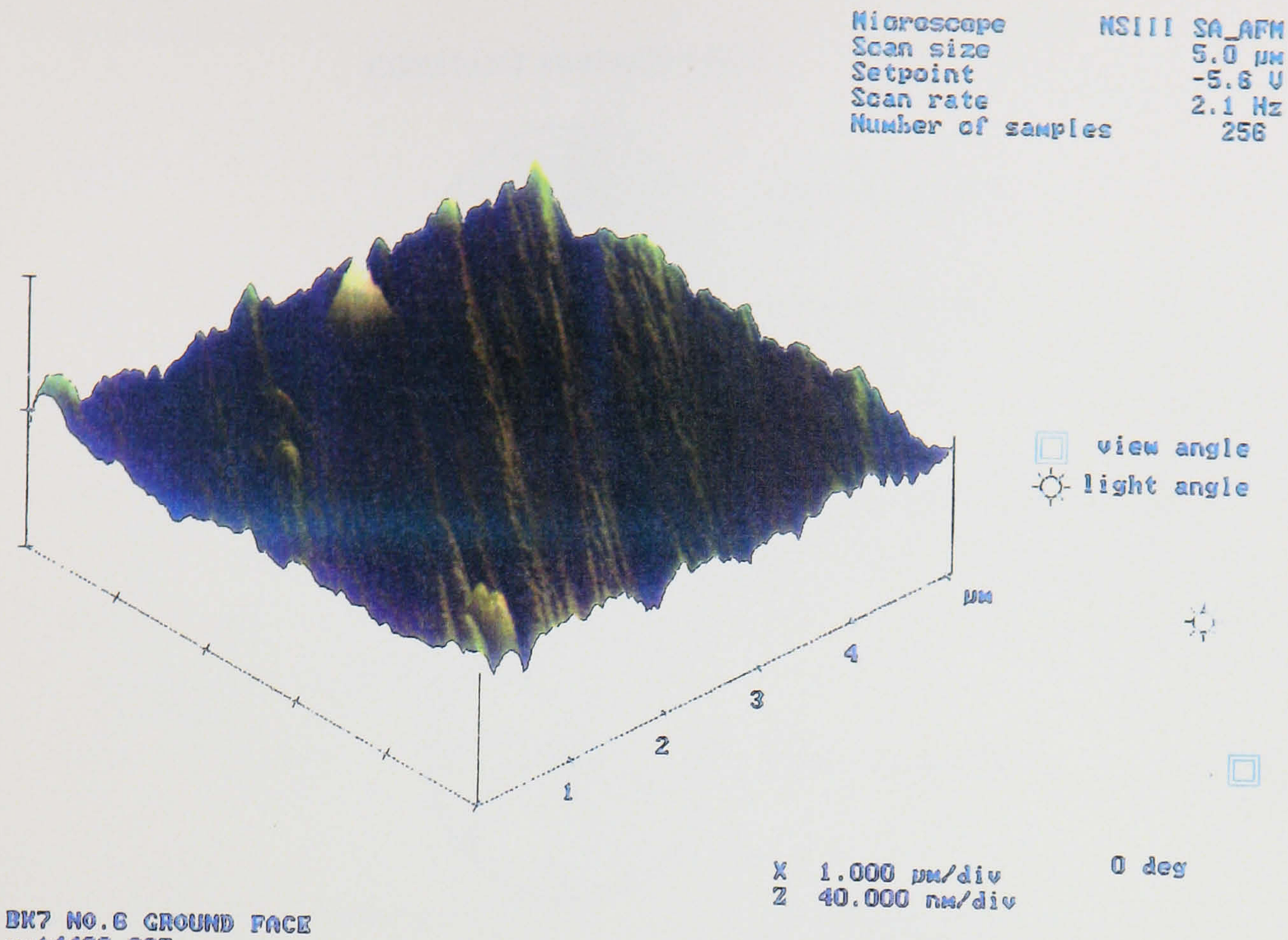

Figure 91 : A.F.M. Micrograph showing Ductile Ground BK7

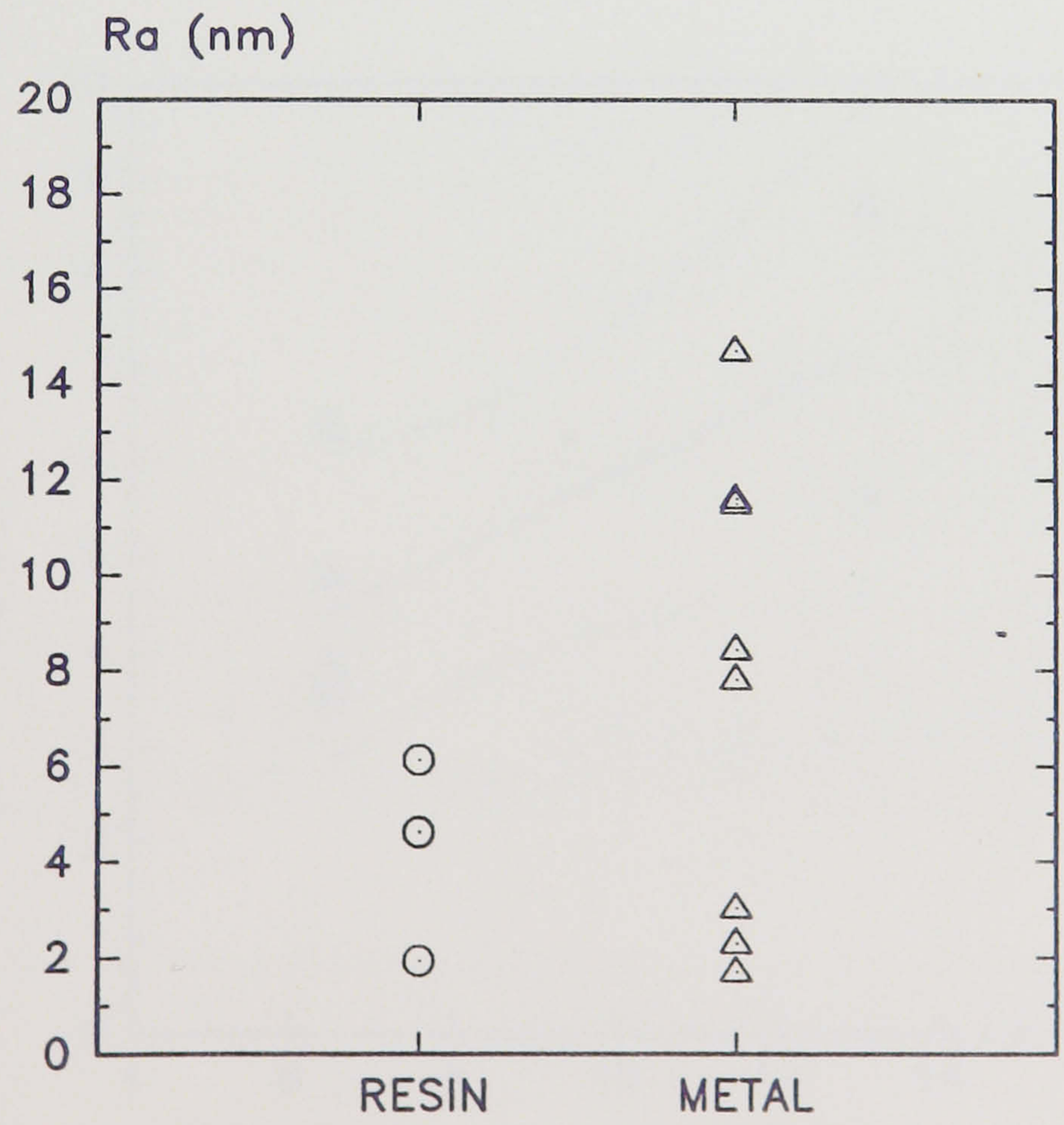

Figure 92 : Graph showing Surface Roughness / Wheel Bond Type (resin and metal)

CONSTANT SURFACE SPEED

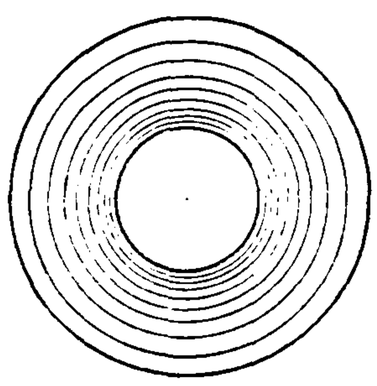

- Concentric surface ripple

- Upper speed limit.

CONSTANT ROTATIONAL SPEED

- Spiral surface ripple

Figure 93 : Schematic of Surface Pattern of CSS and CRPM Grinding Modes

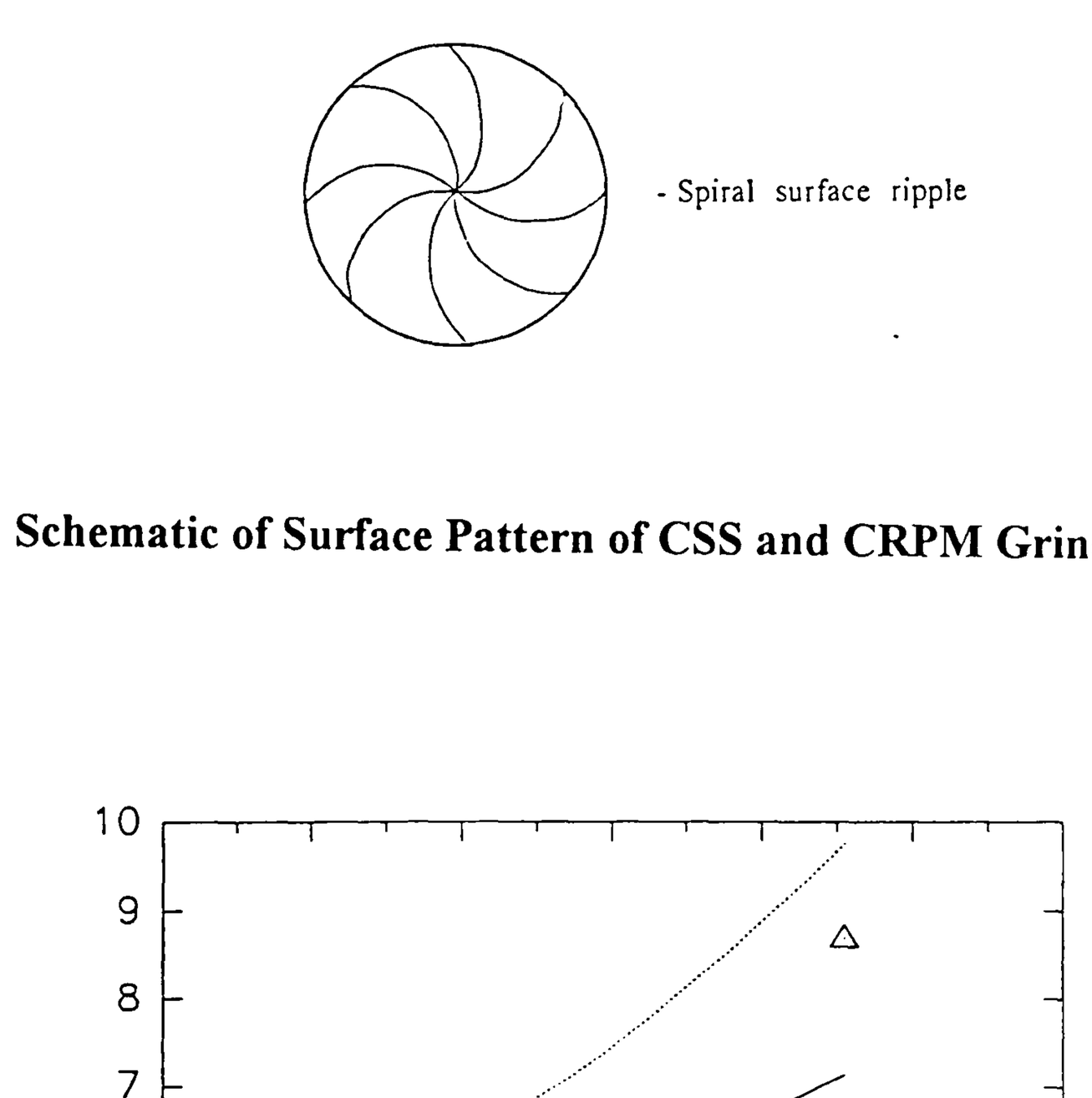

Figure 94 : Graph showing Surface Roughness / Angular Velocity (V_w)

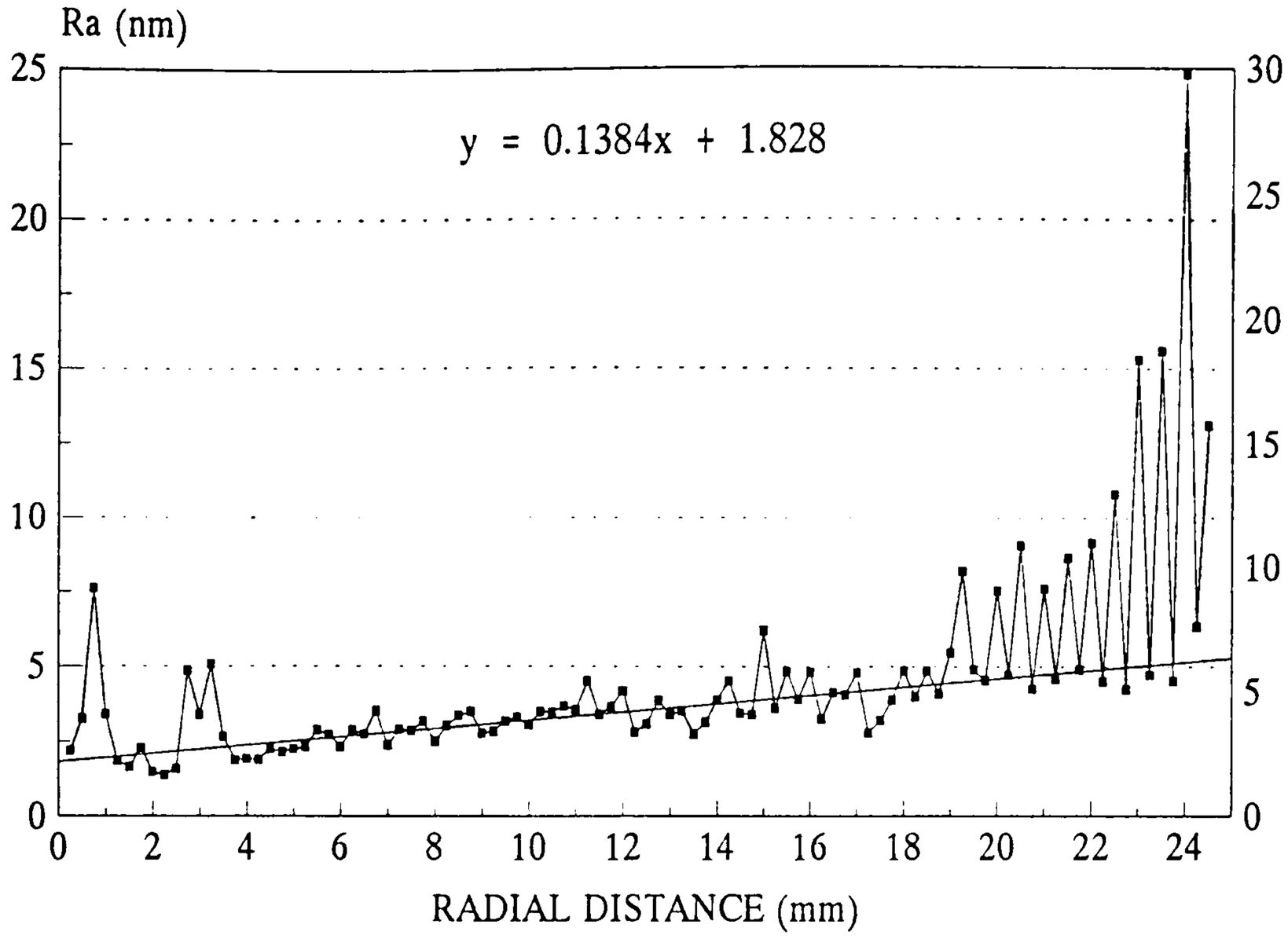

Figure 95 : Graph showing Surface Roughness / Radial Position, CSS Mode

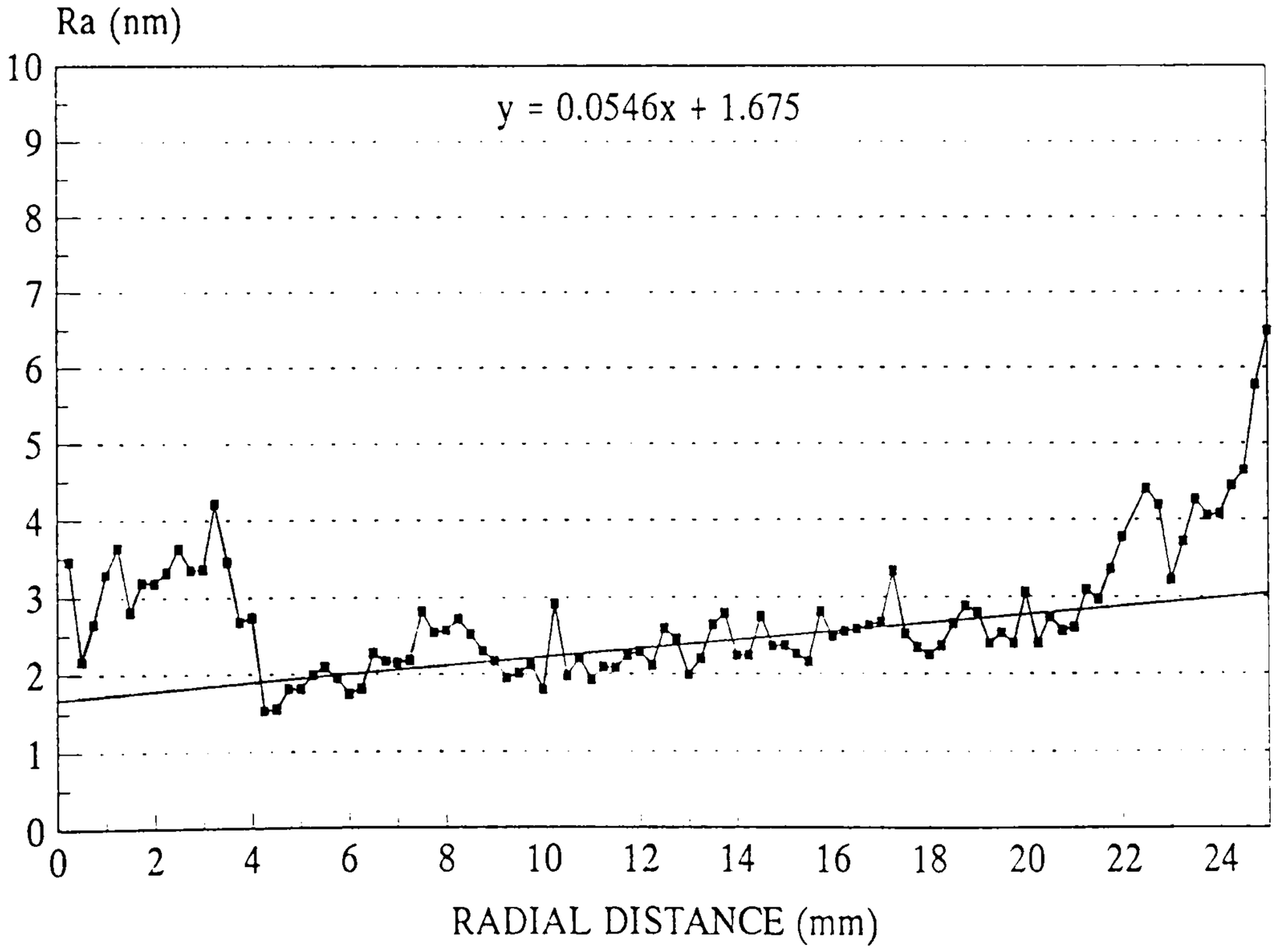

Figure 96 : Graph showing Surface Roughness / Radial Position, CRPM Mode

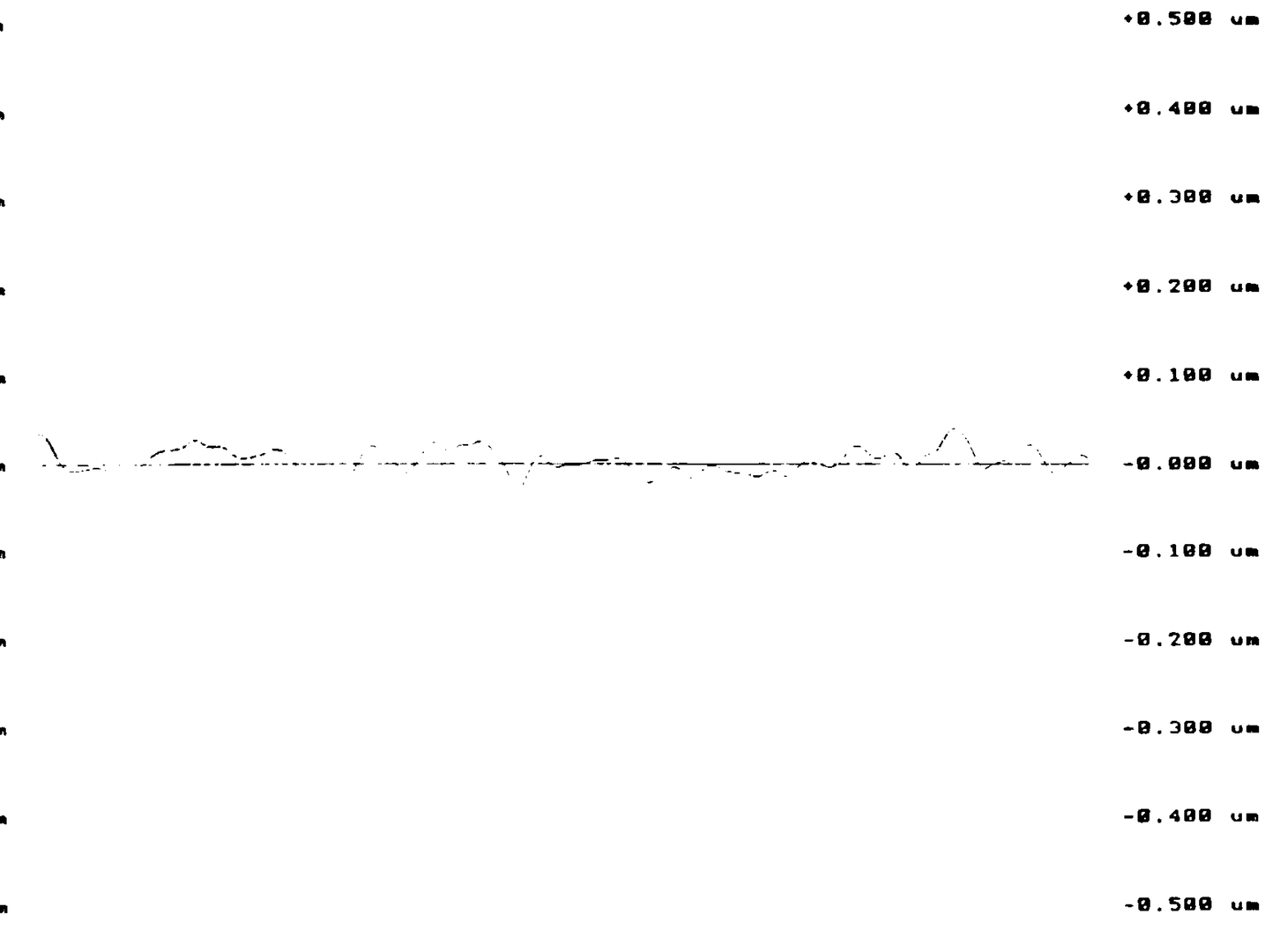

Figure 97 : Surface Waviness of CSS Ground BK7 Sample

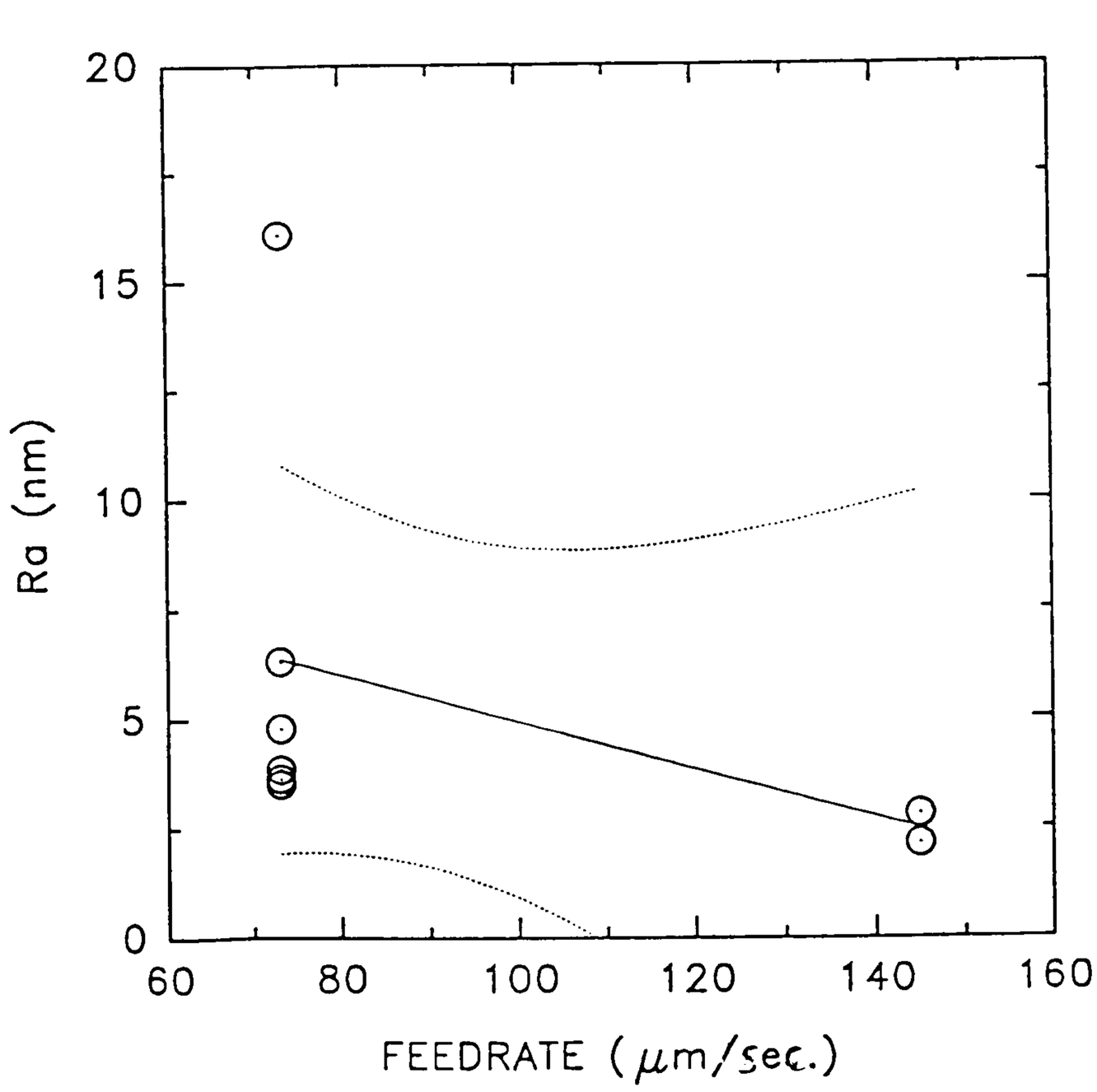

Figure 98 : Graph showing Surface Roughness / Linear Feedrate (V_l) at 8 mm Radius Position on Ground BK7 Samples

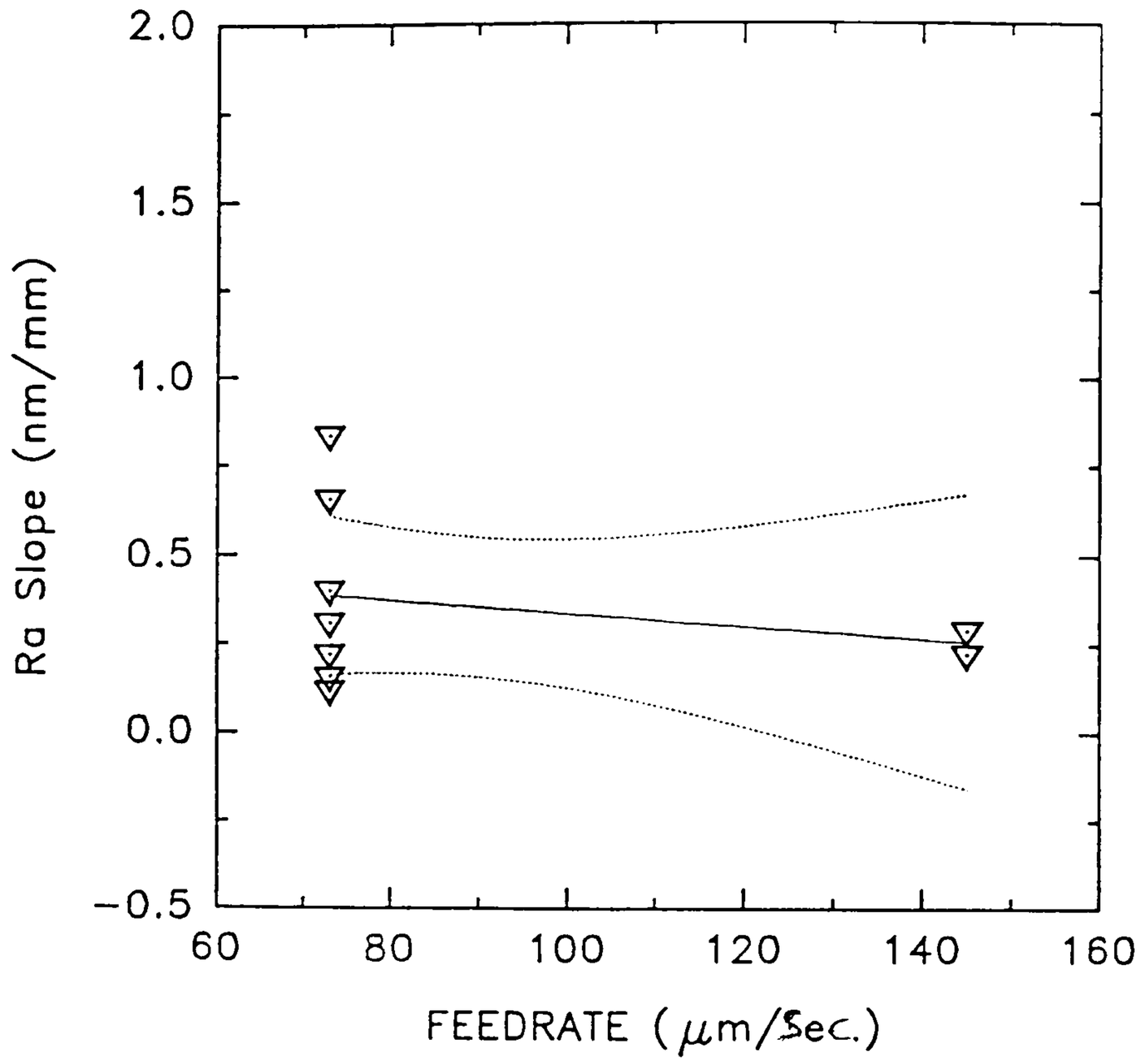

Figure 99 : Graph showing Surface Roughness / Linear Feedrate (V_l) Slope across Ground BK7 Samples

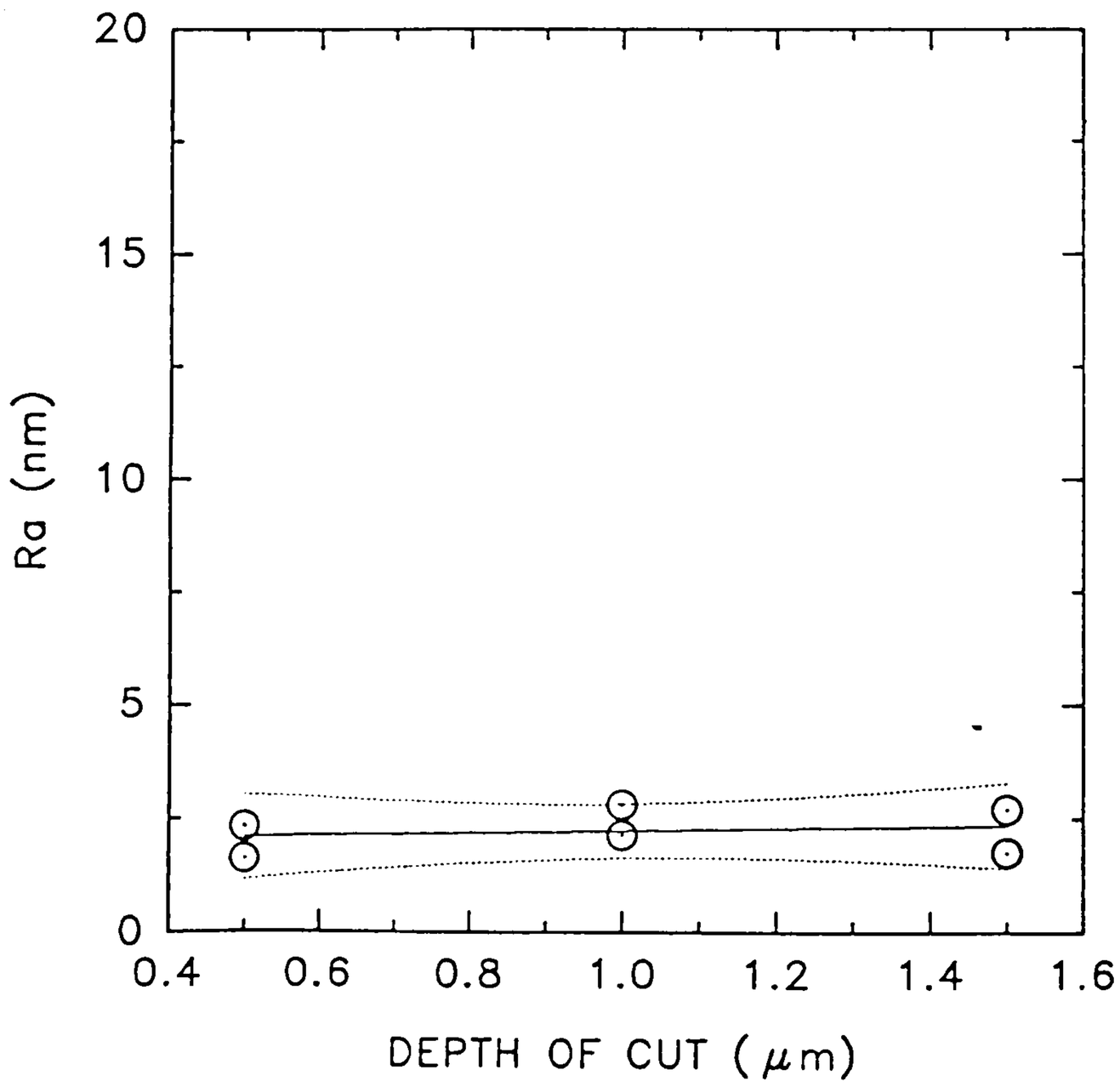

Figure 100 : Graph showing Surface Roughness / Depth of Cut (d) at 8 mm Radius Position on Ground BK7 Samples

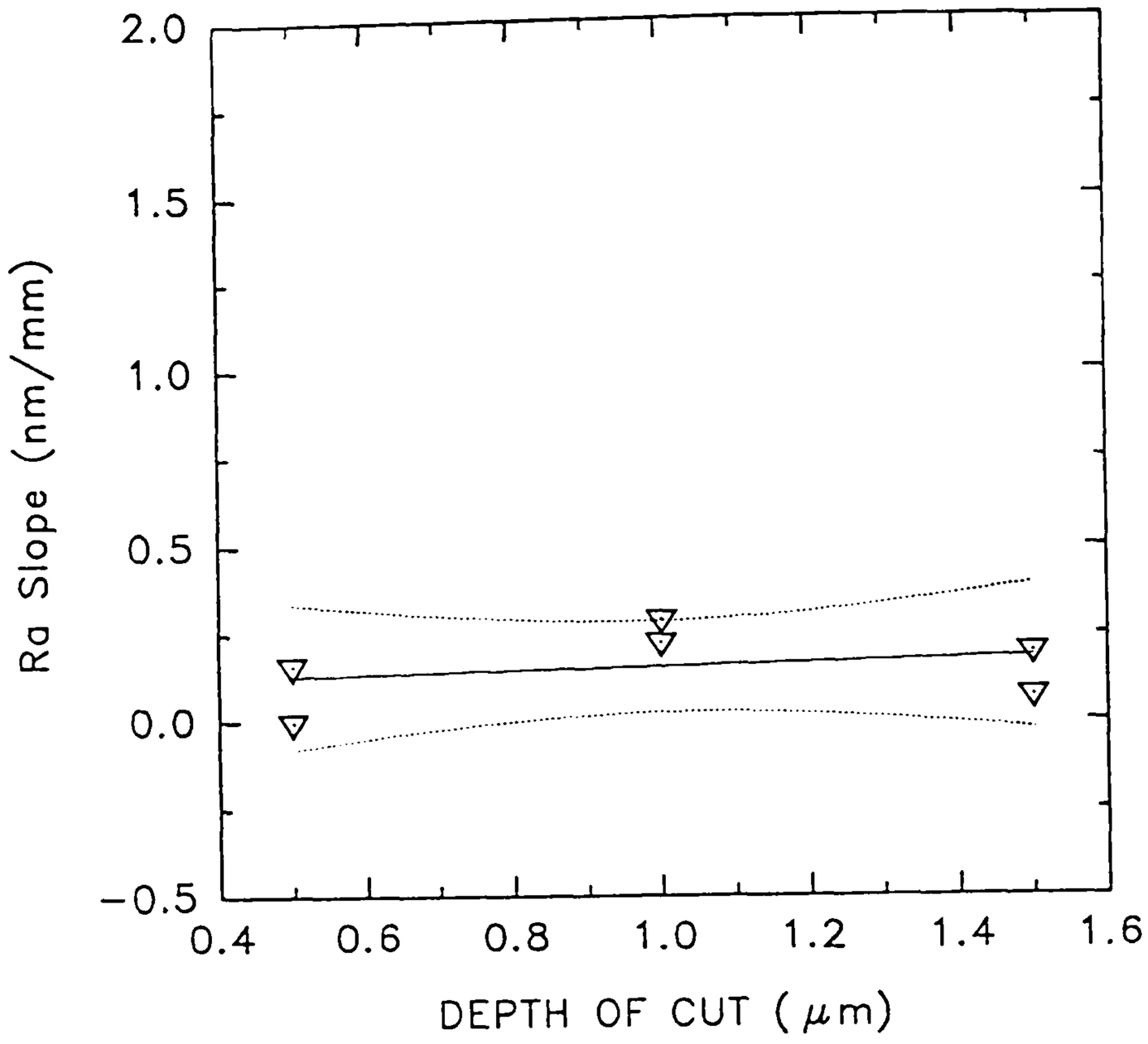

Figure 101 : Graph showing Surface Roughness / Depth of Cut (d) Slope across Ground BK7 Samples

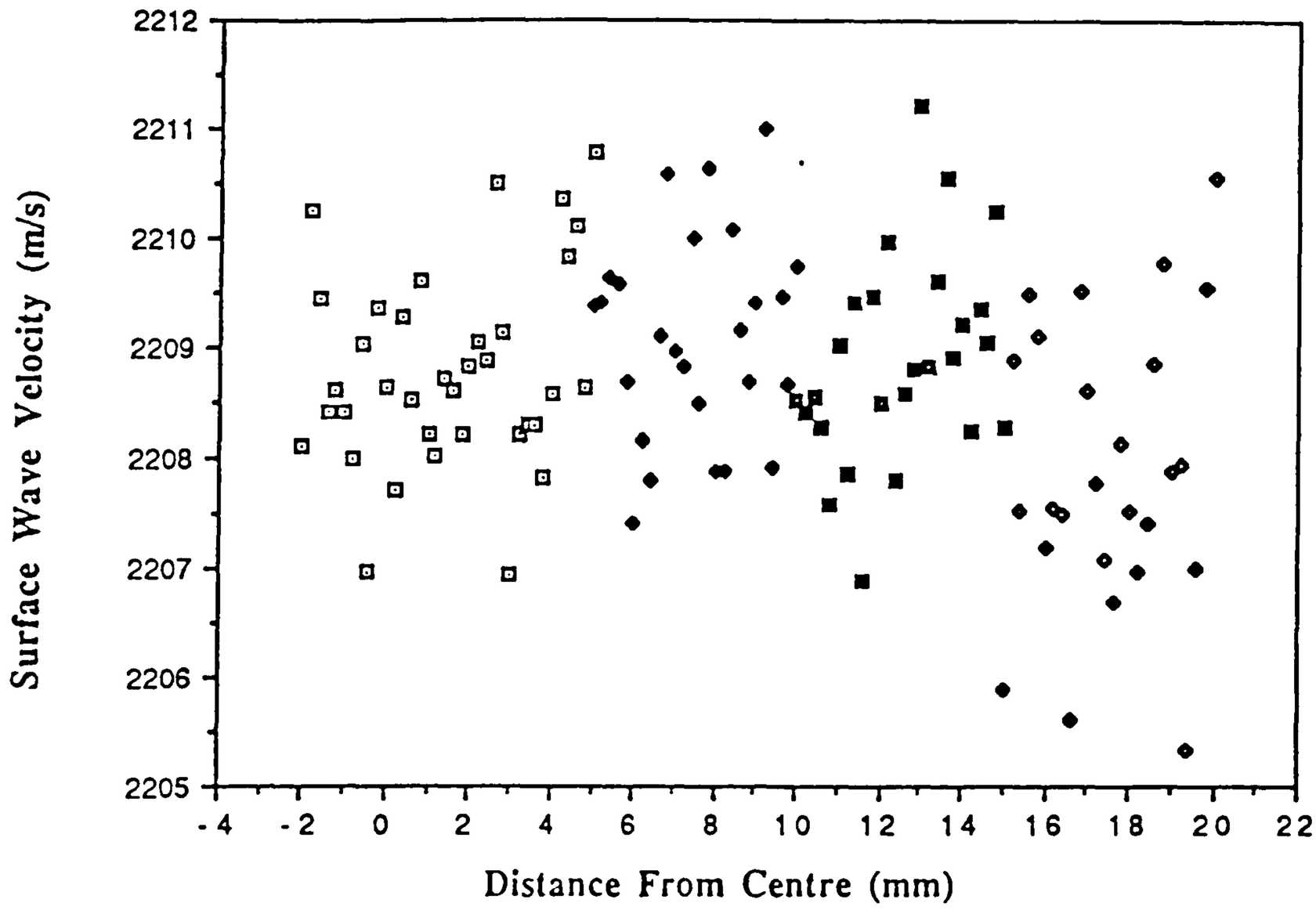

Figure 102 : Surface Wave Velocity Radial Scan on Polished SF10 Glass Surface

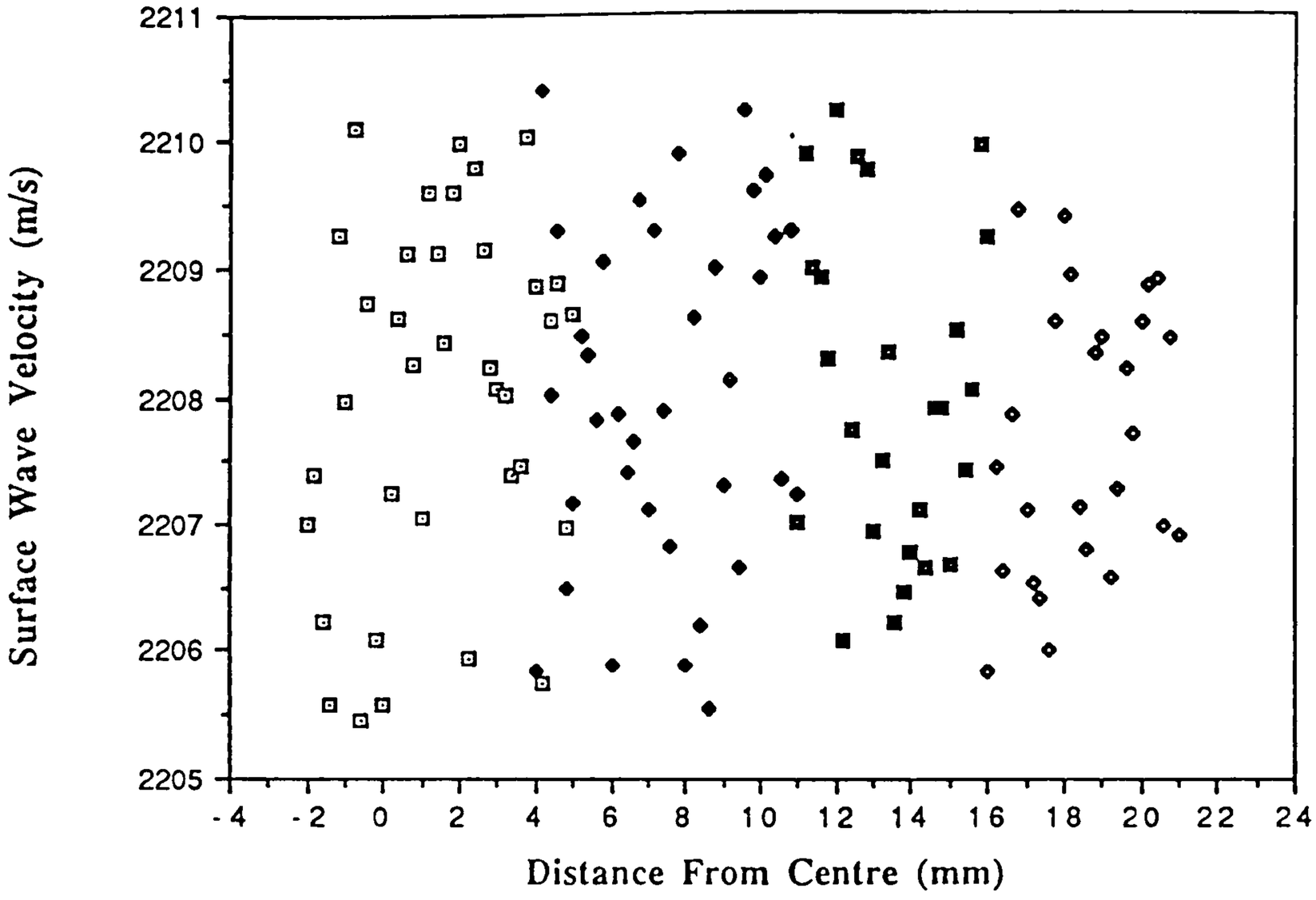

Figure 103 : Surface Wave Velocity Radial Scan on Ground SF10 Glass Surface

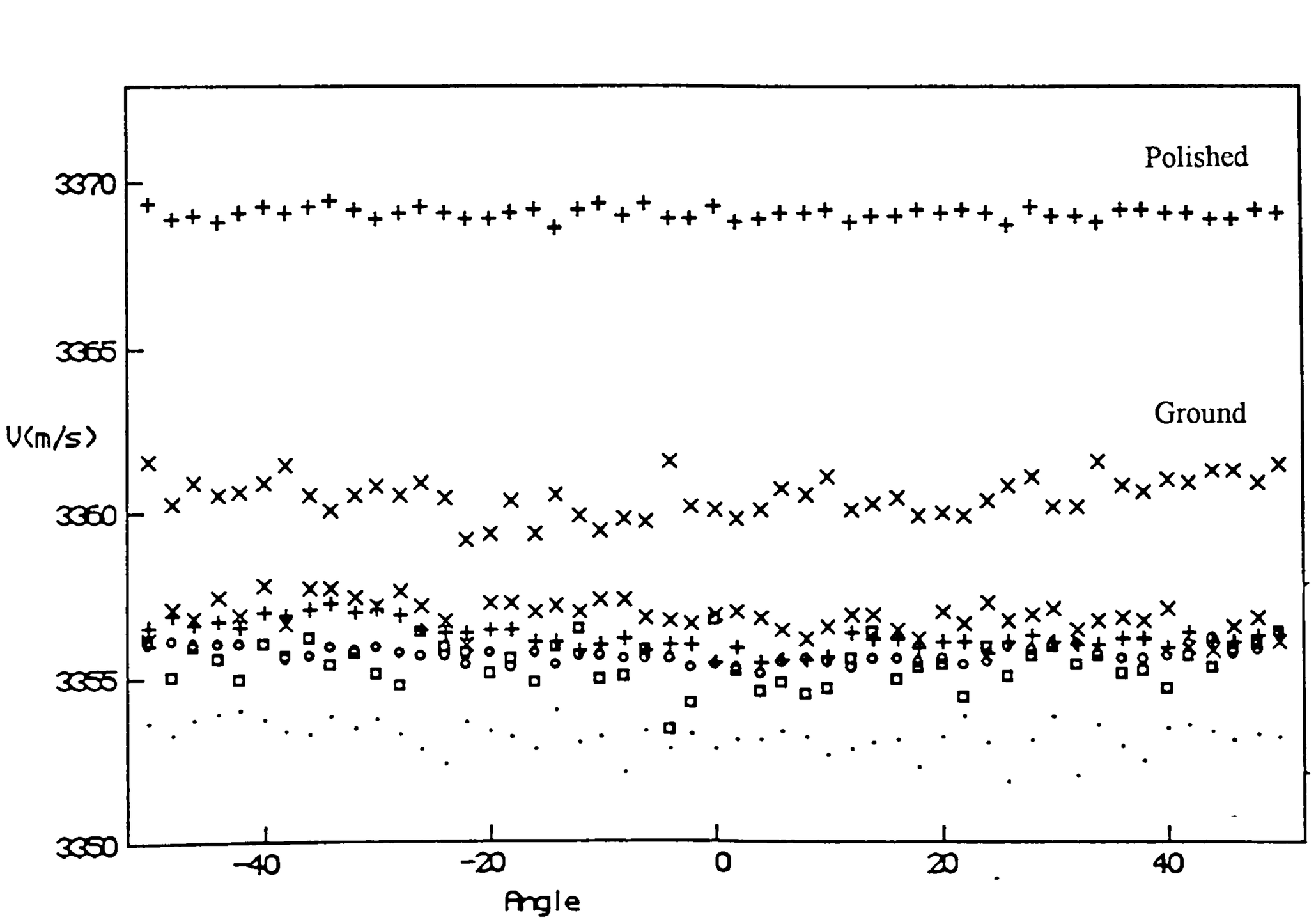

Figure 104 : Surface Wave Velocity of BK7 Ground Samples
Azimuthal Scans at 12 mm

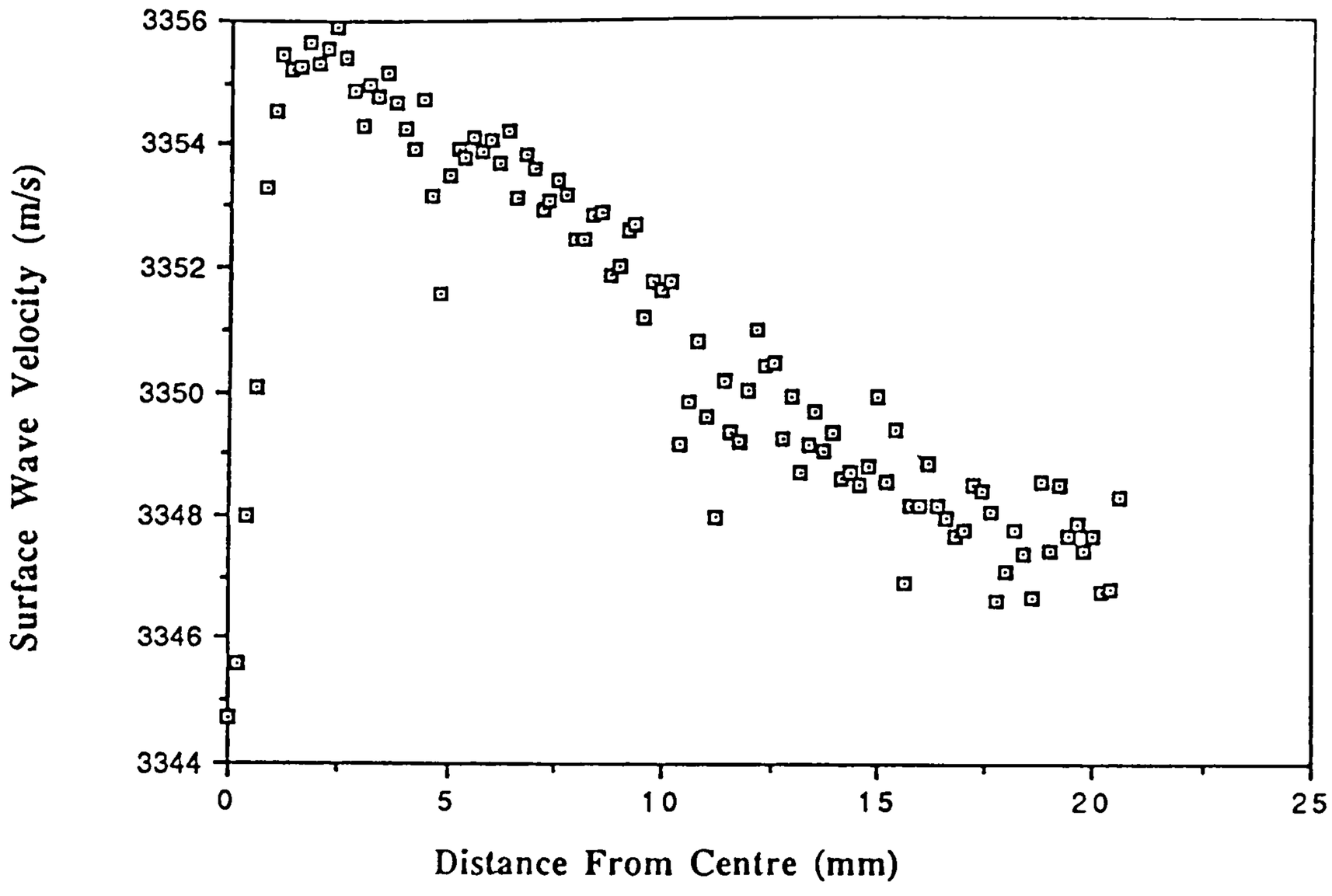

Figure 105 : Surface Wave Velocity Radial Scan on CRPM Mode Ground BK7 Sample No. 17

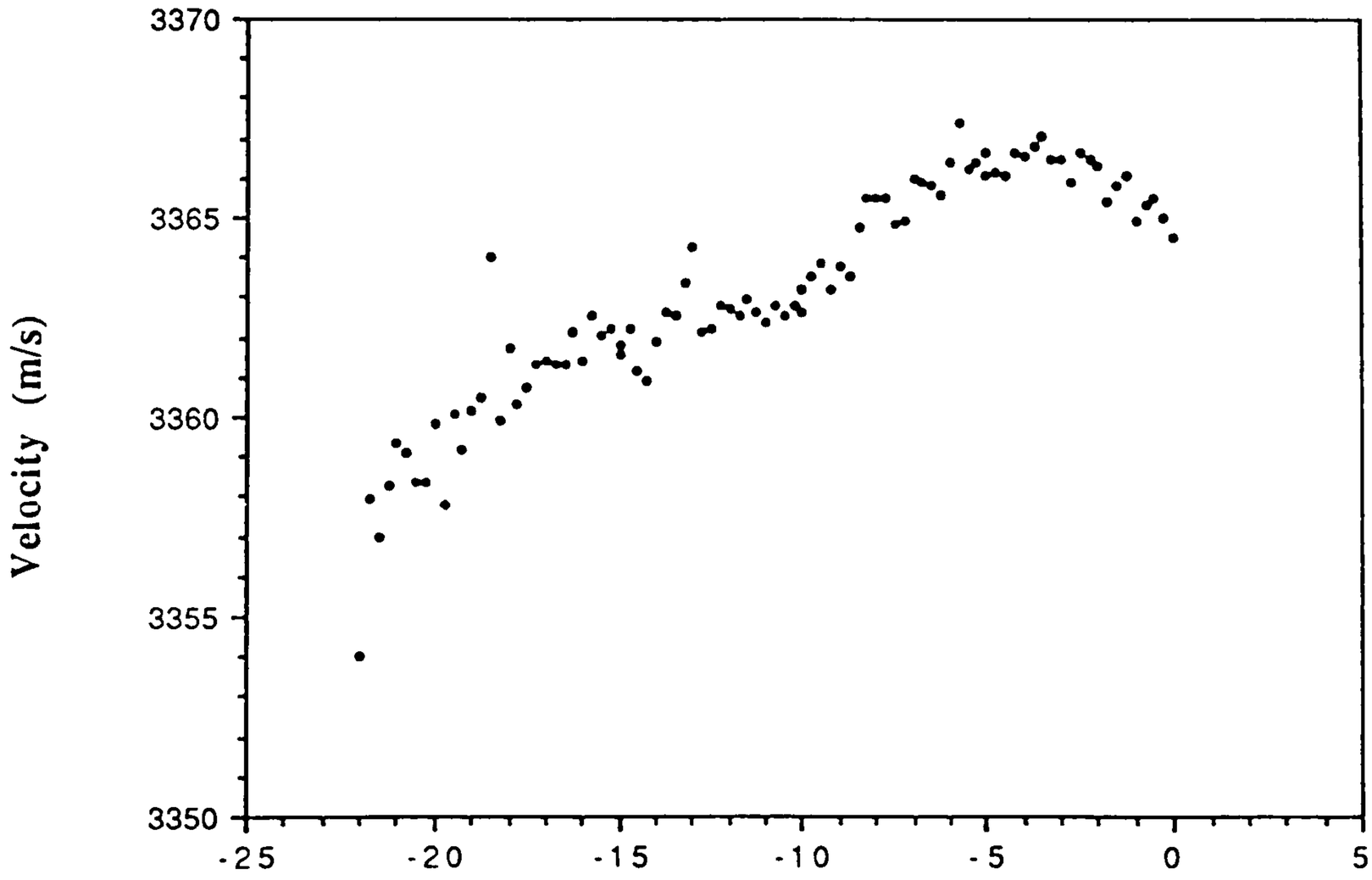

Figure 106 : Surface Wave Velocity Radial Scan on CRPM Mode Ground BK7 Sample No. 18

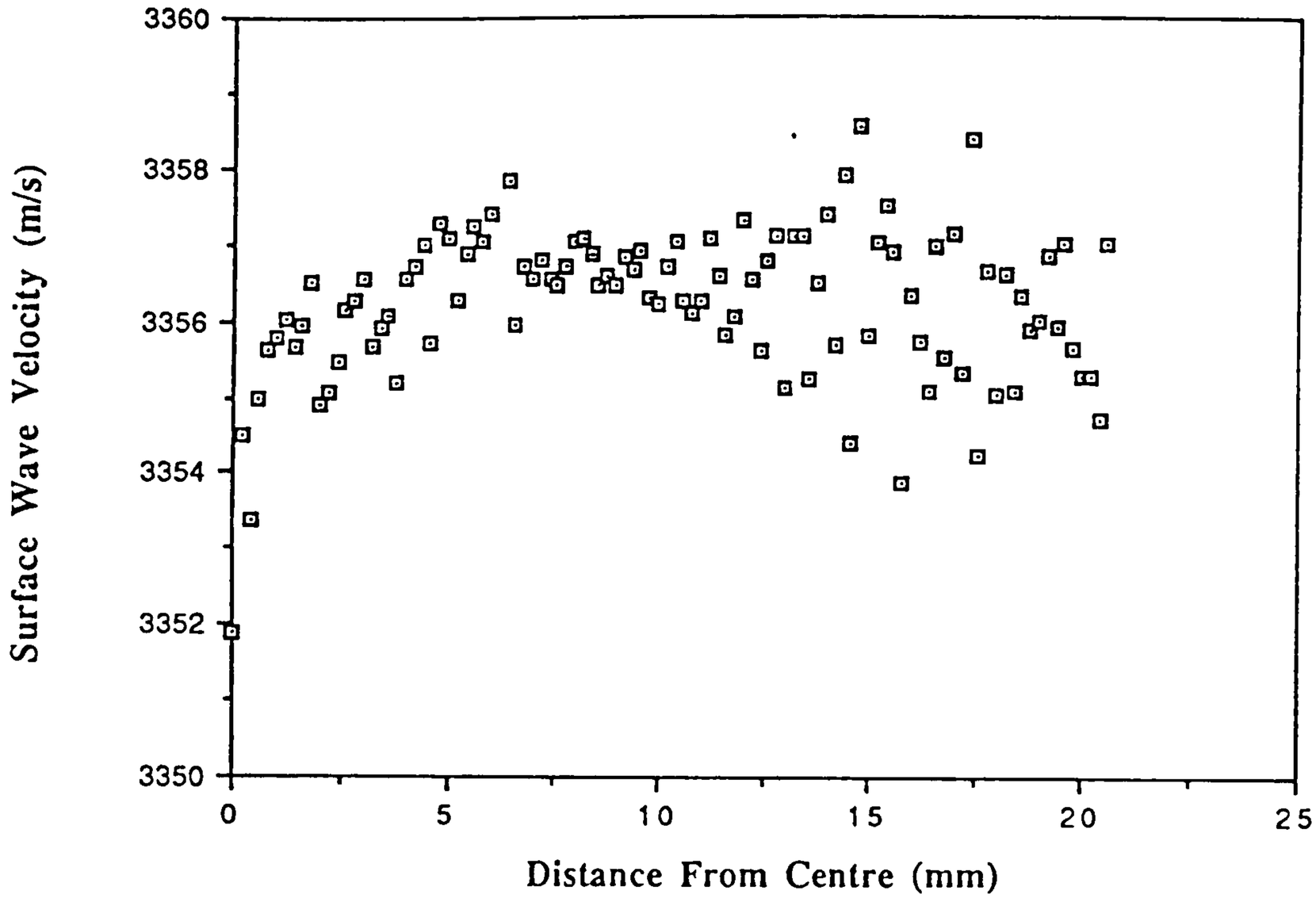

Figure 107 : Surface Wave Velocity Radial Scan on CSS Mode Ground BK7 Sample No. 15

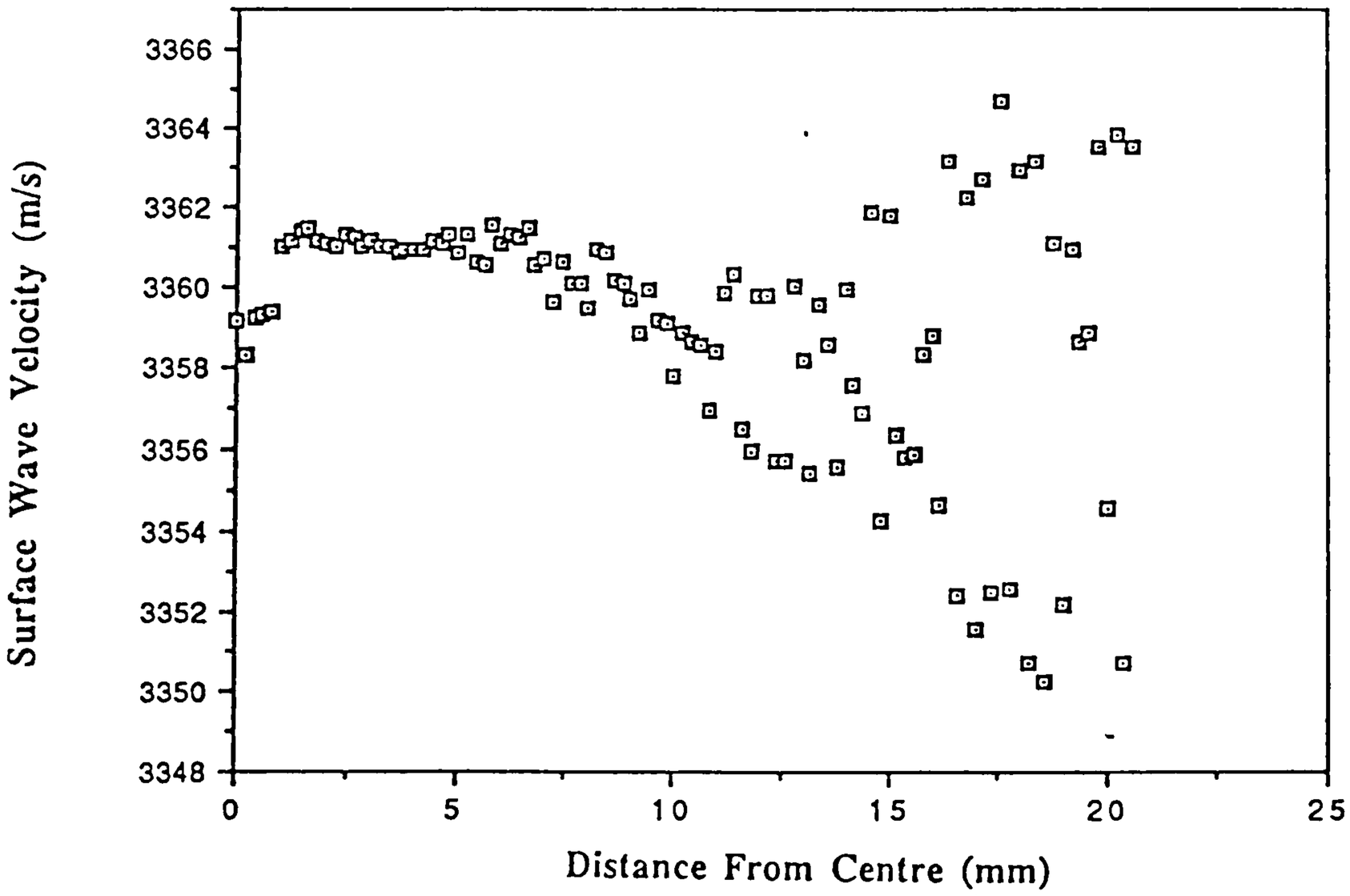

Figure 108 : Surface Wave Velocity Radial Scan on CSS Mode Ground BK7 Sample No. 19

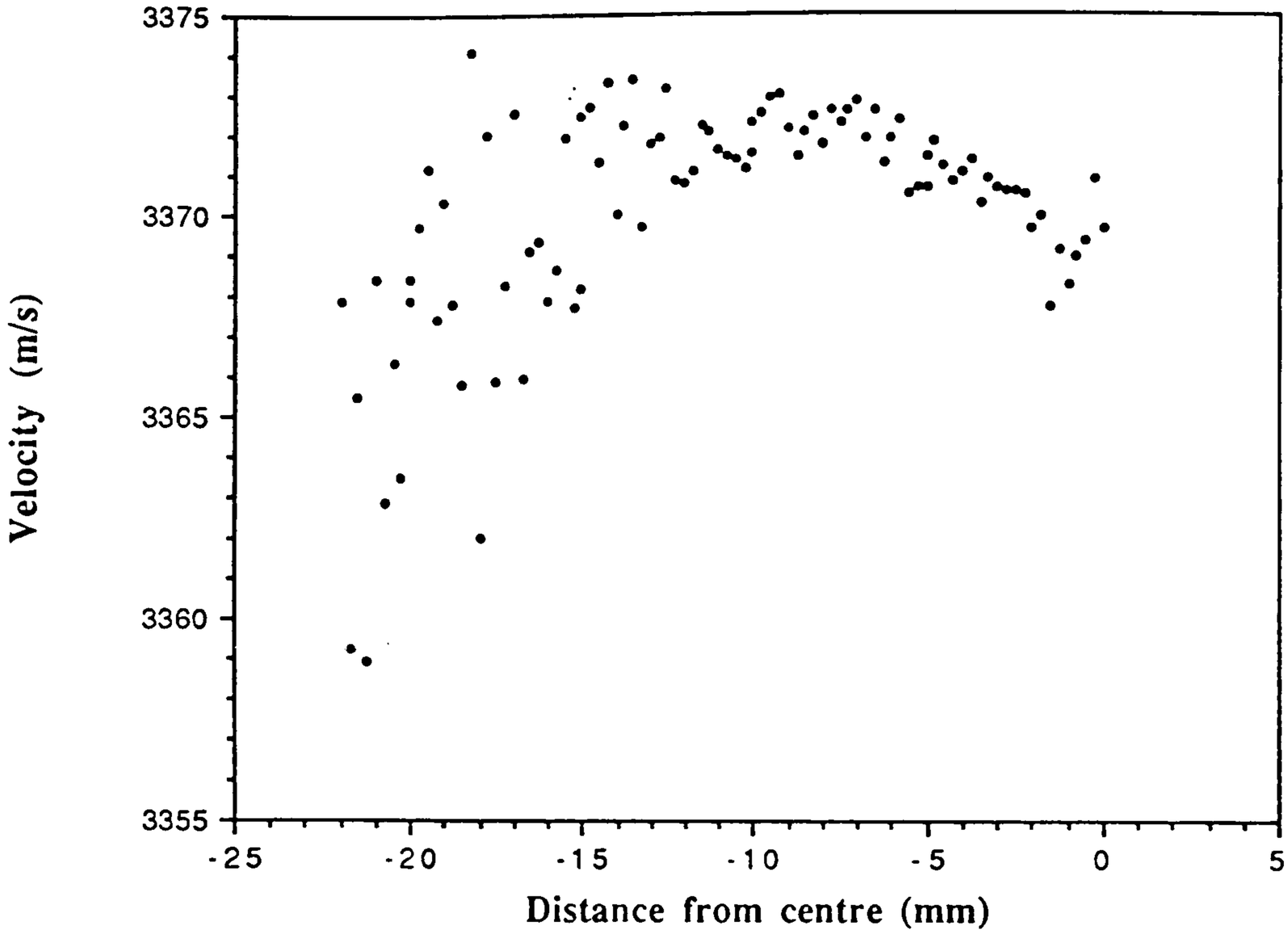

Figure 109 : Surface Wave Velocity Radial Scan on CSS Mode Ground BK7 Sample No. 4

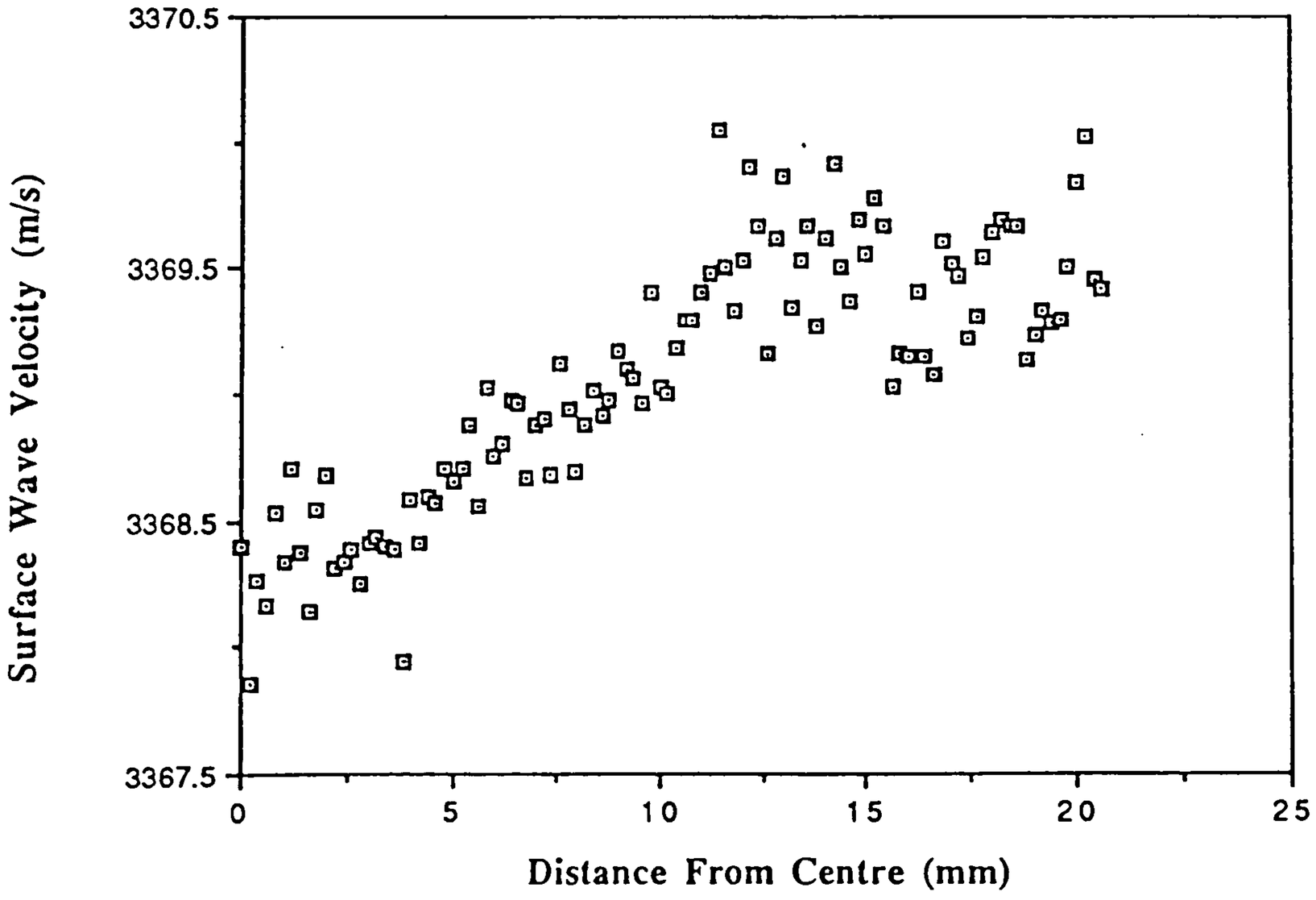

Figure 110 : Surface Wave Velocity Radial Scan on Polished BK7 Sample

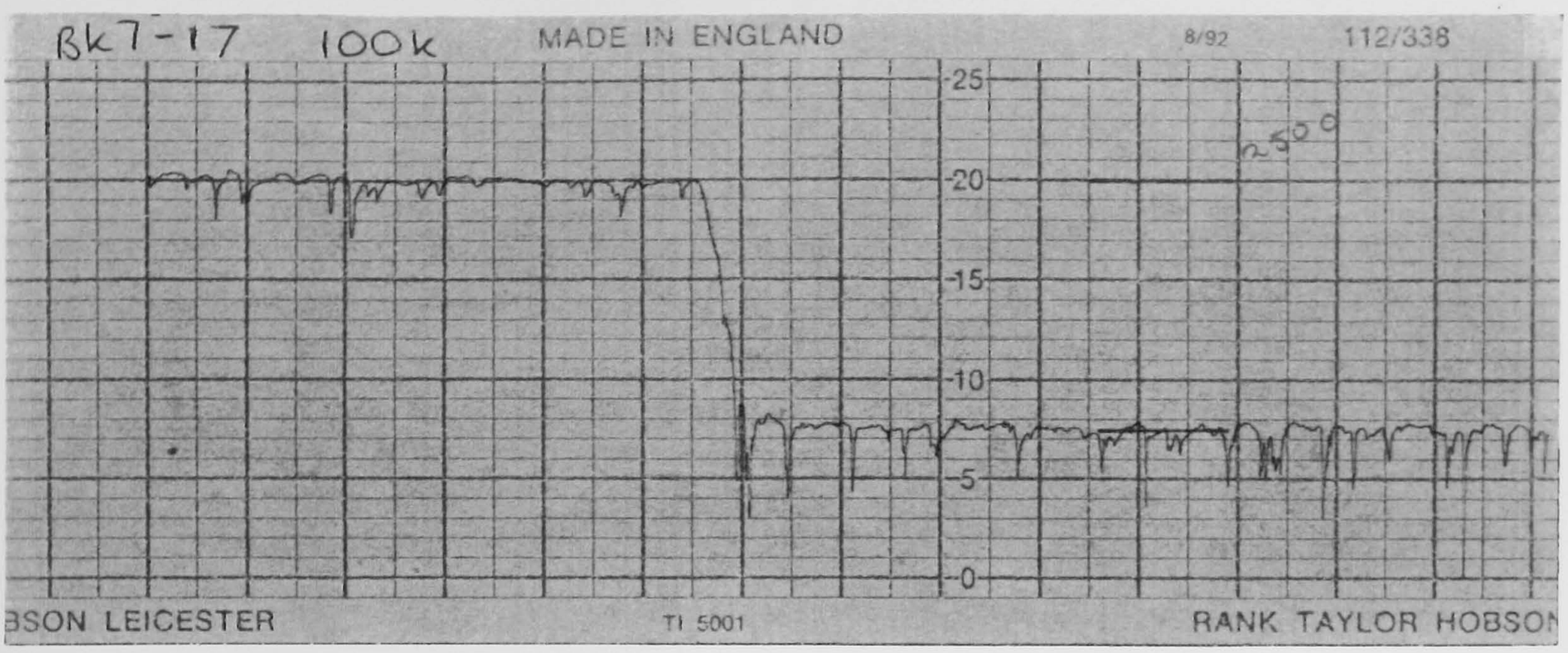

Figure 111 : Talystep Trace showing Etched Step Height for Assessment of Sub-Surface Damage

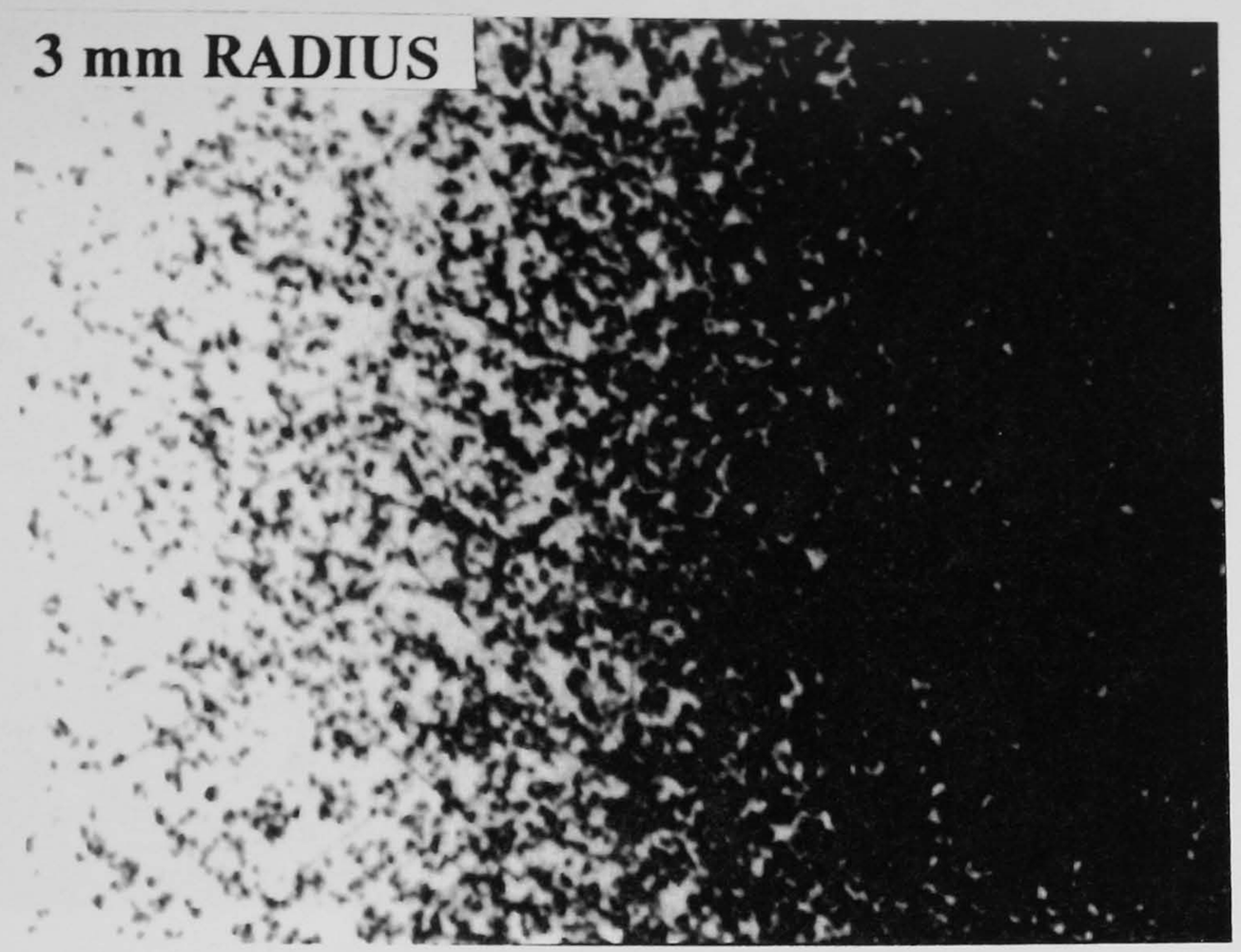

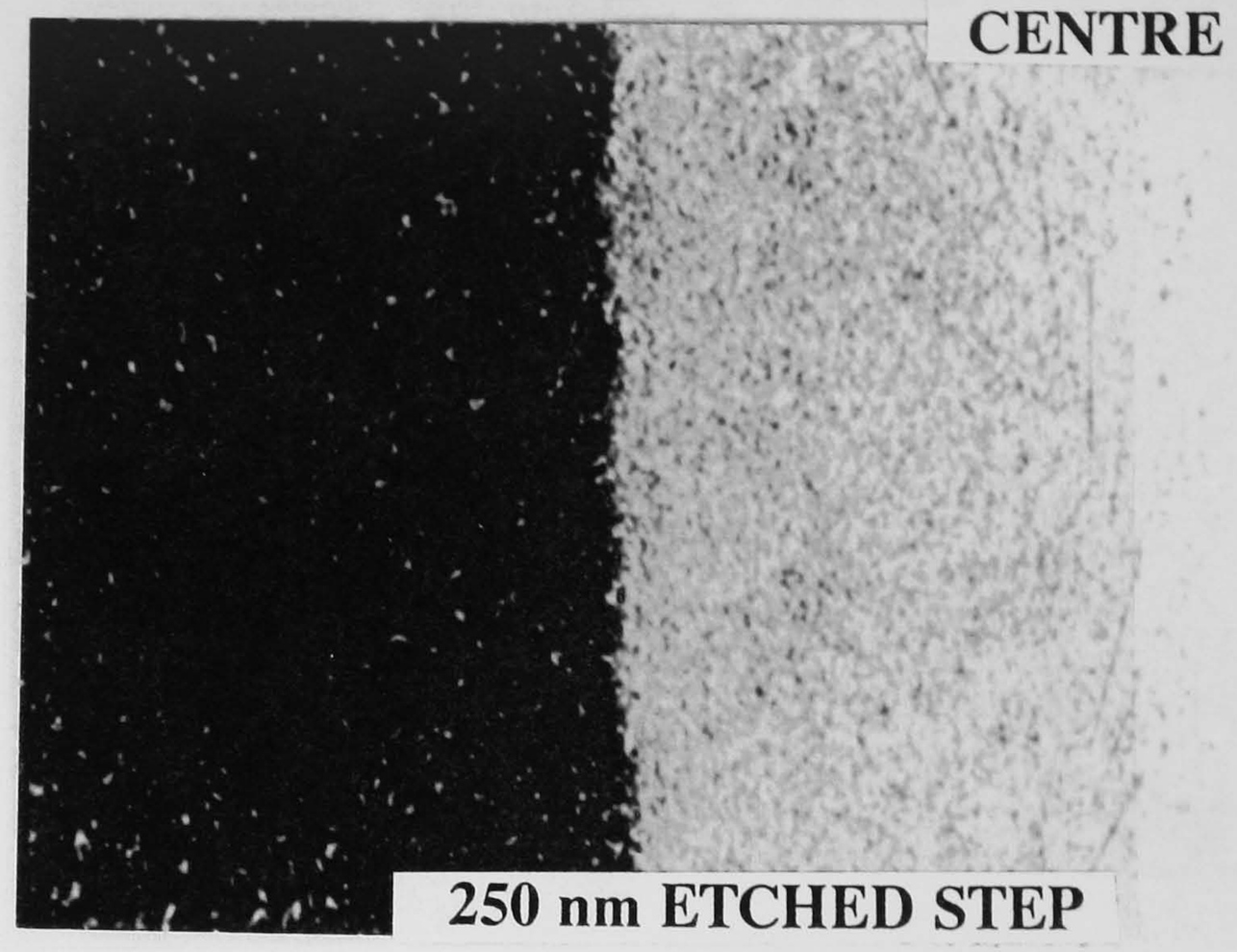

Magn X 86

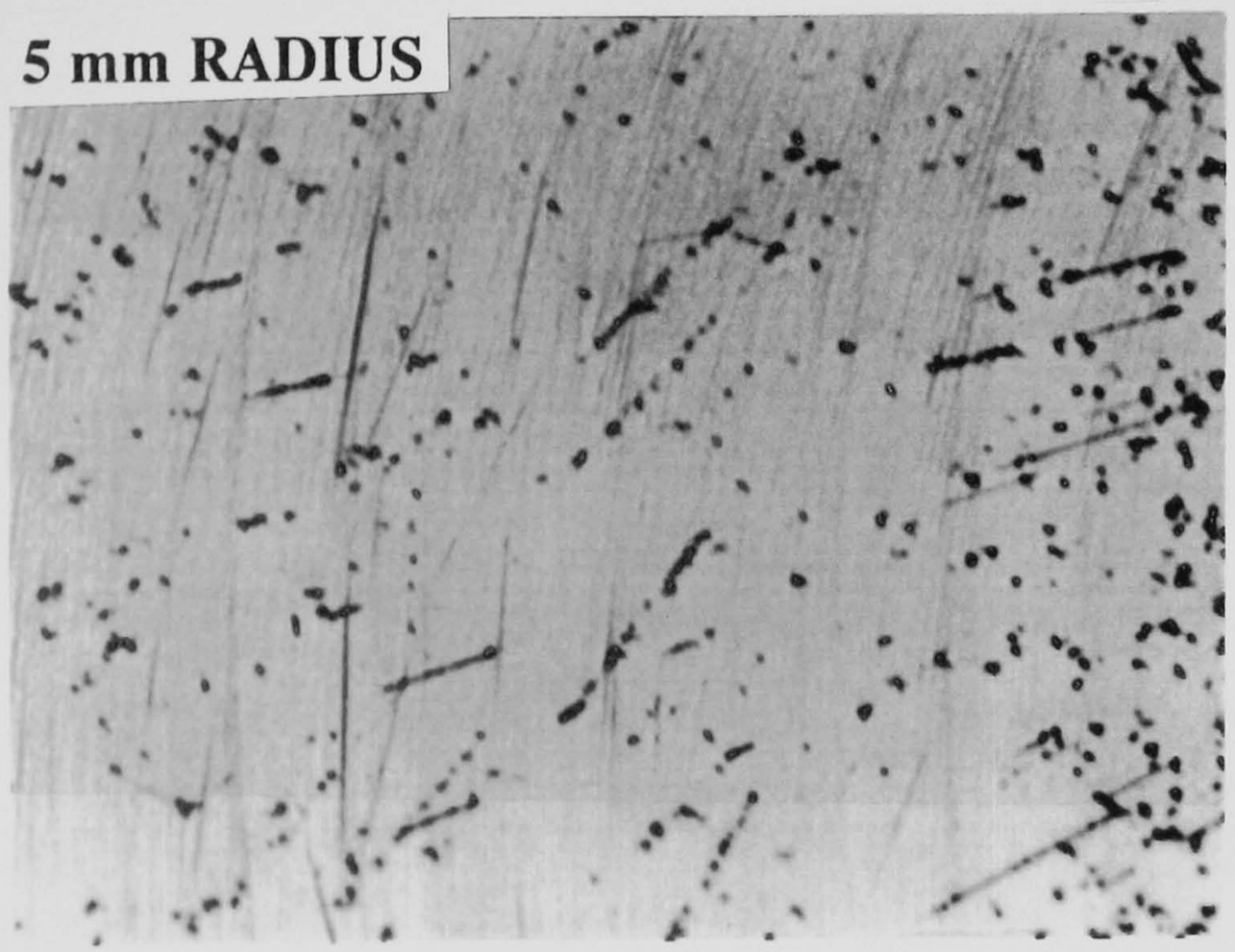

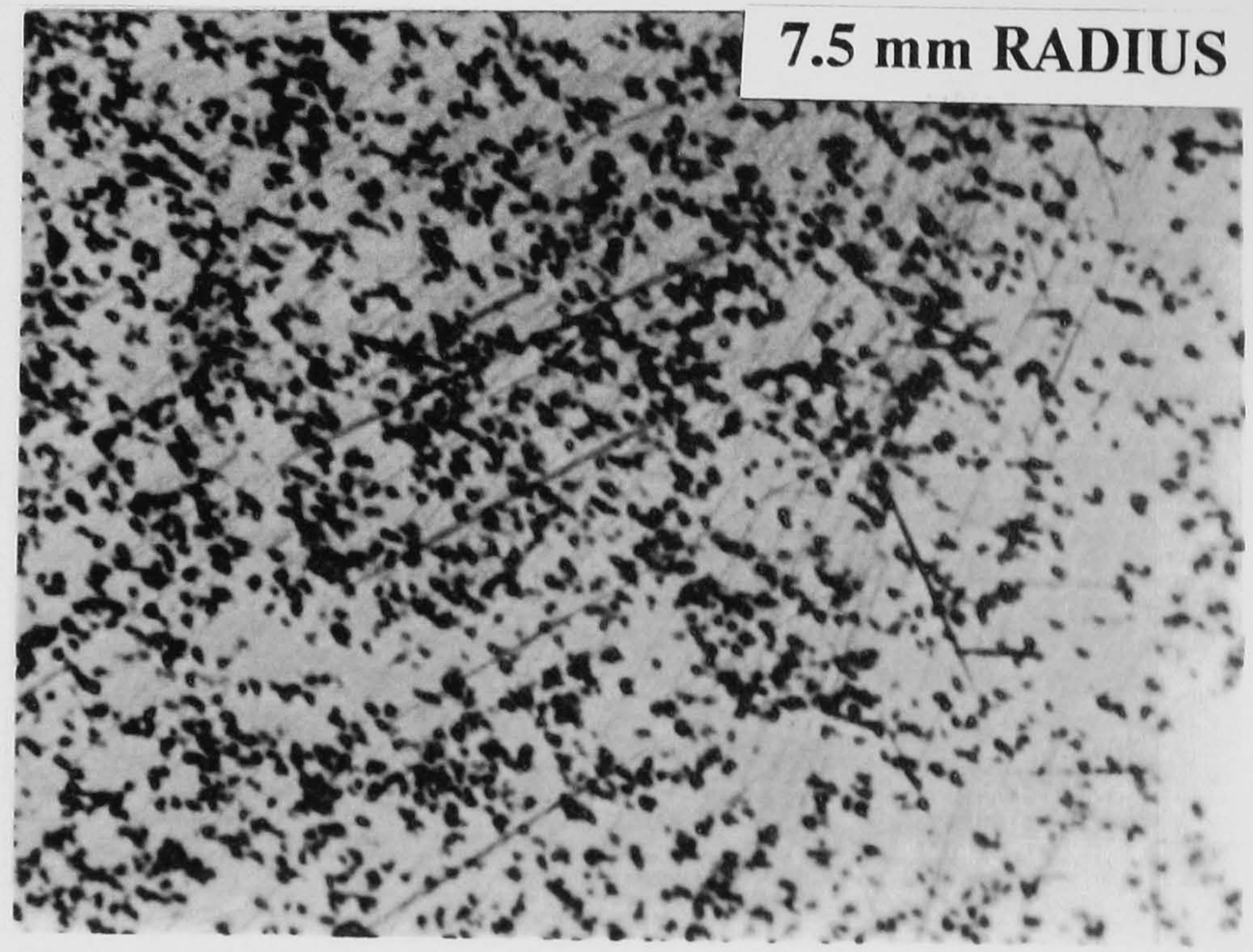

Figure 112 : Photomicrographs of Etched Regions of BK7 Sample 17

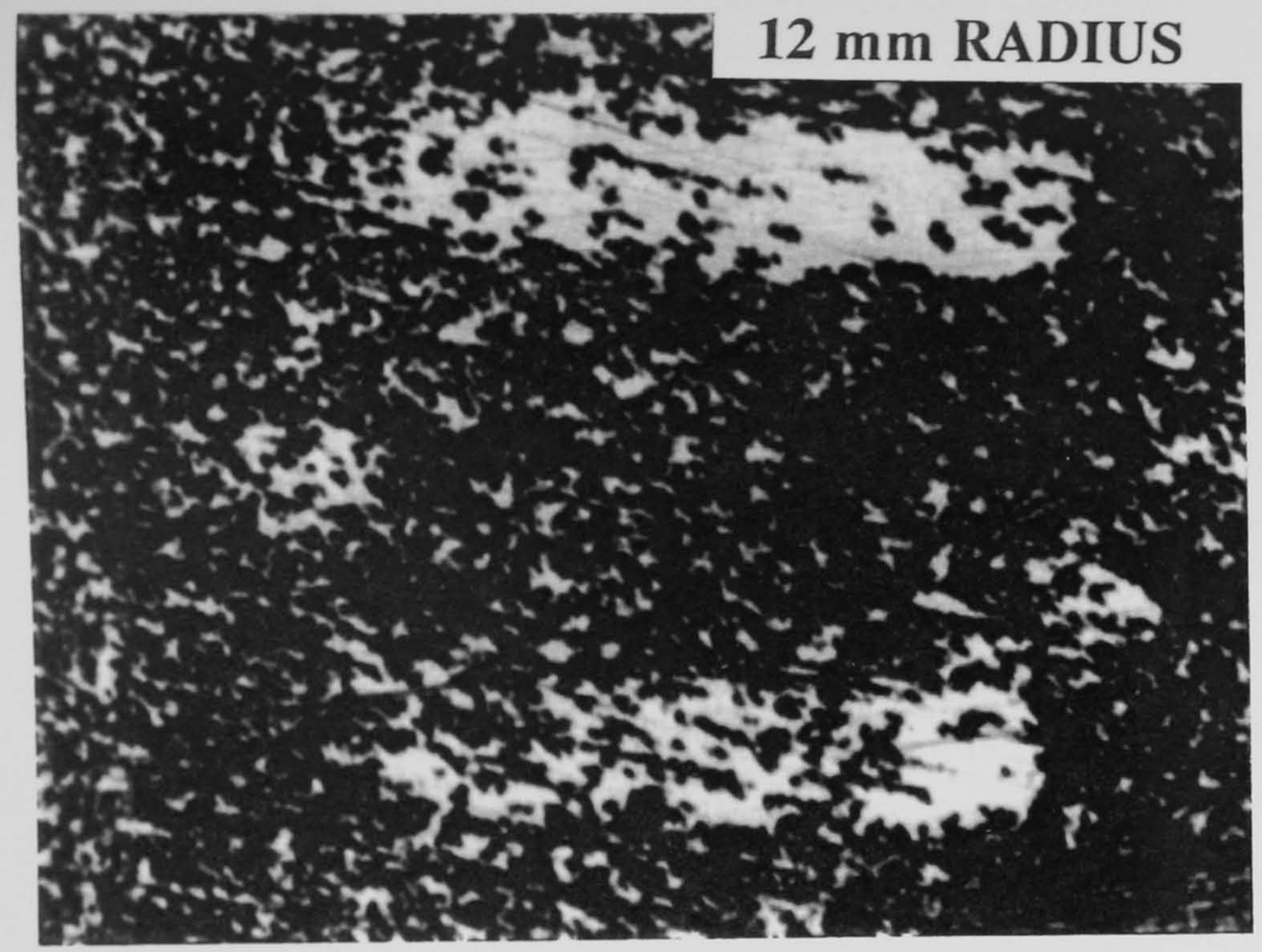

Magn X 86

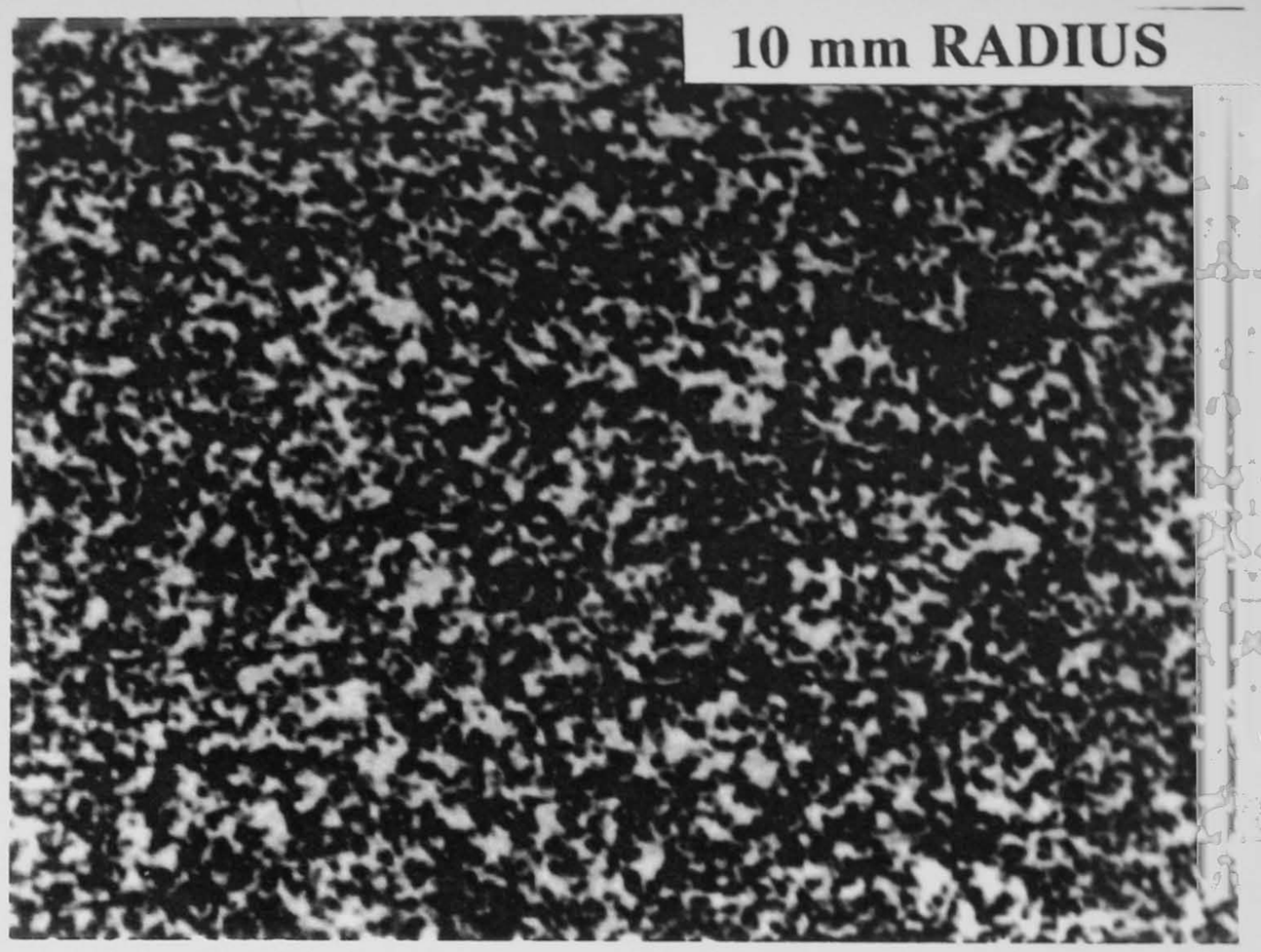

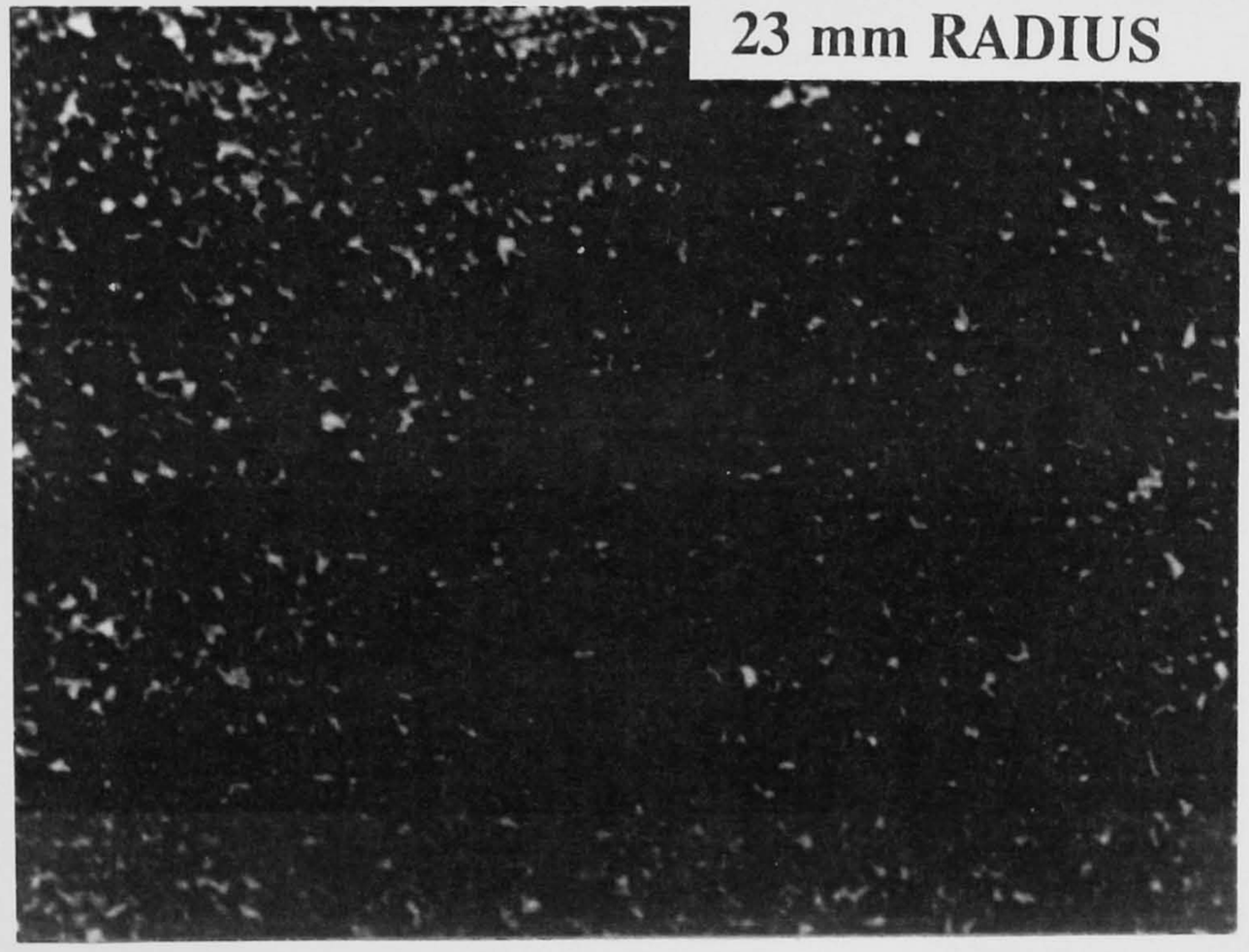

Figure 113 : Photomicrographs of Etched Regions of BK7 Sample 17

Figure 114 : Photomicrographs of Etched Regions of BK7 Sample 15

15 mm RADIUS

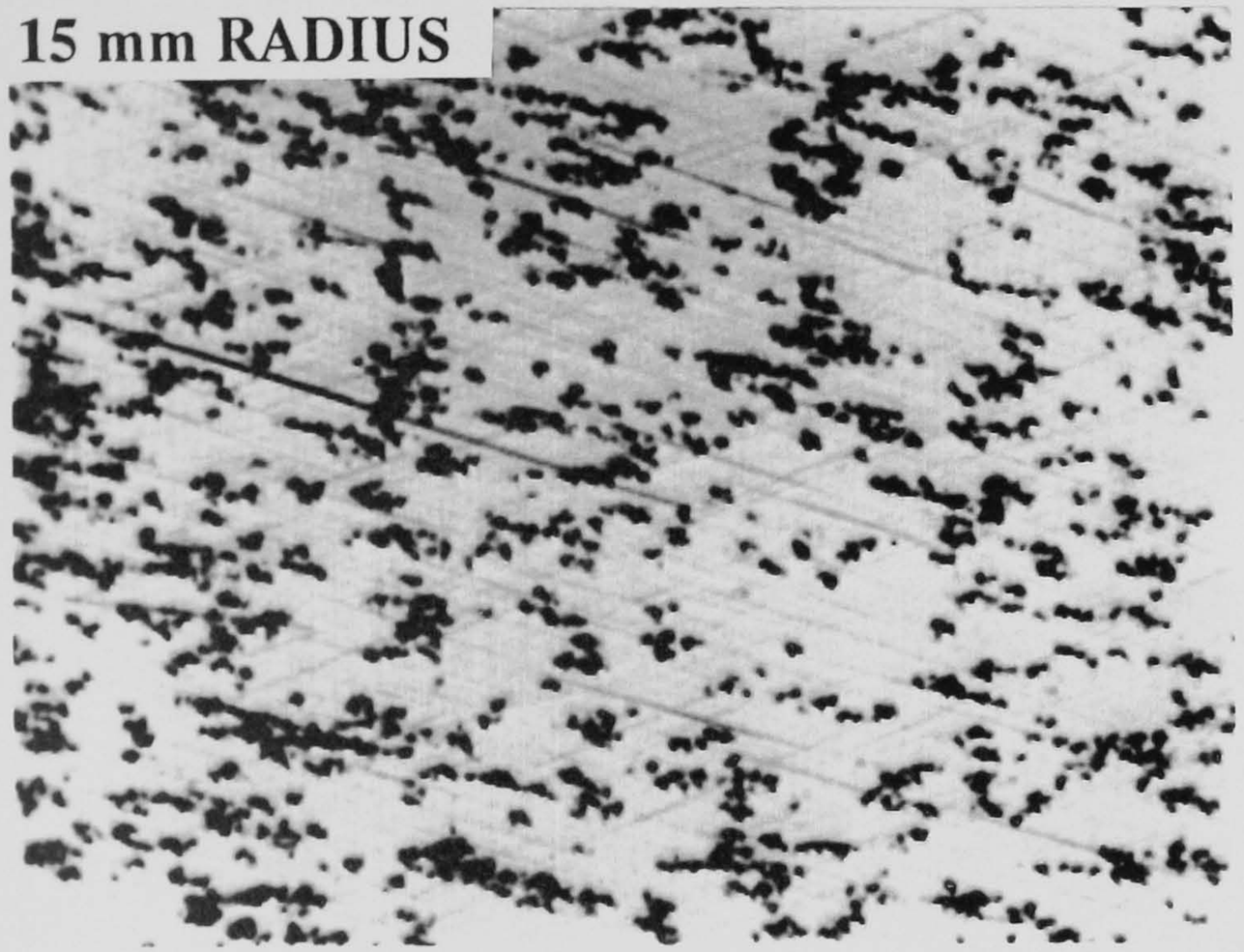

Magn X 86

23 mm RADIUS

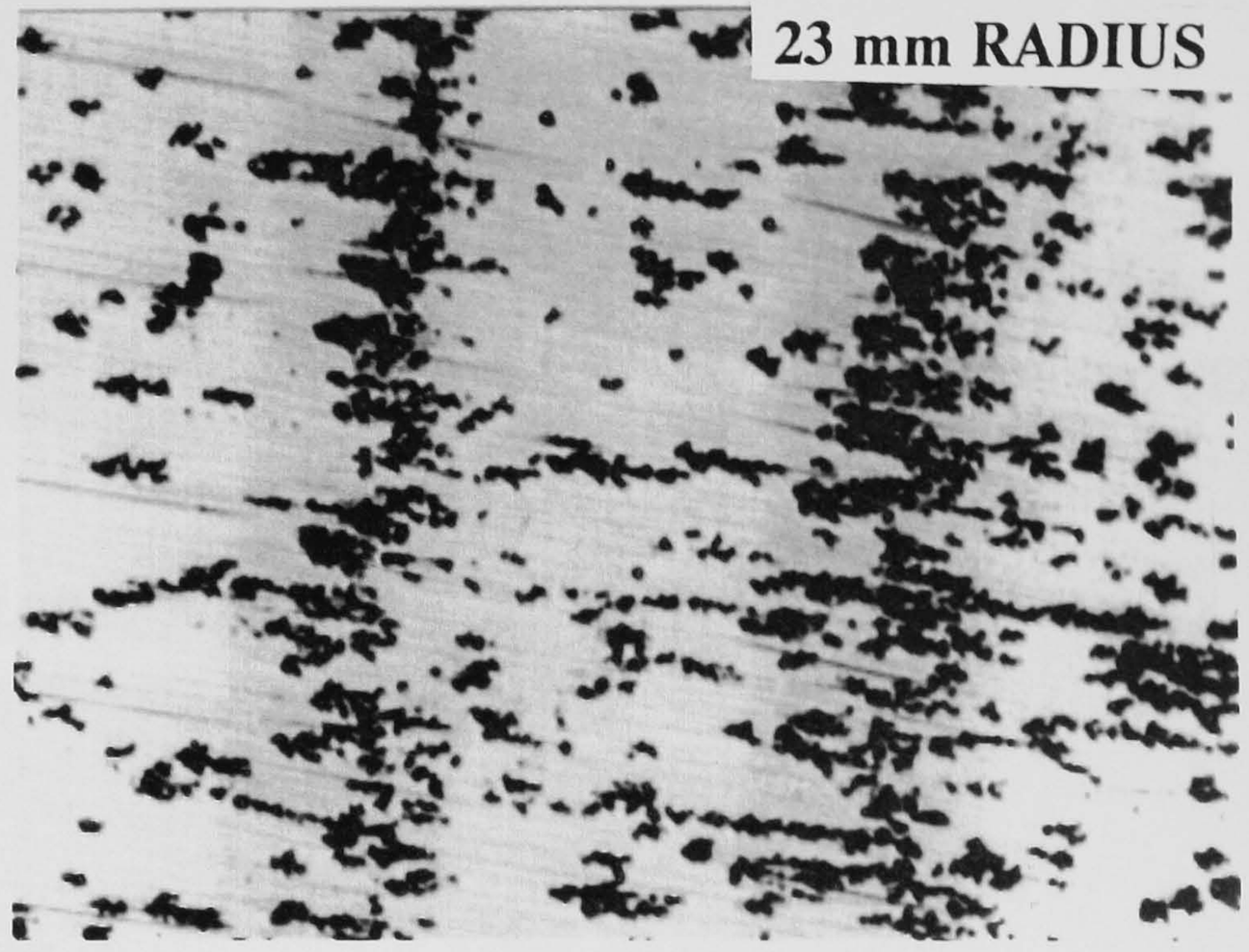

Figure 115 : Photomicrographs of Etched Regions of BK7 Sample 19

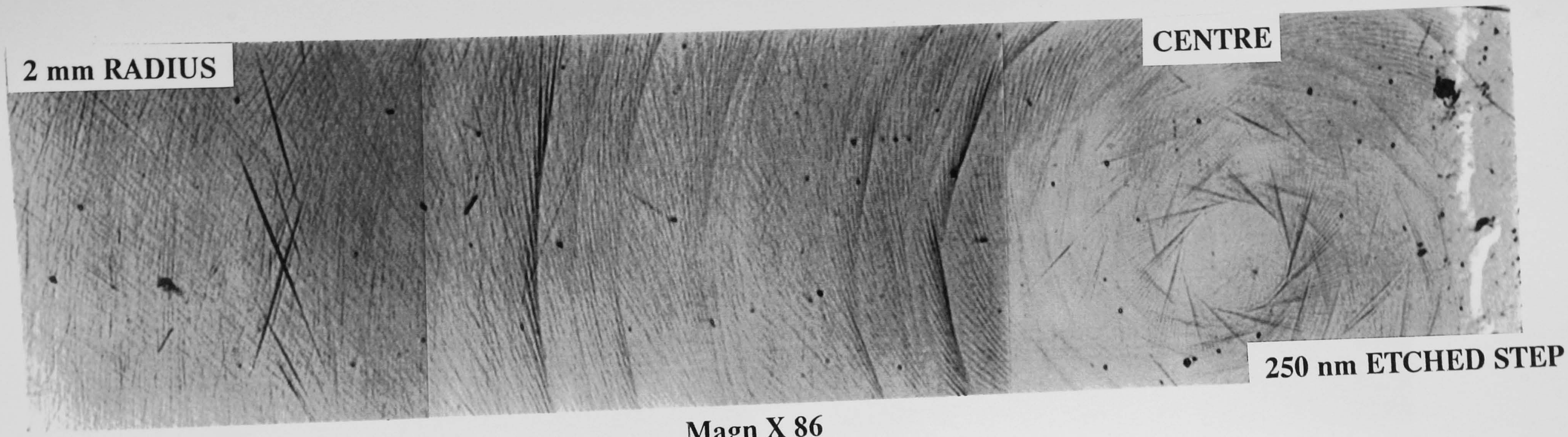

Figure 116 : Photomicrographs of Etched Regions of BK7 Sample 19

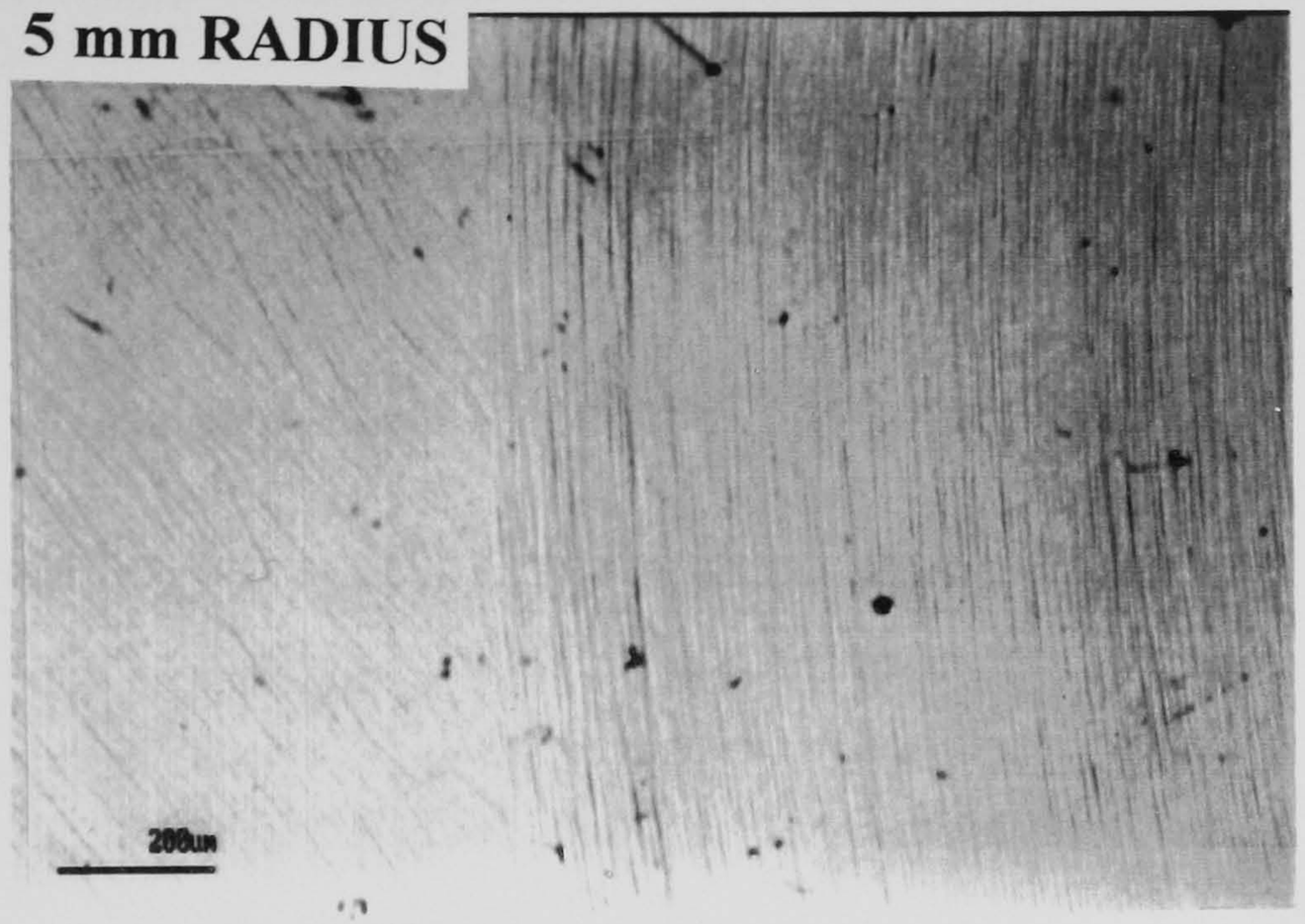

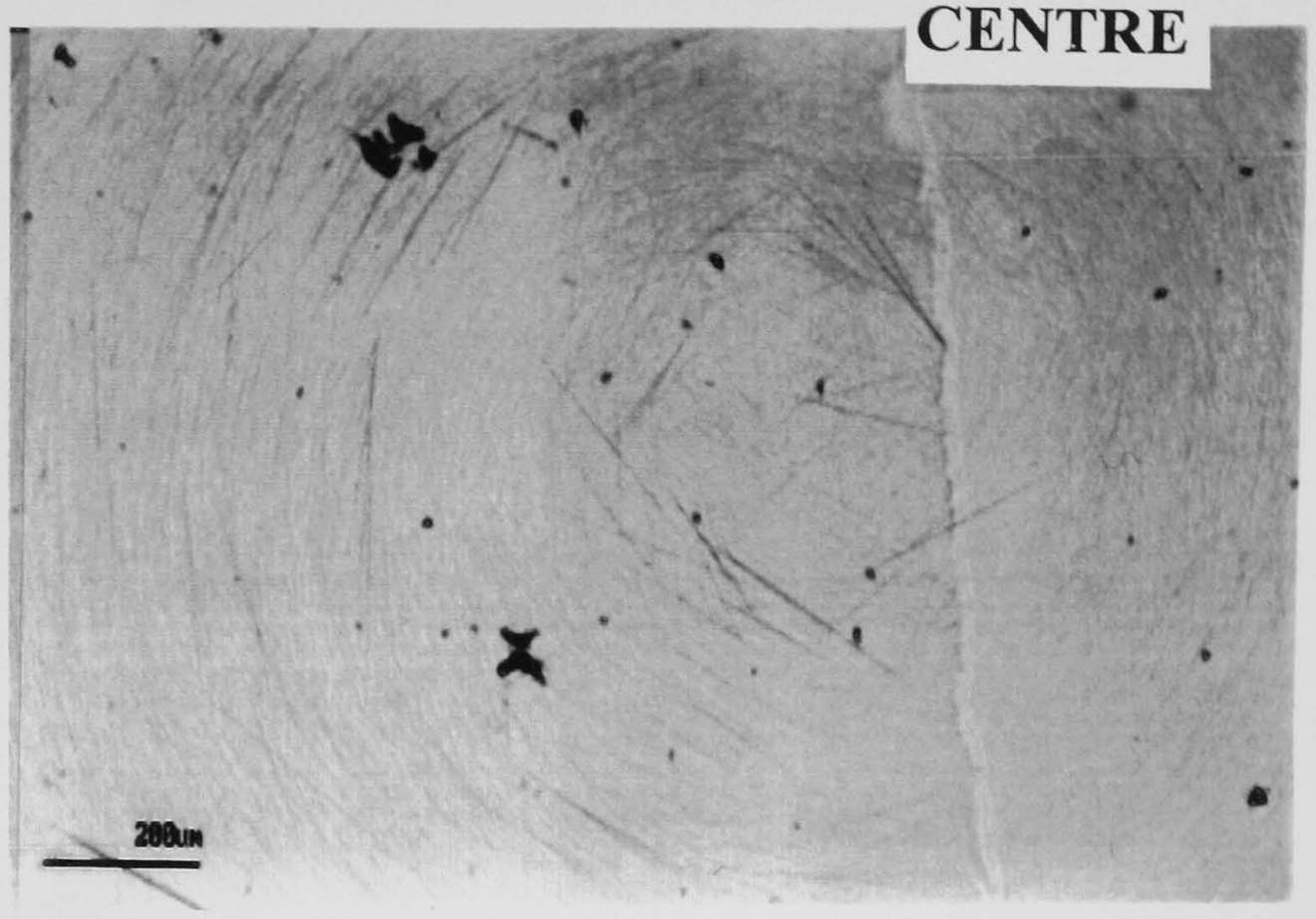

Magn X 86

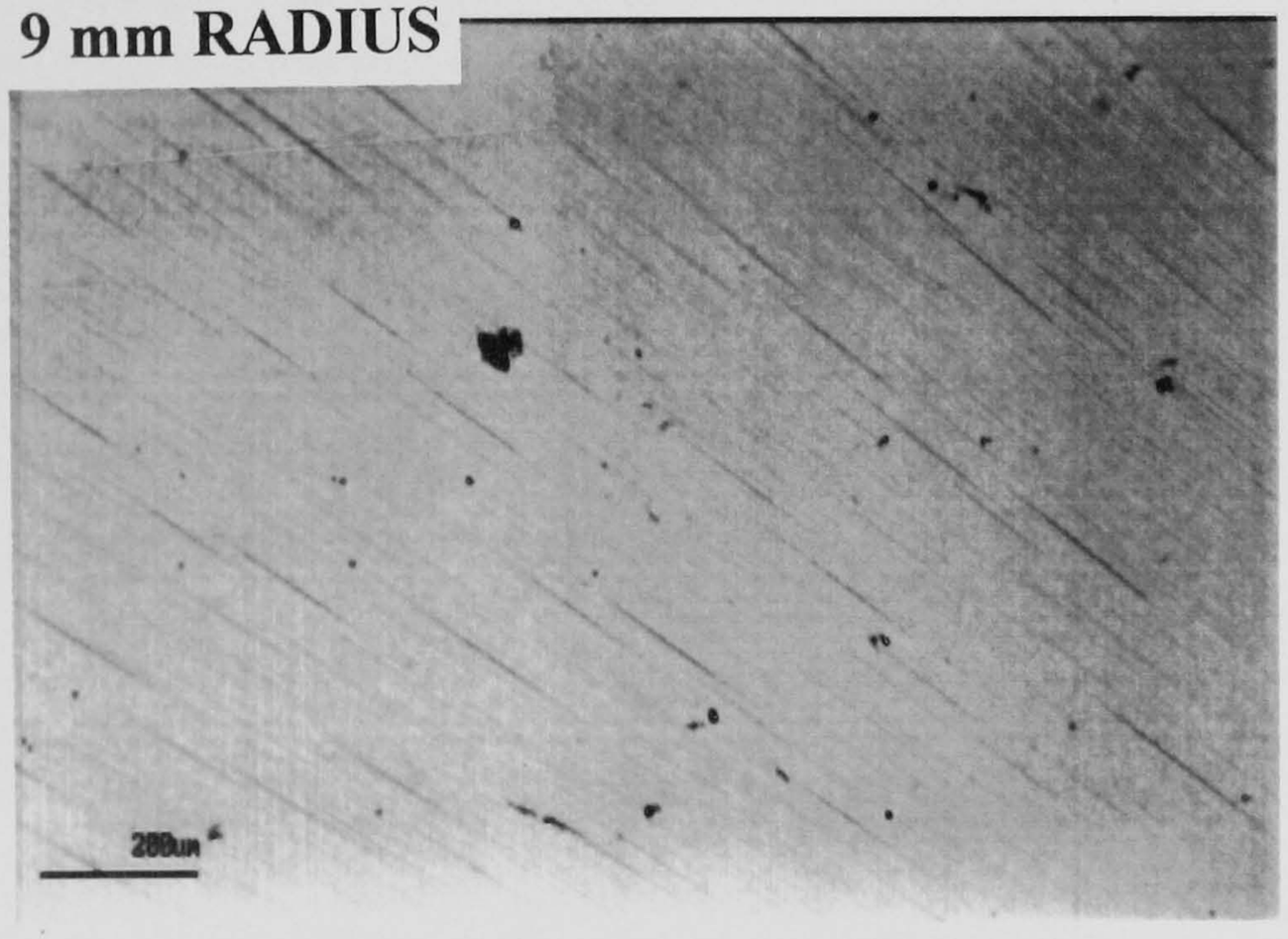

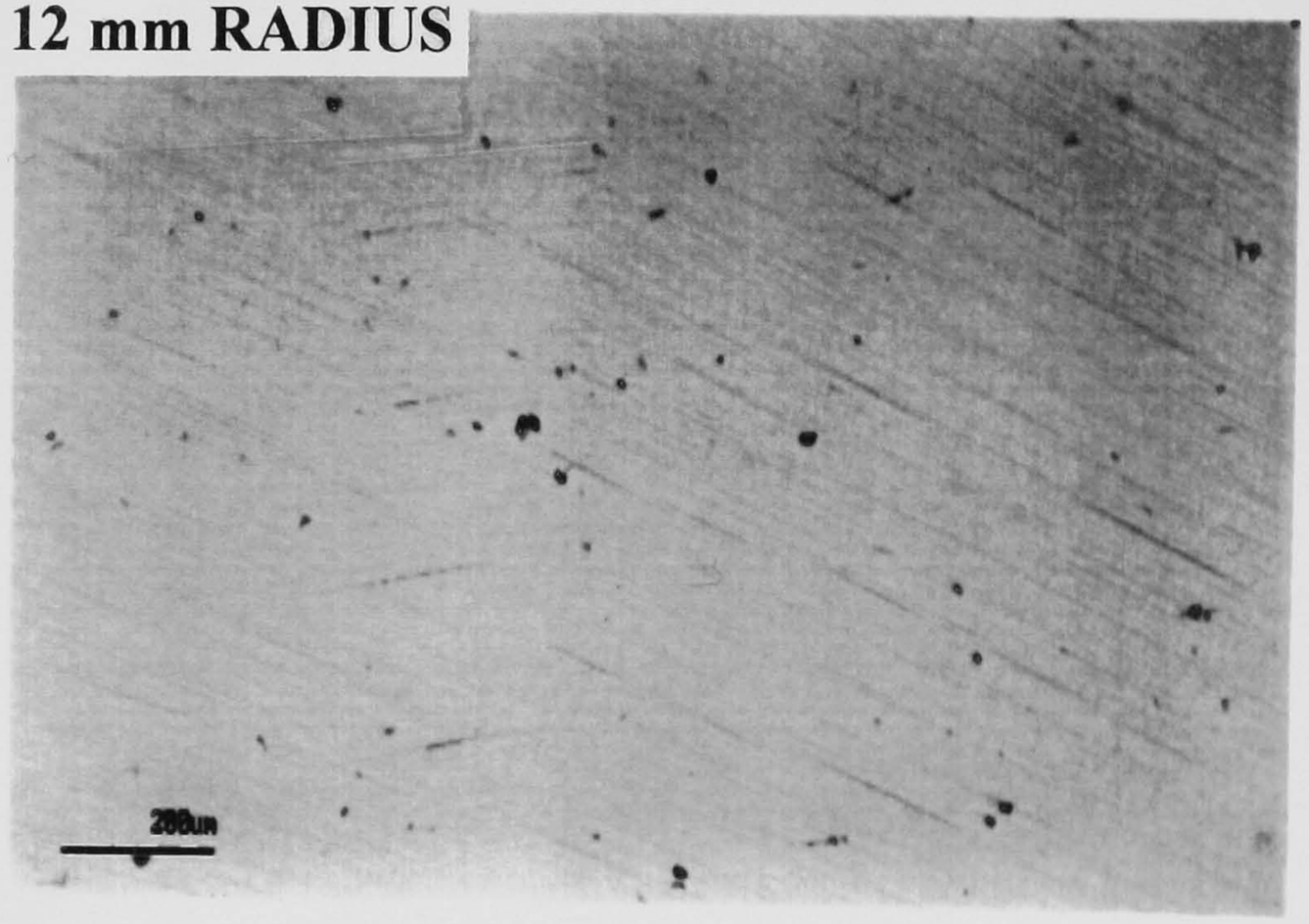

Figure 117 : Photomicrographs of Etched Regions of BK7 Sample 4

19 mm RADIUS

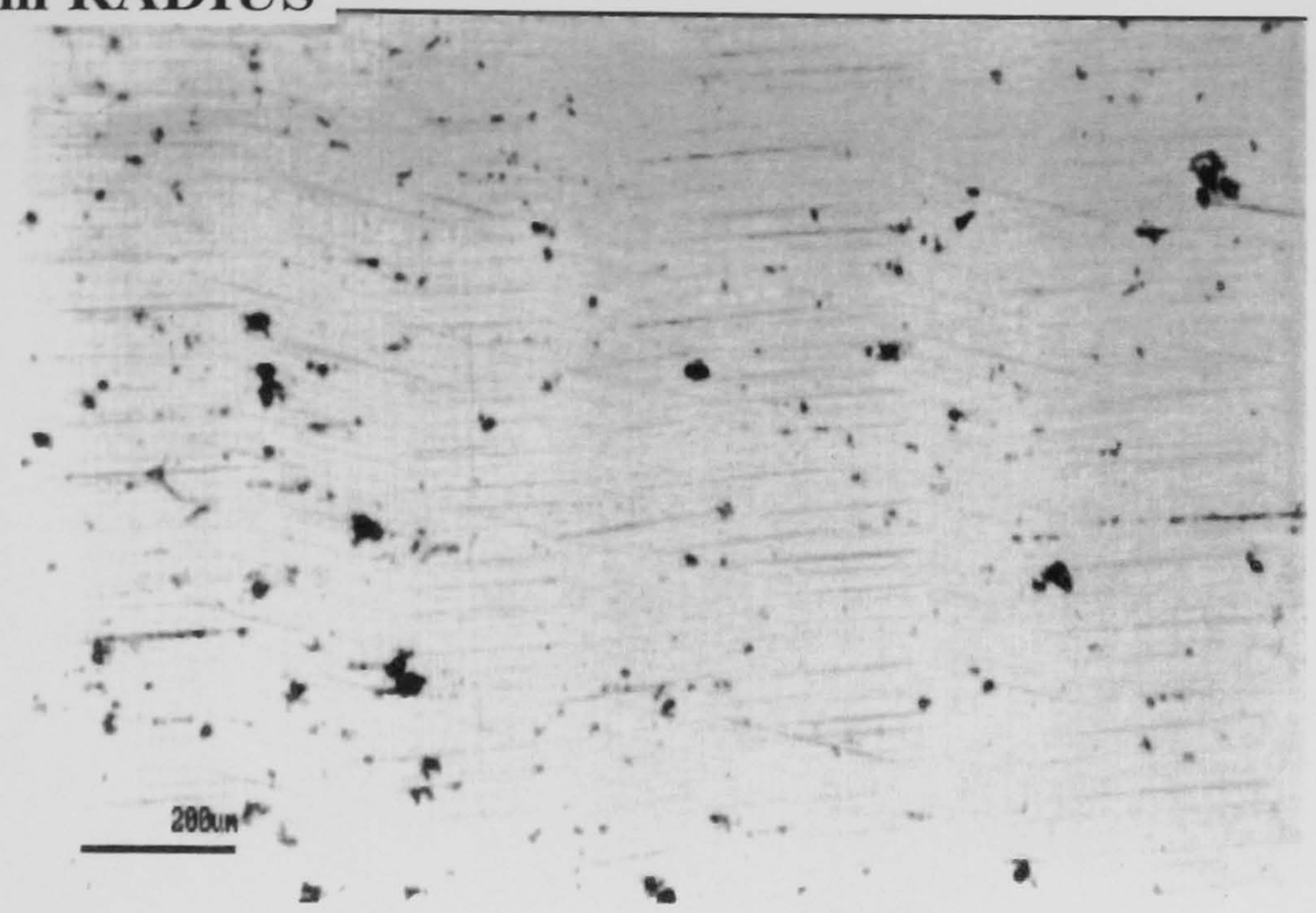

17 mm RADIUS

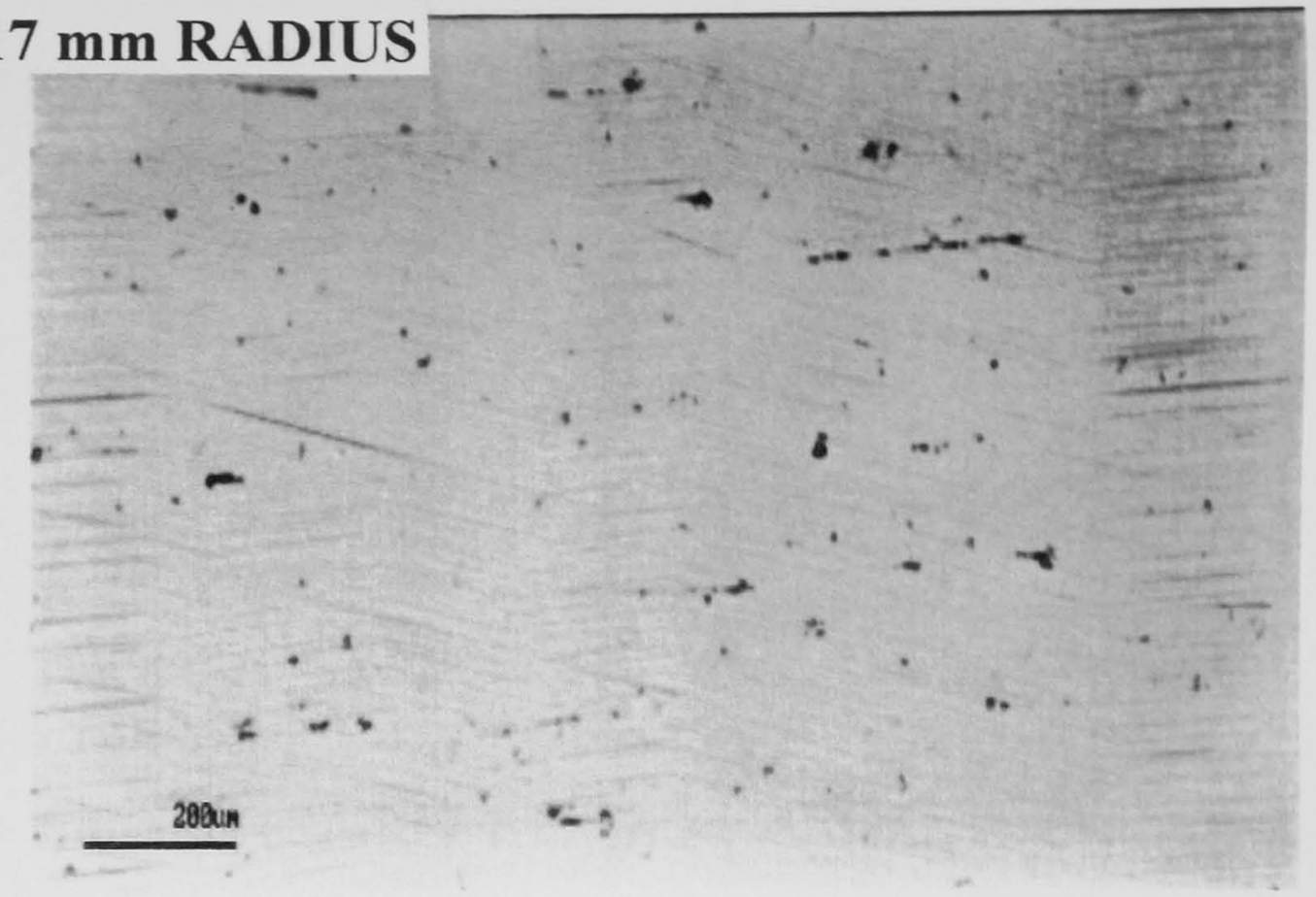

Magn X 86

EDGE

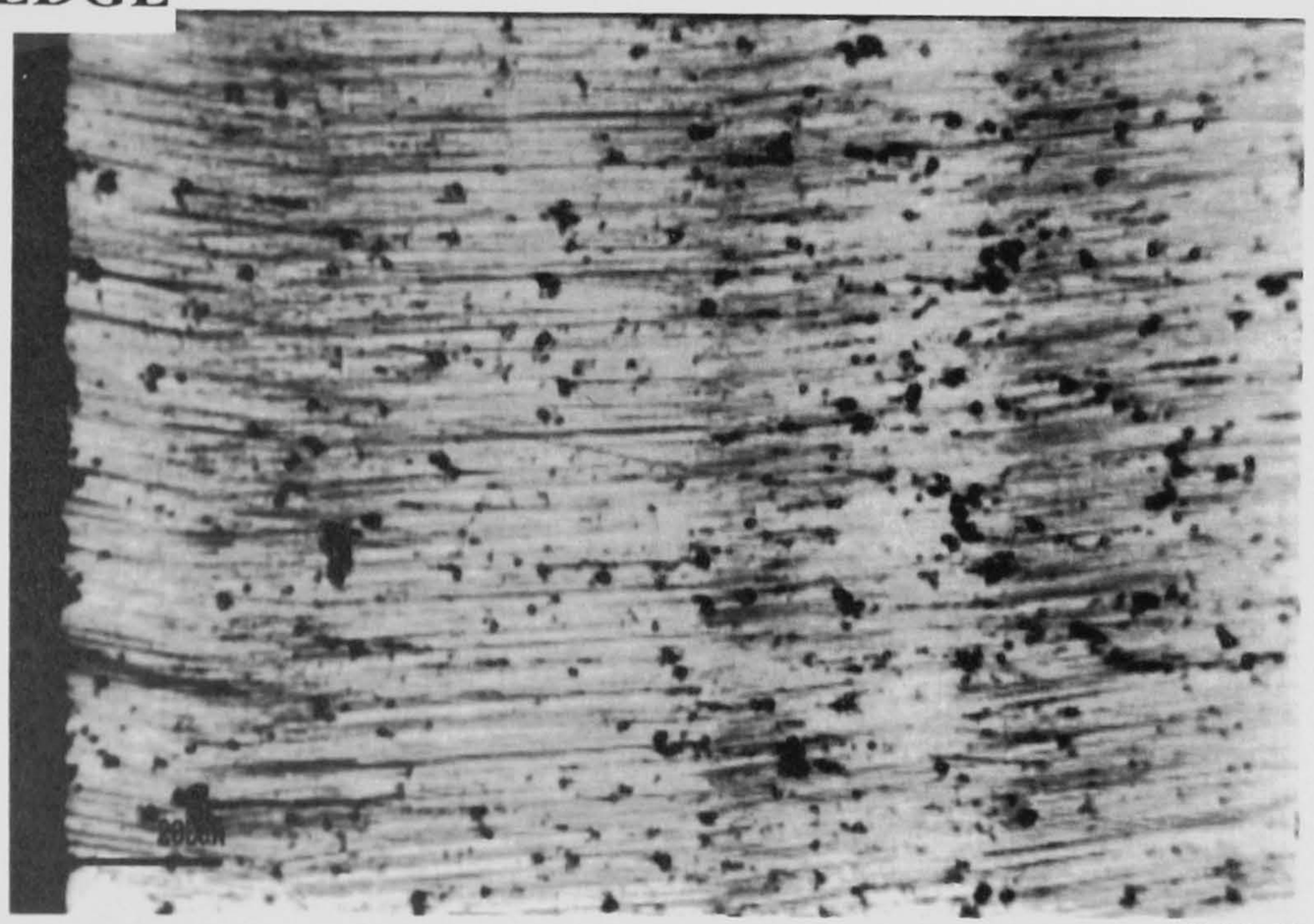

22 mm RADIUS

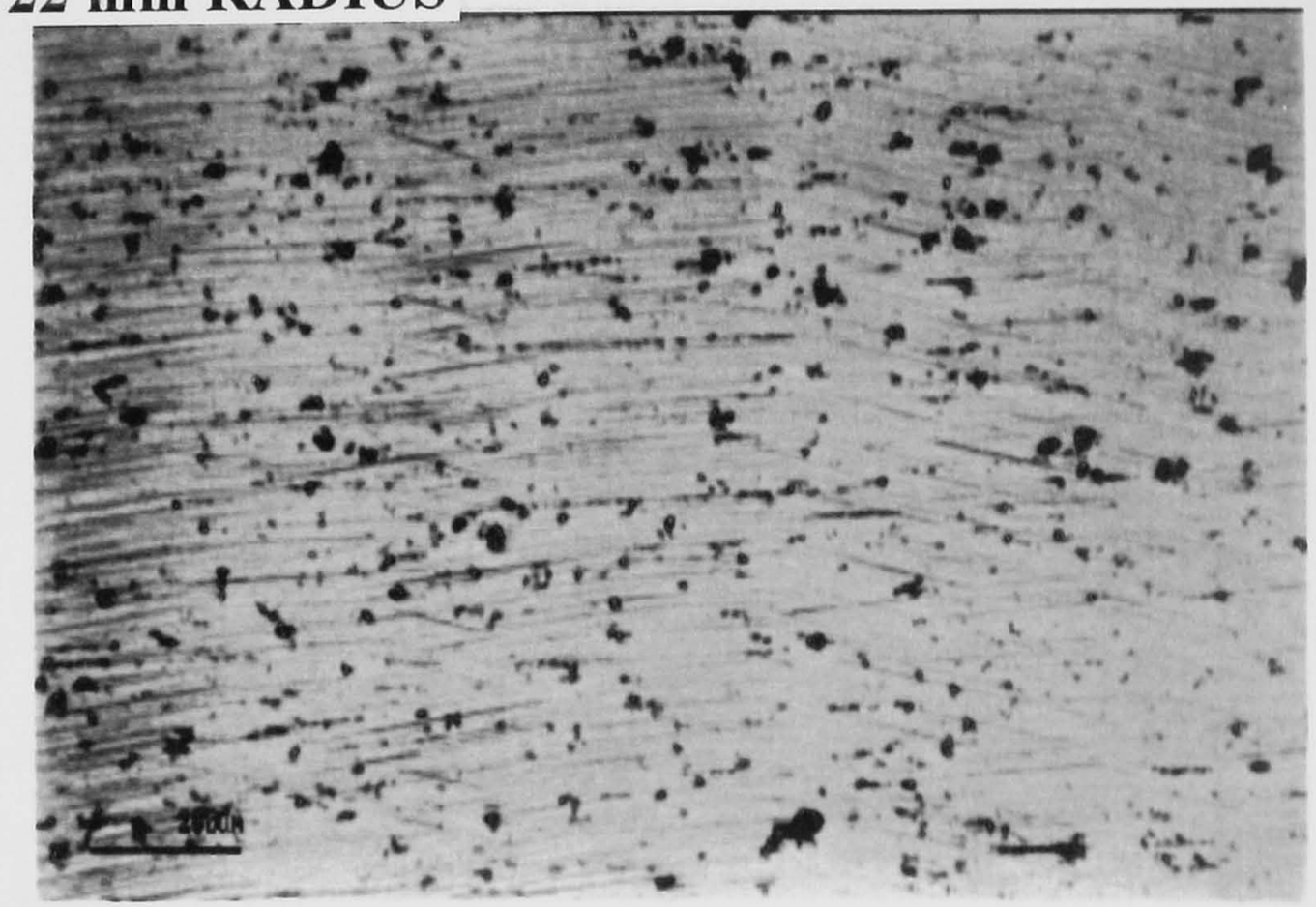

Figure 118 : Photomicrographs of Etched Regions of BK7 Sample 4

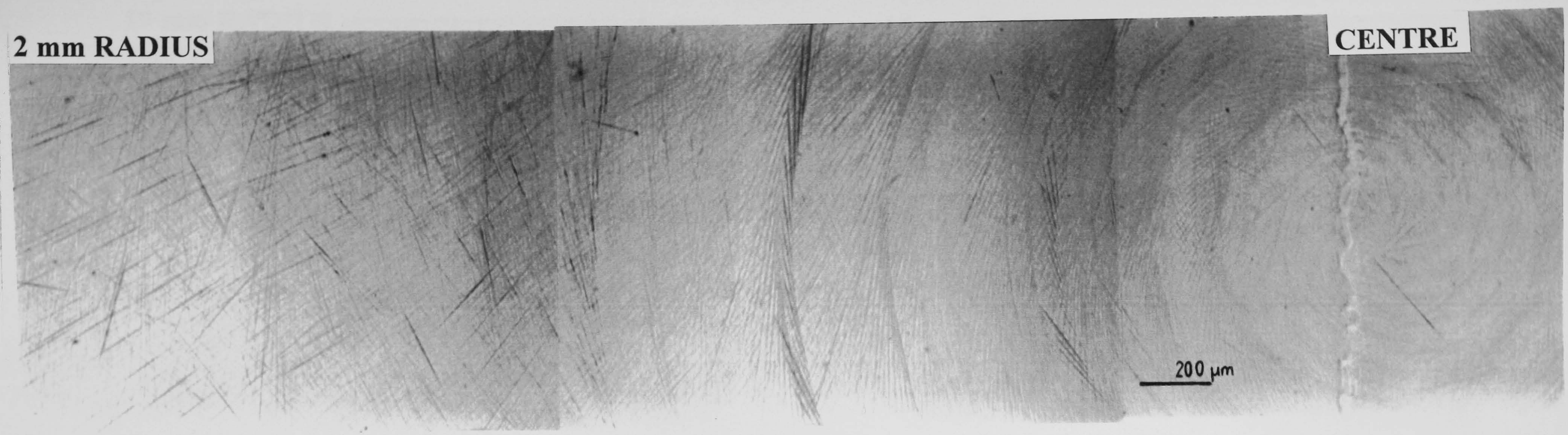

Magn X 86

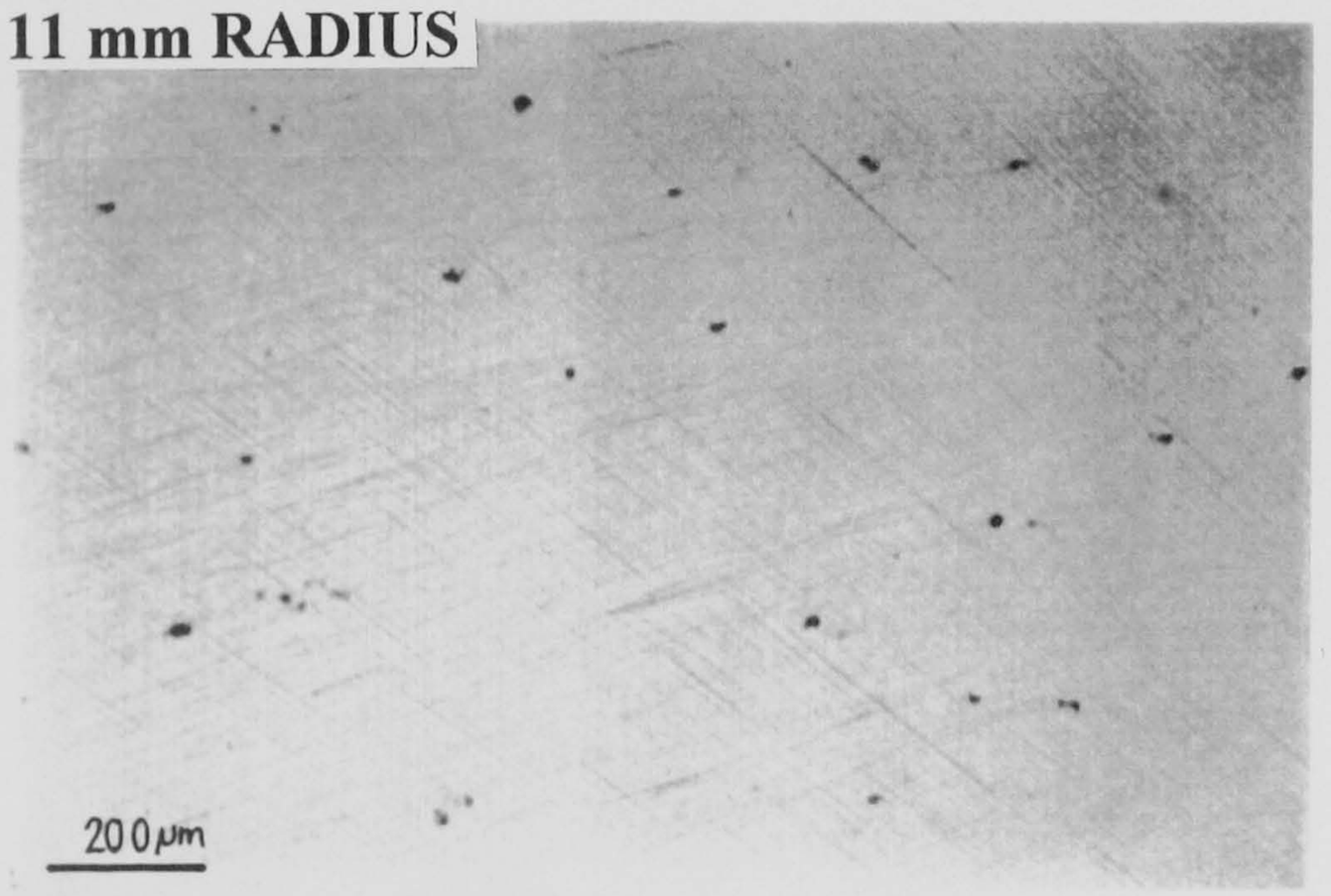

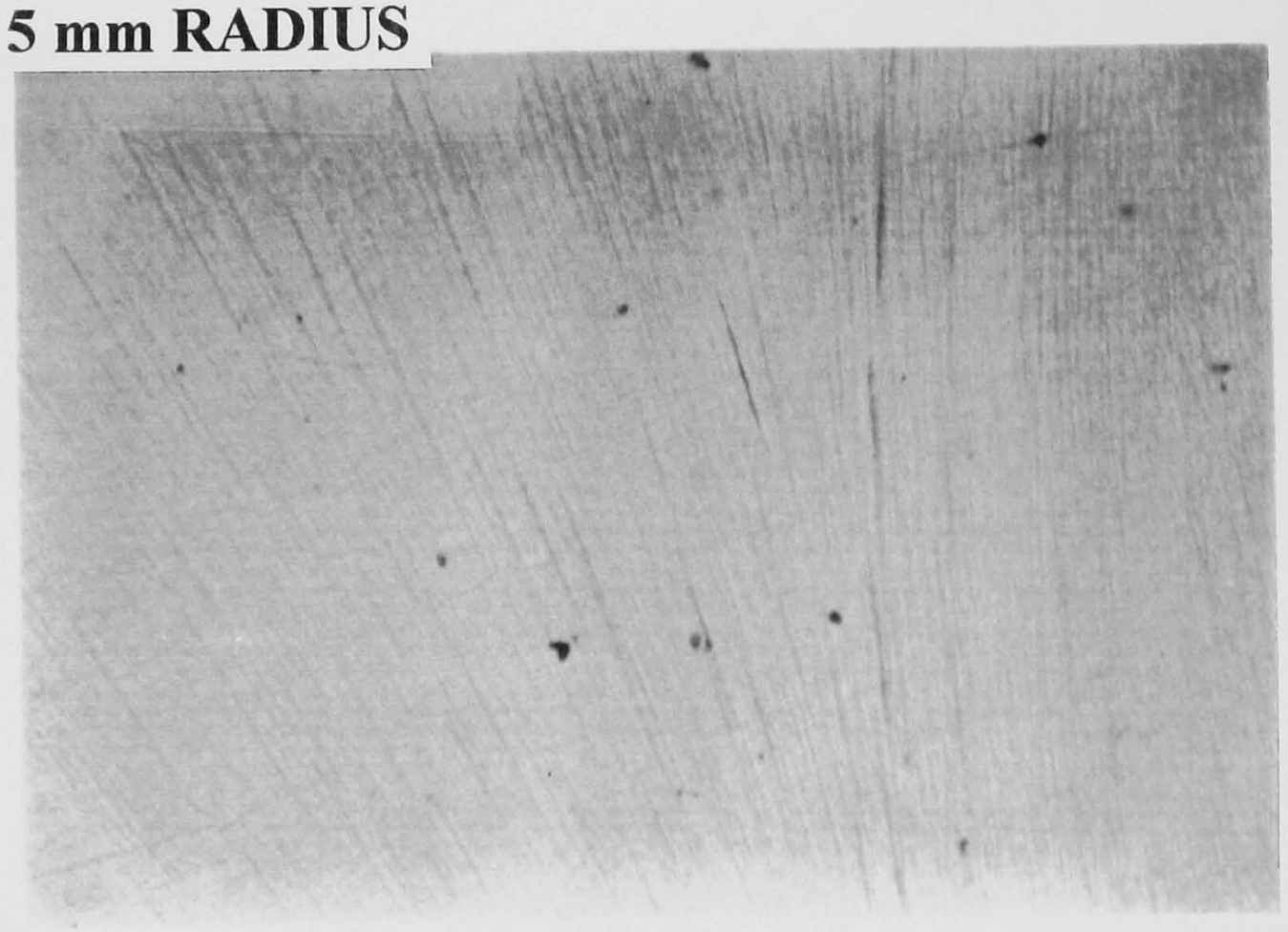

Figure 119 : Photomicrographs of Etched Regions of BK7 Sample 14

19 mm RADIUS

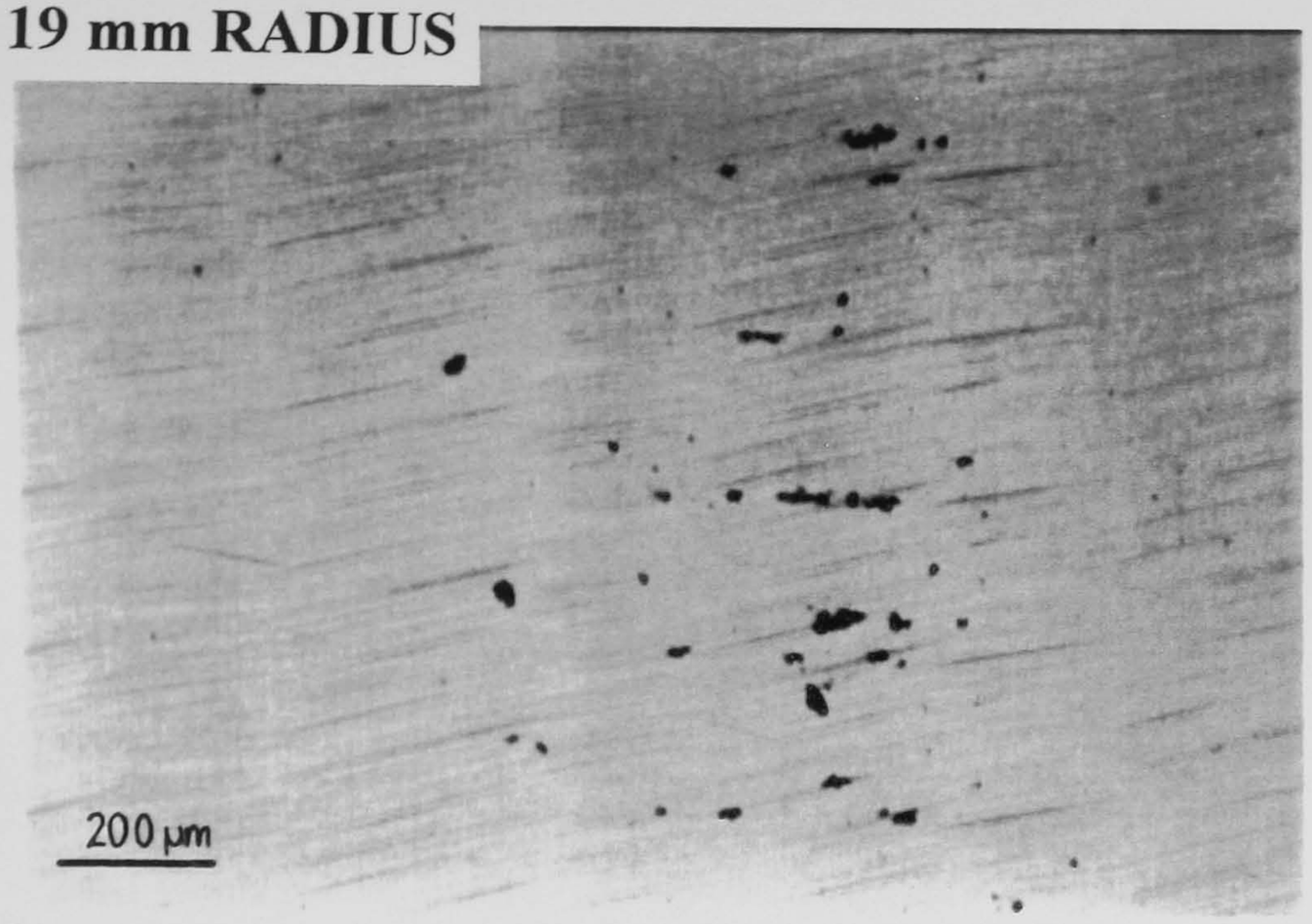

15 mm RADIUS

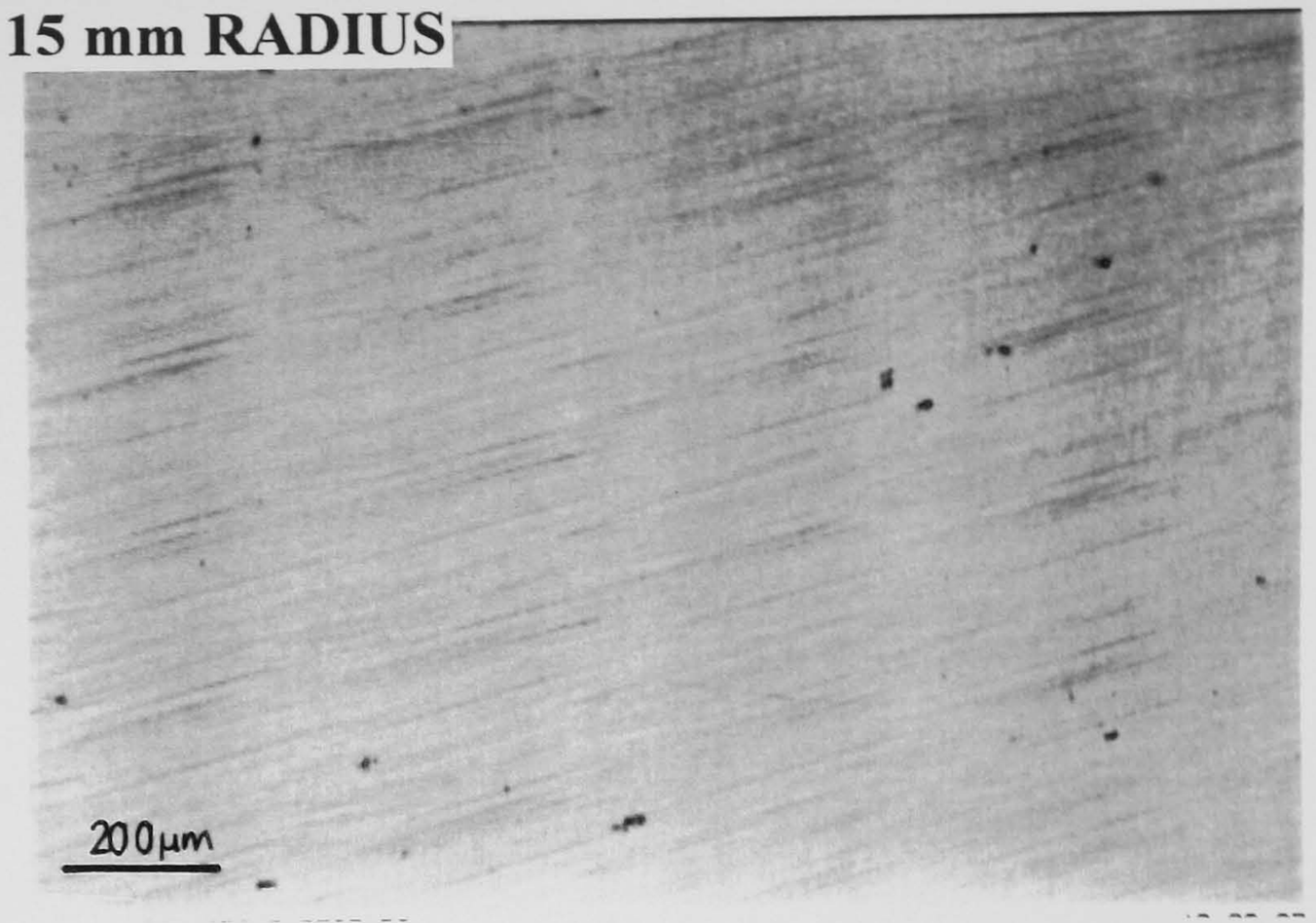

Magn X 86

EDGE

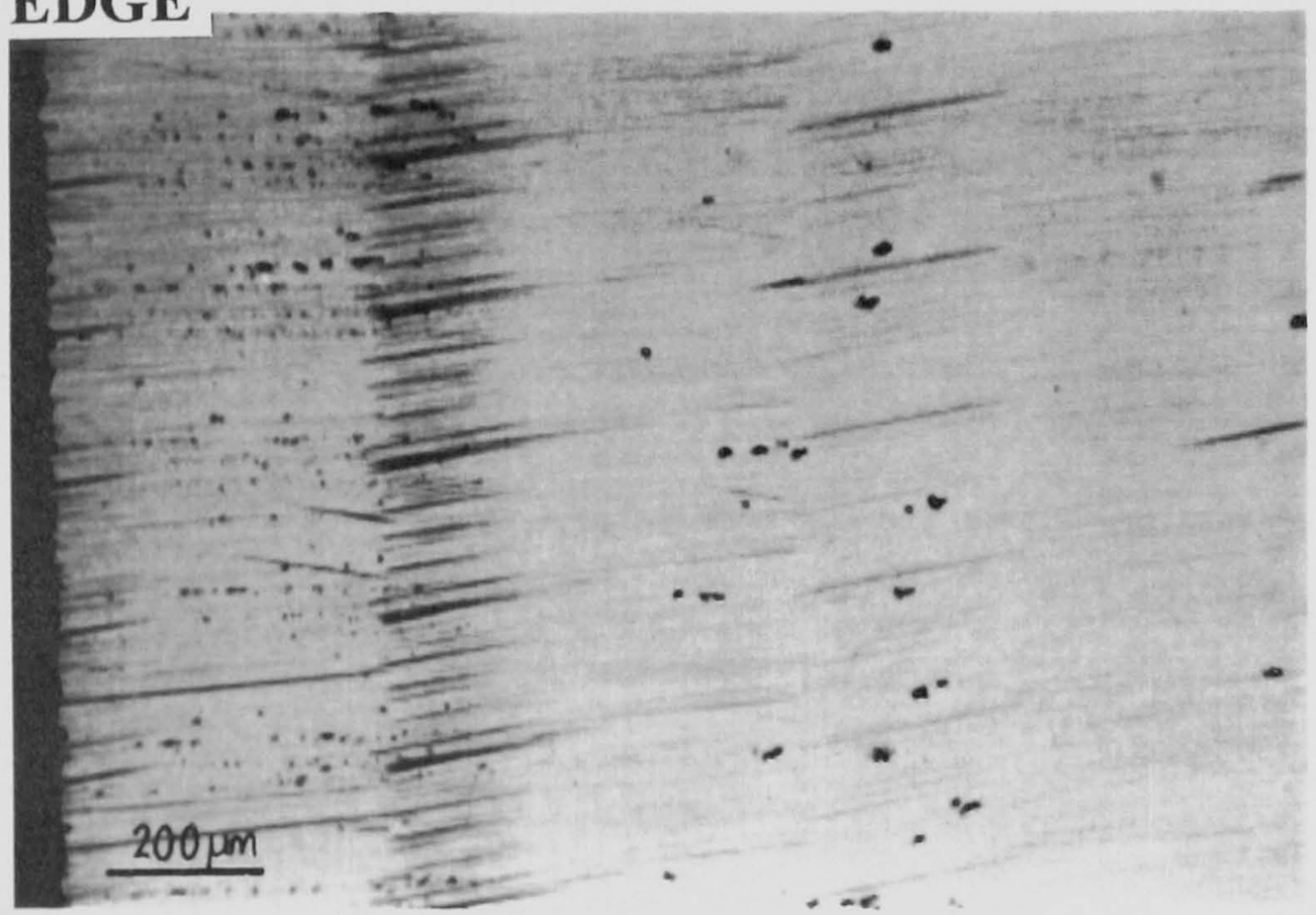

22 mm RADIUS

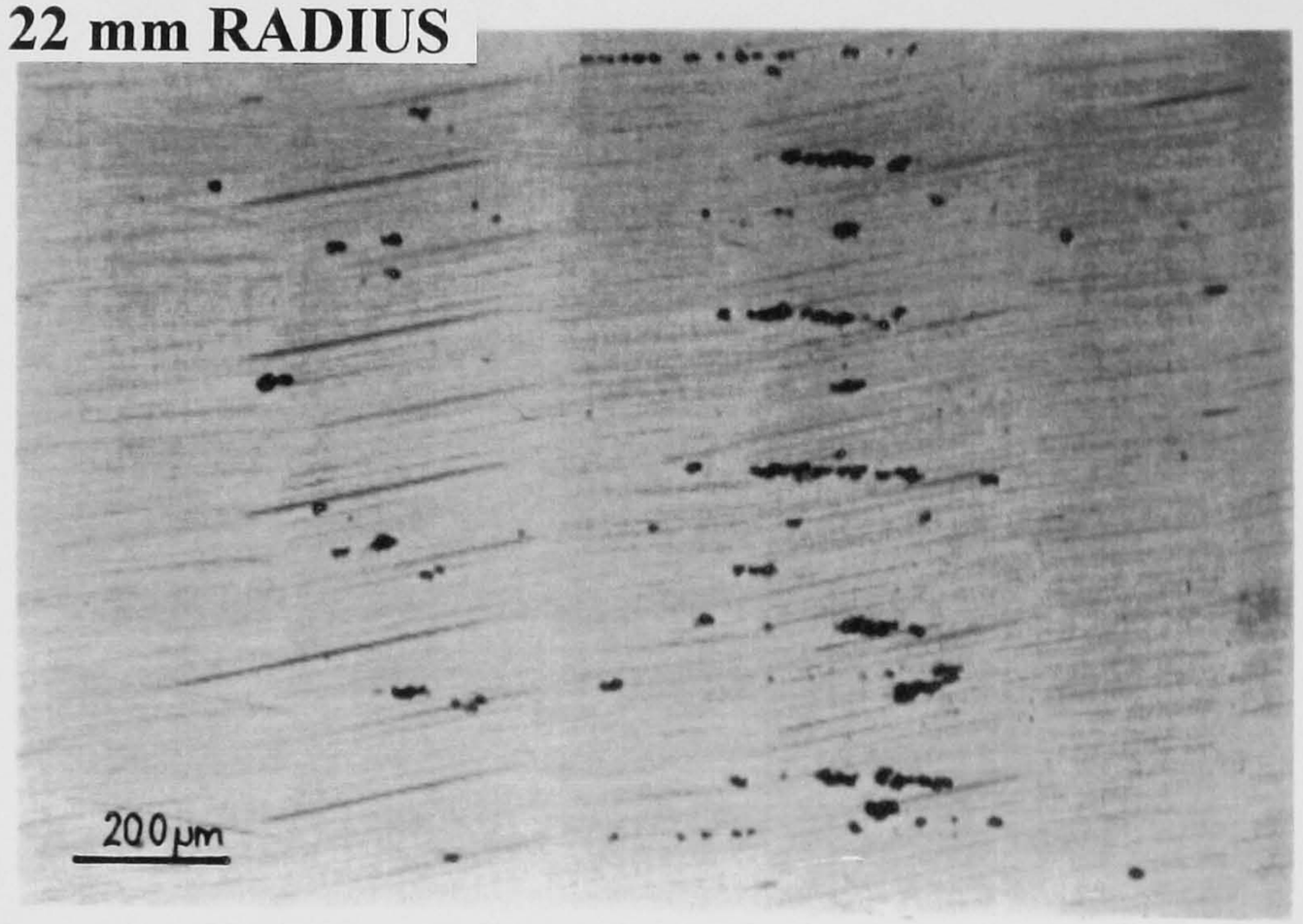

Figure 120 : Photomicrographs of Etched Regions of BK7 Sample 14

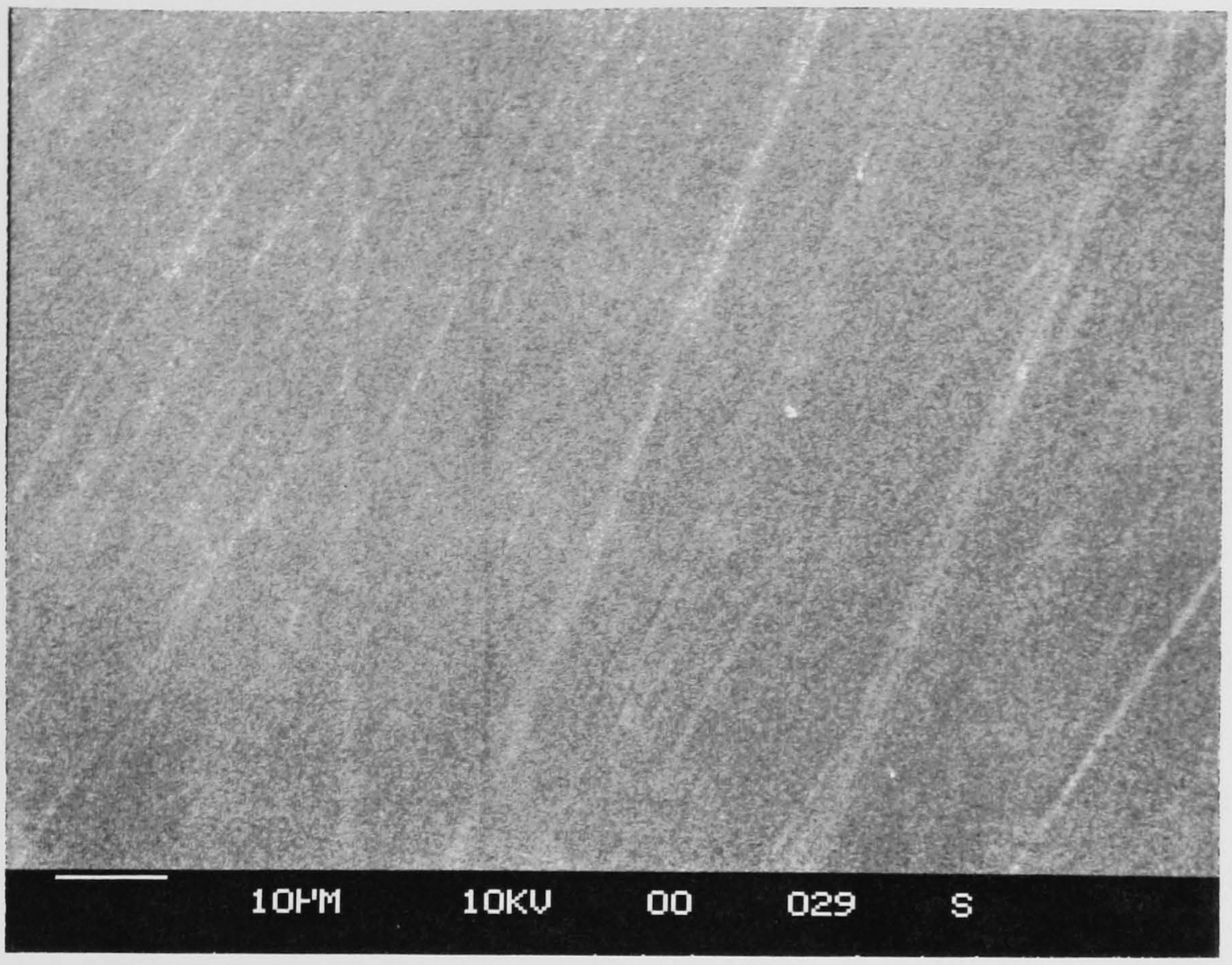

Figure 121 : SEM Micrograph of Ground LaSFN30 Glass

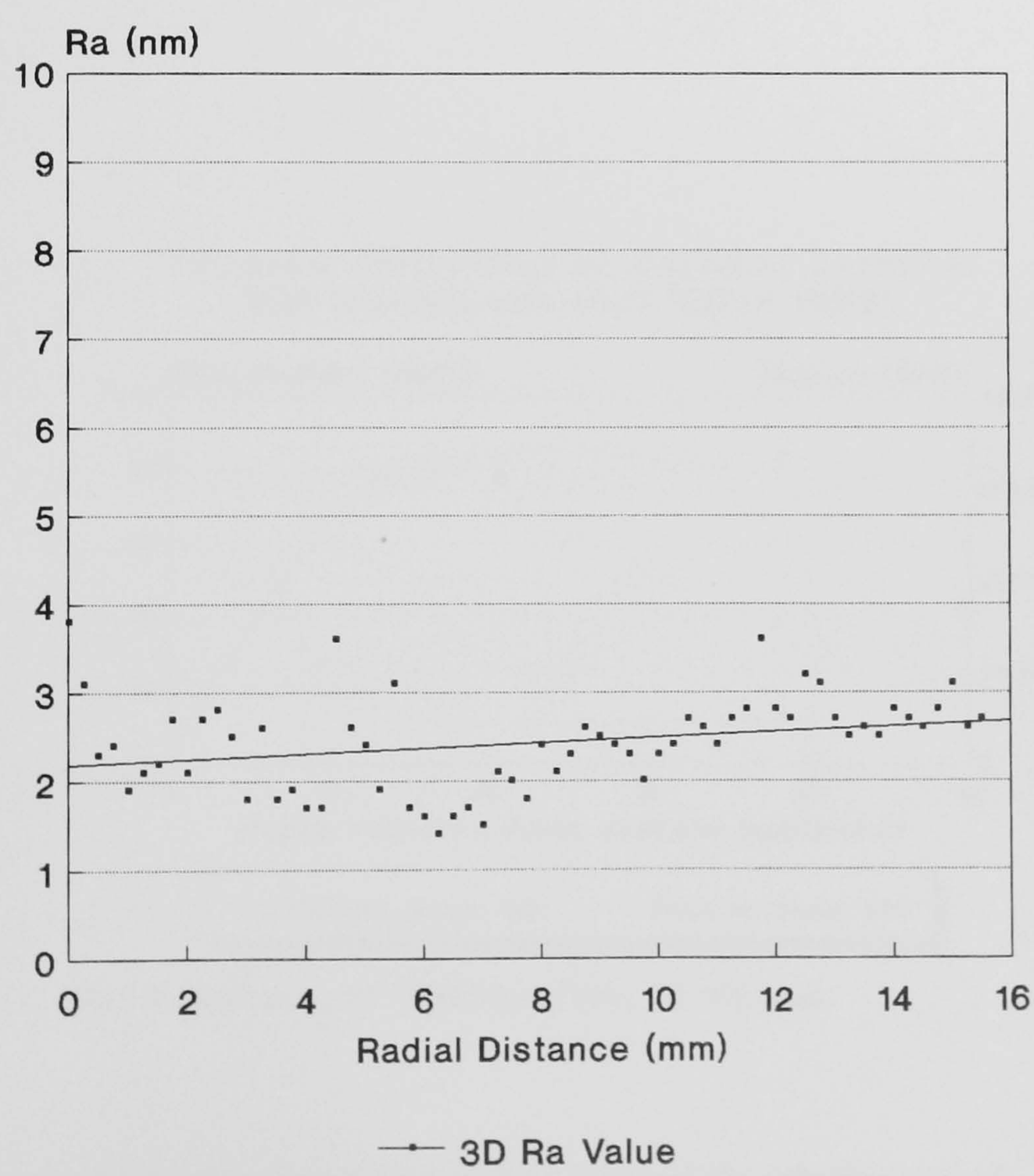

Figure 122 : Surface Roughness Versus Radial Position Ground Zerodur

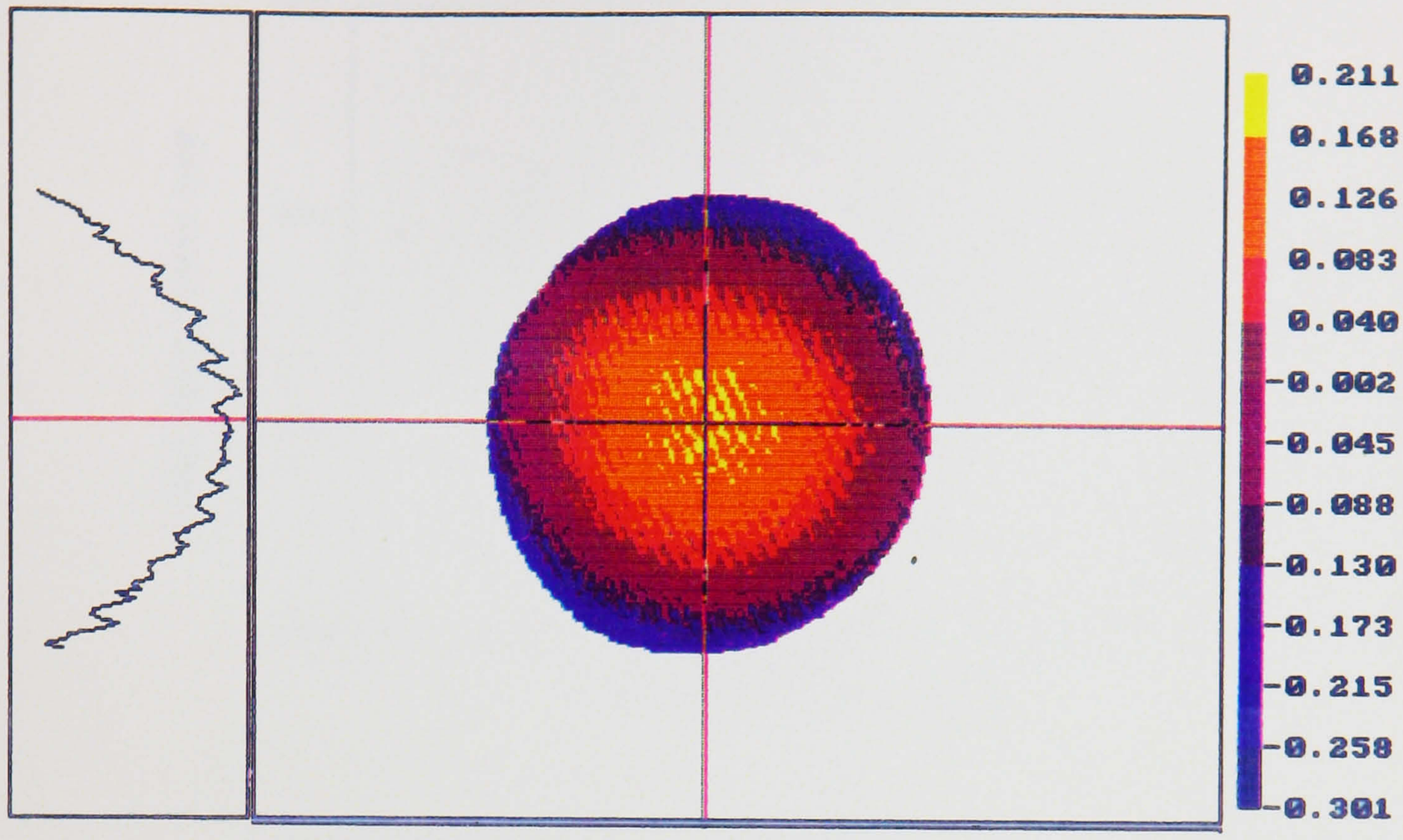

Figure 123 : Twyman Distortion from Residual Stress Induced by "Ductile" Mode grinding

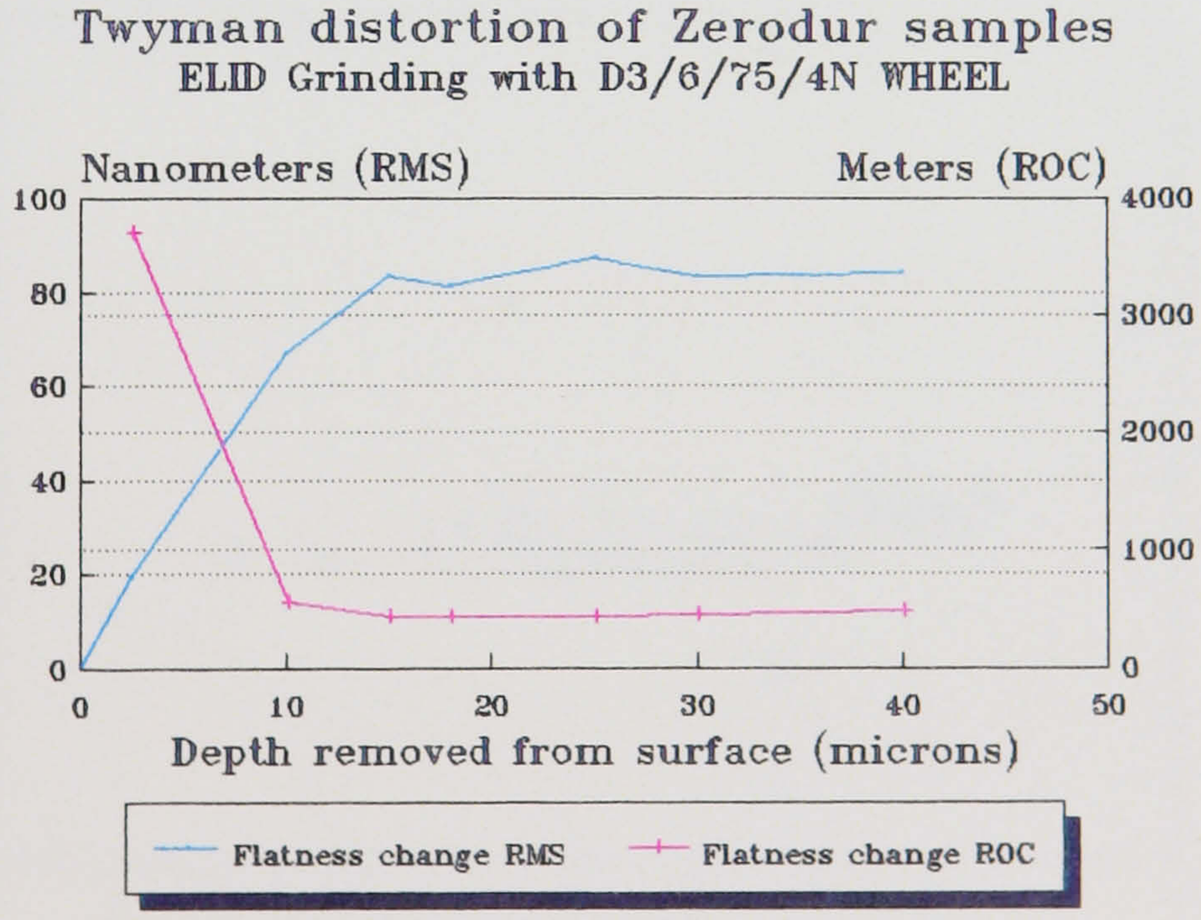

Figure 124 : Twyman Distortion Versus Depth Removed by "Ductile" Mode Grinding

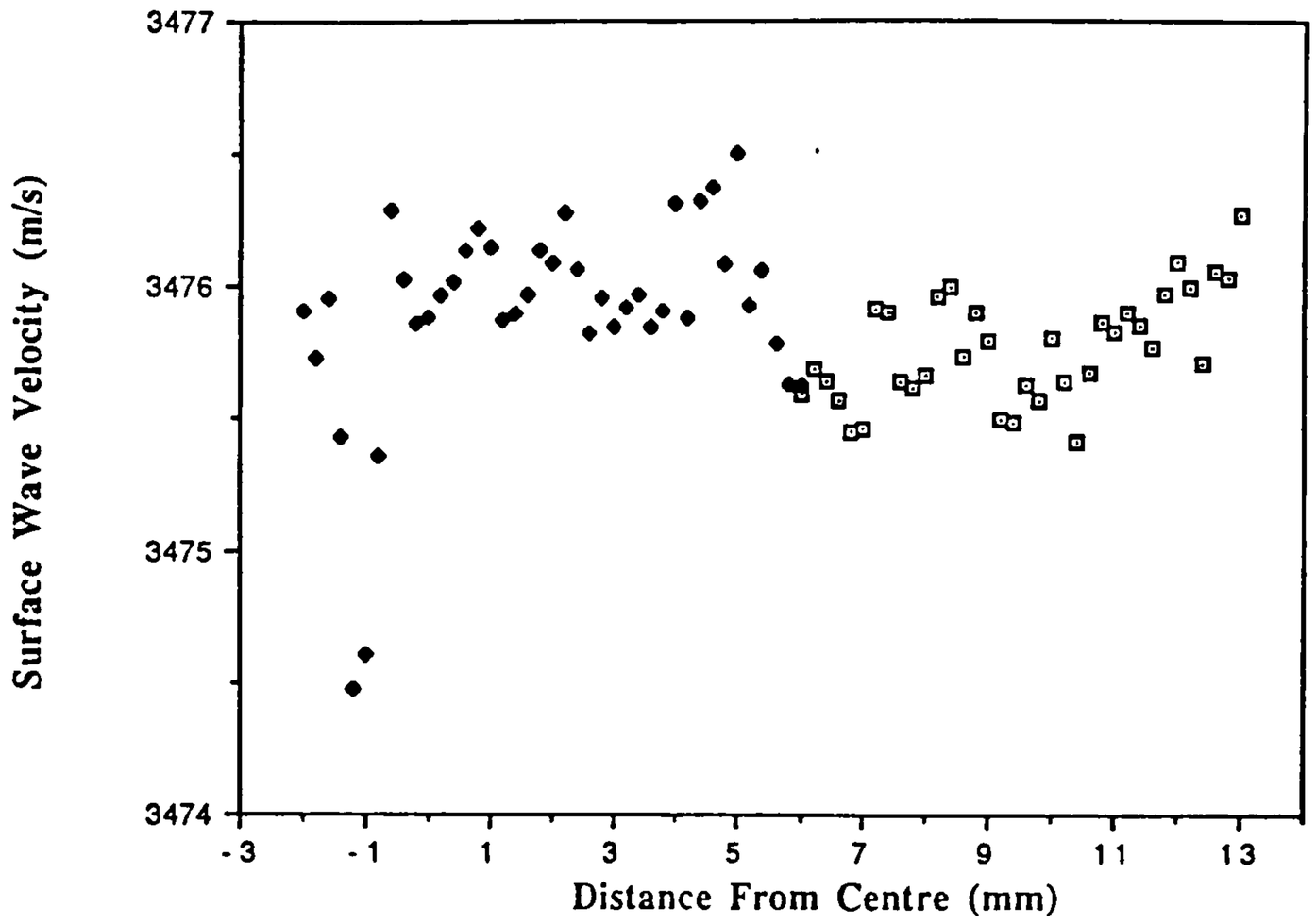

Figure 125 : Surface Wave Velocity (Radial Scan) for Polished Zerodur

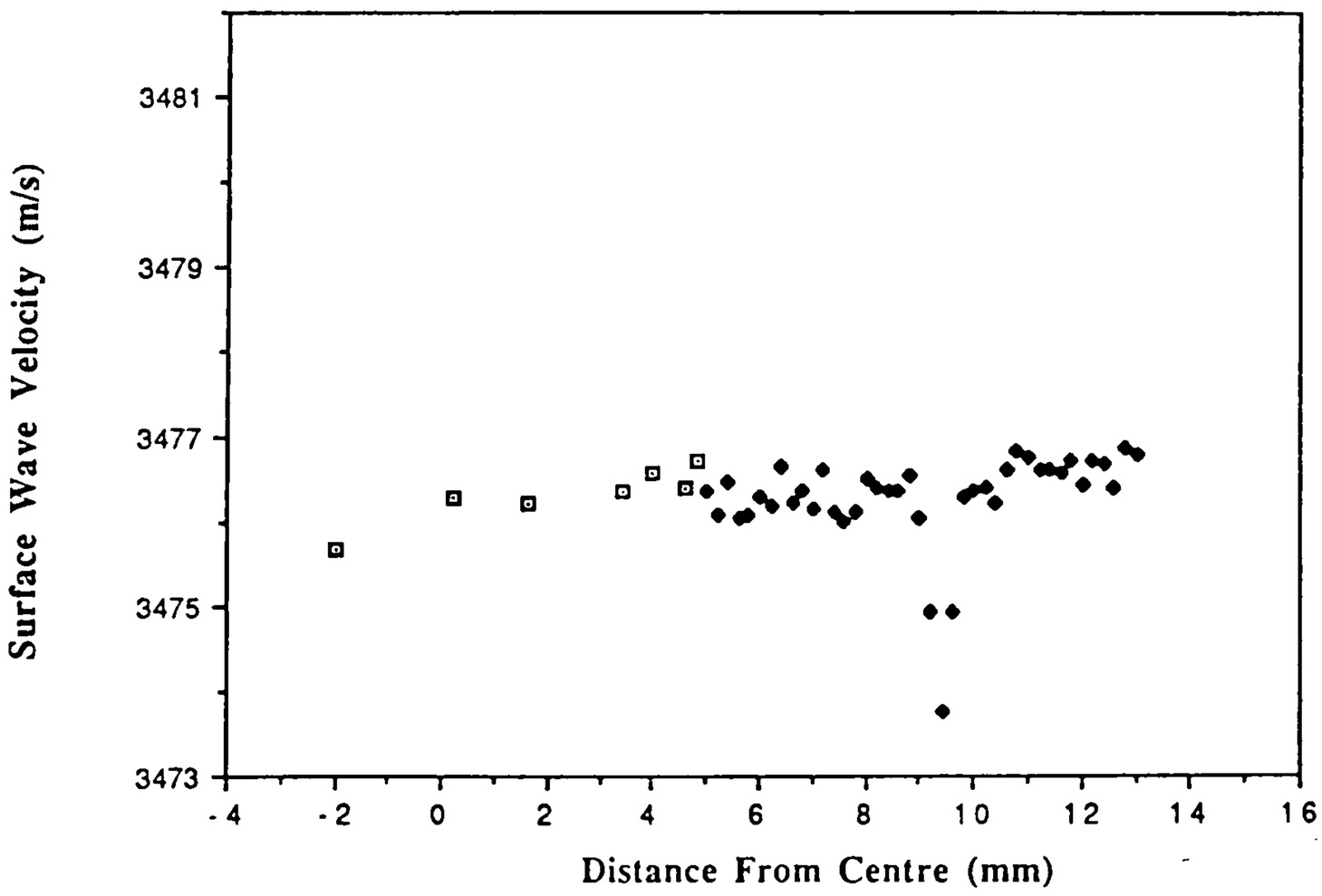

Figure 126 : Surface Wave Velocity (Radial Scan) for "Ductile" Ground Zerodur

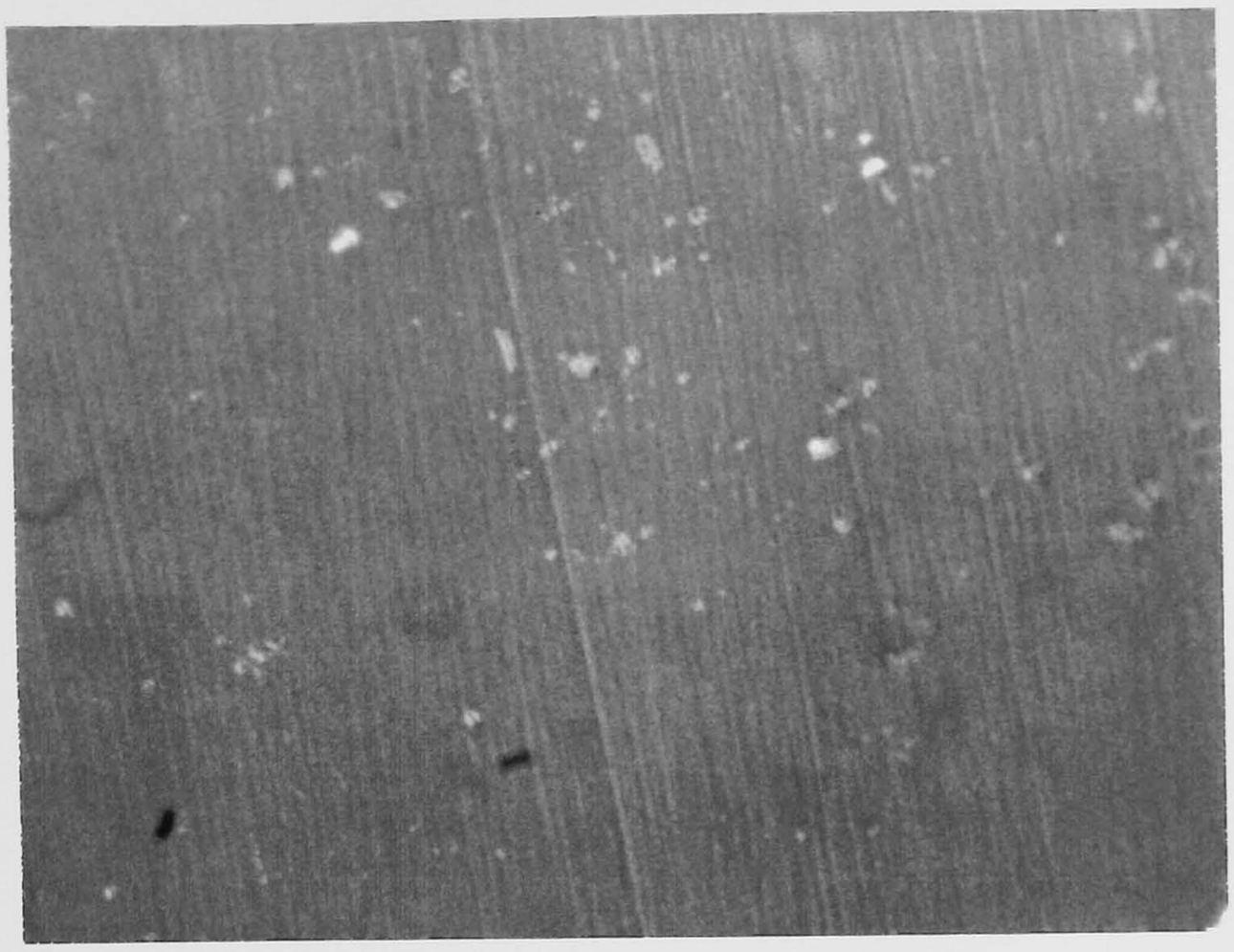

Figure 127 : Photomicrograph of Ground Zerodur after Polishing for 1.5 µm

Figure 128 : Photomicrograph of Ground Zerodur after Polishing for 8 µm

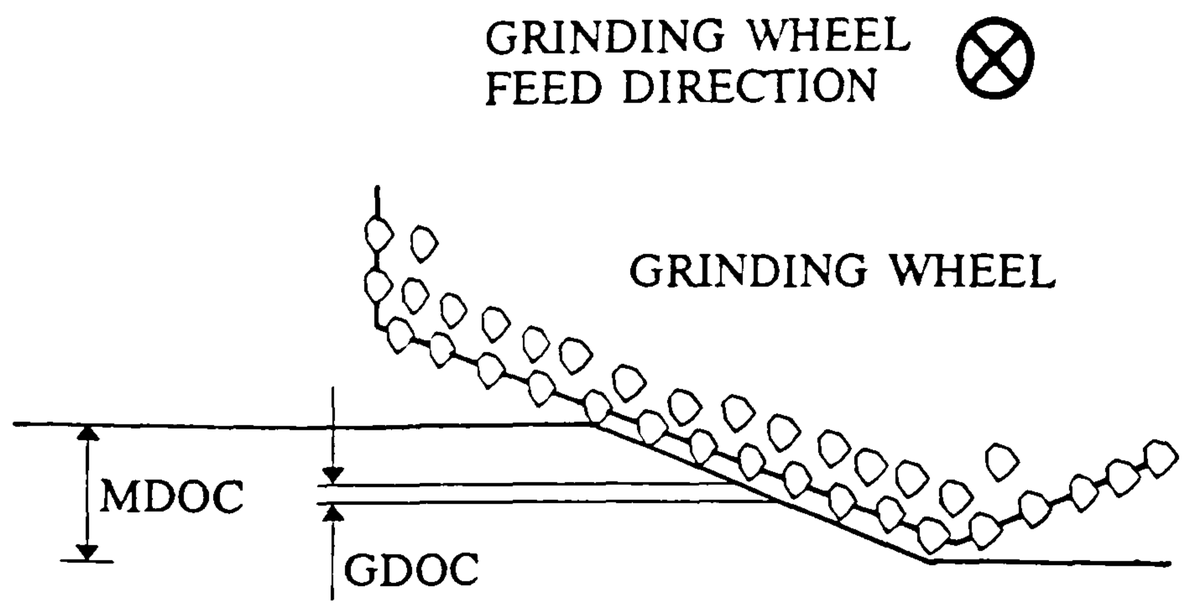

- EXAMPLE

  - Median grit size = 4.5 um
  - Concentration = 75
  - Chamfer angle = 14 minutes

- GDOC = 25 nm

Figure 129 : Schematic of GDOC Parameter

Appendix 1

ELECTROLYTICALLY ASSISTED "DUCTILE" MODE DIAMOND GRINDING OF BK7 and SF10 OPTICAL GLASSES

M J Ball, N A Murphy and P Shore*

Pilkington plc, Group Research Laboratories
***Cranfield Unit for Precision Engineering (CUPE)**

1.0 ABSTRACT

Samples of BK7 and SF10 optical glass were "ductile" ground using a cast-iron diamond ring tool with an electrolytic in-process dressing system. Selected machining parameters gave nanometric quality surfaces (Ra< 2nm) with minimal sub-surface damage. Relatively rough brittle fractured surfaces were obtained by machining the glasses with the same diamond wheel but without the assistance of electrolytic dressing. The grinding force (normal) generated whilst ductile machining was significantly greater than for brittle fracture grinding.

The work described in this paper reveals a significant advance in the machining of optical glass. This novel and complex process requires further investigation to provide a full understanding of the science involved.

2.0 INTRODUCTION

The manufacture of precision optical glass elements generally involves grinding and polishing using relatively simple machines. Grinding is achieved with either diamond impregnated tools or with loose abrasives (diamond, carborundum, alumina) carried in water or a water soluble coolant/lubricant. Glass is normally polished on specifically formulated polyurethane pads or pine wood pitch with a cerium oxide/water slurry.

A minimum of two grinding stages i.e., generation and smoothing followed by at least one polishing operation are required in making a single blemish free, spherical surface of precise radius of curvature from a glass blank. A lens is then only produced by generating the desired radius of curvature on the reverse side whilst reducing the centre thickness of the element to that specified by the optical designer. The generated surface is then smoothed and polished in a similar manner to the first surface.

Precision optical elements are usually combined with others to form a system or instrument. The edge of each lens must therefore be ground concentric with its own optical centre. Edging the lenses ensures that all the elements within the system can be assembled on a common optical axis.

Slight modifications to the basic grinding and polishing principles allow a skilled craftsman to make shallow aspherical surfaces, in addition to spherical surfaces and optical flats; all with minimal sub-surface damage. Shallow aspherical surfaces can only be achieved by multi-stage smoothing and multi-stage polishing. Automated generators and polishing machines are beginning to take their place in modern optical manufacturing establishments, but the move away from traditional production methods is slow.

Two developments in optics which are being actively pursued are; 1, the desire to use steep aspherical glass lenses in systems and 2, the need for optical surfaces which are free of sub-surface damage. It is claimed that one aspherical surface can replace two spherical surfaces in an optical system thus reducing the weight and length of instruments. Damage-free surfaces and sub-surfaces are required primarily for high power laser systems to avoid destruction of the optics by energy concentration at defects. Both developments are prime objectives for the NION project (ref 1).

The work reported in this paper was undertaken to explore the viability of "ductile" grinding of optical glasses, and to establish the manner by which this process can be utilised on the NION ultra precision CNC Aspheric Generator which is currently under construction at CUPE. This is based on the Cranfield Precision Engineering Nanocentre CNC Aspheric Generator, a three axis state of the art machine for single point diamond turning or, by virtue of its high 'loop-stiffness', ductile grinding of complex shape components in brittle materials.

2.1 Diamond Turning Glass in a "Ductile Mode"

Research has shown that polished optical glass surfaces exhibit "ductile" movement when impacted with a Vickers hardness test diamond (ref 2). More recent work has shown that these macroscopically brittle materials can be machined in a non-brittle fracture mode by fine single point diamond turning (ref 3, 4).

The advantage offered by diamond turning, which is a hard loop process, is associated with the capability of precisely controlling the tool's position relative to the workpiece. Such processes generally require more sophisticated machine tools which offer, through the use of advanced CNC systems, the ability to produce complex components which are precise and accurate.

 0-8194-0703-8/92/$4.00

Soft loop machining processes such as lapping and polishing, are those where the relative position of the tool to the workpiece is force controlled. In this case precise control of the tool's path across the workpiece is difficult for shapes other than simple geometric forms.

Diamond turning in the absence of a coolant is essentially a mechanical removal process. The volume of material which can be removed in a single pass by this process in the so-called ductile manner, has been found to be dependant on the type of glass being machined. Transition from the ductile mode to brittle fracture mode has been observed when single point diamond turning. The occurrence of this transition is frequently described in terms of a "critical depth of cut" which has been calculated from theory and verified experimentally. To utilise this mechanical process reliably the machine tool must have a positioning capability smaller than "the critical depth of cut".

The "critical depth of cut" is small, i.e. 0.1 - 0.3 μm, as is the associated feedrate, which results in a slow ductile mode removal rate. The commercial viability for single point diamond turning of hard glass optics without the addition of a coolant or some form of chemical assistance is in considerable doubt.

2.2 Grinding of Glasses in a "Ductile Mode"

The use of a grinding process in a "ductile" mode offers a number of advantages over single point turning. A somewhat simplistic view of grinding is that it is analogous to a multi-point turning process. The higher number of cutting points (grits) yield a higher machining rate, thus improving the commercial viability for ductile mode machining.

Whilst grinding is a multi-point mechanical process it is known to be controlled also by non-mechanical mechanisms. This is particularly true when grinding glass in a "ductile mode". Previous work (ref 5) suggested that diamond grinding is controlled by purely mechanical actions when using large grit wheels with a relatively high stock removal rate. Recent work by Golini (ref 6) emphasized the importance of chemical mechanisms in small grit (0.75-3μm) loose abrasive machining. Brown (ref 7) has also shown that chemical effects play a significant role in stock removal rates using micron size abrasives.

Izumitani (ref 8) concludes that the polishing of optical glasses with cerium oxide/water slurries is predominantly via chemical reaction of the water with the glass surface forming a relatively soft hydrated layer. As it is formed, this layer is planed away by the cerium oxide grains (0.5-2μm diameter) trapped in the rotating polishing pad. The stock removal rate is determined by a combination of the chemical durability of the glass (rate of formation of the hydrated layer) and the hardness of the hydrated layer. Ductile mode grinding, and traditional polishing of optical glass involve both chemical reaction and "inert abrasive particles" of approximately the same size but with different relative hardness. However, it would be unwise to postulate that ductile mode grinding is a simple extension of traditional glass polishing or vice versa.

2.3 Low Damage "Ductile Mode" Grinding

Investigation into "low damage" mode diamond grinding of brittle ceramic materials (ref 9) has shown that the use of fine grit wheels together with a stiff and precise machine, prevents or minimises micro-cracking and produces nanometric quality surfaces. The strength of components ground in this way is also significantly enhanced. The necessary use of small grit grinding wheels poses difficulties in creating and then maintaining a sufficiently "open" wheel. Typically, grinding debris adhering to the wheel surface reduces the level of grit protrusion, and hence, degrades the cutting efficiency of the wheel.

2.4 Grinding Wheel Dressing

Conventional dressing methods for diamond wheels generally use an abrasive stick which is pushed into the grinding wheel to preferentially abrade the wheel bond. This abrasive process provides the necessary grit protrusion and removes grinding debris from the wheel surface. When applied to fine grit wheels this method fails to provide the necessary control over the wheel's topography. Consequently the surface finish produced on the workpiece is poor and the magnitude of the grinding force is uncontrolled, thus hindering the attainment of high precision form accuracy.

An electrolytic dressing technique (ref 10) has been developed for mirror finish surface grinding. This technique is used with grinding wheels having an electrically conductive bond. Electrolysis chemically modifies the grinding wheel surface; the modified layer of the grinding wheel being dependent mainly on the wheel bond material. Currently the most suitable bond material is cast-iron, since the chemically modified layer has a low adhesion to the wheel and is easily removed during initial contact with the workpiece.

The necessary equipment for this electrolytic technique as applied to a cup shape grinding wheel is shown schematically in Figure 1. An electrical potential is placed across the stationary electrode and the grinding wheel, and coolant is fed between the electrode and the wheel. Figure 2 shows the manner in which the modified layer is produced. After the truing operation is complete, electrolysis of the coolant is commenced. Initially the wheel surface (clean cast-iron) provides good conductivity and consequently a high current passes between the wheel and static electrode. After a short period of time has elapsed an insulating oxide layer forms on the interactive surface of the cast-iron and results in a drop in the drawn current. Grinding is started when the drawn current reaches a specified level, whereupon a slight increase in the drawn current is noticed as the loosely adhered modified layer is broken away during the initial contact with the workpiece. A consistent level of grain protrusion is obtained by this electrolytic cycle and it is considered that this process stabilises the grinding forces.

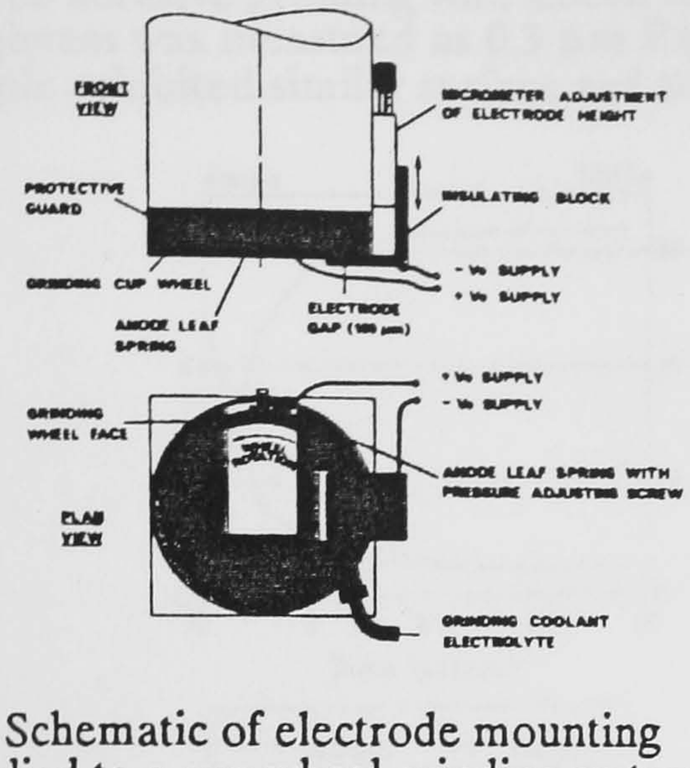

Fig. 1 Schematic of electrode mounting as applied to a cup wheel grinding system

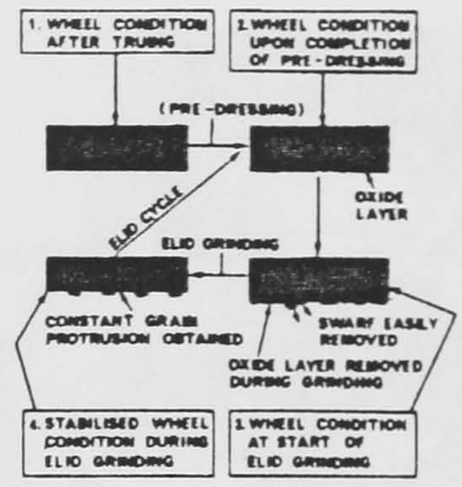

(After Ohmori & Nakagawa)

Fig. 2 Stages of in-process electrolytic dressing.

3.0 EXPERIMENT

3.1 Introduction

Fixed abrasive grinding tests were performed on BK7 (low density borosilicate glass) and SF10 (high density lead silicate glass). Tests carried out on the BK7 samples were made using a two-level, three factor experimental design, whereas less formal exploratory tests were made on the SF10 glass samples. The physical properties of BK7 and SF10 are given in Table 1. Cast-iron bonded diamond wheels of 3-6 and 1-2 μm grit size were used with conventional abrasive and electrolytic dressing methods.

Glass type	Knoop Hardness Hk	Density ρ(g/cm^3)	R.Index n_d	Abbe No V_d
SF10	370	4.28	1.72825	28.41
BK7	520	2.51	1.51680	64.17

Data taken from the Schott glass catalogue

Table 1. PHYSICAL PROPERTIES OF SF10 & BK7 GLASSES

3.2 Electrolytic Dressing System

Assessment of the electrolytic system shown in Figures 3 and 4 was carried out by monitoring the current and voltage drawn between the electrode and the grinding wheel during initial electrolysis. Figure 5 shows the measured electrical characteristics of the system, which correlate well with those for the system described in reference 9.

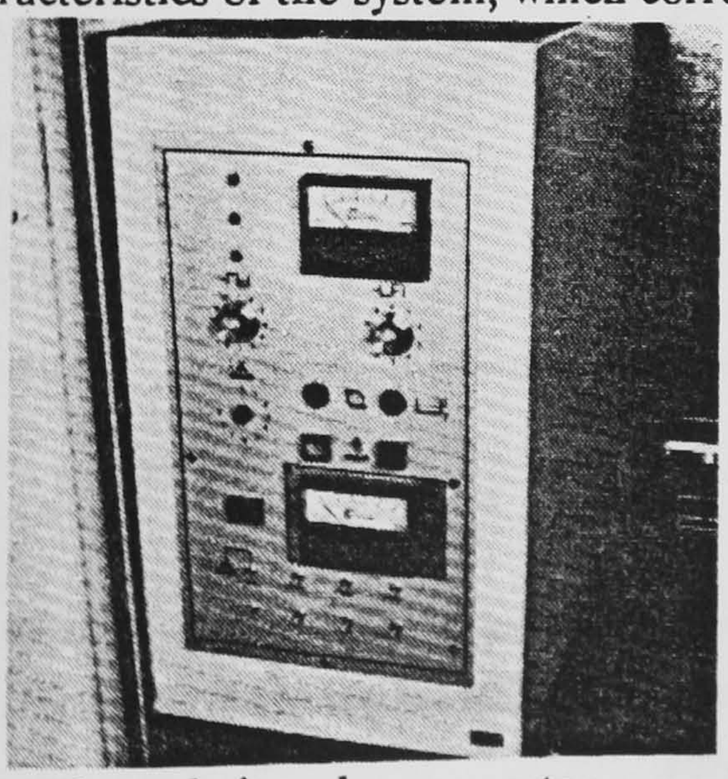

Fig 3. Electrolytic pulse generator.

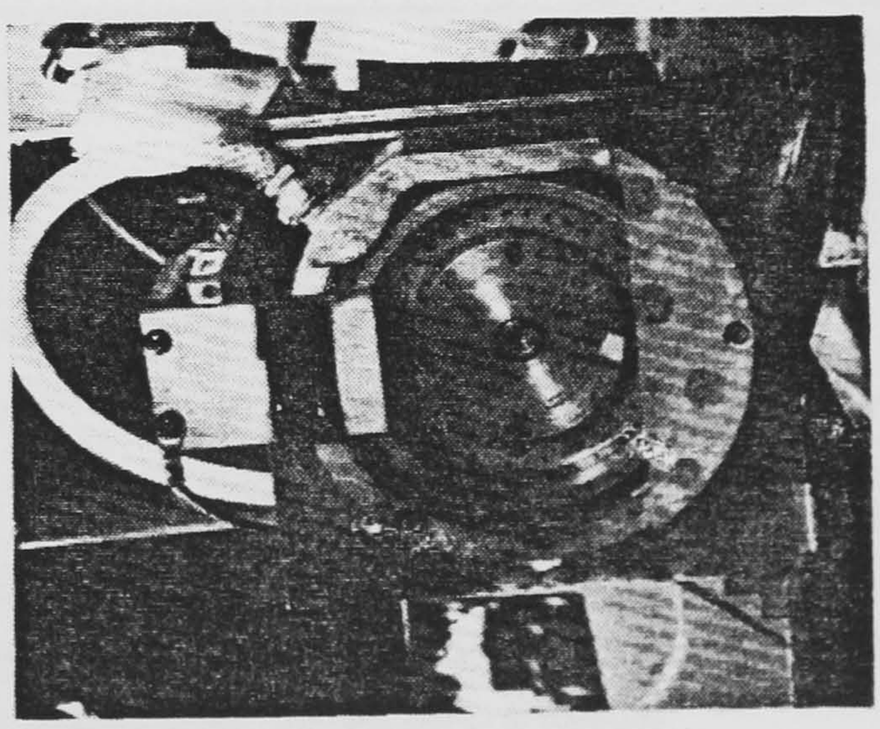

Fig 4. Electrolytic dressing for cup wheel set up.

3.3 Preparation of Glass Samples

Surface grinding tests were performed on 25 mm diameter prepared samples, the flat surfaces of which were produced by free abrasive grinding with silicon carbide particles of 14 μm diameter in a water based fluid. The resulting surface roughness was measured as 0.3 μm Ra (2.8 μm P-V_{max}). This initial preparation was carried out to ensure that each sample exhibited similar surface and sub-surface properties.

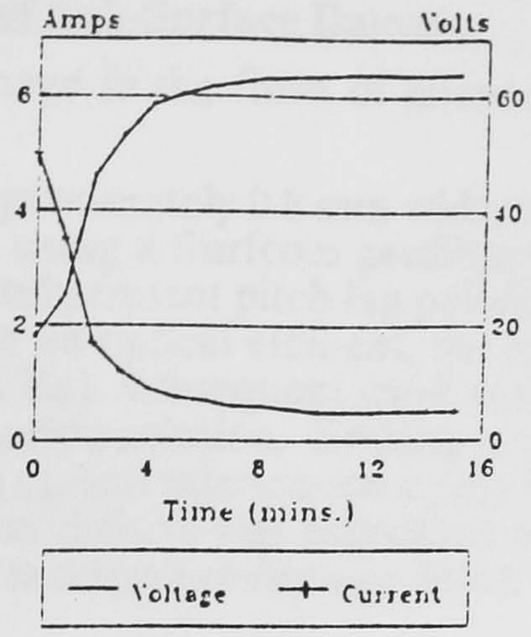

Fig 5. Electrical characteristics of the dressing system

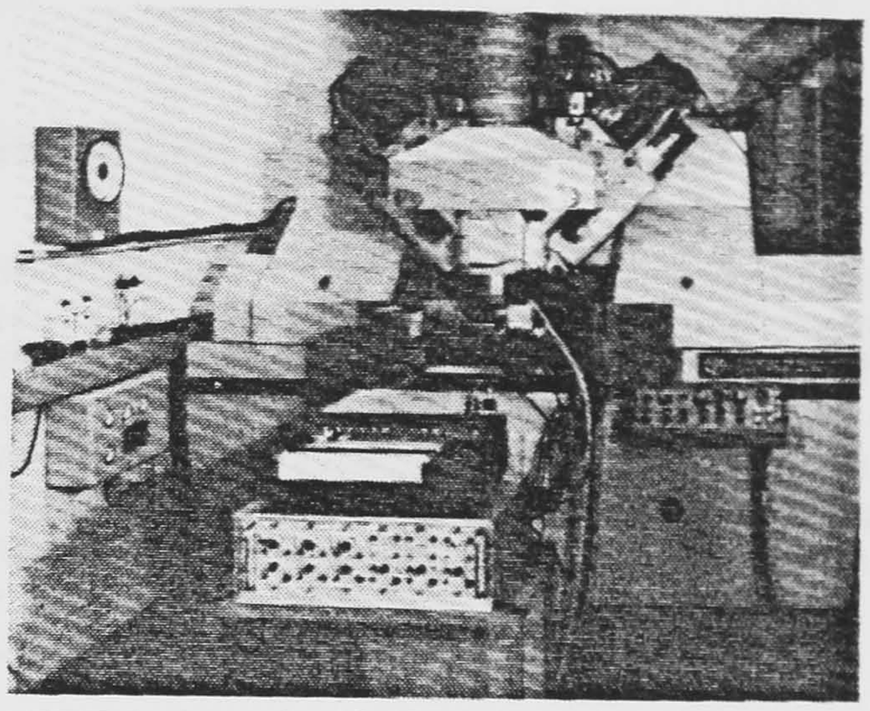

Fig 6. CPE Ltd 7 axis grinding machine, for computer disk read/write (flying) head production

3.4 Machine Tool and Grinding Tests

All tests were carried out on a 7 axis grinding machine (see Figure 6) manufactured by CPE Ltd. This machine offers a grinding wheel positioning capability in the order of 0.1 μm, and possesses a high "loop-stiffness" (static 135 N/μm).

Truing of the grinding wheel prior to dressing was accomplished using a diamond truing wheel mounted on a motor driven air bearing spindle, this was precisely fed across the grinding wheel at set depths of cut and feedrate.

Details of the grinding tests and the surface quality produced are given in Table 2. The BK7 samples were ground using two levels of depth of cut, feedrate and total stock removed and with conventional and electrolytic dressing methods. The grinding force in the normal direction was monitored during grinding with a dynamometer.

Higher material removal rates were investigated with the softer SF10 glass samples to assess the scope of the ductile removal mode with this material when using electrolytic dressing.

Description	Test No.	Stock removed (μm)	Final feed (mm/sec)	Final DOC (μm)	Ra (nm)	P-V_{max} (nm)
Electrolytically assisted grinding of SF10 glass.	1/1	55	1.5	5.0	-	24
	1/2	107	1.5	1.0	-	18
	1/3	117	1.5	0.5	7.9	36
	1/4	123	0.375	0.5	5.5	20
	1/5*	142	0.375	0.1	1.7	14
	1/6	83	0.25	0.1	3.8	32
Conventional grinding of BK 7 glass	2/1	70	0.75	1.0	49.0	430
	2/2	70	0.375	1.0	68.5	460
	2/3	70	0.75	0.5	21.7	180
	2/4	70	0.375	0.5	37.4	310
	2/5	35	0.75	1.0	52.3	460
	2/6	35	0.375	0.5	31.1	270
Electrolytically assisted grinding of BK 7 glass.	3/1	70	0.75	1.0	1.9	23.2
	3/2	70	0.375	1.0	10.2	76.4
	3/3	70	0.75	0.5	9.4	85.7
	3/4	70	0.375	0.5	2.1	23.1
	3/5	35	0.375	0.5	10.9	75.4

All tests used a 3/6μm/100 conc. cast iron bond wheel, except test 1/5 which used a 1/2μm/100 conc. cast iron wheel.

Table 2.GRINDING TEST DATA AND SURFACE FINISH

3.5 Assessment of Surface Topography

The quality of the ground surfaces was measured using a Talystep surface profilometer fitted with a 0.1 μm radius stylus applied at 0.01 g force. All values for Ra and peak to valley roughness measurements were assessed over 5 cut off lengths of 0.25 mm. Evaluation of the surface integrity and material removal mode was carried out using; Normarski optical, scanning electron and transmission electron microscopes.

3.6 Assessment of Sub-Surface Damage

Sub-surface damage in the form of micro-cracks was assessed by a series of light polishing and wet chemical etching operations.

A fine groove approximately 0.8 mm wide, was etched across the diameter of a number of ground samples and its precise depth measured using a Surfcom profilometer. This groove established a datum against which the depth of material removed during subsequent pitch lap polishing with 0.33 μm cerium oxide/water slurry could be measured. To simulate the production of an optical element, the sample was initially polished to a high quality surface of approximately 5 nm P-V max (0.5 nm Ra). Subsequent small amounts of stock were polished away with intermediate etching in dilute aqueous ammonium bifluoride solution. Etching revealed micro-crack defects lying immediately below the polished surface, and with the aid of an optical microscope under Nomarski illumination, the number of defects per unit area could be counted. The density of the defects was expressed as the number of defects per square mm. This form of experiment gave an indication of the mechanical damage depth profile of a component ground with electrolytic assistance.

4.0 DISCUSSION OF RESULTS

4.1 Investigation of Dressing Methods

Diamond grinding wheels were prepared by abrasive and electrolytic methods. These wheels were then evaluated by scanning electron microscopy. Figures 7, 8 and 9 are back scattered electron micrographs, Figure 7 is of a conventionally dressed cast-iron bonded 1-2 μm diamond wheel. The grits, which appear as black areas, can be clearly seen as having both good distribution and protrusion.

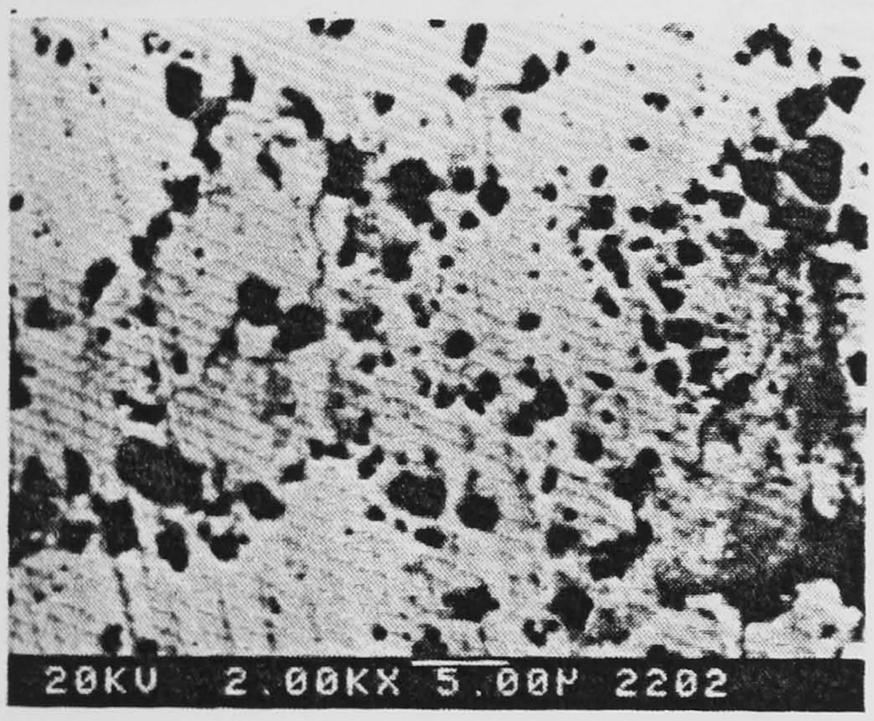

Fig 7. Backscattered SEM photomicrograph of conventionally dressed 1-2 μm diamond wheel.

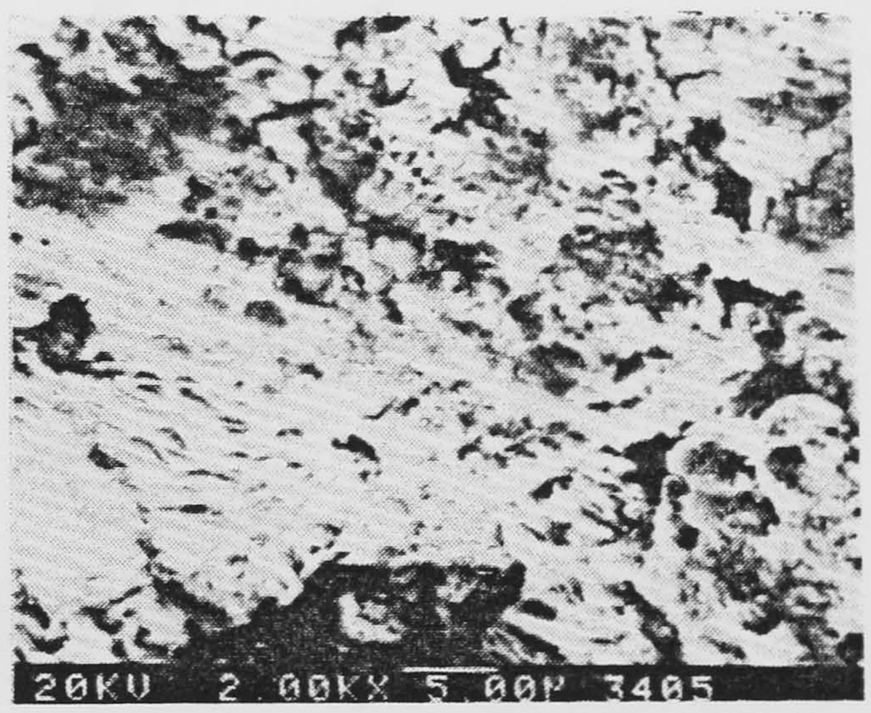

Fig 8. Backscattered SEM photomicrograph of 3-6 μm diamond electrolytically dressed wheel.

Figure 8 shows a small representative area of a 3-6 μm wheel immediately after electrolytic dressing. The photomicrograph shows that the diamond grains are completely hidden by a fine granular oxide layer. Figure 9 shows a similar area of the same wheel after mechanical abrasion of a workpiece with the black diamond grains now visable. It is considered that Figure 9 is representative of the condition of the wheel during its interaction with the workpiece.

Break up of the oxide layer can be seen in Figure 10, and from this photomicrograph the approximate depth of the oxide layer produced during the initial dressing can be estimated as 10 μm.

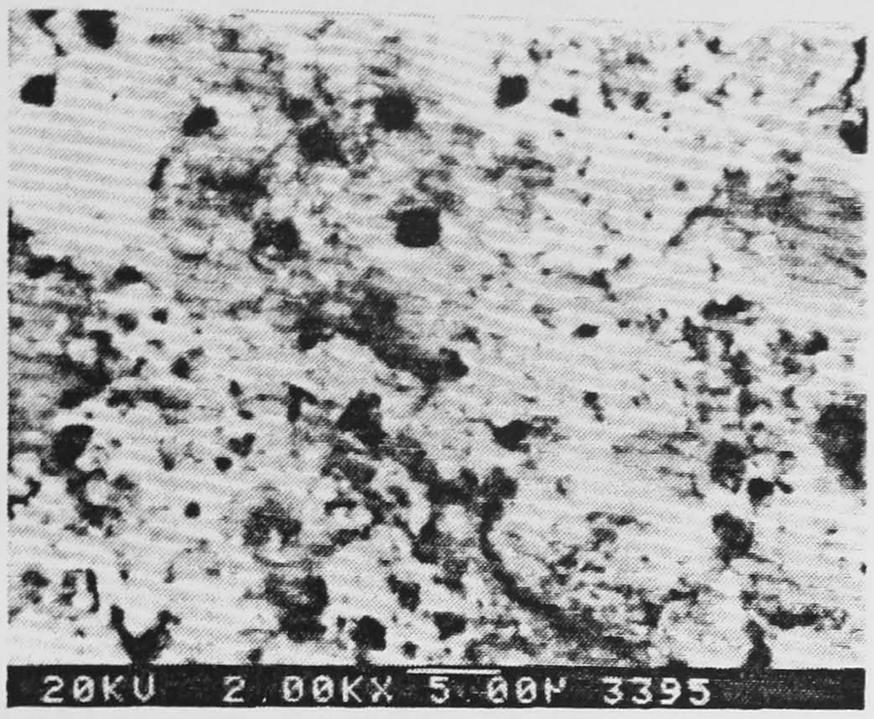

Fig 9.Backscattered SEM photomicrograph of an abraded 3-6 μm electrolytically dressed diamond wheel.

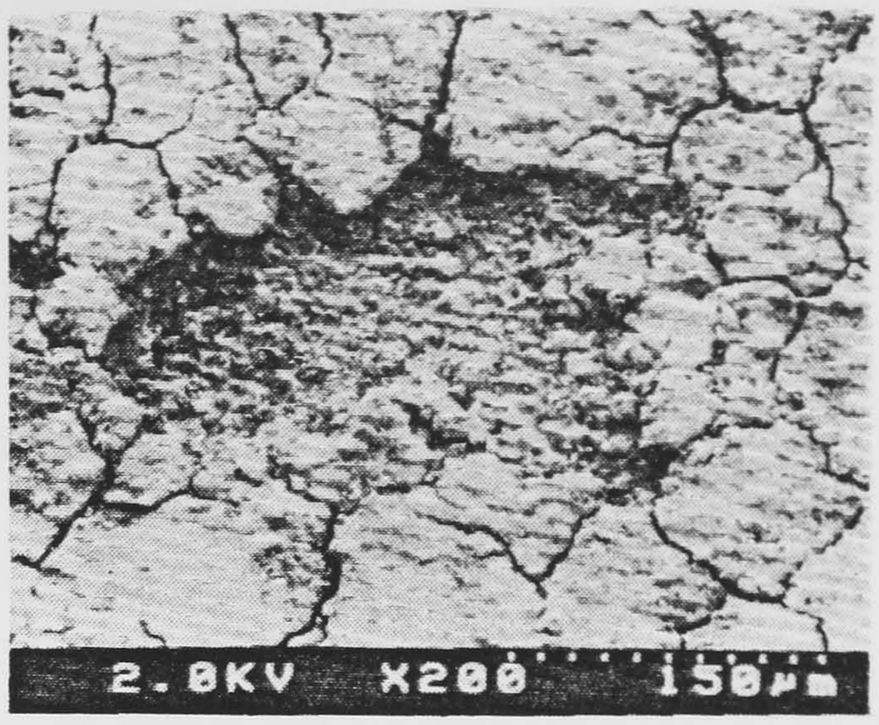

Fig 10.SEM photomicrograph of the oxide layer produced on a 3-6 μm wheel.

4.2 Grinding Tests

A two-level, three factor designed experiment was carried out on the BK7 samples for both conventional and electrolytic dressing techniques. Figures 11 and 12 show the resulting surface finish and normal grinding force obtained using the two different dressing techniques.

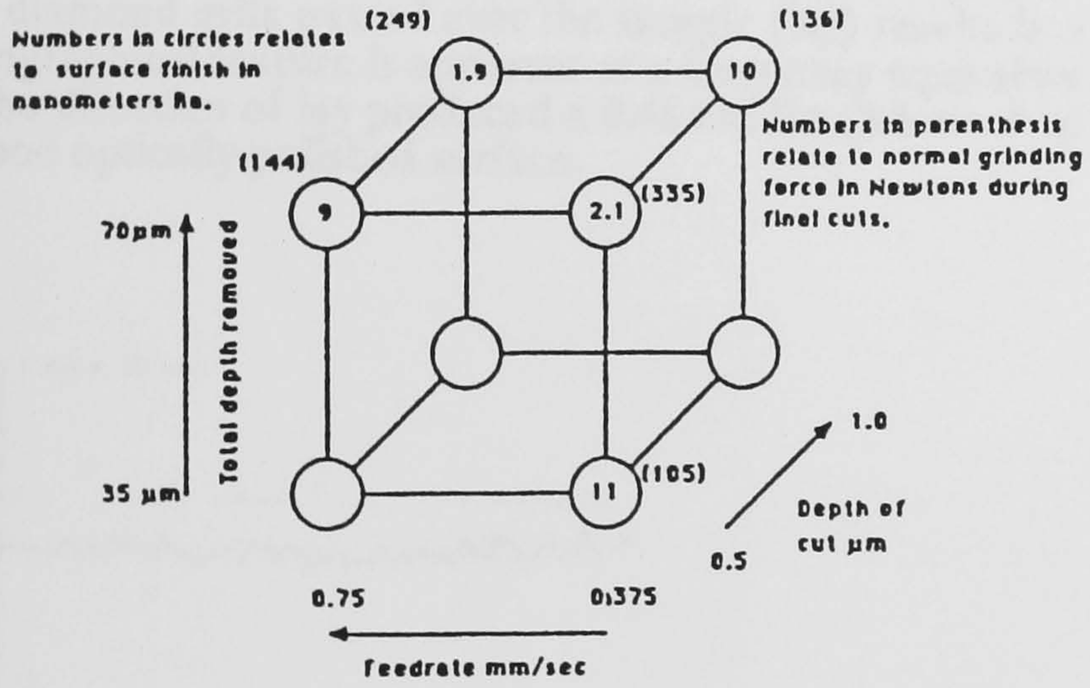

Fig 11.Electrolytically assisted grinding of BK7.

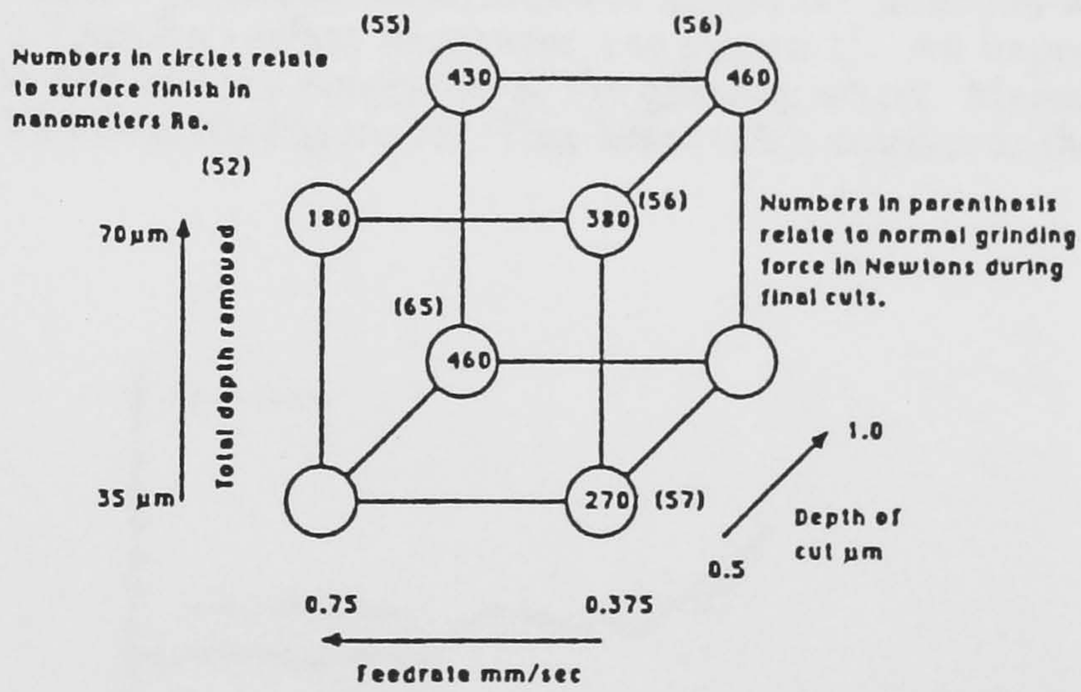

Fig 12.Conventionally dressed diamond grinding of BK7.

A dramatic improvement in surface quality resulted from employing the electrolytic dressing system; this was found to be the case in all test runs. The poor surface qualities obtained when using conventional dressing appear to have little dependence on the three specified factors at the assessed levels. Low normal grinding forces were encountered and the surfaces were shown to be of a totally brittle fractured nature.

The surface quality produced by the same machining parameters with the addition of electrolytic assistance was found to be in the 1-10 nm Ra range. The importance of the total depth removed is shown by a general increase in surface quality with the greater depth removed. These surfaces, when investigated by transmission electron microscopy, generally proved to be a combination of ductile and brittle fracture modes (see Figure 13). Whether the brittle fracture areas were initially induced during the free abrasive sample preparation or were propagated during the test runs is unknown. Test run 3/1 resulted in a surface which appeared to be consistent with pure ductile mode stock removal. A noticeable increase of the normal grinding force was experienced during these test runs, with the best quality surface finish being obtained when the highest value of normal force was encountered.

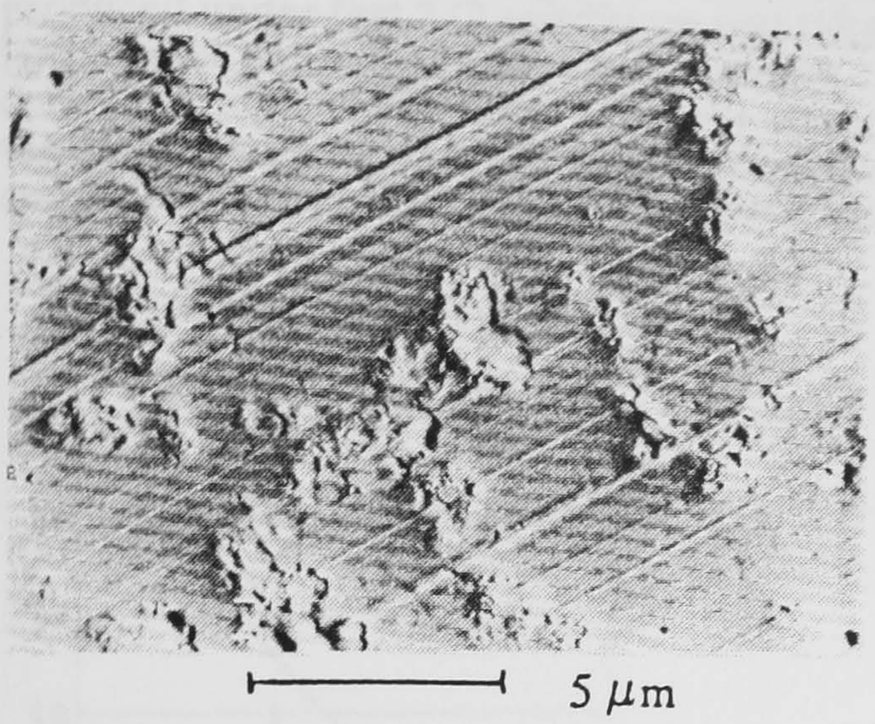

Fig 13.TEM replica of a brittle/ductile ground surface of BK7.

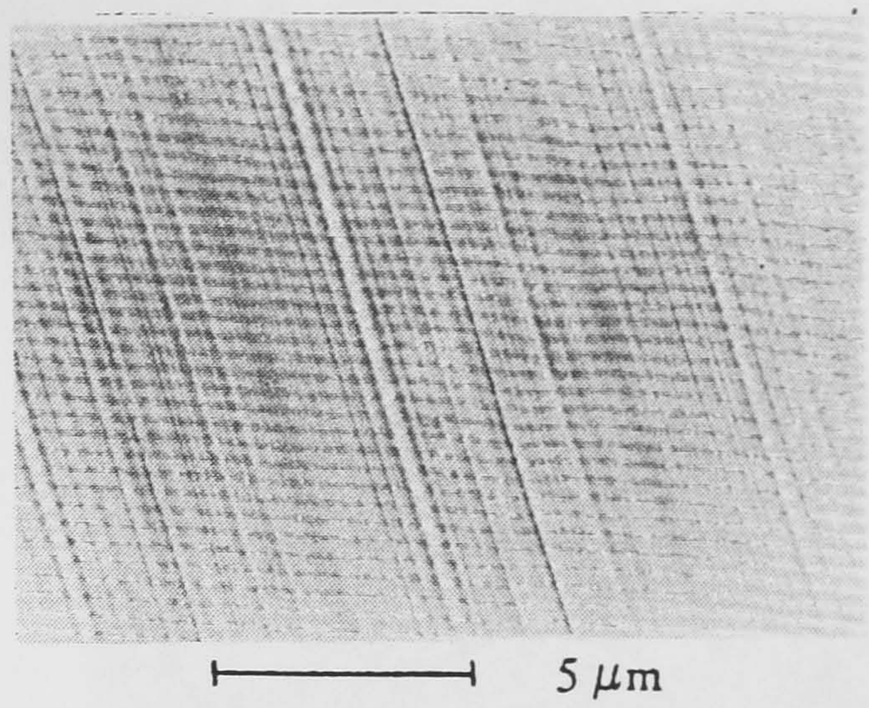

Fig 14.TEM replica of a purely ductile ground surface of SF10.

Electrolytically assisted grinding trials were also carried out on the SF10 glass. TEM investigation of the resulting surfaces showed these samples to have only ductile type movement, see Figure 14. Surface roughness values were found to be in the region of 1-10 nm Ra. The same 3-6 μm wheel was used as for the BK7 except in the case of test run 1/5; this test used an 1-2 μm diamond wheel. A single measurement of the surface finish is not sufficient to describe these ductile ground surfaces, due to the high directionality of the microtexture produced. Measurement across the direction which the diamond grits passed over the sample (lay) results in a 1.7 nm Ra surface roughness, see Figure 15. An important topographical feature is apparent at a frequency equivalent to the feed per revolution of the grinding wheel. Measuring in the direction of lay produced a 0.48 nm Ra (3.5 nm P to V) value, see Figure 16. This latter value equates to that of a good optically polished surface.

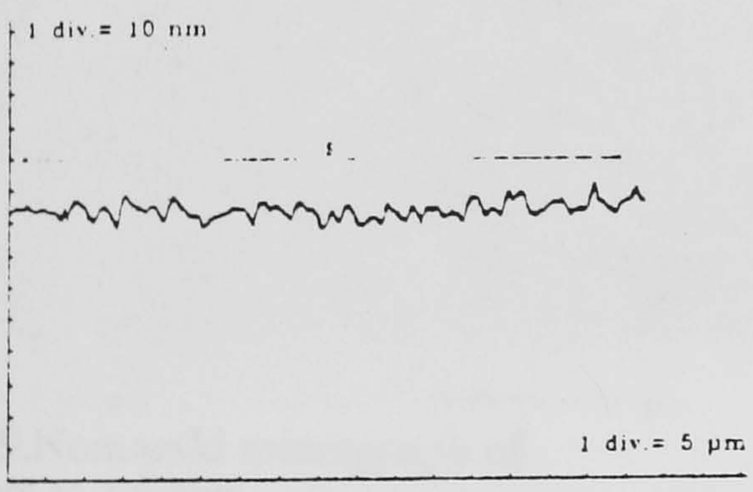

Fig 15.Talystep trace of ductile ground SF10 glass, measured across "lay".

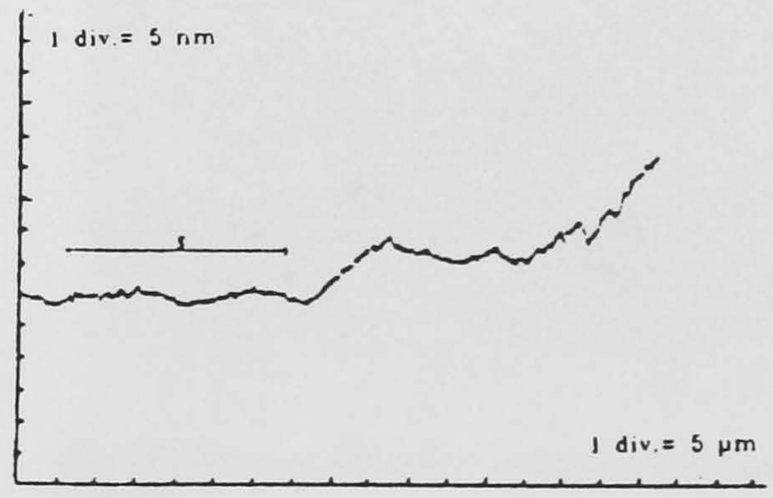

Fig 16.Talystep trace of ductile ground SF10 glass, measured with "lay".

4.3 Sub-Surface Damage

The surface produced on BK7 in test 3/1, which consisted of solely ductile removal, revealed no sub-surface micro-cracks beyond a depth of 2 μm. In a similar way, the ductile machined surface produced on SF10 in test 1/6 was free from micro-cracks beyond a depth of 0.75 μm. Although the specific damage cut-off point was not ascertained for these two surfaces, the indication is that ductile mode material removal does not induce significant sub-surface damage.

Surfaces on BK7 containing both brittle and ductile modes of material removal were commonly observed. The surface produced under test 3/3 conditions was taken to represent this surface topography, and the polish/etch cycle revealed a large initial concentration of micro-cracks. The graph shown in Figure 17 demonstrates a nominally linear decrease in defects per square mm observed as the surface was polished away, with a theoretical zero damage depth of 3.25 μm below the original surface. The Nomarski micrographs in Figures 18,19 and 20 show three consecutive stages in the experiment, and from these the initial cracks can be seen to be in the order of 2 μm long.

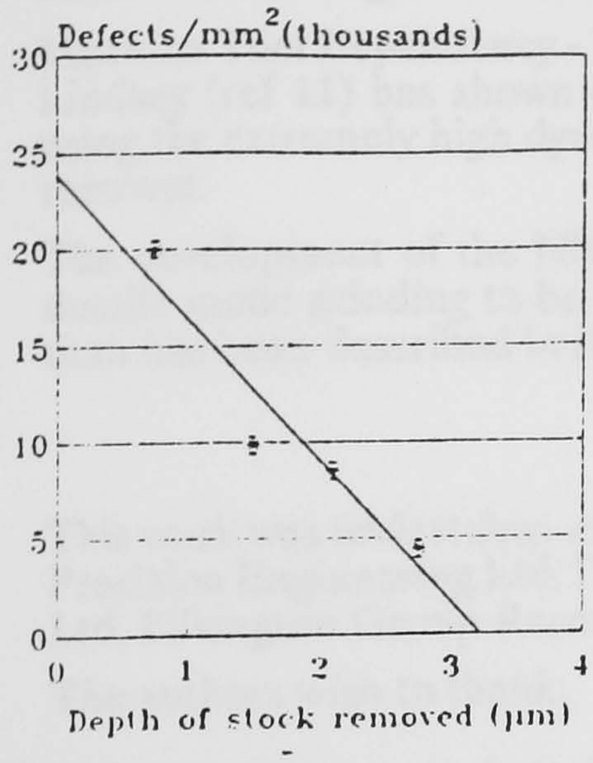

Fig 17.Graph of defects per unit area against depth of penetration.

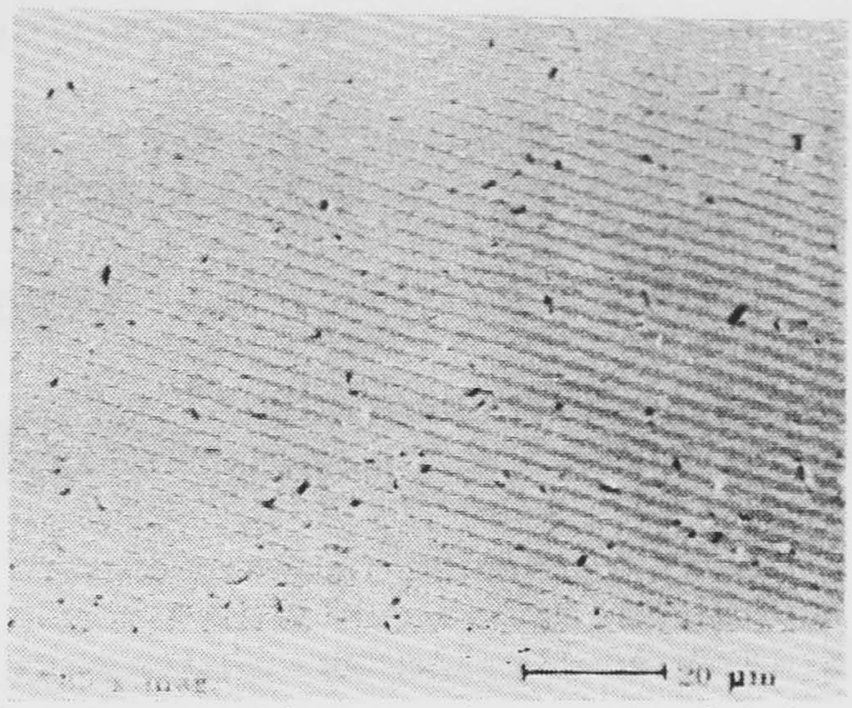

Fig 18.Nomarski photomicrograph of defects at 0.75 μm depth.

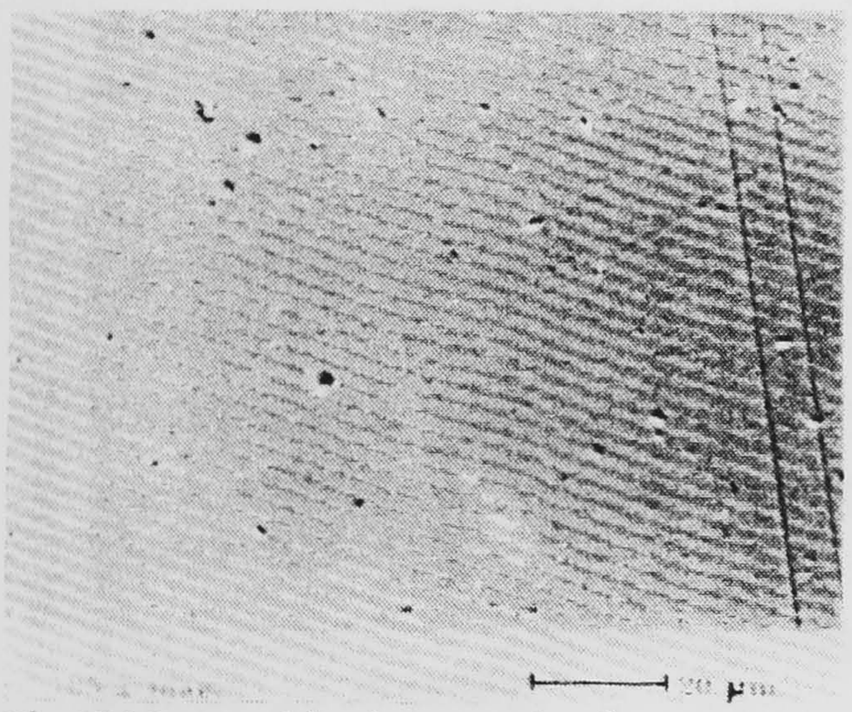

Fig 19.Nomarski micrograph of defects at 1.5 μm depth.

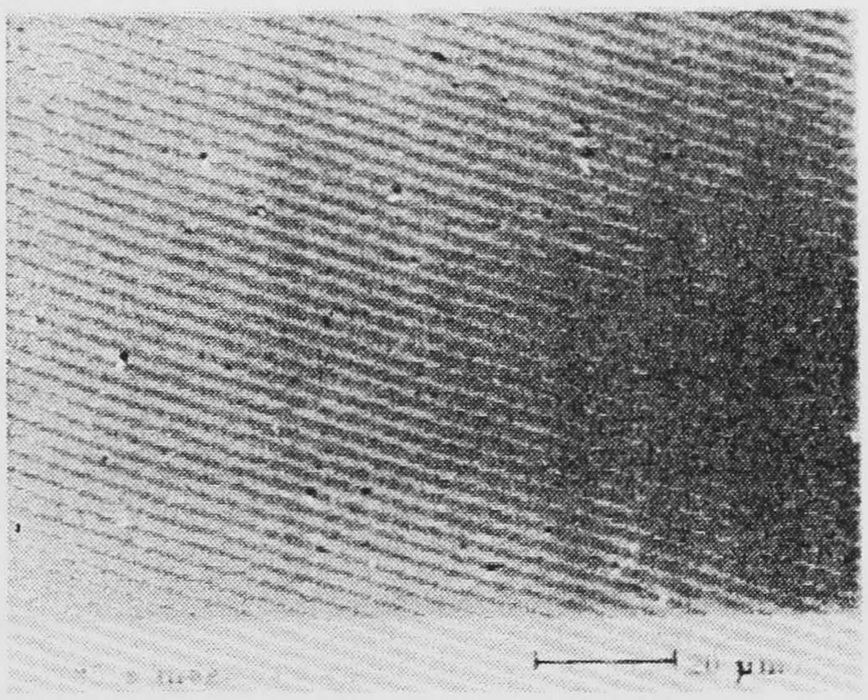

Fig 20.Nomarski micrograph of defects at 2.75 μm depth.

It is imperative that sub-surface stress induced by grinding should be recognised as damage; this has not been investigated in the work presented here.

4.4 Conclusions

BK7 and SF10 optical glass can be machined in a ductile mode using cast iron bonded diamond grit wheels with electrolytic assistance.

The surface finish attained by electrolytically assisted machining BK7 and SF10 optical glasses is vastly superior to that obtained using the same wheel and machining parameters in a traditional grinding operation.

The electrolytically assisted fixed abrasivé grinding process was shown to be capable of producing optical quality surfaces (0.5 nm Ra) albeit in a unidirectional manner on a microtextured surface of 1.7 nm Ra.

Sub-surface microcracks in the glasses investigated were restricted to a maximum depth of 2 μm when machined in a ductile mode with electrolytic assistance.

The magnitude of the grinding force is indicative of the grinding mode; higher forces are associated with ductile mode machining whilst lower forces are associated with brittle fracture mode machining.

4.5 Direction for Further Work

In order for ductile mode grinding to be widely accepted as a production process for machining optical glass elements, further work is required in the following areas:-

Material Removal Mechanism - A detailed scientific understanding must be sought regarding the mechanisms involved in the electrolytically assisted grinding process. Research in this area needs to resolve the individual contributions to the ease of machining, from the electrolytic, chemical, and mechanical effects.

Machine Tool Dependency - The ability to machine glasses in a ductile mode is considered to be machine tool dependent. Lindsey (ref 11) has shown that high quality surface finishes can be obtained with minimal sub-surface damage when using the extremely high dynamically stiff research machine known as Tetraform ^{R} with relatively high rates of material removal.

The development of the NION ultra precision CNC aspheric generator will shortly enable a detailed investigation of ductile mode grinding to be made, both producing finer quality surfaces and at a much higher rate of material removal than has been described in this paper.

5.0 ACKNOWLEDGEMENTS

This work was undertaken as part of a DTI (UK) Link Nanotechnology project. This project is also funded by Cranfield Precision Engineering Ltd, DeBeers Industrial Diamond Division (PTY) Ltd, Framatome, S.A., IBM (UK) Laboratories Ltd, Pilkington Group Research, REOSC.

The authors wish to thank;

Pilkington Group Analytical Services for the Talystep, Surfcom, T.E.M. and Normarski data and photomicrographs.

De Beers Industrial Diamond Division Ltd for valuable advice on grinding wheel topography and SEM photomicrographs

This paper is published with the permission of the Directors of Pilkington plc. Dr A Ledwith, Director of Group Research and Professor P A McKeown, Director of CUPE.

6.0 REFERENCES

1. NION,(UPMR) project. A Department of Trade and Industry (UK) LINK Nanotechnology programme based at the Cranfield Institute of Technology,1989-1992.

2. A G Evans,K T Faber,"Crack growth resistance in microcracking brittle materials."J.Am Ceramic Soc.1984,67(4) 255-260

3. K E Puttick,M R Ruddman,K J Smith,A Franks,K Lindsey,"Single point diamond machining of glasses." Proc. R.Soc London.A426,19-30 (1989).

4. M G Schinker, W Doll,"Basic investigations into the high speed processing of optical glasses with diamond tools." Proc. SPIE,381,32-38 (1989).

5. H Mairlot "The texture of ground glass surfaces." Industrial Diamond Review,61-66,February 1972.

6. D Golini, S D Jacobs "Physics of loose abrasive microgrinding."Applied Optics Vol 30.July 1991.

7. N.J.Brown,B A Fuchs,"Shear mode grinding." 43 rd Annual symposium,IEEE (1989).

8. T Izumitani, "On materials science and technology" Materials structure and physical properties. Vol 17, Glass II. 1979 Academic Press.

9. P Shore, "State of the art in "damage-free" grinding advanced engineering ceramics" British Ceramics Proc, Vol 46, 1990. R Morrell. Inst of Ceramics.

10. T. Nakagawa, H Ohmori,"Mirror finish surface grinding of silicon wafers with in-process electrolytic dressing." Annals of CIRP (1990).

11. K Lindsey, "Tetraform Grinding", International Conference - "Commercial applications of precision manufacturing of the sub-micron level", London, November 1991. SPIE Proceedings Vol 1573

Appendix 2

Application of a Nanometric Resolution Optical Tool Setting System to Aspheric Generation

P. Morantz, R.F.J. Read, P. Shore

Cranfield Precision Engineering
Cranfield Institute of Technology
Bedford, MK43 0AL, England

A previously announced[1] method for setting the position of a tool has now been applied to aspheric generation, on a diamond turning aspheric generator. The method uses advanced image processing techniques, in conjunction with a high magnification optical imaging system, to measure (with nanometric resolution) the position and orientation of chosen segments of a tool edge relative to a fixed machine reference point.

This setting technique has several advantages over alternative methods: it provides non-contact measurement, can make three-dimensional measurements and is capable of extremely high accuracy; thus permitting 'right first time' tool setting to the accuracy required by modern aspheric generators. Furthermore, it has the capability of mapping entire tool geometry to allow wear/shape compensation, within a machining programme.

There are two principal techniques which are used with the system.

The first is to move the tool in two orthogonal directions, using machine motion axes, and take successive measurements of the position of the tool edge as it is scanned. See figure 1.

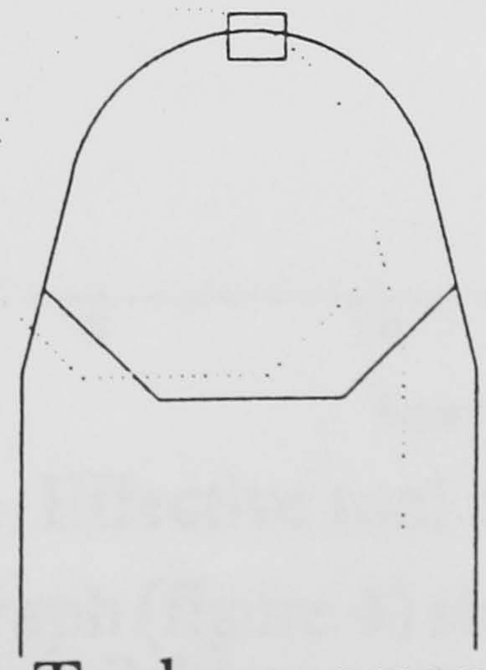

Figure 1. Tool movement in x-z

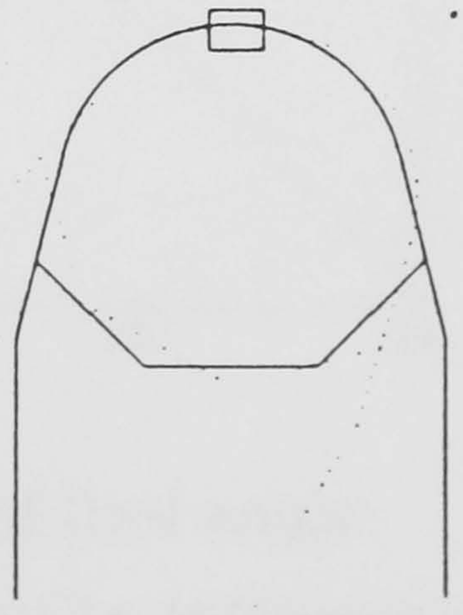

Figure 2. Tool rotation

On machines which have a tool rotary axis, for tool normal one point machining, an additional technique is used to establish the concentricity of tool geometric and rotary axis centres. See figure 2.

The system has been used to perform complete tool edge geometry mapping on several diamond tools. The graphs below show data gathered, using the optical tool setting system in conjunction with an aspheric generator, from a 0.5 mm radius tool with zero top-rake. The data were acquired by rotating the tool about an axis as close as possible to its geometric centre (figure 2), so that a portion of 30° of the tool edge passed through the probe acquisition area.

In the first graph (figure 3) shown below, the effective tool radius as the tool is rotated (as in figure 2), is plotted against the angular position of the tool. The general trend of the graph is a function of the centring of the tool geometric centre to the rotary axis. In the second graph (figure 4), the departure of this measured effective radius from the expected (and conventionally relied upon) perfect circular arc is plotted against tool rotation angle.

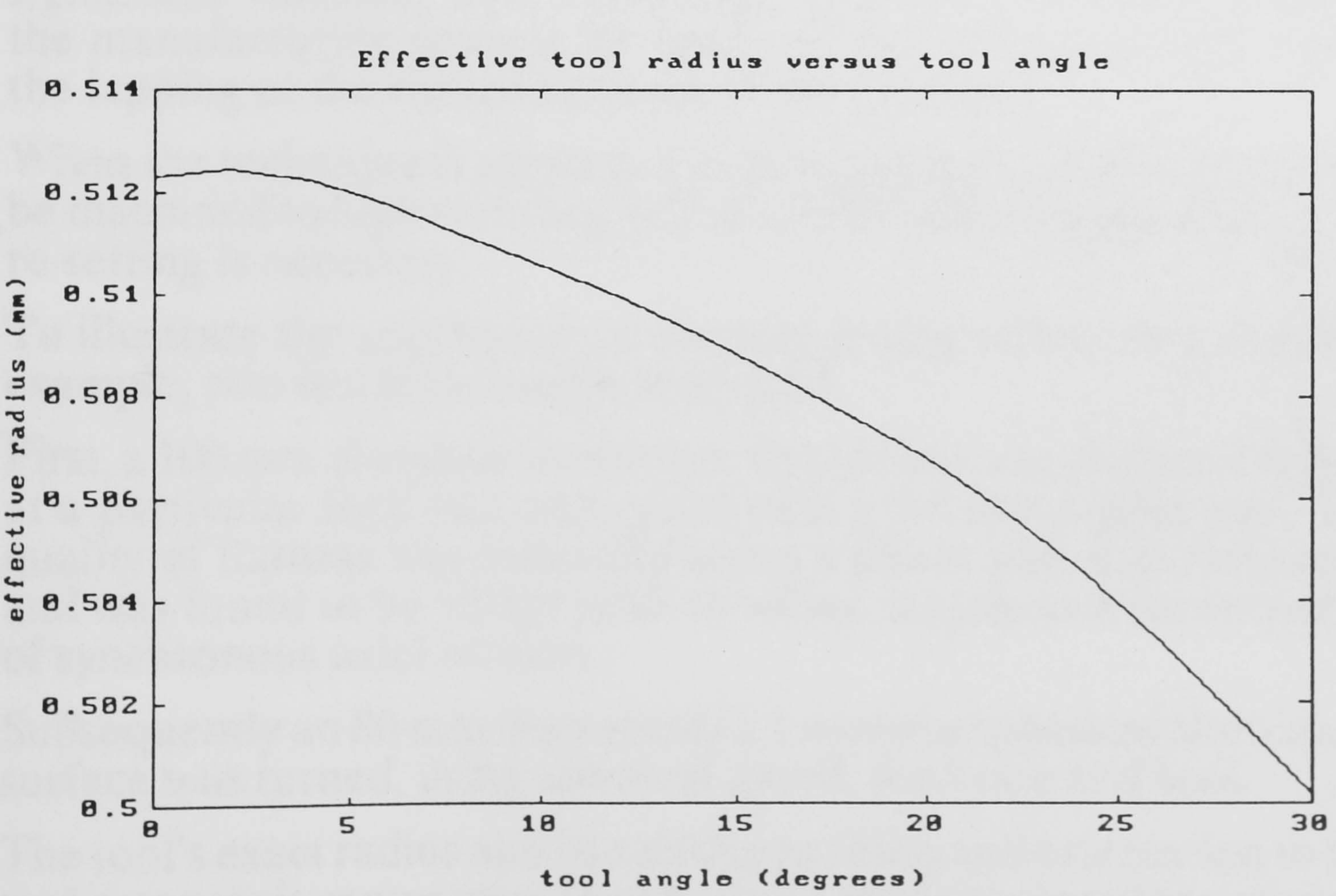

Figure 3. Effective tool radius as a function of tool angle.

This second graph (figure 4) shows the tool error profile, information not normally available to an aspheric generator. This error profile would affect the accuracy of any cutting operation which used more than one point on the tool. So the information can be used to si[illegible]uracy of aspheric generation, or to allow th[illegible] cost tools or even to prolong tool life.

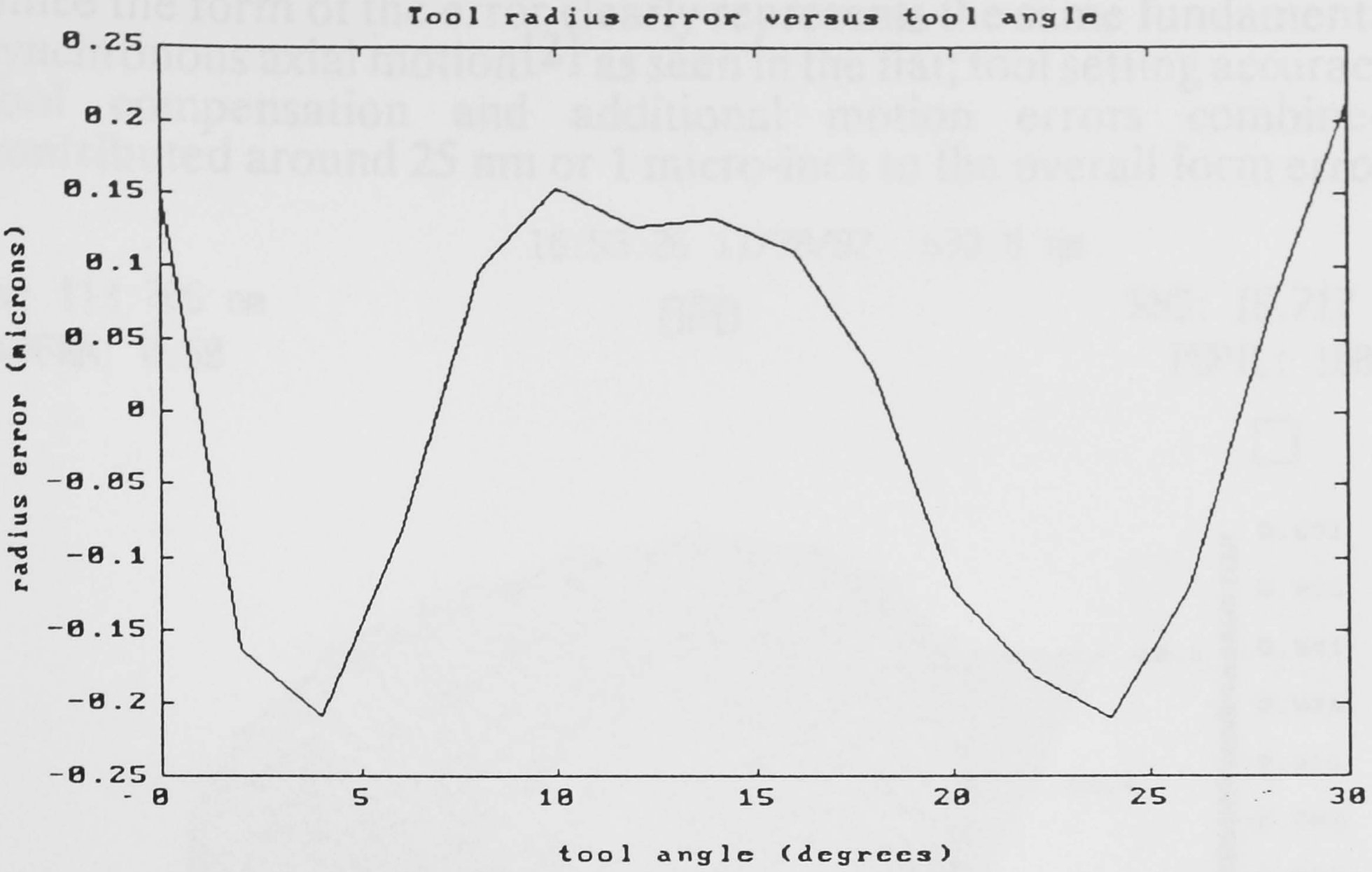

Figure 4. Tool radius error as a function of tool angle.

In figure 3 note the significant wear at the zero tool angle. This is because this tool had been used for facing prior to tool measurement. In figure 4, the departure of the tool from perfect form shows a significant 'waviness' of the tool edge. This is a common artefact of the manufacturing process for diamond tools, which occurs during the lapping of the curved surfaces of the diamond.

When the technique is applied to turning surfaces, profiled parts can be machined to high accuracy, with a single toolsetting operation. No re-setting is necessary.

To illustrate the application of the tool setting system to a practical example, two test pieces were machined.

First, a 100 mm diameter aluminium flat surface was diamond turned at a particular feed rate and speed with a 0.5 mm radius tool. The quality of flatness was measured using a phase shift interferometer and was found to be 90 nm peak to valley, largely as a consequence of synchronous axial motion.

Subsequently an 80 mm diameter f/1.1 concave spherical aluminium surface was turned, using identical speed, feed rate and tool.

The tool's exact radius and its relative position and orientation to the tool rotary axis centre were found using a single tool setting program. These parameters were automatically assigned to the part program used to generate the concave surface. The accuracy of the surface was measured and found to be 113 nm peak to valley (see figure 5).

Since the form of the error clearly represents the same fundamental synchronous axial motion[2] as seen in the flat; tool setting accuracy, tool compensation and additional motion errors combined, contributed around 25 nm or 1 micro-inch to the overall form error.

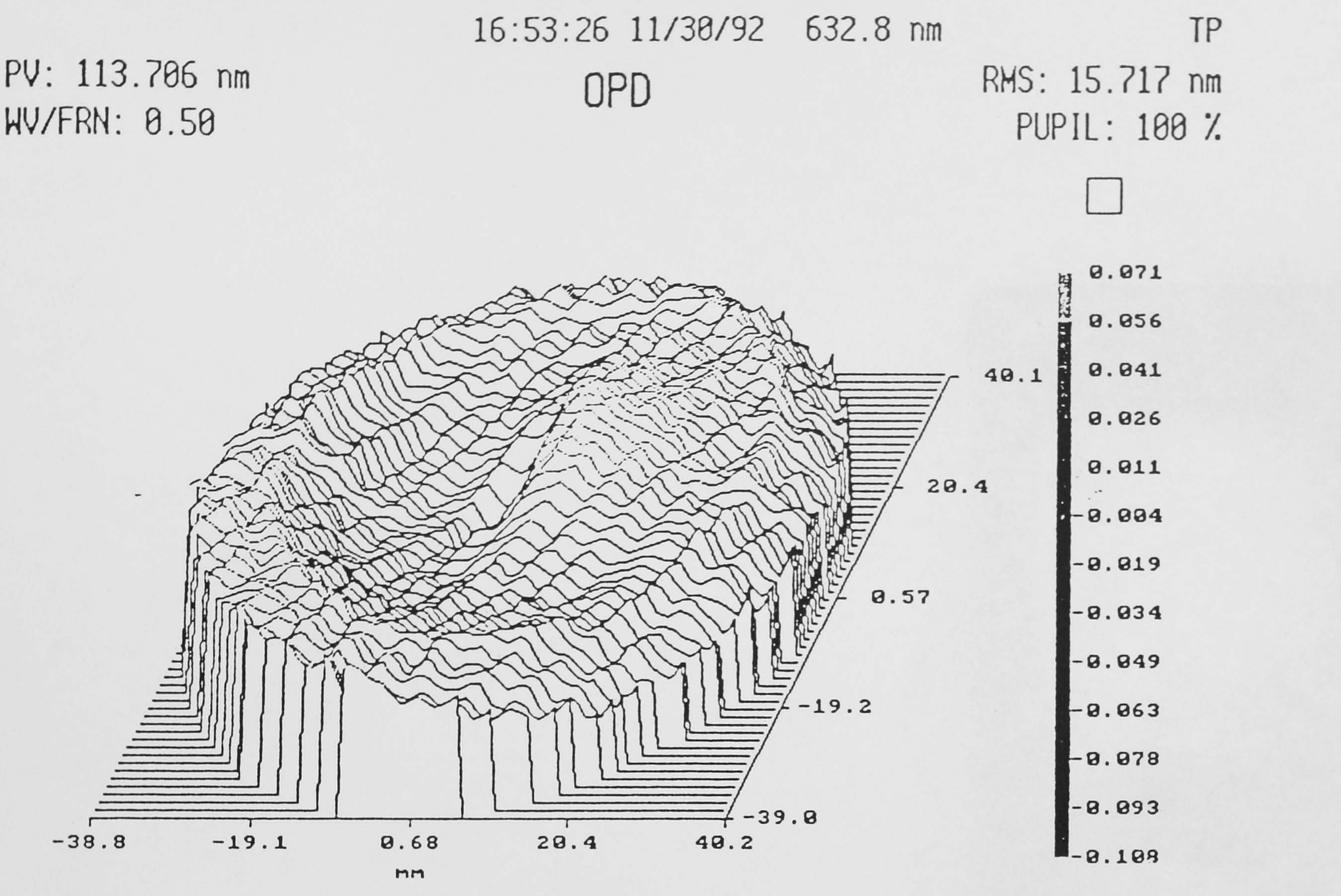

Figure 5. Form error of the spherical surface.

This work was undertaken as part of a DTI (UK) Link Nanotechnology Ultra Precision Machining Research project with additional funding from Robert Bosch (Gmbh), Cranfield Precision Engineering Ltd., DeBeers Industrial Diamond Division (PTY) Ltd., Framatome, S.A., IBM (UK) Laboratories Ltd., Pilkington Group Research and REOSC Optique.

References

1. Morantz P. "A Nanometric Precision Non-Contact Toolsetting System", American Society for Precision Engineering Annual Meeting Conference Proceedings, October 1992
2. Gerchman M. C. "The Effects of Fundamental Axial Spindle Motion on the Optical Performance of Diamond Turned Surfaces", American Society for Precision Engineering Annual Meeting Conference Proceedings, October 1991